IAEA-TECDOC-933

Creep-fatigue damage rules for advanced fast reactor design

Proceedings of a Technical Committee meeting held in Manchester, United Kingdom, 11–13 June 1996

INTERNATIONAL ATOMIC ENERGY AGENCY IAEA

The IAEA does not normally maintain stocks of reports in this series. However, microfiche copies of these reports can be obtained from

INIS Clearinghouse
International Atomic Energy Agency
Wagramerstrasse 5
P.O. Box 100
A-1400 Vienna, Austria

Orders should be accompanied by prepayment of Austrian Schillings 100,– in the form of a cheque or in the form of IAEA microfiche service coupons which may be ordered separately from the INIS Clearinghouse.

The originating Section of this publication in the IAEA was:

Nuclear Power Technology Development Section
International Atomic Energy Agency
Wagramerstrasse 5
P.O. Box 100
A-1400 Vienna, Austria

CREEP-FATIGUE DAMAGE RULES FOR ADVANCED FAST REACTOR DESIGN
IAEA, VIENNA, 1997
IAEA-TECDOC-933
ISSN 1011–4289

Printed by the IAEA in Austria
March 1997

FOREWORD

The excellent heat transfer properties of the sodium coolant used in liquid metal cooled fast reactors (LMFRs) transmit any changes in the coolant temperature rapidly to the structural components of the reactor. Thermal transients that are sufficiently rapid may cause local yielding of the material, setting up residual stresses. These residual stresses can relax at high temperature, converting elastic strains into creep strain. Repetition of such transients can therefore result in progressive damage by both fatigue and creep mechanisms or, in the presence of primary stresses, to progressive deformation (ratcheting). Interaction of these damage processes might, potentially, result in more severe damage than the individual mechanisms acting in isolation. While design code rules have been developed for design against creep, fatigue, creep-fatigue and ratcheting, these rules tend to contain conservatism to ensure that component failure is avoided.

Present trends in LMFR design are aimed at providing designs which can compete economically with other energy sources. Because of the relatively high capital cost of LMFRs, this implies the need for both high availability and plant lifetimes in excess of 40 years. Reduction of over-conservatism in design, while avoiding failure over lifetimes of at least 300 000 hours, is therefore a motivation for the development of improved design rules against creep-fatigue damage.

The IAEA, following the recommendations of the International Working Group on Fast Reactors, convened a Technical Committee Meeting on Creep-Fatigue Damage Rules to be used in Fast Reactor Design. The objective of the meeting was to review developments in design rules for creep-fatigue conditions and to identify any areas in which further work would be desirable.

The meeting was hosted by AEA Technology, Risley, and held in Manchester, United Kingdom, 11-13 June 1996. It was attended by experts from the European Commission, France, India, Japan, the Republic of Korea, the Russian Federation and the United Kingdom.

The IAEA wishes to thank all the participants of the Technical Committee meeting for their valuable contribution, especially the Chairman, C. Picker from the United Kingdom.

EDITORIAL NOTE

In preparing this publication for press, staff of the IAEA have made up the pages from the original manuscripts as submitted by the authors. The views expressed do not necessarily reflect those of the governments of the nominating Member States or of the nominating organizations.

Throughout the text names of Member States are retained as they were when the text was compiled.

The use of particular designations of countries or territories does not imply any judgement by the publisher, the IAEA, as to the legal status of such countries or territories, of their authorities and institutions or of the delimitation of their boundaries.

The mention of names of specific companies or products (whether or not indicated as registered) does not imply any intention to infringe proprietary rights, nor should it be construed as an endorsement or recommendation on the part of the IAEA.

The authors are responsible for having obtained the necessary permission for the IAEA to reproduce, translate or use material from sources already protected by copyrights.

CONTENTS

SUMMARY

1. Session 1: General Design Methods

Chairmen: C. Poette, France, V. Zhukov, Russian Federation, H.-Y. Lee, Republic of Korea, Y. Wada, Japan

The French RCC-MR design code was evaluated on typical applications in fast reactors structures. Minimum life evaluations obtained were not very different from design values, while mean and maximum evaluations confirmed the large margins provided by the code. A sensitivity study in France was carried out and permitted identification of the most influential material parameters to be made. The most influential parameters on the creep-fatigue assessment were found to be the Sr curves, the symmetrisation factor Ks, the creep law and the cyclic stress/strain curves. There is currently no intent to modify the RCC-MR code in the light of the study, although over-pessimism results from the combination of lower bound properties, where these are physically impossible.

The "Normative method for calculation of long-term cyclic strength" is recommended in Russia to estimate cyclic damage of equipment being operated under significant creep conditions in the range 350-500°C for carbon, carbon manganese and high chromium steels and in the range 450-600°C for corrosion-resistant austenitic steels. The method relies on direct relations between allowable elastic stress amplitude and allowable number of cycles for both categories of material. The key parameters such as non-metallic inclusions, corrosion-aggressive media, welded joints, etc. are taken into account by the use of suitable coefficients. An example of application of the method to assess the joint between the upper tube sheet of the BN600 intermediate heat exchanger and the outer shell showed that the total accumulated damage for this component was well below the allowable value.

The shakedown method was developed in the UK primarily for the assessment of progressive deformation (ratcheting), but provides for creep damage calculation and the determination of an accurate strain range for fatigue. The method had been applied to examples such as a T-butt weld and a cylinder with moving sodium level and compared with finite element (FE) analyses. The method is conservative, but less so than the RCC-MR elastic route. It was concluded that the use of the shakedown principle fulfils the following purposes:

- it excludes ratcheting;
- it limits strain accumulation;
- it provides a basis for creep damage calculation and permits strain range prediction for fatigue analysis in creep conditions;
- it involves only elastic analysis in determining the shakedown state, which obviates the need for time-consuming and costly cyclic inelastic analysis;
- it avoids the problem of defining complicated constitutive laws.

Application in Japan of secondary creep to a ductility exhaustion approach led to the latter being assessed using a time fraction rule. Some results of the work were summarised as follows: (1) the time fraction procedure gives a good creep-fatigue life prediction for both Type 304 and 316FR SS, and (2) the assessment of ductility exhaustion as a time fraction can be derived analytically from the exhaustion of secondary creep. The time fraction procedure is easily applicable for various factors such as weldments, environmental effects and elastic follow-up. No account is taken of the effect of strain rate on the creep ductility, which is accounted for in some ductility exhaustion methodologies.

The R5 creep-fatigue initiation method (UK) covers multiaxial stress states. Fatigue is assessed using Miner's law, with the total endurance split into initiation and growth cycles. Initiation is assessed by entering the curve of initiation cycles vs strain range using a Tresca equivalent strain range. Growth is assessed by entering the curve of growth cycles vs strain range using a Rankine equivalent strain range. The variation of the ductility with strain rate is taken into account in the method. To assess creep-fatigue, the total damage would be the linear sum of the fatigue and creep damage components.

The current creep-fatigue design approach of the RCC-MR (1989) design code is used in India to examine features characteristics of FBR and included the effects of materials data, weldments and neutron irradiation. The ORNL constitutive model and, especially, the Chaboche viscoplastic model were used in the assessment of these components.

The requirements for further R&D studies include:

- the definition of stress-strain hysteresis loops and creep, stress relaxation and cyclic curves for Mod 9Cr1Mo steel,
- the need for data to validate the recommended RCC-MR design rules for welds, such as the effects of weld metal, welding procedure, type of weld and inspection,
- the need for data for method validation, such as materials data scatter, idealisation of finite element analysis (geometry, boundary conditions, loading and materials modelling) and experiments for benchmarks to include multiaxality, weldments and stress concentrations at high temperature.

The ductility exhaustion approach is used in the UK to assess creep damage and a short crack growth concept. The fatigue cycles are assessed using the Rankine strain range, rather than the von Mises equivalent strain range. Use of crack growth to assess fatigue damage, plus a crack arrest concept, permits the extension of the methodology to cover the effects of thermal striping and vibration. The overall procedure also employs a L-shaped creep-fatigue interaction diagram and this is based on an understanding of the interaction of creep and fatigue damage mechanics and the results of creep-fatigue endurance tests covering a range of conditions. The compressive strain hold effect of Mod 9Cr1Mo due to enhanced surface crack initiation is taken into account by assuming that small surface cracks are present at the outset. The lower bound ductility values for Types 316/316L(N) weld metal were obtained from experimental data.

2. Session 2: Design Methods for Mod 9Cr1Mo Steel

Chairman: D. Buckthorpe, UK

The application of the PNC (Japan) design procedure to Mod 9Cr1Mo steel was valid, since, although cavity formation was not seen in short term tests, it was observed in specimens tested for over 1 year of total duration. Creep-fatigue tests with up to 10 hour hold periods showed lower lives with tensile hold periods compared with compressive holds and cyclic tests showed cyclic softening behaviour for the material. For short time holds, there was evidence of a large scatter in relaxation behaviour between tests with and without cyclic softening, whereas for longer hold periods the behaviour was similar for both. Application of the PNC procedure shared the same tendency and correlations were made creep rupture, creep rate and production of creep strain. The long time creep rupture data were now available for Mod 9Cr1Mo, up to 100000 hours duration. The procedure has also been applied to 2¼ Cr1Mo steel, which showed similar tendencies, and an analogy was made between 2¼ Cr1Mo and Mod 9 Cr1Mo, concerning creep-fatigue damage estimation for the

procedure. Comparisons were made between experimental data (short hold times) and the time fraction ductility exhaustion procedure (which included long hold times), showing good agreement over the experimental range. The creep-fatigue behaviour of the material, under compressive hold conditions and up to 10 hour hold periods, showed the formation of sharp cracks due to an oxidation effect. However, the behaviour became saturated as the cracks filled with oxide and the behaviour in tension was more severe. The benefits with compressive hold periods seen in austenitic steels were therefore ignored for Mod 9Cr1Mo steel. The main discussion points raised were on the ductility exhaustion approach which used Reduction of Area rather than elongation, the creep strain behaviour, which seems to show the softened material creeping at a slower rate than unsoftened material and on the behaviour with compressive holds.

The analytical evaluation of the Ks symmetrisation factor (used in RCC-MR) for Mod 9Cr1Mo, using the Chaboche viscoplastic model was done in India. Mod 9Cr1Mo steel exhibits cyclic softening behaviour. For the analytical simulations, additional kinematic hardening and softening parameters were used in the formulation to simulate the material behaviour, together with 20 material parameters. These parameters were based on uniaxial monatonic and cyclic material curves in RCC-MR. Results were presented for the monotonic and cyclic stress-strain curves. The softening behaviour was simulated in the cyclic calculations, with stabilisation after 10 cycles. Results were obtained for a temperature of 500°C and strain rate of 6.7 x 10^{4}/s covering strain ranges between 0.1% and 1.25% and the Ks curve was constructed. The approach was also checked against the case of type 316 L(N) steel for comparison and a favourable comparison with the RCC-MR Ks diagram 316 L(N) for steel was shown. The points raised in discussion were mainly on the availability of experimental data to support the results. It was noted that some work had been carried out in Europe, but, because it was based on 316 L(N) steel behaviour, did not provide a full enough data description in order to define a Ks curve.

3. Session 3: Design Methods for Weldments

Chairmen: K. B. S. Rao, India and C. Picker, UK

Creep-fatigue evaluation on butt welded joints of Type 304 SS was done in Japan (PNC). Results pertaining to the metallurgical discontinuity-induced strain concentration under uniaxial mechanical loading of welded joints were shown. The differences in cyclic deformation properties between base and weld metals leads to strain redistribution in welded joints, and strain was found to increase in the weld metal with strain cycling. This mechanism has been treated as a two element model. The strain concentration factors for vessel-type structures were calculated. The PNC creep-fatigue life evaluation procedure was applied to Type 308 weldments. The strain range was estimated from the strain concentration factor and fatigue damage was estimated from the total strain value. Creep damage was evaluated using the damage diagram determined from the total strain value. The diagram was determined analytically using mechanical properties of basic metal, the cyclic stress-strain curve, the creep-strain-time and the creep-rupture curve.

Data relating to total-axial-strain-controlled low cycle fatigue (LCF) tests were obtained in India for 550 and 650°C on Type 304 SS base material, Type 308 SS weld metal and 304-308 SS weldments prepared by the manual metal arc welding process. The results indicated that the LCF resistance of the base material is superior to that of the weldment at both temperatures. A reduction in fatigue life take place for all the material conditions as the temperature was raised from 550 to 650°C. The phase transformations and morphological changes that were occurring during LCF testing were noted. The delta-ferrite in the welds

and weldments was shown to transform to $M_{23}C_6$ and σ- phase during LCF testing. The transformed portion of delta-ferrite increased with increasing number of cycles to failure and increasing temperature. The loss in life with increasing temperature, in all the three material conditions, was believed to result from an increase in inelastic strain generated in a cycle and from the effects of oxidation-associated crack initiation and propagation. The sigma phase was shown to cause embrittlement locally and to lead to the formation of microcracks at the austenite-sigma interfaces, which shortens the microcrack propagation stage in the all-weld and weldment material. Solution treatment of the weldment prior to LCF testing caused an improvement in fatigue life of 304/308 SS weldments. The LCF behaviour of 308 SS welds containing defects was compared with that of Type 304 SS base metal and 308 SS sound weld metal. The presence of porosity at the specimen surface was particularly harmful and reduced the fatigue life by a factor of seven relative to sound weld metal. A combination of porosity and slag inclusions was found to be more deleterious than the case when either was present alone. Type 316 LN base metal exhibited better fatigue resistance than weld metal at 500°C, whereas the reverse was true at 600°C. The welded joint showed the lowest life at both temperatures. The better fatigue resistance of weld metal was related to the brittle transformed delta ferrite and the high density of dislocations at the interface. This inhibited the growth rate of cracks by deflecting the crack path. The lower fatigue endurance of welded joints was ascribed to the shortening of the crack initiation phase by surface intergranular crack initiation and to the poor crack propagation resistance of the coarse-grained region in the heat affected zone. The results comparing the creep-fatigue interaction behaviour of Type 304 SS base metal and 308 SS weld metal were briefly touched upon. The 308 SS welds were found to exhibit lower values of life under creep-fatigue interaction conditions.

4. Session 4: Application of Methods

Chairmen: B. Riou, France, and S. K. Bate, UK

An experiment involving thermal shock testing of a tubeplate feature in a saltbath had been used as a benchmark test to compare the UK strain-based creep-fatigue assessment method and the RCC-MR method. Finite element analyses of the test had been made in Europe using six different combinations of Finite element code and constitutive equations. The results of these analyses showed a wide range of results. Although this was, to some extent, due to differences in input data there also appeared to be significant discrepancies between the methods.

The use of the Chaboche elastic-viscoplastic model to predict the thermal ratchet behaviour of a 304 SS cylinder under an axial moving temperature distribution and ratcheting in a pressurised pipe has been validated through comparison with experimental results. The analytical results of thermal ratcheting were shown to be in good agreement with experimental results over the first five cycles. It was, however, noted that the Chaboche model is likely to over estimate the accumulated deformation. In addition, the variation of material properties with temperature and the creep-relaxation effect, not presently considered, is to be evaluated in future analyses.

The French recent developments in support to rules for creep and creep-fatigue analyses dealt with the test programme "SOUFFLE" which is aimed at providing a better understanding of the phenomena involved in welded joints under fatigue and creep-fatigue loadings. The results with fatigue loading showed that the fatigue strength reduction factor (J_f) to be considered should take into account not only the material effect but also geometrical and elastic follow-up effects. Work of interpretation is underway in order to determine the real strain in the weld. Simplified methods (Roche's method and Zarka's method) are being

compared with elastic-plastic calculations and Roche's method has been shown to lead to a conservative estimate of the strain ranges.

5. CONCLUSIONS

1. The most important conclusion of the workshop was that there was a wide range of results when the same experiments were analysed by different methods. Three input fields to such analyses are the stress analysis route (elastic, simplified elastic or inelastic), materials data (lower bound, representative or actual) and failure criterion (e.g. RCC-MR/N47 or other). The meeting proposed that a carefully controlled study should be made to examine the discrepancies between the methods.

2. Descriptions were provided of new developments in the Russian Federation, Japan and the UK. Existing code rules are used in India, the Republic of Korea and Europe, with the shakedown and strain-based procedures also being used in Europe, the latter for trial use only. A study of the sensitivity of the RCC-MR method to the input parameters had provided a useful insight into how assessments could be optimised.

3. There had been interest in the UK and Japan in developing ductility exhaustion to assess creep damage. In Japan this was expressed in terms of a time fraction but in the UK R5 and Fast Reactor procedures, the cumulative strain was compared with the ductility, taking account of the effect of strain rate on ductility.

4. The differences in deformation behaviour between weld metal and base metal in weldments, the evolution of this difference with cycling and discrepancies in endurance between these constituents makes the behaviour of weldments, particularly those in austenitic stainless steels, very complicated. Some success in predicting the behaviour of such weldment has been achieved, but some of these developments have yet to be formalised into practical methodologies.

5. The formation of sigma phase from delta-ferrite in austenitic weld metals at high temperature has been shown to reduce the ductility of welds by encouraging cracking at the sigma-to-austenite interface. The reduction of the delta-ferrite content, while retaining a necessary minimum level to avoid cracking during welding, and the use of lower alloy contents in the weld metal, might offer some scope for improving the rupture ductility.

6. While validation of methods is being pursued, more work is needed, particularly for weldments and for Mod 9Cr1Mo steel.

7. The design codes such as ASME N47 and RCC-MR were developed initially for austenitic stainless steels, and most work has been carried out on this class of material. Work is in progress to provide adequate methodologies to assess creep-fatigue damage in Mod 9Cr1Mo steel which cyclically softens. More experimental work is required, most notably to evaluate the symmetrisation factor Ks. Mod 9Cr1Mo steel is less prone to creep cavitation than austenitic stainless materials, but shows a greater sensitivity to surface crack initiation. This has to be taken into account in developing creep-fatigue assessment methods.

MATERIAL VARIABILITY IN ELASTIC ASSESSMENT

B. RIOU, M. SPERANDIO
NOVATOME, FRAMATOME,
Lyon, France

J. GUINOVART
European Commission,
Bruxelles, Belgium

Abstract

The structures of Fast Reactors (FRs) are subjected to high temperatures and their design is checked mainly against elastic rules. The aim of this paper is to study the influence of uncertainties in material properties on creep-fatigue assessment according to the elastic route of the RCC-MR code, so as to evaluate the subsequent margins. This work has been conducted by FRAMATOME, in cooperation with GEC, NNC and SIEMENS, in the frame of the activities of the Working Group on Codes and standards of DG XI/C (Nuclear Safety of Installations). The material considered is the 316L(N) austenitic stainless steel (RCC-MR 1S type material). The work is divided into two phases: the first one consists of the identification of the scatterband of material properties used in the elastic creep-fatigue assessment route of the RCC-MR code and the second of the study of the influence of the scatter on the results of elastic calculations and creep-fatigue assessment, with the aim to evaluate the difference in lifetime as a function of the set of material properties used and the relative importance of each material property. The lattest will be based on one example of application typical of FRs structures. The example chosen consists of a plate to shell junction subjected to a thermal transient. Calculations are carried out using design material properties, mean material properties and properties leading to minimum and maximum life duration. Results of creep-fatigue analyses with material properties leading to minimum life duration are shown to be similar to those with design material properties, giving results of the same order of magnitude. Results with mean material properties and properties leading to maximum life duration exhibit significant margins compared to design analyses. Sensitivity analyses carried out on the basis of the maximum and minimum material property values show that properties which are the most significant for creep-fatigue assessment are the S_r curves, the K_s factor, the creep law as well as the cyclic curves. The influence of the fatigue curves was not significant in the benchmark considered.

1. INTRODUCTION

The aim of this work is to study the influence of uncertainties in material properties on elastic calculations and creep-fatigue assessment according to the RCC-MR code [1], so as to evaluate the subsequent margins. The material considered is the 316L(N) material (RCC-MR 1S type material).

The work is divided into two parts:

- Identification of the scatterband of material properties used in the analysis,
- Study of the influence of the scatter on the results of elastic calculations and creep-fatigue assessment, with the aim to evaluate the margins and the relative importance of each material property. This part is based on one example typical of FRs structures.

The companies participating to this work were: FRAMATOME, GEC, NNC and SIEMENS [2].

2. IDENTIFICATION OF THE SCATTERBAND OF MATERIAL PROPERTIES

The material properties used in the elastic creep-fatigue analyses according to the RCC-MR code are the following:

- YOUNG's modulus E,
- Poisson's ratio ν,
- mean coefficient of thermal expansion α_m,
- Yield strength $R_{0.002}$,
- cyclic curves (and the strain enhancement coefficients K_ε and K_σ defined with them),
- fatigue curves,
- symmetrisation factor K_s,
- creep stress to rupture S_r,
- creep laws.

The following sections identify the scatterband of each material property and provide the background to this identification.

2.1. YOUNG's modulus E

The data bank of Young's Modulus of the 316L(N) austenitic stainless steel comprises static measurements using large gauge length tensile specimens taken from 3 plates corresponding to 3 casts of 316L(N) steel at temperatures from 20 °C to 750 °C: a total number of 61 results are included in the data bank.

There is not enough data (7 or 6 per temperature) to calculate significant standard deviations at the different temperatures. In addition, the width of the scatterband is similar at 400 °C, 500 °C, 600 °C and 700 °C (12 or 13.10^3 MPa) and is accidently smaller at 20 °C. As a consequence, no attempt was made to define a temperature dependent standard deviation.

The analysis of the results of Young's Modulus versus temperature was performed using linear regression and a 90 % confidence scatterband was established statistically. The corresponding upper bound and lower bound values are given in table I in addition to the RCC-MR values.

The present RCC-MR values of the Young's Modulus are in this scatterband but rather in the upper half part. This is due to the difference in the data base. The RCC-MR mean curve was derived from data or casts of grades 316L (PHENIX) and ICL 167 CN fabricated prior to the specification of 316L(N) steel. Today, these data are excluded from the 316L(N) data base. Nevertheless, the analysis indicates that the difference in the Young's Modulus between 316L(N) steel (present data base) and 316L steel (ICL 167 CN data) is not statistically significant.

TABLE I. YOUNG'S MODULUS E (10^3 MPa)

θ (°C)	20	100	200	300	400	500	600
RCC-MR	192	186	178	170	161	153	145
Upper bound	197.5	191.1	183.1	175.2	167.3	159.4	151.5
Lower bound	179.4	173.1	165.3	157.5	149.6	141.7	133.8

2.2. POISSON's ratio ν

There are some doubts about the physical reality of the measured variability of Poisson's ratio for the following reasons:

- The Poisson's ratio is obtained by comparison of the measurement of two elastic strains or of two velocities of sonic waves and this is not very accurate,
- As the value of Poisson's ratio for plasticity is 0.5, if microplasticity is not fully avoided during the measurement, a value higher than the elastic one will be obtained.

The Poisson's ratio will be therefore considered equal to 0.3 without any material variability.

2.3. Mean coefficient of thermal expansion α_m

Available data for the mean coefficient of thermal expansion α_m between 20 °C and θ °C are given:

- by the RCC-MR for 316L(N) steel,
- by the RCC-M for 316L and 316 steels,
- by the code case N47 of ASME for 316 steel.

A realistic estimation of the scatterband of the values of α_m can not be obtained from these data for the following reasons:

- RCC-MR curve was established from the data measured for a particular cast,
- RCC-M values are mean values of some published data excluding handbook data,
- ASME CC N47 values are also mean values derived from another group of published data.

The scatter of published data has been examined formerly by FRAMATOME in the case of 304 steel. The width of the scatterband of the data was 1.5 10^{-6} /K at 400 °C as well as at 200 °C and did not appear to be temperature dependent.

As only one cast of 316L(N) steel was tested, there is no proof that the scatter of the values for α_m is reduced in comparison to that observed with 316 or 304 steel.

Therefore, it was proposed to use for the upper bound and lower bound values of the mean coefficient of thermal expansion those which are derived from the mean coefficient of thermal expansion α_m given by the RCC-MR code and a width of $\pm$ 0.75 10^{-6}/K at all temperatures from 20°C to 600°C: the corresponding values are given in table II.

TABLE II. MEAN COEFFICIENT OF THERMAL EXPANSION α_m (10^{-6}/K)

θ (°C)	20	100	200	300	400	500	600
RCC-MR	15.90	16.4	17.00	17.5	17.9	18.3	18.7
Upper bound	16.65	17.15	17.75	18.25	18.65	19.05	19.45
Lower bound	15.15	15.65	16.25	16.75	17.15	17.55	17.95

2.4. Yield strength $R_{0.002}$

The yield strength $R_{0.002}$ is only used for the calculation of the symmetrisation factor K_s. The scatterband defined for K_s will be established considering the mean value of the yield strength and as a consequence no scatterband is provided in the present study for $R_{0.002}$.

2.5. Cyclic curves

The definition of a scatterband is based on the results of a CEC study for which results of 260 low cycle fatigue tests on 316L(N) from EDF, CEA, UNIREC, ECOLE DES MINES, AEA and IA have been collected and evaluated to describe the cycling hardening behaviour. Data comprise test results on five different casts. Test temperatures were the following (number of tests given in brackets): 20 °C (16), 450 °C (10), 550 °C (69), 600 °C (134), 650 °C (22) and 700 °C (9), i.e. 80 % of the tests are at the two temperatures of 550 and 600 °C.

In the CEC study only scatterbands for each cast at a certain test temperature had been determined, but no overall scatterband for 316L(N). For cyclic data at 550 and 600 °C, it can be shown that most of the data fall within a scatterband of $\pm$ 10 %. This is also true for small strain amplitudes. It is therefore suggested that upper bound / lower bound cyclic curves are determined by dividing / multiplying the mean stress values from RCC-MR curve by a factor of 1.1. Since there are no indications for a temperature dependency of the scatterband, this factor applies for all temperatures.

The corresponding equations (elastoplastic equivalent strain range $\overline{\Delta\varepsilon_t}$ as a function of the equivalent stress range $\overline{\Delta\sigma}$) are given below:

a/ *Mean cyclic curves*

$$\overline{\Delta\varepsilon_t}\,[\%] = 100 \cdot \frac{2\,(1+\nu)}{3E} \cdot \overline{\Delta\sigma} + \left(\frac{\overline{\Delta\sigma}}{K}\right)^{1/m}$$

with K = 718 and m = 0.319.

b/ *Upper bound cyclic curves*

$$\overline{\Delta\varepsilon_t}\,[\%] = 100\,\frac{2\,(1+\nu)}{3E} \cdot \frac{\overline{\Delta\sigma}}{1.1} + \left(\frac{\overline{\Delta\sigma}}{K \cdot 1.1}\right)^{1/m}$$

c/ *Lower bound cyclic curves*

$$\overline{\Delta\varepsilon_t}\,[\%] = 100\,\frac{2\,(1+\nu)}{3E} \cdot \overline{\Delta\sigma} \cdot 1.1 + \left(\frac{1.1 \cdot \overline{\Delta\sigma}}{K}\right)^{1/m}$$

2.6. Fatigue curves

The RCC-MR fatigue design curves for 316L(N) austenitic steel were obtained from average strain controlled fatigue curves recommended by the EFR R&D community and derived from a statistical analysis of an extensive number of continuous cycling fatigue results using the multiple regression method [3]. The high cycle part was completed by extrapolation and smoothing giving continuous curves between 10^2 and 10^8.

In deriving the fatigue design curves the following approach was used :

- Introduce factors of 2 on total strain range ($\overline{\Delta\varepsilon}$) and 20 on number of cycles (N),
- Lowering the high cycle part of the curve by introducing a factor equal to 1.3/1.5 at 10^9 cycles and 1 at 10 cycles to be consistent with the RCC-MR definition of equivalent strain (RB 3227.9) from the Von Mises equivalent strain range (the factor 1.3/1.5 accounts for the increase of the Poisson's ratio from 0.3 in the elastic regime to 0.5 in the low cycle fatigue regime).

These curves are not to be used for stress controlled situations with cycle numbers in excess of 10^6.

ASME have published design curves in code case N47 [4] at temperatures between 100°F and 1300°F. A single curve is given to represent the behaviour between 538 °C and 650 °C. At RT the agreement between the ASME and RCC-MR curves is good, however at 550 °C the present RCC-MR curves predict higher endurances.

The statistical method of [3] does not yield confidence limits to the data. However, visual inspection of the data about the best fit curves suggested that the scatter is approximately ± 25 % on strain range.

For definition of upper and lower bounds to the average data the ± 25 % scatterband has been used. To obtain smoothed curves the ± 25 % scatterband has also been used to complete the high cycle fatigue part.

For corresponding average, upper and lower bound fatigue curves for the sensitivity calculations some further adjustment is required at the high cycle part to be consistent with the RCC-MR definition of equivalent strain by introducing a factor 1.3/1.5 at 10^9 cycles. The resulting fatigue curves are shown in figure 1 at 550°C.

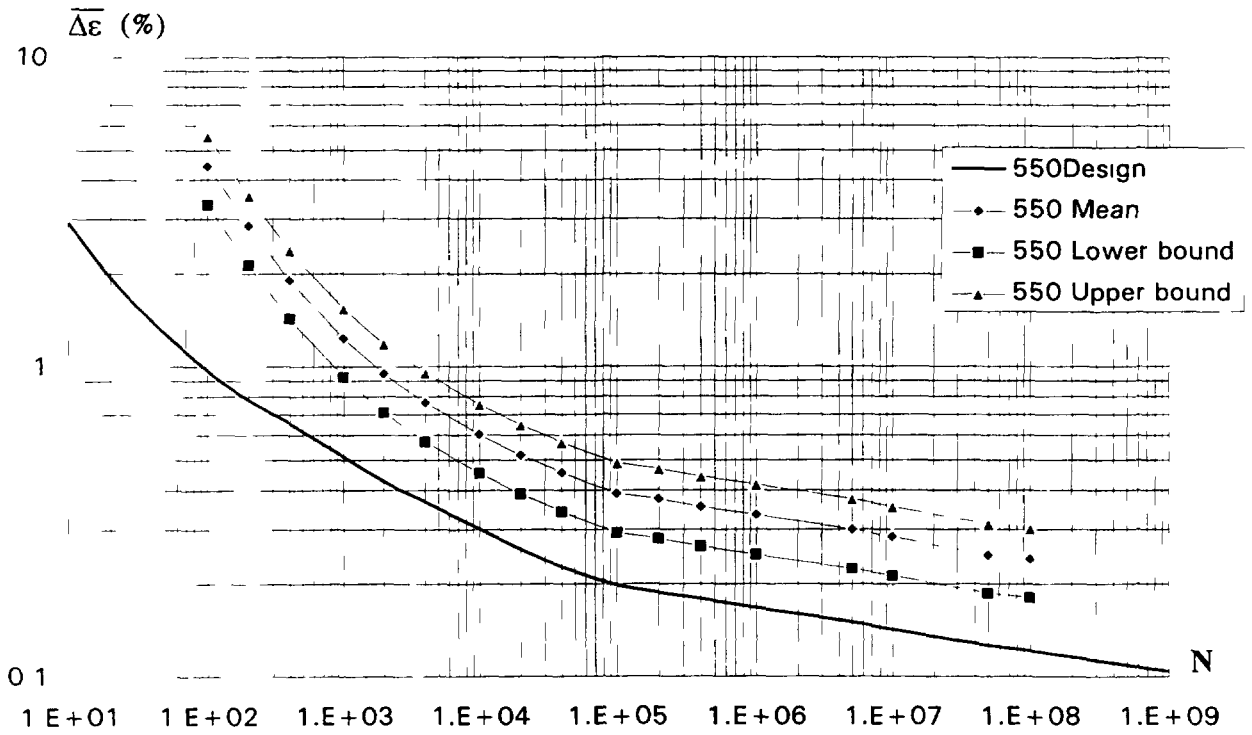

FIG. 1. Fatigue curves at 550°C

2.7. Symmetrisation factor K_s

The symmetrisation factor K_s is used in the RCC-MR code for the estimation of the equivalent stress (denoted σ_k) during hold time for creep-fatigue damage assessment. The K_s coefficient accounts for the possible symmetrisation along the stress axis of the stress-strain loops under large loadings. It is given as a function of the ratio:

$$R = \frac{\Delta\sigma^*}{2\,(R_{0.002}\,(\theta^*))_{min}}$$

where:

- $(R_{0.002}\,(\theta^*))_{min}$ is the minimum yield stress at temperature θ^* (maximum temperature during hold time),
- $\Delta\sigma^*$ is the stress range corresponding to the elastoplastic strain range $(\overline{\Delta\varepsilon_{el+pl}})$ on the cyclic curve.

K_s factor for the 316L(N) SS has been established on the basis of the following type of tests (performed at 550 °C and 600 °C):

- cycling with a given strain range $\Delta\varepsilon_t$ after monotonic prestraining at $\varepsilon^{initial}$ (tests A),
- cycling with a given strain range $\Delta\varepsilon_t$ after cyclic prestraining at $\Delta\varepsilon_t^{initial}$ (tests B),
- cycling between 0 and $\Delta\varepsilon_t$ (tests C).

The K_s curve recommended in the RCC-MR code is an upper bound of the experimental values obtained from tests A and C. Data from tests B were not taken into account because:

- cyclic prestrainings ($\Delta\varepsilon_t^{initial}$ = 1.96 % or 1.2 %) were considered as unrealistic when compared to service cycles,
- observed $\Delta\sigma_{exp}$ values deviated from $\Delta\sigma$ values calculated with the mean cyclic curve.

Experimental values of K_s obtained with test B would be above the present K_s curve.

The RCC-MR curve is in fact the upper bound of tests A and points from tests C correspond principally to K_s = 0.5. Type A tests are known to have more severe loading conditions than type C tests whereas type C tests are likely to be more representative of actual loading conditions that may occur on a FR component.

Due to the low number of data points, it is not possible to propose upper bound, average and lower bound curves defined statistically.

However, in order to be able to study the sensitivity of elastic analyses to the K_s curve, it is proposed to define a lower bound curve based on tests C. The corresponding curve is defined by the following formula :

$$K_s = \frac{1}{12}\left(\frac{5.5}{R} + 1\right)$$

The resulting curve is shown in figure 2. This curve should also be used as a mean curve when studying the influence of the scatter of material properties.

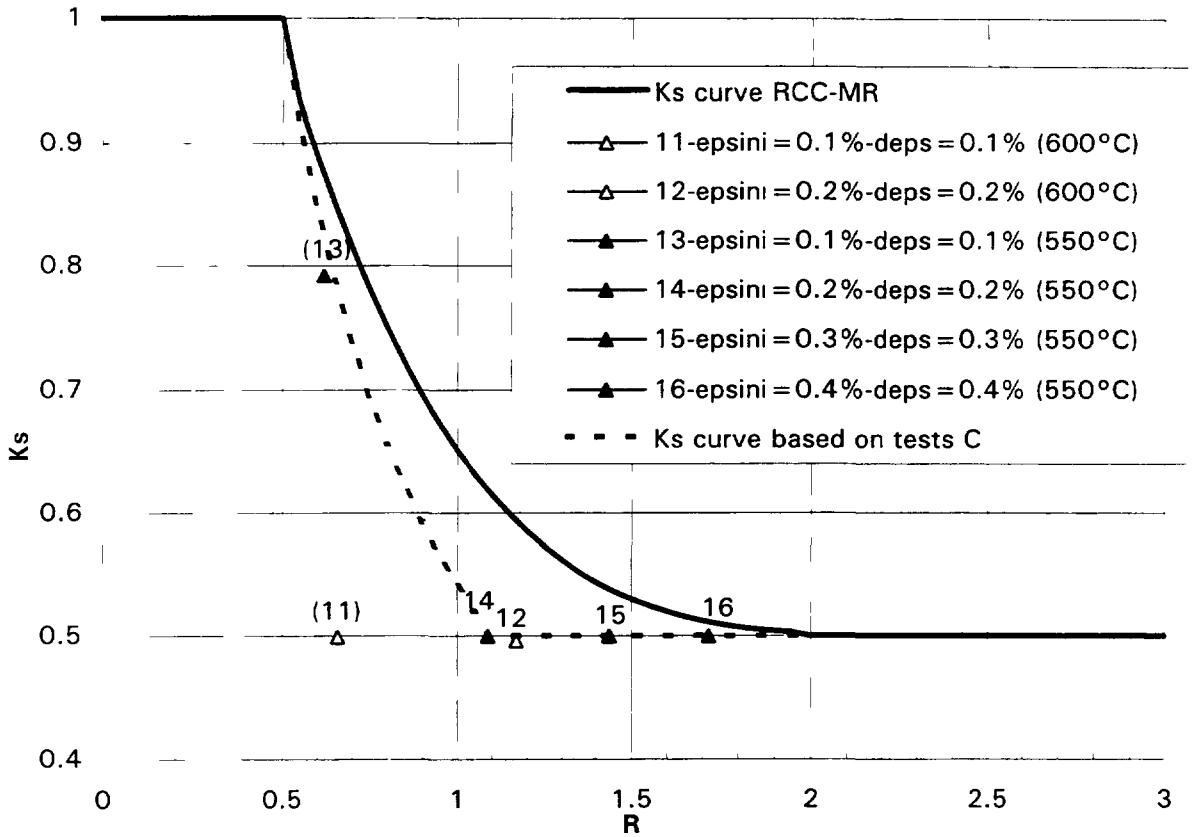

FIG. 2. K_s Symmetrisation curves

2.8. Stress to rupture S_r

The collected data are at 550 °C and comprise 137 data points corresponding to different casts. The data have been collected from a 1986 edition of the French GTM data base, from recent WGCS AG2/AG3 reports and from internal UK sources.

The study of the data shows a preponderance of high-stress data points above the RCC-MR average curve and a preponderance of low-stress data points below this curve. This would indicate a steeper mean curve than given by RCC-MR. On the other hand, closer examination of the data suggests that the stronger casts tend to have been tested at the higher stresses and that the trends of variation for each individual cast (or, at least, for those having a fairly broad range of stress-levels) are roughly parallel with the RCC-MR curves. The indication, therefore, is that (a) the RCC-MR gives a reasonable picture of the determinate dependance of stress for each cast, (b) the overall scatter is largely due to cast-to-cast variability and (c) there is also some degree of random scatter within each cast.

The analysis of the data shows a mean curve which differs by only about 5 % from the RCC-MR mean curve. Even if a more precise estimate can be proposed, it is recommended that the average and minimum properties of RCC-MR should be retained unchanged, namely minimum property equal to $S_r^{avc}(t_r)/1.25$. With regard to the maximum property, equal widths of upper and lower scatterbands (on a logarithmic stress-plot) would indicate a choice of $1.25\ S_r^{avc}(t_r)$. This is rather high compared with the precise evaluation for the maximum property but not excessively so and is recommended for simplicity.

As noted at the beginning of the paragraph, the collected data are at 550 °C. It is however reasonable to extend the proposed scatterband to temperatures around 550 °C relevant for the benchmark case to be studied in the second part of the work.

2.9. Creep laws

The available data-base is at 550 °C. The casts concerned are a subset of those studied in 2.8.

The RCC-MR creep law is expressed in terms of the following quantities:

- ε_f primary creep strain
- t_{fp} time to the end of primary creep
- ε_{ffp} creep strain at the end of primary creep
- $\dot{\varepsilon}_f$ secondary/minimum creep-rate

Due to the complexity of the formulation of the primary creep strain (which is dependent on the hold time, stress and temperature), it is decided to study the scatter on the last three quantities and to deduce from them the upper and lower bound formulations for the primary creep strain.

The selection of tests in the data base was therefore simply in terms of those for which at least one of the last three quantities could be identified. In all, the number of available data points amounted to:

- for t_{fp} : 25
- for ε_{ffp} : 18
- for $\dot{\varepsilon}_f$: 35

The available data have been studied imposing the RCC-MR prediction as the mean value and this led to the following upper and lower estimates:

a/ *time to the end of primary creep*

$$t_{fp}^{max} / t_{fp}^{RCC\text{-}MR} = 10.422$$

$$t_{fp}^{min} / t_{fp}^{RCC\text{-}MR} = 0.0960$$

b/ *creep strain at the end of primary creep*

$$\varepsilon_{ffp}^{max} / \varepsilon_{ffp}^{RCC\text{-}MR} = 7.0754$$

$$\varepsilon_{ffp}^{min} / \varepsilon_{ffp}^{RCC\text{-}MR} = 0.1413$$

c/ *secondary/minimum creep-rate*

$$\dot{\varepsilon}_f^{max} / \dot{\varepsilon}_f^{RCC\text{-}MR} = 6.583$$

$$\dot{\varepsilon}_f^{min} / \dot{\varepsilon}_f^{RCC\text{-}MR} = 0.1519$$

The upper and lower estimates (with the RCC-MR predictions as imposed means), and the RCC-MR formulae, are compared with the available data and, with the exception of a single point, the data are contained by the estimates. Note however that only in the case of the secondary/minimum creep rate, are the data points evenly clustered around the RCC-MR line. In the other cases the data values tend to be some 50 % greater than predicted by RCC-MR.

At the relatively high stress levels of most of the data it is permissible to accept that the trends of change with respect to stress are reasonably predicted by the RCC-MR lines. It is however shown that the RCC-MR law, though fairly satisfactory as a numerical representation of most of the available 550 °C data, is probably misleading in terms of extrapolation to stress-levels of 100 MPa or below.

Even so, it may be observed that, though the low-stress predictions are on the unconservative side for the secondary/minimum creep they are conservative for the maximum primary creep strain and the two effects would tend to balance out. On the other hand, the time-scale of primary creep appears to be excessively predicted at low stresses so that the compensating effect of excessively predicted maximum primary creep need not come into play at relevant time scales.

As far as the scatterband on the primary creep strain is concerned, it should be lower than that of the creep strain at the end of primary creep and the latter should be used conservatively for the primary creep strain.

The collected data are at 550 °C. It is however reasonable to extend the proposed scatterband to temperatures around 550 °C relevant for the benchmark case to be studied in the second part of the work.

The scatterbands recommended in this paragraph are rather broad. This is partly due to inherent cast-to cast variability but is considered also to be influenced by the basic stress-dependencies of the creep law having only moderate accuracy.

It is strongly recommended that such stress-dependencies should be re-examined in terms of data available since the original issue of the creep law. It is considered that a revised law would make it much easier to deal confidently with low-stressed creeping regions and, moreover, would allow narrower scatter bands to be adopted at higher stresses.

3. DATA TO BE USED FOR STUDYING THE INFLUENCE OF THE SCATTER

Four classes of data are defined:

- design data,
- mean data,
- data for minimum behaviour (leading to minimum life time),
- data for maximum behaviour (leading to maximum life time).

It is to be noted that, for the last two categories, the choice has been made to define these sets of data without taking into account any relation between the material properties but considering them independently with the objective to maximise or minimise the life time.

The following sections explain how these sets of data have been derived.

3.1. Design data

Design data are those recommended in appendix A3.1S of the RCC-MR Code [1].

3.2. Mean data

Mean data are those recommended in the RCC-MR Code except:

- the fatigue curves which are those described in 2.6,
- K_s factor whose values are recommended 2.7.

3.3. Data for minimum behaviour (minimum life time)

The data for minimum behaviour consist of the following:

- upper bound Young's modulus,
- Poisson's ratio equal to 0.3,
- upper bound mean coefficient of thermal expansion,
- mean 0.2% yield strength,
- upper bound cyclic curves
- K_ε coefficient based on the lower bound values of the cyclic curves (it is assumed here conservatively that the part of the cyclic curve to be used for the NEUBER correction is close to the lower bound cyclic curve whereas the part of the cyclic curve to be used for the calculation of $\overline{\Delta\sigma^*}$ is close to the upper bound cyclic curve),
- K_σ coefficient based as K_ε on the lower bound values of the cyclic curves,
- lower bound fatigue curves,
- K_s factor as recommended in the RCC-MR code,
- creep stress to rupture S_r as recommended in the RCC-MR code,
- creep strain law derived from that given in RCC-MR after having taken into account scatterbands defined in 2.9. By considering that the benchmark studied in the second part of the work should remain in the primary creep regime, the modifications compared to RCC-MR law consists in multiplying C_1 by the ratio between the lower estimate of the creep strain at the end of primary creep and the RCC-MR corresponding value $\left(\frac{e_{fip}^{min}}{e_{fip}^{RCC-MR}} = 0.1413 \right)$.

  It is to be noted that the corresponding coefficients will minimise stress relaxation and will therefore maximise the creep damage. The same coefficients should also be used for calculating the creep strain increment and thereafter the fatigue damage when performing the creep-fatigue analyses leading to maximum lifetime.

It is to be noted that the Young's modulus which is used in the formula defining the cyclic curves and in those used for the relaxation law is chosen as the mean Young's modulus in order to avoid to cumulate at the same time the scatter on the cyclic curves and that on the Young's modulus.

3.4. Data for maximum behaviour (maximum life time)

The data for maximum behaviour consist of the following:

- lower bound Young's modulus,
- Poisson's ratio equal to 0.3,
- lower bound mean coefficient of thermal expansion,
- mean 0.2% yield strength,
- lower bound cyclic curves
- K_ε coefficient based on the upper bound values of the cyclic curves,
- K_σ coefficient based as K_ε on the upper bound values of the cyclic curves,
- upper bound fatigue curves,
- lower bound symmetrisation factor K_s,
- creep stress to rupture as recommended in the RCC-MR code but multiplied by a factor 1.25^2 as recommended in 2.8,
- creep strain law as described in 3.3. but multiplying C_1 from RCC-MR by

$$\frac{\varepsilon_{tfp}^{max}}{\varepsilon_{tfp}^{RCC-MR}} = 7.0754 \ .$$

4. DESCRIPTION OF THE EXAMPLE OF APPLICATION

The following sections provide a complete description of the example, as well as the results of the corresponding design analysis.

4.1. Description of the example

The example of application chosen for studying the influence of the scatter of material properties is representative of geometry and loads met in FRs structures. It consists of a plate-to-shell junction of a type equivalent to that used in the above core structure of FRs. The geometry is shown in figure 3. The structure is only subjected to a thermal load.

The material considered is the 316 L(N) stainless steel corresponding to 1S type material as defined in the RCC-MR code.

4.2.Thermal boundary conditions and thermal load

The structure is divided into three zones (see figure 3):

- zone 1 : AB,
- zone 2 : CD,
- zone 3 : EF.

The heat transfer coefficient applied on these three zones is h = 5 000 W/m^2 °C typical of Na-stainless steel exchanges. Adiabatic conditions are applied on BC and FA extremities.

The load cycle considered consists of a thermal transient, a start-up and an hold period at θ = 560 °C. The thermal transient consists of a hot shock and a cold shock. The Na temperatures applied on zones 1 to 3 are provided in table III. It is to be noted that this thermal transient is a fictitious one and that it should lead to stresses higher than those obtained in a real structure. It is assumed that the start-up does not contribute to the stress range.

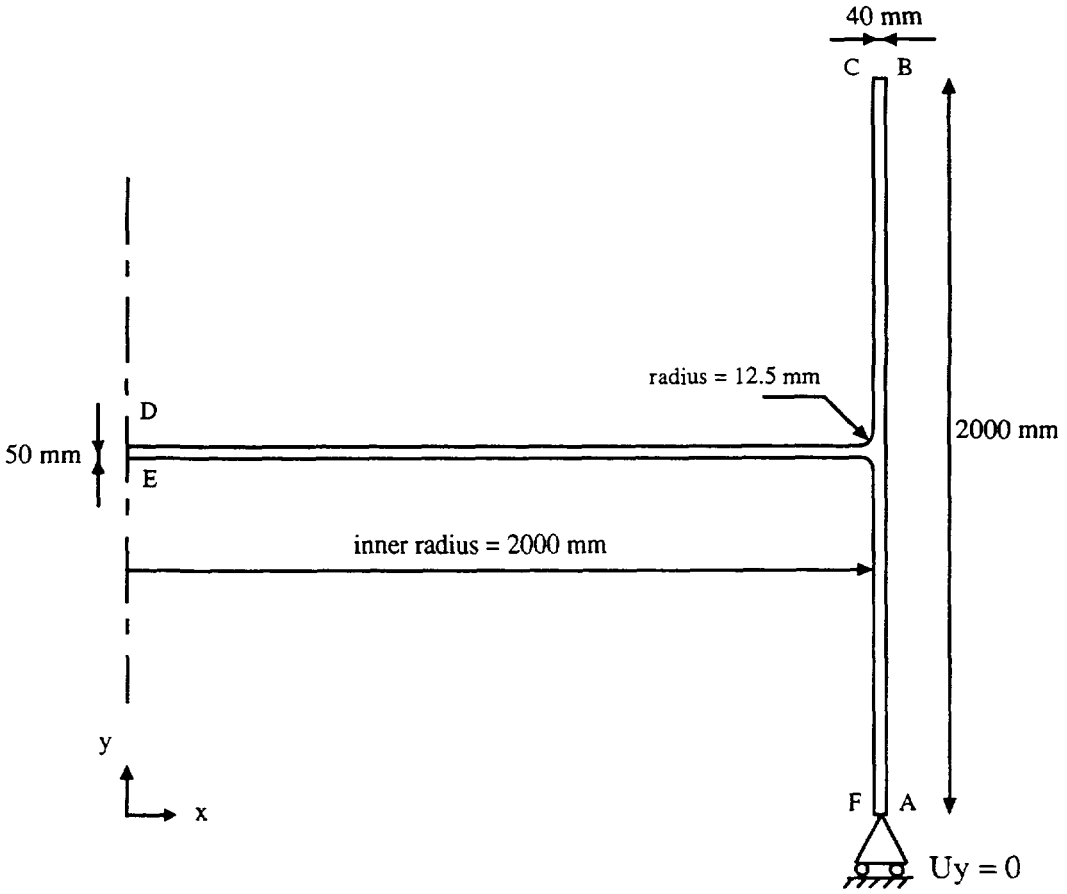

FIG. 3. Geometry of the plate-to-shell junction

TABLE III. DESCRIPTION OF THE THERMAL LOAD (θ_{Na} in °C)

time (s)	Zone 1	Zone 2	Zone 3
0	560	560	560
50	580	580	580
100	550	510	530
200	500	460	480
350	450	430	440
600	400	400	400

4.3. Mechanical boundary conditions

The boundary conditions applied for the mechanical calculations consist of a restraint vertical displacement ($U_y = 0$) at the lowest extremity of the structure.

4.4. Data for creep-fatigue analysis

The data to be used for the creep-fatigue assessment are the following:

- Number of occurrences N_{occ} = 500 cycles.
- Temperature at operating conditions θ^* = 560 °C.
- Hold time per cycle T_m = 350 hours.

4.5. Thermal and thermomechanical calculations

Thermal and thermomechanical calculations have been carried out with SYSTUS computer code [5].

Physical properties taken into account for the thermal calculations are the following :

- thermal conductivity $\lambda = 20.10^{-3}$ W/mmK
- specific heat $C_p = 560$ J/KgK
- density $\rho = 7.8\ 10^{-6}$ kg/mm^3.

The elastic calculations are carried out on the basis of the temperature fields of the thermal calculations and using the RCC-MR material properties [1]. The maximum stress range is obtained in the upper groove ring (see figure 4) between instants t = 50 s and t = 200 s. The value of stress range obtained is $\overline{\Delta\sigma} = 245.4$ MPa.

4.6. Results of the creep-fatigue assessment

The creep-fatigue assessment is performed according to RCC-MR RB 3260. The results are the following:

creep usage fraction W = 3.31,
fatigue usage fraction V = 0.01,

which leads to the allowable number of cycles N_r = 150 cycles.

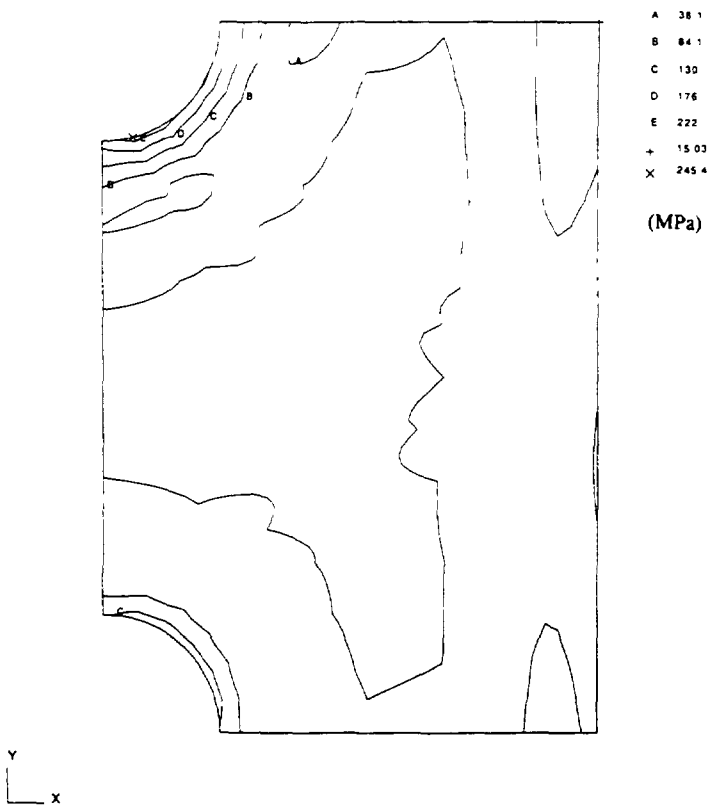

FIG. 4. Von Mises equivalent stress range

5. STUDY OF THE INFLUENCE OF THE SCATTER OF MATERIAL PROPERTIES

This step consists in comparing the results of:

- elastic calculations,
- creep-fatigue assessments,

using material properties corresponding to:

- design values,
- mean values,
- minimum behaviour values ("minimum" material properties),
- maximum behaviour values ("maximum" material properties).

For the example considered, the results obtained with design material properties are not significantly different from those with "minimum" values (see table IV). Taking into account the accuracy when determining the scatter on material properties, it can only be stated that both results are of the same order of magnitude.

Analyses carried out with mean and "maximum" material properties exhibit significant margins compared to the design case. The decrease of the creep usage factor is greater than 97 % with mean material properties compared to the design analysis and is greater than 99 % with "maximum" material properties.

TABLE IV. INFLUENCE OF THE SCATTER OF MATERIAL PROPERTIES

	Design material properties	**Mean material properties**	**% (*)**	**"Minimum" material properties**	**% (*)**	**"Maximum" material properties**	**% (*)**
$\overline{\Delta\sigma}$ (MPa)	245.4	245.4	0	265.3	8.1	219.4	-10.6
$\overline{\Delta\varepsilon}_{el+pl}$ (%)	0.168	0.168	0	0.193	14.7	0.145	-13.6
σ_k (MPa)	149.0	117.1	-21.4	157.4	5.6	113.0	-24.2
$\overline{\Delta\varepsilon}$ (%)	0.207	0.185	-10.6	0.312	50.9	0.148	-28.6
W	3.31	0.09	-97.4	3.95	19.4	0.005	-99.8
V	0.01	0	-100	0.01	4.7	0	- 100
$N_r = f(W,V)$ (cycles)(**)	150	5 800	3 767	126	-16	102 017	67 911

(*) Values of percentage in the table correspond to $\frac{X - X_{design}}{X_{design}} \times 100$ where $X = \overline{\Delta\sigma}, \overline{\Delta\varepsilon}_{el+pl}, \ldots$

(**) For $V < W$, $N_r = \frac{N_{occ}}{W(N_{occ}) + 7/3\ V(N_{occ})}$

6. SENSITIVITY ANALYSES

The aim of these analyses is to evaluate the relative importance of each factor. For this purpose, each material property (E, α, ...) is set the one after the other to its "minimum" and "maximum" values whereas other properties are set to the mean values and results are compared with the analysis with mean material properties.

The conclusions of the sensitivity analyses, for what concerns the plate-to-shell junction example, are the following:

- Influence on the stress at the beginning of the hold period σ_k

  Material properties which have the most significant effect on σ_k are the cyclic curves (+ 10 %/- 1.9 % compared to results with mean values) and the K_s factor (+ 22.7 %/0 %). It is to be noted that "maximum" material properties have less effect than "minimum" values. This is due to the K_s factor which is saturated at 0.5 in the latter case.

- Influence on the total equivalent strain range $\overline{\Delta\varepsilon}$

  Material properties which have the most significant effect on $\overline{\Delta\varepsilon}$ are the K_s factor (+ 9.5 %/0 %) and the creep law (+ 23.4 %/- 7.5 %).

- Influence on the creep usage fraction W

  The most significant material properties for the creep usage fraction W are the cyclic curves (+ 75.4 %/- 11.1 %), the K_s factor (+ 222.7 %/0 %), the creep law (32.6 % / -68.5 %) and the S_r curves (378.7 % /-79.2 %).

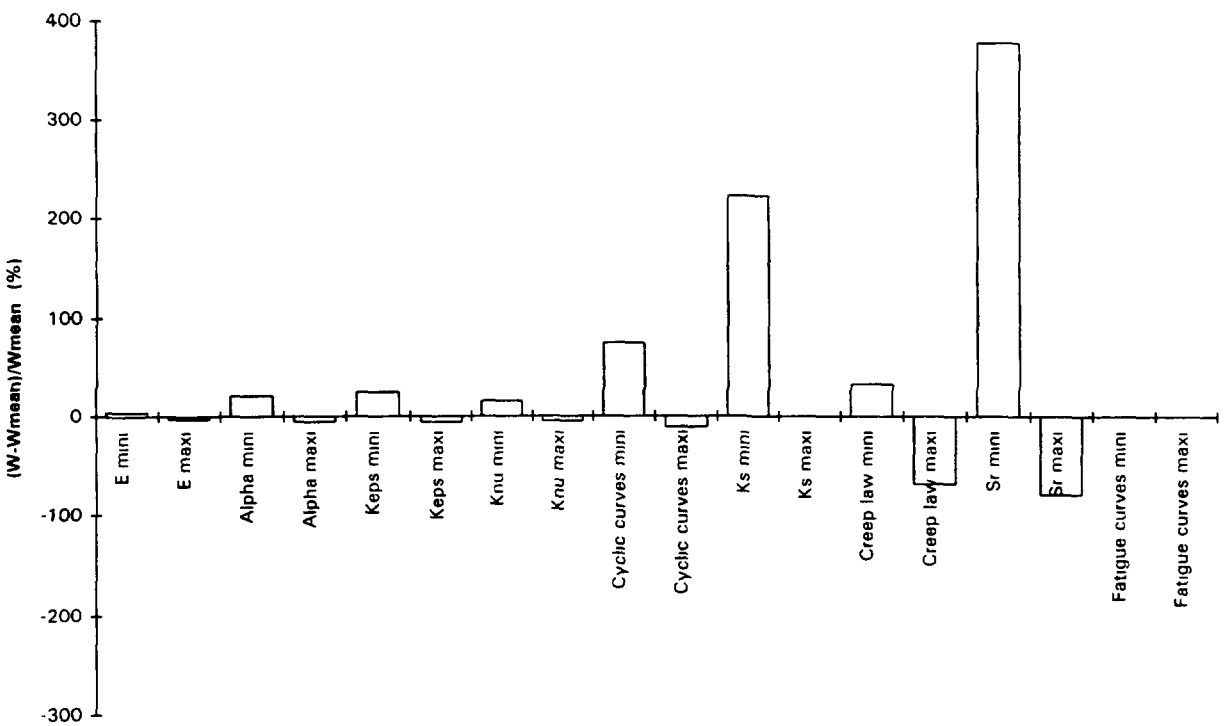

FIG. 5. Influence of the material properties on W

Figure 5 shows the relative importance of the different material properties.

- Influence on the fatigue usage fraction V

  The benchmark case which is considered do not enable to draw conclusions as regards the fatigue usage fraction. It is however obvious that material properties which have a significant effect on $\overline{\Delta\varepsilon}$, as well as fatigue curves, will have a significant effect on V.

- Influence on the allowable number of cycles N_r

  Due to the low level of fatigue damage, material properties significant for the allowable number of cycles N_r are the same than those listed for the creep usage fraction W.

7. COMPLEMENTARY ANALYSES : INFLUENCE OF THE SCATTER OF MATERIAL PROPERTIES IN THE INSIGNIFICANT CREEP REGIME

The benchmark studied previously concerns a case for which the creep damage is predominant against the fatigue damage.

Academic fatigue analyses have been performed in the insignificant creep regime at θ = 425°C and with $\overline{\Delta\sigma}$ = 400, 500 and 600 MPa (without primary load).

Calculations carried out with material properties leading to minimum life time lead to results with significant margins compared to those carried out with design material properties. The margin is all the more important that the stress range considered corresponds to the high cycle fatigue regime. The increase in the allowable number of cycles is ranging between 227% to 2754% compared to the design case.

8. FUTURE WORK

(i) The study considered the influence of the scatter of material properties without taking into account any relation between these material properties. A more refined study could show more margins between creep-fatigue analyses with material data leading to minimum life time and design analyses.

(ii) This work could be completed with a real benchmark for which fatigue damage is significant. A LWR case could be considered with either the RCC-MR or the RCC-M analyses.

(iii) The study considered the effects of material property variation using elastic analysis. A sensitivity study on the effect of mean, minimum and maximum material property variation is underway for an inelastic analysis which is expected to complement these results.

9. CONCLUSIONS

The influence of the scatter of material properties has been studied covering two phases. The first phase consisted of the definition of design, minimum, mean and maximum material property data required for the RCC-MR elastic route code assessment. The second phase covered sensitivity assessment of these different property values when applied to the RCC-MR elastic creep-fatigue route. For the lattest, a benchmark case representative to FRs structures and loadings has been studied

Creep-fatigue analyses were carried out using design material properties, mean material properties and properties leading to minimum and maximum lives. The results of the design and minimum life assessment were shown to be similar giving results of the same order of magnitude. Results with mean material properties and properties leading to maximum life duration exhibited significant margins compared to design analyses.

The sensitivity analyses carried out on the basis of the maximum and minimum material property values showed that properties which are the most significant for creep-fatigue assessment are in the order of importance:

- the S_r curves,
- the K_s factor (except for high level of stress ranges for which the symmetrisation factor would be saturated at 0.5 value),
- the creep law,
- the cyclic curves.

The influence of the fatigue curves was not investigated due to the type of benchmark studied. It is however obvious that this is also an important material data for creep-fatigue assessment.

REFERENCES

[1] RCC-MR, Règles de conception et de construction des matériels mécaniques des îlots nucléaires RNR, AFCEN, édition Mai 1993.

[2] Framatome report NVMD.DC.95.0987 RIO/TRR rev. C "Material Variability in Elastic Assessment - Final Report"

[3] WOOD, D.S.,WYNN, J., WILLIAMSON, K., "Derivation of design curves for the elevated temperature fatigue endurance of type 316 stainless steel", International Journal of Pressure Vessels and Piping, 37 (1989) 171-188

[4] Code Case N47, ASME Boiler and Pressure Vessel Code, edition 1989.

[5] SYSTUS user's guide, June 1994, revision B.

DESIGNING OF FAST REACTOR EQUIPMENT AND PIPELINES: NORMATIVE METHOD FOR CALCULATION OF LONG-TERM CYCLIC STRENGTH

V. ZHUKOV, A. KIRYUSHIN
OKBM, Nizhny Novgorod,
Russian Federation

XA9743953

Abstract

The paper deals with the method for calculational analysis of long-term cyclic strength recommended by "Norms for strength ..." to estimate cyclic damage of equipment items being operated at temperatures which cause creep and loaded by repeated thermal or mechanical forces.

The paper gives formulae interrelating amplitude of allowable conditional elastic stresses $[\sigma_{AF}]$ and allowable number $[N_0]$ of cycles, as well as calculational fatigue curves for alloyed steels, corrosion-resistant austenitic steels at loading duration of $2 \cdot 10^5$ hours.

The paper describes the method for calculational analysis of long-term cyclic strength for items made from steels with non-metallic inclusions, for items contacting with corrosion-agressive media, welded joints etc.

An example of calculational analysis of long-term cyclic strength by the use of recommended normative method is given.

It is shown that the item analyzed as an example (the joint of upper tube sheet of BN-600 intermediate heat exchanger and outer shell) has cyclic strength meeting the requirements of "Norms for strength ..." valid in Russia.

1. GENERAL PROVISIONS

Calculational analysis of low-cyclic strength and long-term cyclic strength is an important problem to be solved in the course of designing of equipments for fast nuclear reactors. It is associated with the fast that temperature stresses are a basic loading for equipment items and pipelines. In many cases these stresses exceed considerably the yield strength of the structural material and can result in initiation and propagation of fatique cracks or non-reversible progressive deformation (ratcheting).

The document "Norms for strength calculation of NPP equipment and pipelines" ("the Norms") [1] defines methods for calculational analysis of both fatique and creep-fatique strength. The former method is used in temperatures range up to temperature T_t where creep does not appear. The value of T_t is equal to 623K (350°C) for carbon, alloyed chromium-manganese and high chromium steels, high-temperature chromium-molybdenium-vanadium steels and ferro-nicelium alloys T_t is 723K (450°C).

Later the method is applies to analysis of strength of structural items being operated at temperatures which cause creep and loaded by repeated thermal and mechanical forces.

Characteristics of long-term strength and ductility given in Tables 1 and 2 of the Norms are used for the calculational analysis. In these Tables $R^{20}_{p0.2}$ is the minimum yield strength at the temperature T = 20°C;

TABLE 1 MEAN VALUES OF CONDITIONAL ULTIMATE LONG-TERM STRENGTH R^T, *MPA*

Steel,	$R^{20}_{p0\,2}$	R^{20}_m	T,	Time, hr								
alloy	MPa	MPa	K(°C)	10	30	10^2	$3\,10^2$	10^3	$3\,10^3$	10^4	$3\,10^4$	10^5
09X18H9	>196	>490	773 (500)	361 (36.8)	342 (34.9)	333 (34)	314 (32)	285 (29.1)	256 (26.1)	238 (24.3)	209 (21.3)	190 (19.4)
			823 (550)	323 (33)	313 (31.9)	290 (29.6)	275 (28.1)	237 (24.2)	200 (20.4)	171 (17.4)	152 (15.5)	133 (13.6)
			873 (600)	266 (27.1)	257 (26.2)	232 (23.7)	195 (19.9)	166 (16.9)	152 (15.5)	119 (12.1)	100 (10.2)	85 (8.67)

TABLE 2 MEAN VALUES OF LONG-TERM ULTIMATE DUCTILITY OF MATERIALS

Steel,	$R^{20}_{p0\,2}$	R^{20}_m	T,	Ductility	Time, hr									
alloy	MPa	MPa	K(°C)	%	10	30	10^2	$3\,10^2$	10^3	$3\,10^3$	10^4	$3\,10^4$	10^5	$2\,10^5$
09X18H9	>196	>490	773	A_t^T	28	25	21	16	15	14	12	11	9	8
			(500)	Z_t^T	44	38	33	29	25	22	19	17	14	13
			823	A_t^T	29	24	20	17	14	12	10	10	10	10
			(550)	Z_t^T	46	40	34	30	26	23	16	16	16	16
			873	A_t^T	22	18	17	22	27	24	15	10	7	5
			(600)	Z_t^T	33	31	34	42	32	23	16	13	17	9

R_m^{20} - the minimum ultimate strength at T = 20°C; R_{mt}^T - the minimum ultimate long-term strength at calculation temperature within time t; A_t^T, Z_t^T - the characteristics of long-term ductility (relative elongation and contraction respectively).

Structural items assessed for long-term cyclic strength should meet:

1. strength conditions which are adopted at choice of main sizes in the entire range of working temperatures;

2. strength conditions which are adopted in an analysis for long-term static strength.

2. CALCULATION FOR LONG-TERM CYCLIC STRENGTH (RECOMMENDED METHOD)

The method is applied to items made from ferritic alloy steels in temperature range from T_t to 773K (500°C) and to items made from corrosion resistant austenitic steels and iron-nickel alloys in temperature range from T_t to 873K (600°C) at a number of cycles up to 10^7.

Determination of allowable number of cycles $[N_o]$ for specified stress amplitudes or of allowable stress $[\sigma_{aF}]$ amplitudes for the given number of cycles may be performed by two methods:

1. by the correlations relating allowable amplitude of conditional stress to allowable number of cycles;

2. by calculational fatique curves which characterise the dependence between $[\sigma_{aF}]$ and $[N_o]$.

Amplitude of operational stress should not exceed the value $[\sigma_{aF}]$ for the given number of cycles N. If a stress amplitude is specified the number of operational cycles N should not exceed the value $[N_o]$.

If loading process consists of a number of cycles with stress amplitude $[\sigma_{aF}]_i$ and corresponding cycle numbers N_i the strength condition for accumulated fatique damage should be met:

$$\sum_{i=1}^{k} \frac{N_i}{[N_o]_i} = a \le [a_N], \qquad \text{where}$$

N_i - the number of i- type cycles during operating life,

$[N_o]_i$ - allowable number of i- type cycles,

k - total number of cycles types;

a - accumulated fatique damage the ultimate value of which is $[a_N] = 1.0$

For steels with ratio $\frac{R^T_{p0\,2}}{R^T_m} \le 0.7$ at $[N_o] \le 10^{12}$ the allowable amplitude of conditional elastic stress (or the allowable number of loading cycles) may be determined by the following formulae:

$$\left.\begin{aligned}[\sigma_{aF}] &= \frac{E^T \cdot e^T_c}{n_\sigma \cdot (4 \cdot [N_o])^m} + \frac{R^T_c}{n_\sigma \cdot \left[(4 \cdot [N_o])^{m_e} + \frac{1+r}{1-r}\right]} \\ [\sigma_{aF}] &= \frac{E^T \cdot e^T_c}{(4 \cdot n_N \cdot [N_o])^m} + \frac{R^T_c}{(4 \cdot n_N \cdot [N_o])^{m_e} + \frac{1+r}{1-r}}\end{aligned}\right\} \quad (1)$$

If the allowable number of cycles $[N_o] < 10^6$, it is permissible to calculate $[\sigma_{aF}]$ by the formulae:

$$\left.\begin{aligned}[\sigma_{aF}] &= \frac{E^T \cdot e^T_c}{n_\sigma \cdot (4 \cdot [N_o])^m} + \frac{R^T_{-1}}{n_\sigma \cdot \left(1 + \frac{R^T_{-1}}{R^T_m} \cdot \frac{1+r}{1-r}\right)} \\ [\sigma_{aF}] &= \frac{E^T \cdot e^T_c}{(4 \cdot n_N \cdot [N_o])^m} + \frac{R^T_{-1}}{1 + \frac{R^T_{-1}}{R^T_m} \cdot \frac{1+r}{1-r}}\end{aligned}\right\} \quad (2)$$

The minimum value is selected from to values $[N_o]$ or $[\sigma_{aF}]$ calculated by formulae (1) and (2).

For pearlitic steels at $[N_o] < 10^{12}$ and $\frac{R^T_{p0\,2}}{R^T_m} < 0.7$ the Norms recommend the use of the following formulae:

$$[\sigma_{aF}] = \frac{B^T \cdot E^T \cdot e^T_m}{(n_N \cdot [N_o])^{m_1}} \cdot \frac{1-r}{2} \cdot K^2_{(\sigma)} + \frac{R^T_c}{(4 \cdot n_N \cdot [N_o])^{m_e} + \frac{1+r}{1-r}} . \quad (3)$$

In these formulae $n_\sigma = 2.0$, $n_N = 10.0$ are strength margin coefficients for the stresses (n_σ) and the number of cycles (n_N); m, m_1 - material properties; r - stress cycle asymmetry coefficient; R^T_c - strength characteristic; e^T_c - ductility characteristic; E^T - elasticity modulus at design temperature; B^T, m_1 - characteristics of material; e^T_m - ductility characteristics depending on the value of uniform relative contraction temperature; $K_{(\sigma)}$ - reduced stresses concentration theoretical coefficient.

Methods for the determination of these parameters are presented in section 5.6 (Calculation for low-cyclic strength) and Appendix 7 (Calculation for low-term cyclic strength) of [1].

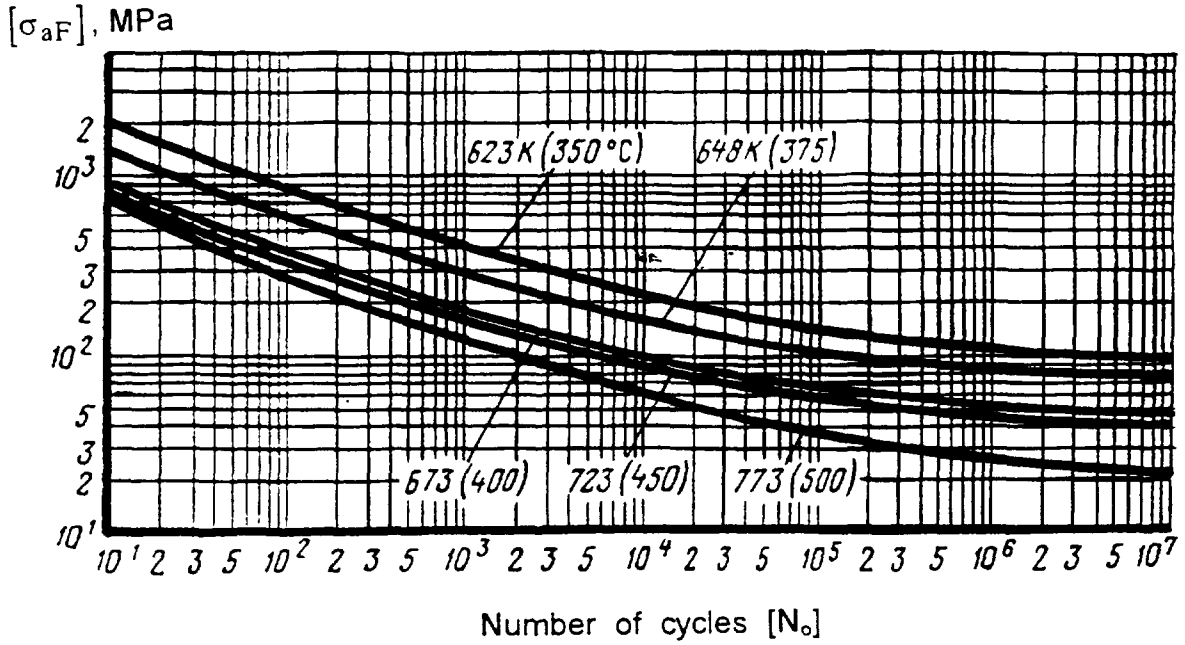

FIG. 1. DATA FOR ALLOYED STEELS DURING LONG-TERM (2· 10⁵ H) OF LOADING

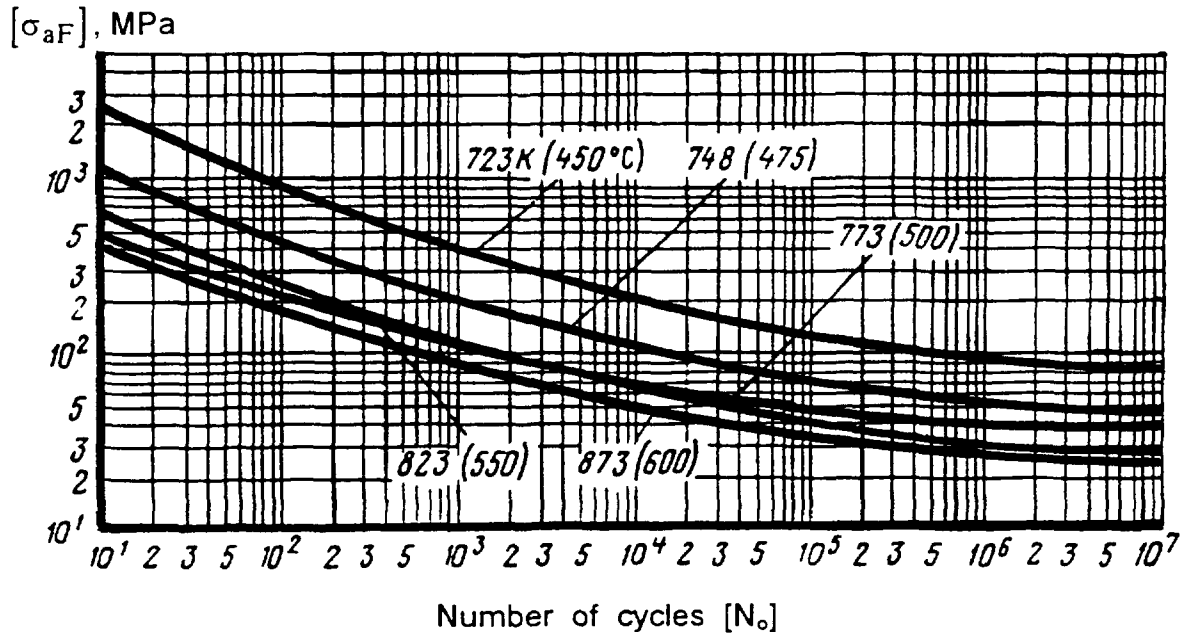

FIG. 2. DATA FOR CORROSION-RESISTANT STEELS OF THE AUSTENITIC CLASS DURING LONG-TERM (2· 10⁵ H) OF LOADING

Calculational fatigue curves for alloy steels with a symmetrical loading cycles are given in Fig.1 Calculational fatigue curves for austenitic steels with a symmetrical loading cycles are presented in Fig.2. When plotting the curves it is assumed that $n_\sigma = 2.0$, $n_N = 10.0$ similar to formulae (1) through (3).

In the analysis of structural items made from similar materials or portions of the items, loaded only by temperature stresses caused by radial temperature differentials (excluding zones of edge effects and average temperature variation) values of coefficients n_σ and n_N in formulae (1) through (3) may be taken as $n_\sigma = 1.5$ and $n_N = 5.0$, if failure of these structures (e.g. thermal baffles) does not result in release of working medium beyond load-bearing elements confining the medium.

When using steels with content of non-metallic inclusions exceeding a 3 points value according to [2] the allowable number of cycles to be determined by calculational fatigue curves at stress amplitude

$$(\sigma_{aF})_B = (\sigma_{aF}) + K_{F_B} \cdot \Delta\alpha \cdot \Delta T \cdot E^T, \qquad \text{where}$$

(σ_{aF}) - calculation amplitude of reduced elastic stresses;

$\Delta\alpha$ - absolute value of difference in thermal expansion coefficients for steel and non-metallic inclusions (see Table 3);

$$K_{F_B} = K_B \left(1 - \frac{1}{1.25 + 10^{-3} \cdot (\sigma_{aF})^2}\right), \qquad \text{where}$$

K_B - coefficient of influence of non-metallic inclusions (see Table 3);

ΔT - cycle temperature range calculated by formulae $\Delta T = T_{max} - T_{min}$;

T_{max} and T_{min} - the maximum and minimum temperature in a cycle of stresses, respectively.

TABLE 3 VALUES OF COEFFICIENTS K_B *AND* $\Delta\alpha$

Material	Impurities content, points	Value of coefficient K_B						$\Delta\alpha\ 10^6$, 1/°C
		Sheet						
		350°C	400°C	450°C	500°C	550°C	600°C	
Austenitic	3.0	-	-	0	0	0	0	
class	3.5	-	-	0	0.07	0.14	0.20	
steels and	4.0	-	-	0	0.08	0.16	0.24	10
welded	4.5	-	-	0	0.09	0.18	0.28	
joints	5.0	-	-	0	0.10	0.20	0.30	

In the analysis of long-term cyclic strength of welded joints the calculation amplitude of stresses is

$$(\sigma_{aF})_s = \frac{(\sigma_{aF})_B}{\varphi_s},$$ where

φ_s - coefficient of long-term cyclic strength reduction for welded joints in compliance with Table 4.

TABLE 4 VALUES OF COEFFICIENT φ_s

Base metal	Welding method	Weld material	Heat treatment after welding	Temperature, °C			
				450	500	550	600
Austenitic steels	Manual	48A-1	Without heat treatment	0 8	0.7	0.6	0.5
			Austenization	1.0	0.85	0.7	0.55

In the analysis of cyclic strength for structural items in contact with corrosion-aggressive media of reactor-grade purity

$$(\sigma_{aF})_k = \frac{(\sigma_{aF})_B}{\overline{\varphi}_k}$$

or

$$(\sigma_{aF})_{ks} = \frac{(\sigma_{aF})_B}{\overline{\varphi}_{ks}},$$ where

$\overline{\varphi}_k$ and $\overline{\varphi}_{ks}$ - coefficients of base metal and welded joint cyclic strength deterioration due to corrosion determined by test. The method for conducting such test is given in [1].

In the analysis of structures exposed to neutrons, the minimum value from the following two values is assumed as the allowable number of cycles:

the number of cycles determined by calculational fatique curves and divided by coefficient φ_F;

the number of cycles determined by formulae (1) through (3) and divided by coefficient φ_F.

Values of the coefficient φ_F are given in Table 5 [1].

TABLE 5 VALUES OF COEFFICIENT φ_F

Material	T K (°C)	φ_F	F_N, m^{-2} (E > 0.1 M_{ev})					
			10^{22}	10^{23}	10^{24}	10^{25}	10^{26}	10^{27}
Austenitic class steels	748-873 (475-600)	φ_F	1.0	0.9	0.85	0.8	0.75	0.6

For items with chromium-nitride coating a stress amplitude

$$(\sigma_{aF})_n = \frac{(\sigma_{aF})}{\varphi_n}, \qquad \text{where}$$

φ_n = 0.75 - for austenitic steels.

The influence of sodium or argon of reactor-grade purity in contact with equipment is not taken into account in the analysis of long-term cyclic strength

3. BN-600 INTERMEDIATE HEAT EXCHANGER. CALCULATION OF LONG-TERM CYCLIC STRENGTH FOR TRANSITION ZONE BETWEEN UPPER TUBE SHEET AND OUTER SHELL

3.1. Formulation of the problem.

The tube sheets (Fig.3) together with heat-exchange tubes form the heat transfer surface of the IHX. They work under pressure of both the secondary coolant (up to 1.0 MPa) and the primary coolant (not more than 0.05 MPa) and experience thermal stresses influence by conditions in the both circuits. These thermal stresses are mainly nonstationary and have a complex character.

The calculational analysis and experimental studies showed that temperature fields in the upper tube sheet are determined mainly by thermal conditions in the performed part.

The calculational scheme given in Fig.4 was adopted for the analysis of the item under consideration. The tube sheet was presented by a solid annular plate. It's thickness was reduced to take into account reduced stiffness due to presence of the holes. The calculational scheme adopted does not take into account the stiffness of heat-exchange tube because they have compensation bends and the force generated by the tubes does not exceed 10% of the force from coolant impacting the tube sheet.

The calculations show that the stress state in the upper tube sheet and the shells to which it is connected depends on the temperature fields which are set up during the following operational transients:

(a) Reactor trip,

(b) Heat transfer loop isolation,

(c) Heat transfer loop start up, when power is not more than 40%.

At some points in time the zone in which the stress exceeds the yield extends through the entire depth of the tube sheet and into the adjoining shells. This creates conditions under which the development of low-cycle fatique cracks and ratcheting can occur.

An A-80 computer program complex was used to calculate temperature distributions along radius and height of the intermediate heat exchanger and to study stresses in the upper tube shells adjoining it. The program complex is based on the finite element method.

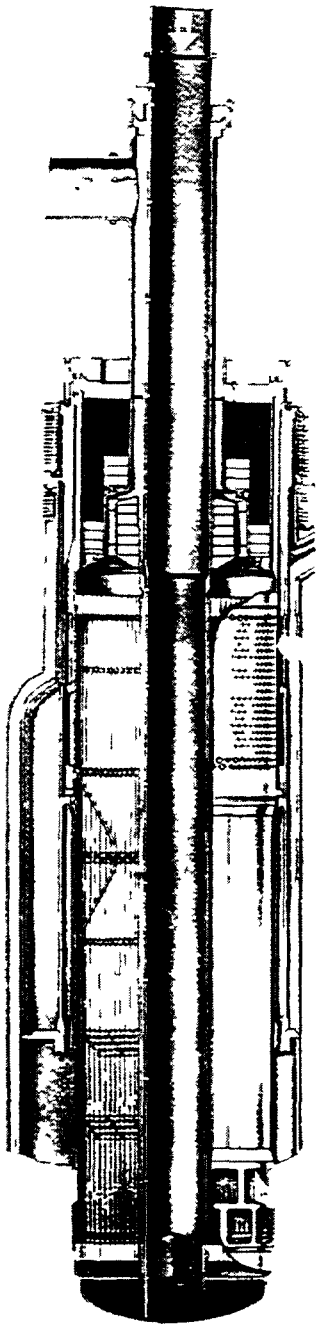

FIG 3 BN-600 INTERMEDIATE HEAT EXHANGER

3.2 Input data for calculation of long-term cyclic strength

The main input information for assessment of cyclic damage is derived from the results of the stress analysis calculations in the zone considered; in addition the data about the number of operational transients are used as well as standard physical and mechanical properties of structural material in the range of operating temperatures with the account of loading period duration

According to the analysis of operating conditions of Beloyarsk-3 NPP with the BN-600 reactor (running since 1980) the following number of transients were realized until 1992 (see Tables 6-8)

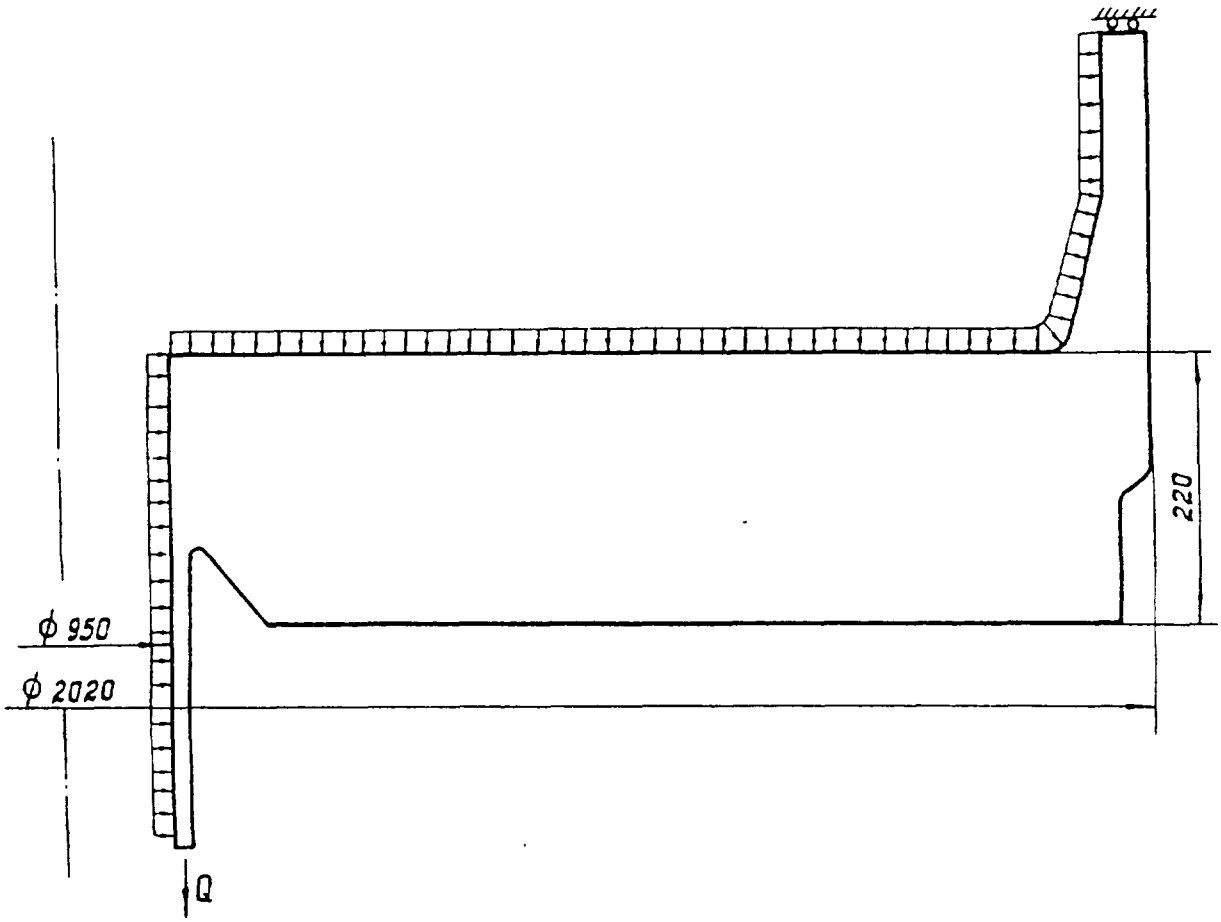

FIG. 4. CALCULATIONAL MODEL FOR THE IHX TUBE SHEEL.

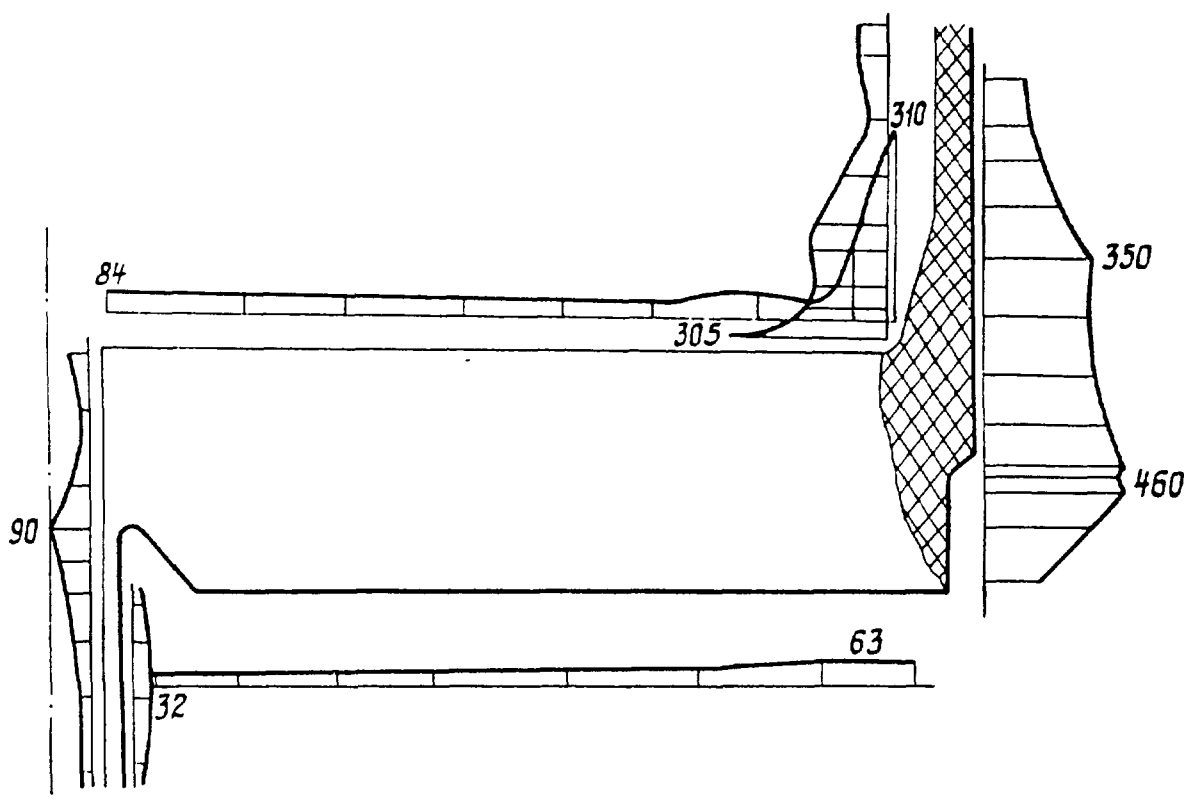

FIG. 5. STEEL INTENSITY DISTRBUTION IN THE TUBE SHEET.

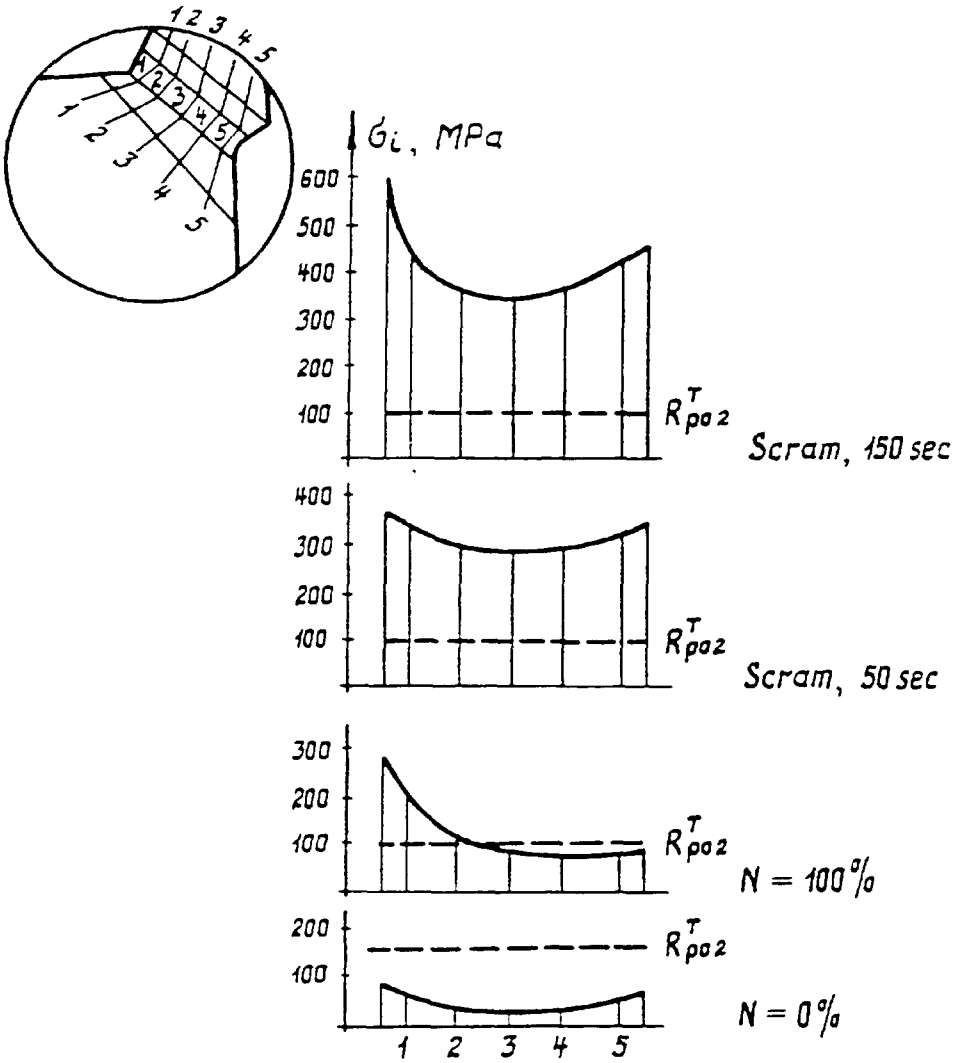

FIG. 6. IHX'S TUBE SHEET TO OUTSIDE CYLINDRICAL SHELL JOINT DISTRIBUTION OF STRESS INTENSITY IN STRESS CONCENTRATION ZONE FOR DIFFERENT MOMENTS OF TIME.

TABLE 6. THE NUMBER OF BN-600 REACTOR SHUTDOWNS WITH CLASSIFICATION ACCORDING TO INITIAL POWER LEVEL.

Mode type	Power level					
	30	40	50	60	75	100
Reactor trip	2	3	1	5	4	4

TABLE 7 THE NUMBER OF BN-600 REACTOR HEAT-TRANSFER LOOP ISOLATIONS WITH CLASSIFICATION ACCORDING TO INITIAL POWER LEVEL

Heat transfer loop, №	Power level, %					
	10	40	50	60	75	100
4	9	2	-	2	2	11
5	2	4	4	-	3	15
6	5	2	-	1	3	13

TABLE 8 THE NUMBER OF HEAT-TRANSFER LOOP START UP EVENTS (POWER LEVEL UP TO 40%)

Heat transfer loop, №	The number of heat transfer loop startup events (1980-1992)
4	18
5	19
6	13

The results of the calculational analysis of strength for intermediate heat exchangers were used to estimate the cyclic damage. These results were validated by strain measurements during BN-600 reactor startup testing and power raising. Table 9 gives data on stresses in a transition zone between the upper tube sheet and outer shell.

Physical and mechanical properties of 09X18H9 steel (base material for the heat exchangers) were adopted in compliance with [1] (Table 10).

TABLE 9 LEVEL OF STRESSES IN THE ZONE OF TRANSITION BETWEEN THE UPPER TUBE SHEET AND THE OUTER SHELL

	Power level, %					
	30	40	50	60	75	100
Temperature variation amplitude, °C	80	110	140	170	180	200
Stress level, MPa	240	330	420	510	540	600

TABLE 10 PHYSICAL AND MECHANICAL PROPERTIES OF 09X18H9 STEEL

Temperature, °C	R_{p02}^T, MPa	R_m^T, MPa	R_{mt}^T, MPa	Z_t^T, %	$\alpha \cdot 10^6$, 1/°C	$E^T \cdot 10^{-3}$, MPa
20	196	491	-	-	16 4	2.05
200	147	400	-	-	17.0	1.90
300	128	380	-	-	17.4	1.80
450	108	314	303	-	18.0	1.67
500	98	304	196	14	18.2	1.65
550	98	294	137	16	18.4	1.62

In Table 10

R_{p02}^T - minimum yield strength at calculation temperature;

R_m^T - minimum ultimate strength at calculation temperature;

R_{mt}^T - mean value of long-term strength for 10^5 hrs (it corresponds approximately to 20 years life span);

α - linear expansion coefficient at calculation temperature;

E^T - modulus of elasticity of material at calculation temperature;

Z_t^T - mean value of conditional ultimate long-term ductility for life span of 10^5 hrs at calculation temperature.

3.3. Calculational estimation of accumulated cyclic damage.

To estimate long-term strength the method recommended in [1] was used. Cyclic damage of items made of austenitic steel can be evaluated by this method in the temperature range

$T_t = 450°C \leq T \leq 600°C.$

The method recommended in [1] is based on correlations between conditional elastic stresses acting in the item under consideration and allowable number of loading cycles.

At operating temperatures specific for the BN-600 reactor fatique effects take place, therefore mechanical characteristics of structural material strength were used in calculations which correspond to the end of specified service life for temperatures which exceed the temperature of creep.

The principle of linear accumulation of damage was adopted to take into account total damage of the material from various transient conditions in compliance with [1].

The analysis of long-term cyclic strength of the heat exchanger units (including the upper tube sheet to outer shell transition zone) was carried out by "CYCLE" program.

The calculational data are presented below in tabular form to estimate cyclic damage of the unit under consideration·

Table 11 - calculational moments of time and corresponding components of stresses;

Table 12 - history of loading for all calculation cycles;

Table 13 and 14 - the results of calculation of damage at reactor operation on power levels N=60% and N=100% respectively (given as an example).

TABLE 11 CALCULATED STRESS COMPONENTS AT EACH TIME STEP

No. of unit	Moment of time	σ_x MPa	σ_y MPa	σ_z MPa	σ_{xy}	No. of material
I	1	0	0	0	0	1
I	2	0	240	0	0	1
I	3	0	330	0	0	1
I	4	0	420	0	0	1
I	5	0	510	0	0	1
I	6	0	540	0	0	1
I	7	0	600	0	0	1

Notes: 1 - moment of time corresponding to initial state of reactor;

2 - 7 - moments of time (numbers of cycles) corresponding to the reactor operation at power of 30%, 40%, 50%, 60%, 75% and 100% nominal one;

σ_x, σ_y, σ_z, σ_{xy} - radial, axial, hoop and tangential (shear) stresses respectively.

TABLE 12 HISTORY OF LOADING CYCLES

No. of cycle	Anticipated number of loading cycles	Number of calculation moments of time in cycle	Maximum temperature of cycle °C	Minimum temperature of cycle °C
2	11	3	500	420
3	23*)	3	500	390
4	1	3	500	360
5	7	3	500	330
6	6	3	500	320
7	15	3	500	300

*) with account of number of heat transfer loops actuation when reactor power does not exceed 40% of rated one.

TABLE 13. REACTOR OPERATES AT 60% POWER

No. of unit	Moment of time	Calculation cycle No. 5			Anticipated number of cycles 7		
		Calculational stresses, MPa					
		Main			Reduced		
		σ_1	σ_2	σ_3	$\sigma_1 - \sigma_2$	$\sigma_1 - \sigma_3$	$\sigma_2 - \sigma_3$
1	1	0	0	0	0	0	0
	5	510	0	0	510	510	0
	1	0	0	0	0	0	0
	Coefficient of asymmetry				-0,797	-0,797	-
	Stress amplitude				313	313	-
	Maximum stress				905		
	Damage for cycle				0,086	0,086	-
	Total damage in cycles 2,3,4, 5				0,143		

The method of stress analysis (including their maximum value for the case when calculated conditional elastic stress exceeds $R^T_{p0,2}$) is described in Section 5.3 of [1].

TABLE 14. REACTOR OPERATION AT 100% POWER

No. of unit	Moment of time	Calculation cycle No. 7			Anticipated number of cycles 15		
		Calculational stresses, MPa					
		Main			Reduced		
		σ_1	σ_2	σ_3	$\sigma_1 - \sigma_2$	$\sigma_1 - \sigma_3$	$\sigma_2 - \sigma_3$
1	1	0	0	0	0	0	0
	7	600	0	0	600	510	0
	1	0	0	0	0	0	0
	Coefficient of asymmetry				-0,766	-0,766	-
	Stress amplitude				398	398	-
	Maximum stress				1170		
	Damage for cycle				0,350	0,350	-
	Total damage in cycles 2,3,4, 5, 6, 7				0,585		

3.4. Conclusion

The results of calculations of the long-term cyclic strength of the IHX's item consideration (a zone of upper tube sheet to outer shell transition) showed the total accumulated damage of the BN-600 heat exchangers, which have been operating since 1980 until 1992, is considerably less than the allowable value ($a = 0,585 < [a_N] = 1,0$).

This result allows us to conclude that the cyclic strength of the BN-600 heat exchanger at present meets the requirements of the Norms [1] in force in Russia.

REFERENCES

[1] - "Нормы расчета на прочность оборудования и трубопроводов атомных энергетических установок. ПНАЭ Г-7-002-86" ("Norms for strength calculation of NPP equipment and pipelines. PNAE G-7-002-86".)

[2] - Сталь. Металлографические методы определения неметаллических включений. ГОСТ 1778-70. ("Steel. Metallographic methods for determination of non-metallic inclusions. GOST 1778-70.)

CREEP/FATIGUE DAMAGE PREDICTION OF FAST REACTOR COMPONENTS USING SHAKEDOWN METHODS

D.E. BUCKTHORPE
NNC Ltd,
Knutsford, Cheshire,
United Kingdom

Abstract

High temperature plant such that to be used in the Fast Reactor operates under conditions which produce creep and plasticity in the presently available materials (eg. Austenitic Stainless steel). For estimation of creep and fatigue endurance in such plant recently established techniques such as the shakedown method developed in the UK primarily as a design tool to prevent the onset of ratcheting allows the prediction of the steady cyclic state to be made and provides less conservative assessments than current elastic assessment routes available in design codes. The method uses essentially elastic analyses of a load cycle and requires the estimation of a constant residual stress field which is used to obtain a reference stress for creep damage estimates and local estimates of fatigue damage. The method also offers significant advantages over time stepping inelastic analysis methods.

The present status of the shakedown method is reviewed, the application of the shakedown based principles to complex hardening and creep behaviour is described and justified and the prediction of damage against design criteria outlined. Comparisons are made with full inelastic analysis solutions where these are available and against damage assessments using elastic and inelastic design code methods. Current and future developments of the method are described including a summary of the advances made in the development of the post process ADAPT, which has enabled the method to be applied to complex geometry features and loading cases.

The paper includes a review of applications of the method to typical Fast Reactor structural example cases within the primary and secondary circuits. For the primary circuit this includes structures such as the large diameter internal shells which are surrounded by hot sodium and subject to slow and rapid thermal transient loadings. One specific case is the damage assessment associated with thermal stratifications within sodium and the effects of moving sodium surfaces arising from reactor trip conditions. Other structures covered are geometric features within components such as the Above Core structure and Intermediate Heat Exchanger. For the secondary circuit the method has been applied to alternative and more complex forms of geometry namely thick section tubeplates of the Steam Generator and a typical secondary circuit piping run. Both of these applications are in an early stage of development but are expected to show significant advantages with respect to creep and fatigue damage estimation compared with existing code methods.

The principle application of the method to design has so far been focused on Austenitic Stainless steel components however current work shows some significant benefits may be possible from the application of the method to structures made from Ferritic steels such as Modified 9Cr 1Mo. This aspect is briefly discussed as a potential application and future development of the method.

1. INTRODUCTION

Design assessment procedures based on the principles of shakedown are important where cyclic thermal stresses are imposed such as in the Fast Reactor. Shakedown is defined as the process whereby a structure reaches dimensional stability within the first few cycles of loading and if the loading is increased progressively above shakedown and the dimensions of the structure do not stabilise but change incrementally in each cycle this gives the condition known as ratcheting. The practical application of shakedown procedures to design problems has become possible with the development of shakedown computer algorithms and a method of assessing shakedown in high temperature plant based on the lower bound theorem[1,2,3] has been developed within the UK nuclear industry and is used for the design of the European Fast Reactor (EFR). The shakedown design method was developed for Fast Reactor components operating in the creep range at large cyclic thermal stresses and moderate levels of primary stress[4] and uses elastically calculated solutions to indicate whether progressive deformation or ratcheting will occur under specified cyclic loading. The method provides an estimate of a reference stress during periods of steady operation at creep temperatures for assessment of creep damage with fatigue damage covered by use of simplified methods.

Structural materials and weldments often possess limited ductility and for strongly strain-hardening materials, such as austenitic stainless steels, the strain accumulation rate does not become constant but eventually reduces to zero after a certain amount of accumulated deformation. For such materials the ratcheting limit can be replaced by an appropriate strain-accumulation limit.

However, even within shakedown part or all of a structure may undergo cyclic plasticity in which there are increments of plastic strain, summing to zero, at different stages of the loading cycle. Such a state is often known as 'plastic shakedown'. It includes the possibility of low-cycle fatigue damage and, in creep conditions, of a strong influence of plasticity upon the stress-levels at which creep damage occurs. At lower levels of loading a state may develop in which, after a moderate number of cycles, all plastic straining ceases and the behaviour is entirely elastic apart perhaps from creep. This is known as 'elastic shakedown' or 'strict shakedown'. It eliminates low-cycle fatigue and simplifies the conditions governing creep damage. Shakedown in any of these senses may be regarded as defining a type of steady cyclic state at each point of a structure. If such states can be predicted, there is an evident basis for sound design and prediction of fatigue and creep/fatigue damage.

The basis of the shakedown method is the mathematical lower bound shakedown theorem applied to structures made from an elastic perfectly plastic material. Although the inelastic step-by-step analysis is nominally capable of predicting the shakedown process, shakedown analysis as outlined in this paper provides a short cut to the inelastic analysis route by going immediately to the prediction of the steady cyclic state.

The explicit use of shakedown methods for the design of high temperature structures is relatively new, though similar concepts are implicit in several design codes, and further development is expected. Improvements have been evaluated to cover a better estimation in regions of alternating plasticity and also under development are less conservative creep and fatigue damage prediction using techniques based on strain quantities rather than stress values.

The purpose of this paper is to provide an outline of the shakedown design rules, including the analysis using ADAPT and to indicate the additional benefits of the method in providing, in many cases, more realistic prediction of creep/fatigue damage than many current

elastic code design routes. Comparisons are made with design code methods and inelastic analysis and example applications on typical high temperature structures are given to demonstrate the usefulness of shakedown as a design tool.

2. SHAKEDOWN - THE BASIC IDEA

To describe the basic idea of shakedown, the more restrictive definition, in terms of elastic shakedown, is considered. Shakedown is defined as the condition whereby, within a small number of load applications the stress and strain response at all points in the structure becomes elastic at all times (in the absence of creep). The assumptions are then made that:

(i) The material is elastic perfectly plastic with temperature dependent properties

(ii) The loading consists of a combination of time varying mechanical loads and independently time varying temperature distributions, in a sequence which repeats at regular intervals (one complete sequence constitutes a single load cycle)

(iii) The finite element modelling of the structural geometry allows a detailed distribution of stresses to be defined, but may include plates, beams, shells, etc, as well as continuum elements.

Fig.. 1 shows the shakedown process is illustrated for the case of a rectangular beam (regarded as containing uniaxial stress) subjected to a repeated primary end load. The bending stress distribution on a section of the beam is illustrated. The elastically calculated stress in the extreme fibre, σ_E, exceeds the material yield stress σ_y. Plastic strain occurs which increases the beam curvature, with a resultant redistribution of stress as shown. On removal of the beam end load a residual stress field ρ, appears obtained by subtracting σ_E from the redistributed stress field produced by yielding. Two points are evident:

(i) The beam has achieved shakedown, since response to re-application of load will be elastic

(ii) The residual stress field is in a state of self-equilibration.

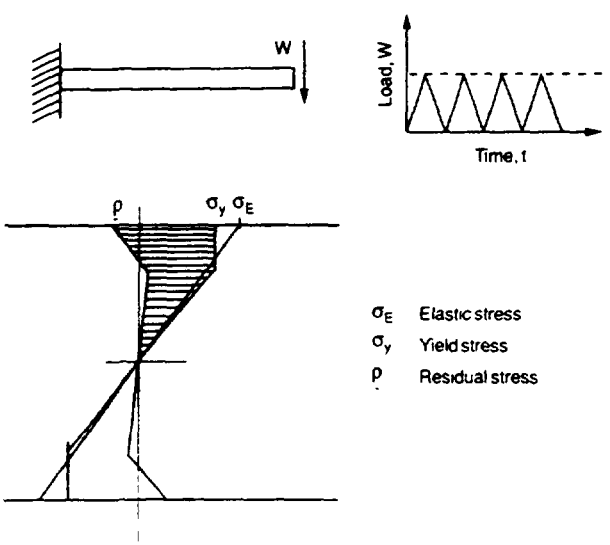

Fig. 1. Shakedown – basic idea

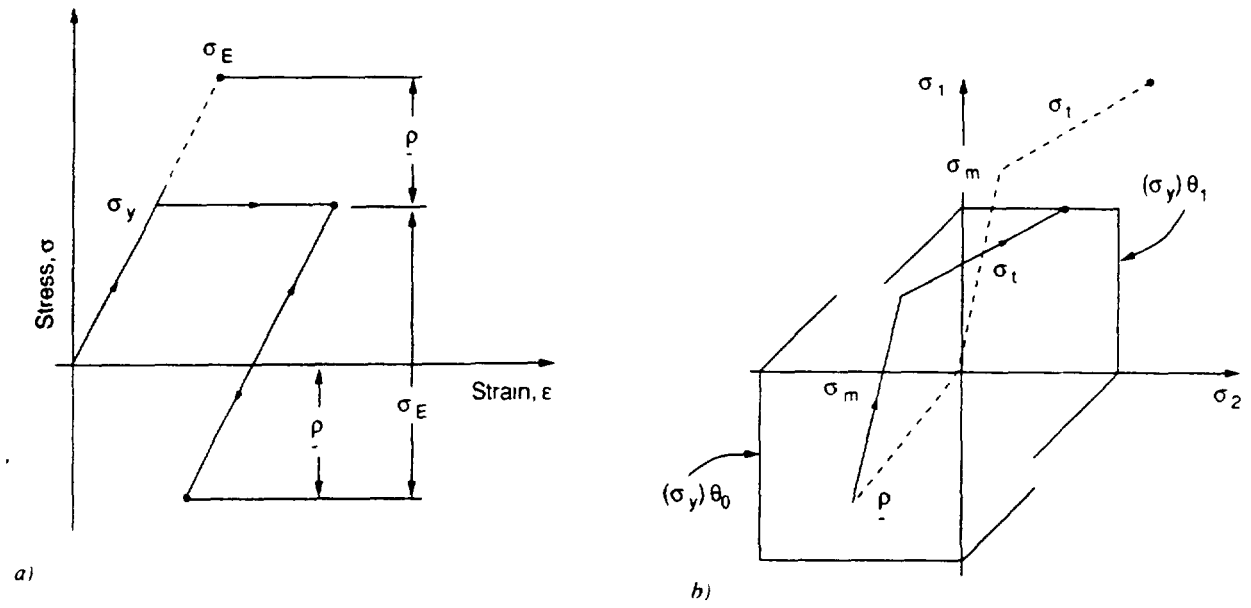

σ_E Elastic stress σ_m, σ_t Elastic mechanical and thermal stresses

$\underset{\sim}{\rho}$ Residual stress $(\sigma_y)_\theta$ Yield stress at temperature θ

σ_1, σ_2 Principal stresses

Fig. 2. a) Uniaxial and b) biaxial representations of shakedown

The shakedown process is further illustrated in Fig.. 2 for a general case in two-dimensional stress space where the elastic stress vectors due to mechanical and thermal loads at a point in a structure are brought within the yield locus by the presence of a vector representing residual stress. (A Tresca yield surface is shown, although the Von Mises formulation is used in the shakedown procedure).

2.1 Types of Shakedown

Using the elastic perfectly plastic material model, it is helpful to distinguish the different forms of shakedown or non-shakedown that may be achieved. These are described below using the terminology applicable to the shakedown method.

(i) Strict or elastic shakedown

Wholly elastic strain changes at all points.

(ii) Overall shakedown

Wholly elastic strain changes over most of the structure volume, including a core region consisting of at least 80 per cent of every section, with local small regions undergoing alternating plastic strain

(iii) General plastic shakedown.

Unlimited regions of the structure undergo alternating plastic strain.

(iv) Ratcheting

Widespread regions of plastic strain changes involving at least one entire structural section and leading to cyclic increments of strain.

2.2 Effect of Material

The shakedown method is applied to structures made of materials which differ from the elastic-perfectly plastic model in having a more gradual yield, especially in cyclic conditions, and in having some cyclic hardening. The actual behaviour, at a point in the structure undergoing the shakedown process, is then as indicated in Fig.. 3. For such materials it is wasteful to seek a completely elastic shakedown since somewhat higher loadings would only induce very moderate plastic strain-ranges. Also, as noted in the introduction, the phenomenon of steady ratcheting - even if it can occur at very high loadings - is normally replaced by ultimately stabilised strain accumulations. In general, it is possible to increase the loading level, resulting in further accumulated strain and attendant hardening until renewed stabilisation.

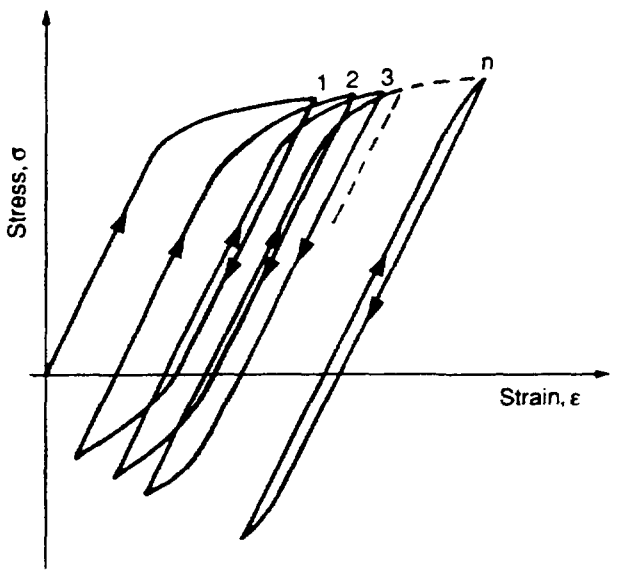

Fig. 3. Shakedown with strain hardening

For such materials it is better to adopt an effective yield stress, much as the 0.2% proof stress is commonly adopted for consideration of monotonic loading problems. The value chosen should correspond to real stress levels within which there is an acceptable amount of accumulated plastic strain according to a design code and suitably small plastic strain-ranges. Reasonable engineering conclusions may then be expected from an elastic-perfectly plastic model based on such a yield stress.

2.3 Effect of Creep

If the loading cycle contains one or more periods of steady or slowly varying load during which time dependant material effects occur, the resultant creep strain will modify the short term shakedown state. Creep can cause relaxation and redistribution of stress during the hold time, in a manner analogous to plasticity. This analogy is employed to determine the steady cycle state following long exposure to creep.

3. IMPLEMENTATION OF THE SHAKEDOWN DESIGN METHOD

The three main features of the shakedown design procedure are the use of an elastic-perfectly plastic model, the lower bound shakedown theorem and shakedown analysis using the ADAPT computer program. These are described in the following paragraphs.

3.1 Choice of the Elastic-Perfectly Plastic Model

The elastic-perfectly plastic model is selected because it is believed to produce conservative predictions of ratcheting potential. This is in contrast to, for example, the kinematic hardening rule which is incapable of describing a ratcheting mechanism. A further reason for the choice is the simplicity of the constitutive law that enables the analysis to be performed using essentially elastic methods and with a minimal set of material parameters.

3.2 The Lower Bound Shakedown Theorem

The lower bound shakedown theorem is employed for the shakedown analysis. It recognises that shakedown takes place as a result of the presence of a favourable residual stress field.

A residual stress field has the following characteristics:

(i) It is a stress that can remain in the structure if all mechanical and thermal loads are reduced to zero and any kinematic constraints are returned to their initial conditions.

(ii) It is in equilibrium throughout the structure

(iii) It is constant with time for shakedown (time-varying residual stress fields can be defined for non-shakedown).

Shakedown can then be understood for cyclic loading as a state where the applied elastically calculated stresses superimposed on residual stresses do not violate the yield condition.

$$[\sigma_E(\underline{x},t) + \rho\ (\underline{x})] < \sigma_y\ (\theta(\underline{x},t)) \qquad \ldots\ (1)$$

The square brackets represent the Von Mises equivalent stress.

From this shakedown criterion, it is clear that for there to be any possibility of achieving shakedown, the stress trajectory representing the elastic stress history $\sigma_E(\underline{x},t)$ at each position must be of such a size as to fit within the yield surface when moved bodily relative to the origin of stress space. This can be seen by reference to Fig. 2b.

The remaining question to be decided is the permissible choice of the residual stress field to be used in testing for satisfaction of the shakedown criterion. The lower bound shakedown theorem, states that if and residual stress field (with the characteristics given above) can be found which satisfied the shakedown criterion then the structure will shakedown.

Such a residual stress field is not in general unique. Many different residual fields can usually be found to satisfy the shakedown criterion, each corresponding to some different initial state of the structure. This is of no detriment to the method. The question becomes more important however for creep conditions which, in fact, induce a unique residual field, independent of the initial state. The effect of cyclic creep within elastic shakedown is to reduce the equivalent stress, at peak positions during a hold period as far as possible until either a steady-state stress distribution is attained or loss of shakedown would occur at some stage in the cycle. This allows an optimisation to be used for estimation of a particular residual stress which in fact minimises creep damage.

The method is limited to cases with loadings within the overall shakedown criteria and though this often covers satisfactory design for long term purposes, there are situations where other methods such as full inelastic analysis are needed to deal with loadings beyond overall shakedown. Likewise, though usually to a lesser extent than in other simplified assessment procedures found in design codes, the built-in conservatisms may sometimes prove too much and inelastic analysis can usefully reduce the damage estimates for problems within shakedown, though developments for improved treatment of creep, are intended to reduce the need. In general however, shakedown analysis is capable of giving an effective assessment of a large proportion of problems for structures subjected to repeated, and especially thermal, loadings over long design lives.

A structure is said to be **at the shakedown limit** when any small increase in load results in failure to satisfy the shakedown criterion at some critical location and at some load step. When this condition is reached, no change in the residual stress field is possible without causing a violation of the yield criterion. **The residual stress field at the shakedown limit is therefore unique**, at least at the critical location.

3.3 The ADAPT Program

The preceding section explains that the demonstration of shakedown requires the generation of a suitable residual stress field, followed by a check that the shakedown criterion is satisfied. The computer program ADAPT is designed to perform these functions, and to proceed on an interactive basis until either shakedown is demonstrated or there is a failure of the solution to converge indicating that shakedown is not possible under the specified loading.

3.3.1 Input to the computer program ADAPT

ADAPT receives as input, the elastic stress history calculated by a finite element program with which it interfaces, and employs the finite element program again as a subroutine to produce equilibrated residual stress fields.

When performing a calculation the finite element idealisation of the structure should be designed to be suitable for elastic plastic analysis, although only elastic analysis is performed. This is because the search procedure produces residual stress fields having

distributions similar to those generated by time stepping inelastic analysis, the detail of which might be lost if the mesh were only designed for typical elastic stress distributions.

A commercially available package such as ABAQUS is employed to calculate the elastic stresses at each integration point for a number of load steps, using the finite element idealisation described above. The load steps are selected using the principle that stresses at times between load steps could be estimated with reasonable accuracy using linear interpolation. By this means, if necessary by trial calculations, it is ensured that a sufficient number of load steps are selected to represent all extreme points in the elastic stress history. The elastic stress history represents the sum of elastic stresses due to all simultaneous mechanical, thermal and kinematic loadings.

The input to ADAPT is completed by the specification of temperature dependant yield stress.

3.3.2 Procedure of ADAPT

The procedure used by ADAPT is described in the following steps

(i) Step 1

For each integration point ADAPT examines the elastic stress history and selects a trial value of residual stress $\rho^L(\underline{x})$ which satisfies the shakedown criterion at that point but need not necessarily form part of a self-equilibrated stress field.

(ii) Step 2

ADAPT enters the $\rho^L(\underline{x})$ values into ABAQUS as initial stress values. ABAQUS then solves for the nearest self-equilibrating stress field $\varrho^S(\underline{x})$ for null load conditions.

(iii) Step 3

ADAPT checks whether $\varrho^S(\underline{x})$ satisfies the shakedown criterion at each point and each load step. If satisfied, a solution to the problem has been demonstrated confirming that shakedown will occur, and the process ends.

(iv) Step 4

If the criterion is not satisfied, ADAPT selects a new trial value of $\varrho^L(\underline{x})$ based on the previous value and $\varrho^S(\underline{x})$ and steps 2 and 3 are repeated.

3.3.3 Results of ADAPT analysis

The result of the analysis is in one of the three classes A, B or C as follows

(i) Strict shakedown

The analysis converges to a solution for the residual stress field with satisfaction of the shakedown criterion at all times and all load steps. For convenience the state of

shakedown is expressed in terms of a **Normalised Shakedown Ratio** (NSR) at each integration point:

$$NSR = \frac{[\underline{\sigma}_E(\underline{x},t) + \rho(\underline{x})]}{\sigma_y(\theta(\underline{x},t))} \quad \ldots\ldots (2)$$

If NSR < 1 at all points and all times, strict shakedown has been demonstrated.

(ii) Overall shakedown

ADAPT will also converge to a solution over the bulk of the structural volume, when small local volumes have values of NSC in excess of unity:

Shakedown (NSR $<$ 1) is shown over the bulk of the structure.

For conservatism, 80 per cent of any structural section is required to have NSR < 1.

Regions where NSR $>$ 1 are interpreted as zones of alternating plasticity.

(iii) Potential Ratcheting

ADAPT may converge to a solution in some cases but show NSR $>$ 1 across much or all of an entire structural section. Under these conditions, ratcheting cannot be excluded as a possibility and the design is therefore rejected.

In more severely loaded cases, ADAPT may fail to converge, indicating that the loading is well beyond shakedown, and the design must be rejected.

In an extreme case where no initial value of $\underline{\rho}^L(\underline{x})$ can be selected over large volumes of the structure, showing that shakedown is not possible the calculation is stopped. This is the case where at too many positions the translated elastic stress trajectory is too extensive to fit inside the yield surface.

4. ASSESSMENT OF DAMAGE USING THE SHAKEDOWN METHOD

4.1 Selection of the Effective Yield Stress

It is important to appreciate that in a structure in a cyclically steady state of stress, the material may undergo stress controlled, rather than strain controlled loading. This is due to the possibly significant presence of primary loads or elastic follow up, and one or both of these effects might operate in virtually any type of structure. It follows that the results used to select an effective yield stress to be used in shakedown analysis should include cyclic load controlled tests, and not only strain cycling tests (which cannot show strain accumulation effects).

A particular reason for using stress controlled testing is that it is able to reveal instability of the response of the steel to axisymmetric repeated loading, which would not be detected in strain cycling tests. This instability is a particular form of material ratcheting often associated with time-dependence in material behaviour. It may occur not only at high temperatures but also, as in type in 316 stainless steel below about 250°C, when 'cold creep' effects are seen.

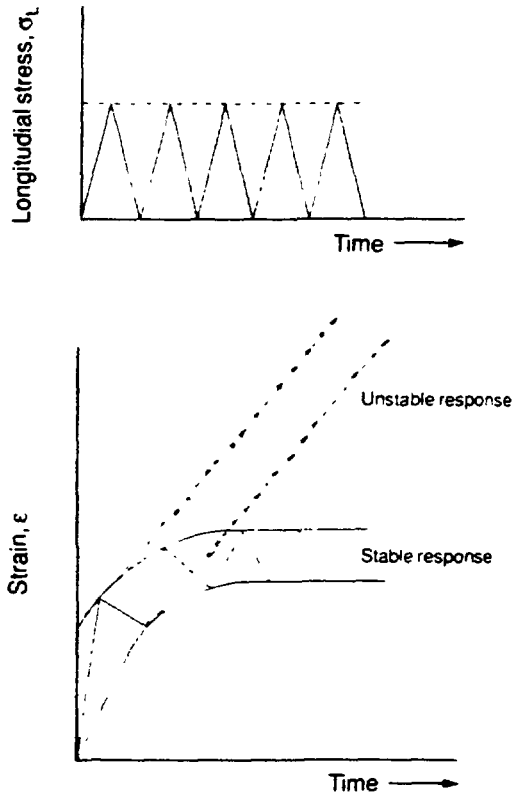

Fig. 4. Schematic strain response to load-controlled cyclic deformation testing

The scheme for performing the material deformation tests is one where a repeated tension of fixed amplitude is applied to a specimen at constant temperature (Fig. 4). The strain response of the test specimen is one of two types, namely:

(i) Stable, or

(ii) Unstable

The response is termed stable if the total strain is asymptotic within a designated number of cycles to a value below a suitable strain limit. The number chosen was 500 for EFR applications of type 316 stainless steel but the strain usually stabilised in many fewer cycles. Unstable response corresponded to the case where the total strain was still increasing at the end of 500 cycles.

For this application of the shakedown method, the choice was made of a maximum strain accumulation of two per cent. The effective yield stress is therefore limited by the results of the deformation tests corresponding to between one and two per cent total accumulated strain at each temperature.

At temperatures below 250°C there was some instability and to ensure a stable response beyond 500 cycles it was necessary to adopt a lower accumulated strain limit. In fact, the stress at the onset of instability was chosen as the effective yield stress under these

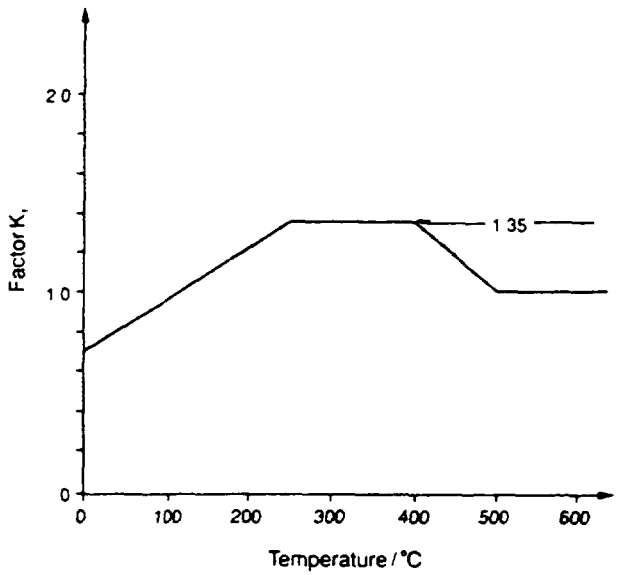

Fig. 5. Factor K_1 for type 316 steel

conditions. The results of the tests were normalised by the 0.2 per cent proof stress of the test material at the test temperature (Sy), and represented as K_1:

K_1 Sy = min (stress at instability,
stress for one to two per cent strain)

From test results obtained with dwell periods at 500°C and above it appeared possible that the strain hardening due to plastic deformation might be retained at higher temperatures over long service periods.

The selected value of K_1 is shown versus temperature in Fig. 5 for Type 316 austenitic stainless steel. Initially a conservative assumption was used for K_1 (reducing to 1.0 at temperatures above 500°C), however, more recent evidence has suggested that K_1 could be maintained at the value of 1.35 up to 580°C. The chosen yield stress of K_1Sy was also found to correspond to adequately small strain ranges after cyclic hardening.

4.2 Effect of Creep on Shakedown

The use of an analogy between creep and plasticity was proposed as a basis for introducing the effects of creep into the shakedown analysis. A requirement was however that the loading should be within the short term strict or overall shakedown limit.

Many different types of loadings and structural geometries occur in practice, leading to a wide variety of stress-strain responses in the steady cyclic state. Two extreme cases can be identified, namely a structure in which primary stresses dominate and at the other extreme a case where the loading is essentially kinematic. Most high temperature structures are subject to cyclic loading between these extremes. The possible types of behaviour at a particular point of a structure are illustrated in Fig. 6 and 7 where it is assumed that the creep dwell takes place at the maximum stress in the stress cycle. In Fig. 6 behaviour is elastic perfectly plastic and emphasis is upon low stress changes with time during the dwell period.

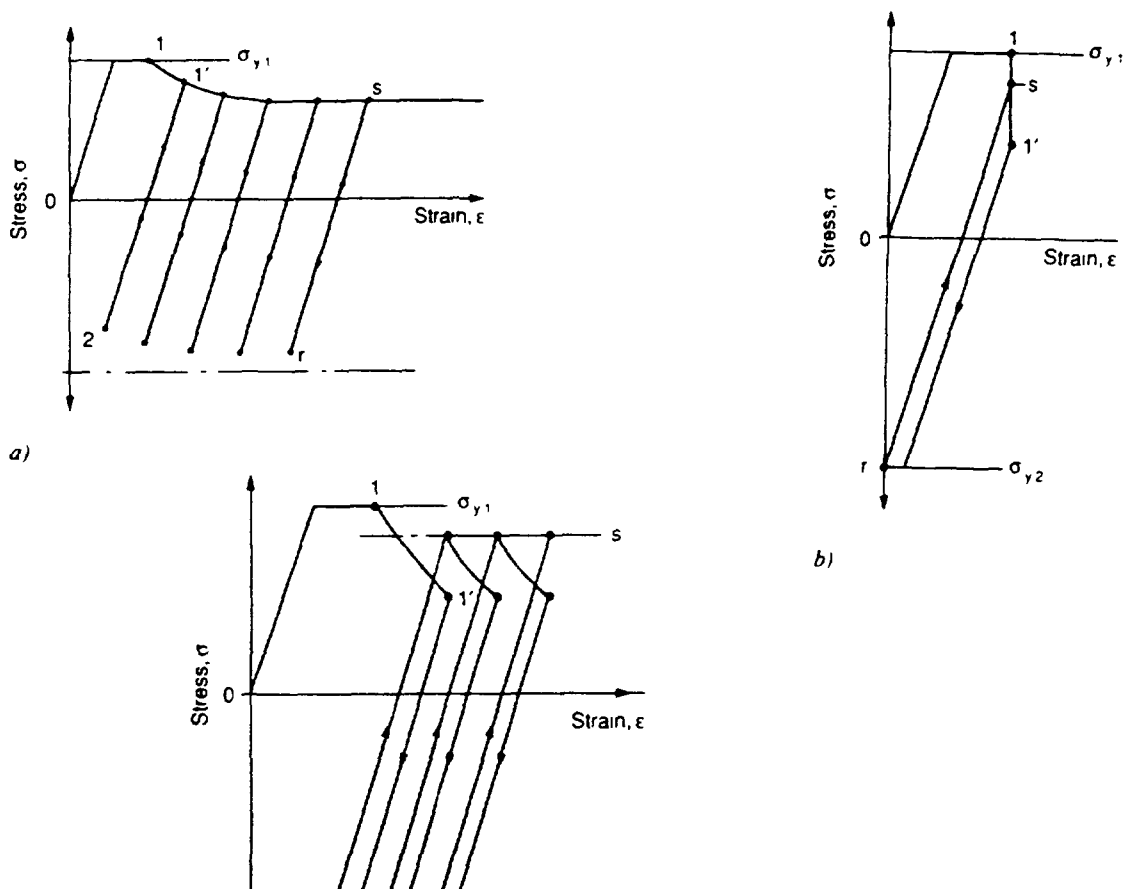

Fig. 6. Stress changes with time during creep assuming elastic–plastic behaviour

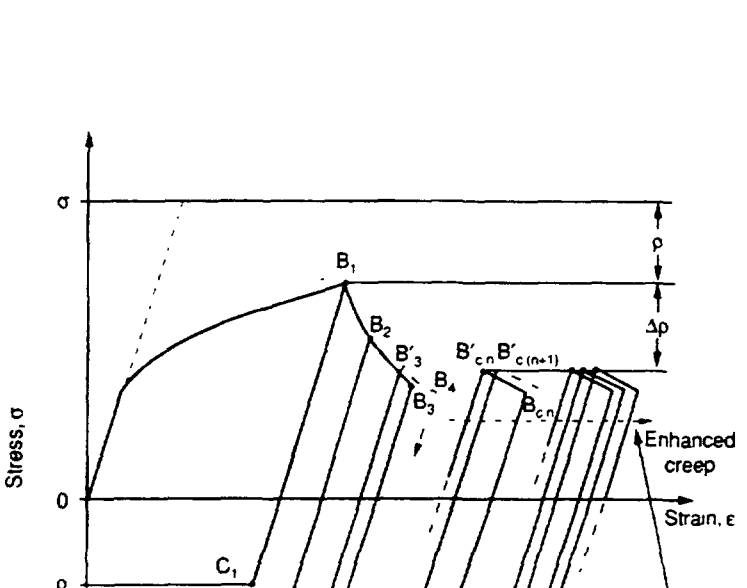

Fig. 7. Stress–strain response under creep modified shakedown showing enhanced creep (some primary stress present during dwell; uniaxial loading assumed)

4.3 Code Assessment

The major steps in the code assessment of a structure and loading using the shakedown method are as below.

(i) Check primary stress limits

The primary stress limits for negligible and significant creep conditions must be satisfied before proceeding to steps (ii), (iii) and (iv). These limits are not discussed here and are given in conventional design codes such as ASME and RCC-MR.

(ii) Demonstrate conformity with the shakedown limit for either strict or overall shakedown

The conditions of steps (i) and (ii) must be satisfied before proceeding to steps (iii) and (iv).

(iii) Calculate creep and fatigue damage

(iv) Calculate accumulated strain

4.3.1 Calculation of Creep Fatigue Damage and Strain Accumulation

(i) Strict shakedown

For a structure and loading which have been shown to be within the short term shakedown limit, the procedure for calculation of the creep damage is outlined in the following steps.

1. Determine the reference stress σ_o and reference temperature θ_o.

   The total stress intensity at all points and times is given by:

   $$\sigma_s (\underline{x},t) = [\sigma^E(\underline{x},t) + \rho(\underline{x})] \quad \ldots\ldots (3)$$

   with corresponding temperature:

   $$\theta(\underline{x},t)$$

Taking the time point at the start of a dwell period (t') locate the point ($\underline{x}$') for which the total stress intensity $\sigma_s(\underline{x}'t')$ in combination with the temperature $\theta(\underline{x}',t')$ produces the shortest time to rupture read from minimum stress to rupture curves.

The reference stress and temperature for the dwell are then:

$$\sigma_o = \sigma_s (\underline{x}',t') \quad \ldots\ldots (4)$$

$$\theta_o = \theta(\underline{x}',t') \quad \ldots\ldots (5)$$

2. Calculate the reference stress correction factor, K_2:

$$K_2 = 1 + 0.13\,(X-1) \qquad \ldots\ldots (6)$$

$$X = \frac{(\sigma^E)_{max}}{\sigma_o} \qquad \ldots\ldots (7)$$

In this expression $(\sigma^E)_{max}$ is the maximum value on the section containing $\underline{x}$' of the equivalent stress corresponding to $\underline{\sigma}^E(\underline{x},t')$. K_2 is not taken less than 1.0.

3. Calculate creep damage, W:

$$W = \frac{t_{tot}}{T_r} \qquad \ldots\ldots (8)$$

Here t_{tot} denotes total duration of steady operation where Tr is the minimum time to rupture at temperature θo and constant stress level equal to $K_2\ \sigma_o/0.9$

4. Optimise residual stress field

The above calculation of creep damage is performed using the results of a shakedown analysis which showed the loading to be within the strict shakedown limit. The residual stress field may not therefore be unique. The possibility exists therefore that the residual stress field can be optimised to reduce the reference stress level and so reduce the calculated creep damage. The procedure to be used is the following:

If the loading is below the short-term strict shakedown limit, perform ADAPT analyses with decreasing trial values of fictitious hot yield stress until the limit is reached. Determine the corresponding reference stress and repeat the damage evaluation.

5. Calculate fatigue damage.

Obtain the elastic stress intensity range $\Delta\sigma_{el}$ at the point with the highest value of shakedown criterion and when the creep deformation is not negligible.

The total strain range for fatigue damage assessment is obtained by calculation of the elastic plus plastic strain range taking into account the effect of stress relaxation during the dwells. The total strain range is calculated from $\Delta\sigma_{el,r}$ which is the sum of the elastic stress range $\Delta\sigma_{el}$ and $\Delta\sigma_{rd}$ the stress relaxation drop.

(a) Calculation of $\Delta\sigma_{rd}$

Determine $\Delta\sigma_{rd}$ as the stress relaxation drop over the period from starting stress σ_a where $\sigma_a = \sigma_s$ (x,t) the stress intensity at the time point at the beginning of the dwell.

$$\Delta\sigma_{el,r} = \Delta\sigma_{el} + \Delta\sigma_{rd} \qquad \ldots\ldots (9)$$

(b) Calculation of $\Delta\epsilon_{tot}$

Determine the total strain range $\Delta\epsilon_{tot}$

$$\Delta\epsilon_{tot} = \Delta\sigma_{el} + \Delta\epsilon_{pl} + \Delta\epsilon_{vol} \quad \ldots\ldots (10)$$

$$\Delta\epsilon_{el} = \frac{2\,(1+\nu)\,.\,\Delta\sigma_{el,r}}{3E} \quad \ldots\ldots (11)$$

$$\Delta\epsilon_{vol} = (K_\nu - 1)\,\Delta\epsilon_{el} \quad \ldots\ldots (12)$$

K_ν accounts for the changes in Poissons ratio in plasticity. $K\nu$ is taken from material property data given in design codes such as RCC-MR for the temperature θ_{max} and stress range $\Delta\sigma_{el}$.

$\Delta\epsilon_{pl}$ represents an enhancement to the elastic strain due to the occurrence of plasticity and measured by the intersection of the material cyclic curve and the hyperbola, $\Delta\sigma\,\Delta\epsilon$ = constant passing through the point $(\Delta\epsilon_{pl}, \Delta\sigma_{pl})$ Fig. 8, the Neuber Law.

(c) Calculation of fatigue damage V

From the fatigue design curves for the material determine the allowable number of cycles M_r at the strain range $\Delta\epsilon_{tot}$.

$$V = \frac{n_r}{M_r} \quad \ldots\ldots (13)$$

where n_r is the number of design cycles of type r.

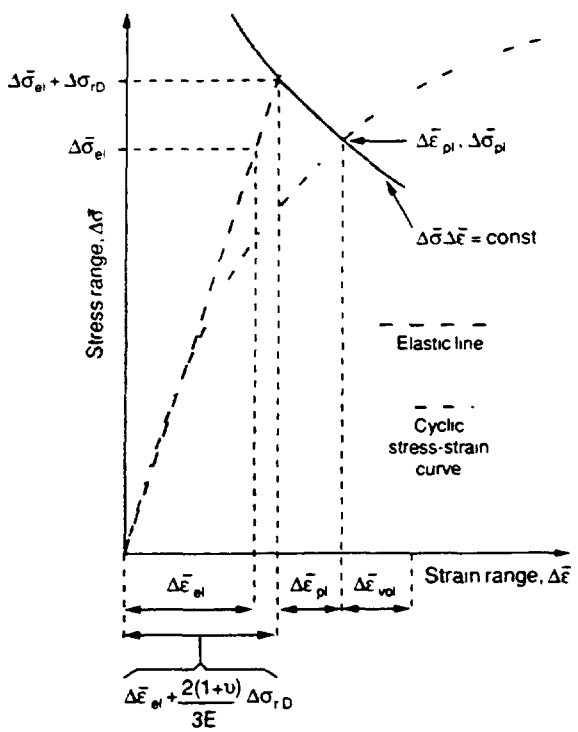

Fig. 8. Calculation of elasto-plastic strain range when creep is significant

6. Calculate Creep-Fatigue Damage

Check for a given point whether the values of W ad V are inside the allowable area a the creep/fatigue interaction diagram. If the point lies outside the diagram the creep/fatigue damage is acceptable.

Repeat steps (a) to (d) for all points where creep and fatigue damage may be considered significant to confirm that all points be with the allowable area on the interaction diagram.

7. Calculate the Strain Accumulation

The creep strain is read from an average isochronous stress-strain curve at the reference stress and temperature and total duration of steady operation, by subtracting the short-term plastic strain given by the curve for zero time:

$$\epsilon_c = \epsilon_c (\sigma_o, \theta_o, t) \quad \ldots\ldots (14)$$

The plastic strain is read from an average monotonic stress-strain curve:

$$\epsilon_p = \epsilon_p (\sigma_o, \theta_o) \quad \ldots\ldots (15)$$

The total accumulated strain summed over all cycles should be limited to two per cent:

$$\epsilon_p + \epsilon_c < 2\% \quad \ldots\ldots (16)$$

(ii) Overall shakedown

As noted earlier, ADAPT will converge to a solution in cases of overall shakedown with a minimum elastic (strict shakedown) core of 80 per cent of the structural section. Regions outside the core are deemed to undergo alternating plasticity. At this stage of the development of shakedown methods and of ADAPT in particular, it is considered desirable to check that the results obtained in the analysis do conform with the physical interpretation. The first step therefore is to check that the ADAPT solution in regions of non-satisfaction of the shakedown criterion, corresponds to symmetrisation of the stress cycle with respect to the hot and cold yield surface. If the above check is satisfactory, the calculation of creep damage and creep strain then proceeds as for the strict shakedown case in item (i) above.

For the calculation of fatigue damage the procedure is again as described in (i) except that the value of σ_{rd} is calculated assuming a starting stress of $\sigma_a = 1.5S_Y$.

It is noted that there is no potential for optimisation of the residual stress in this case, because the residual stress field has a unique definition at the shakedown limit. Beyond this limit the residual stress is subject to some cyclic plasticity and is not constant over the cycle. However, for moderate excursions, as in overall shakedown, the approximately symmetrising estimate obtained above is adequate for evaluation of creep effects, with the K_2 factor in place.

5. FBR APPLICATIONS

To demonstrate the type of design applications permitted by the procedure some example cases have been selected:

(a) Tee butt geometry with small fillet radius.

(b) Free surface investigation of a cylindrical structure partly immersed in sodium.

(c) Thin plate subject to thermal shock.

(d) Large diameter plate subjected to thermal transient loadings.

(e) Tubeplate of an intermediate heat exchanger.

(f) Secondary circuit piping structure.

The latter two cases represent an extension of the method to different forms of structure involving complex geometries and alternative finite element formations. Both of these applications are at an early stage of development but are expected to show significant advantages with respect to creep and fatigue damage estimation compared with existing application of elastic code methods.

5.1 Tee Butt Geometry with Small Fillet Radius

This structure consists of two plates welded together in a T-type joint. The weld and parent materials are taken to have the same properties and only the concentration effect caused by the geometry of the butt weld is examined. Finite element calculations were carried out on a 2-D generalised plane strain idealisation with only two plates modelled because of symmetry conditions (Fig. 9). The upper fillet region gave a maximum stress concentration

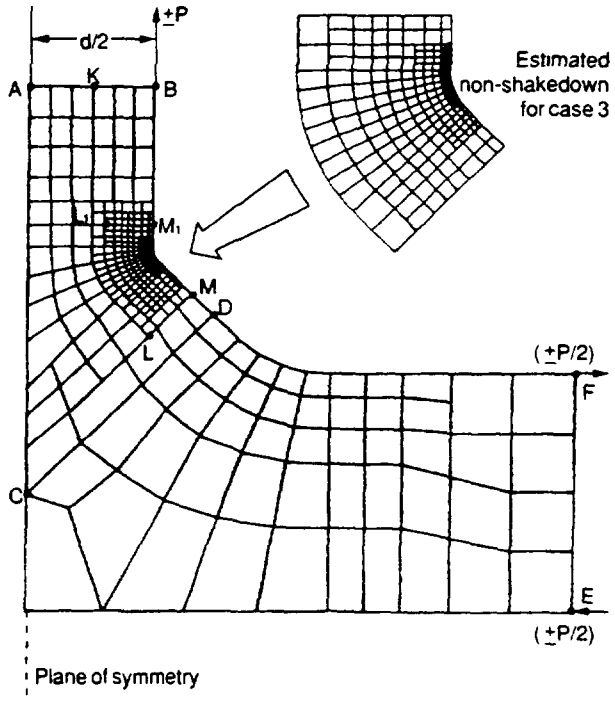

Fig 9. Tee-butt weld problem – finite element model

factor of 2.1, the accuracy of the finite element discretization verified by comparing elastic results with different degrees of refinement. The material properties assumed were for type 316 stainless steel. For inelastic calculations plasticity parameters of a form appropriate for The Oak Ridge National Laboratory (ORNL) constitutive laws were used.

The loading cycle consists of a variable bending moment applied at different temperatures. The moment loading M is applied at the vertical and horizontal legs by a combination of concentrated forces and kinematic constraints to simulate locally pure bending defined by the nominal bending stress σ_{nom} on the vertical leg. The temperatures change proportionately with mechanical load from 540°C to 370°C and sufficiently slowly that no thermal stresses were generated. Three test cases were examined, the details of which are given in Table 1. Problems 1 and 2 were cases where the nominal stress range was 86% of the strict shakedown limit (evaluated by the elastic-perfectly plastic analysis). Problem 3 had a nominal stress range well above this strict shakedown limit. This case was also examined by inelastic analysis first with no creep effects and then with 1000 hr hold period included at the hot condition, using plasticity properties **including** hardening.

5.1.2 Shakedown Analysis and Damage Assessments

The numbers of iterations needed to achieve shakedown are given in Table 1. The result for the steady cyclic stress path at the peak positions in case 2 required seven iterations (equivalent to elastic solutions). This compares favourably with the inelastic analysis which required three times as many solutions. For case 3 shakedown was achieved in an overall sense and convergence was found for practical purposes after about 7 iterations although there were minute changes in the estimated non-shakedown area up to 10 or 11 interactions, this area being conservatively represented with respect to all the inelastic analyses (Fig. 9).

TABLE 1. T-BUTT WELD JOINT, DETAILS OF TEST PROBLEMS

Problem Number	σ_{Hnom} (MPA)	θ_{Hnom} (°C)	σ_{Cnom} (MPA)	θ (°C)	ADAPT No. of Iterations
1	100	540	6	370	5
2	130	540	36	370	7
3	131	540	-40	370	7 to 11

Fatigue damage estimates were made for case 3 using the strain enhancement procedures and compared with estimates from elasto-plastic-creep analyses including hardening. Comparisons were also made with results from elastic assessment routes in design codes ASME N-47 and RCC-MR. The various estimates of strain range are summarised as shown in Table 2.

For the cycle with no dwells, the N-47 estimate is closest to the value obtained in the finite element analysis. This occurs as a result of the different specification of cyclic stress-strain curves. When creep is significant, both N-47 and RCC-MR were shown to be more pessimistic than the shakedown method.

TABLE 2. T-BUTT WELD JOINT, COMPARISON OF STRAIN RANGES (%)

Assessment Method	Cycle with No Dwells	Cycle with Dwells
FE inelastic analysis	0.167	0.169 (6th cycle)
Shakedown method	0.129	0.279
RCC-MR	0.233	0.362
ASME CC N-47	0.186	0.378

5.2 Free Surface Investigation of a Cylindrical Structure Partly Immersed in Sodium

This example is an axisymmetric 316 stainless steel shell of 20 mm thickness which has hot sodium at 550°C on the inside and cold sodium with a free surface on the outside at 395°C. Above the cold sodium is argon gas which is assumed to be a perfect insulator (Fig. 10)

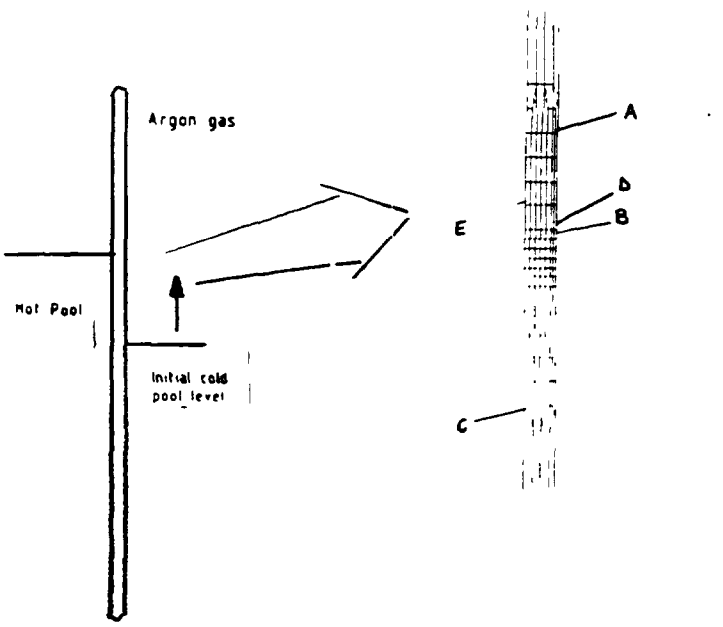

Fig. 10 Cylinder with cold moving surface

The cylinder is subjected to 300 transients where the cold sodium rises rapidly by 1000 mm over a 20s period. After 20 seconds temperatures reduce slowly on both sides of the cylinder down to a uniform 395°C which is followed by a slow return to the starting conditions and a 1000 hour dwell period at which creep is considered to be significant. Above the cold pool surface the metal is at a constant temperature of 550°C. Below the cold pool the outer metal surface is thermally shocked while the temperature on the hot pool side is largely unchanged.

5.2.1 Details of the Analysis

The load cycle was divided into 24 steps with 18 steps representing the rising fluid. Both elastic and inelastic analyses were performed using twenty load steps. Kinematic hardening was used to represent the plasticity together with a subroutine for creep estimation for the inelastic calculations for the shakedown calculation. The residual stress was estimated using the post processor ADAPT.

Using design values of yield stress (K_1S_y) it was not possible to achieve strict shakedown because of peak stresses arising in the structure during the rapid rise in the colder sodium. However it was possible to find a residual stress field that satisfied overall shakedown criterion and nowhere did shakedown exceed 15% of the section. The reference stress and reference temperature at the most highly loaded point was 142 MPa and 543°C respectively.

The results of the creep/fatigue damage assessment for this point are shown Table 4.

TABLE 3. COMPARISON BETWEEN SHAKEDOWN AND INELASTIC DAMAGE ASSESSMENTS FOR MOVING TEMPERATURE FRONT PROBLEM

Shakedown Method	Fatigue	Creep
	0.09	2.94(0.05)
Inelastic analysis	> 0.03	0.86
RCC-MR	-	(0.25)

( ) Creep in compression assumed non-damaging

The shakedown assessment has proved relatively conservative but the following issues were raised:

(i) The positions of maximum creep and fatigue damage were not consistent between the two assessments.

(ii) Considerable reduction of conservatism was achieved if an account was taken of compressive creep being less damaging than tensile creep. Further reduction in conservatism would be possible if only 'tensile' creep damage was counted in the shakedown assessment.

(iii) The ADAPT residual stress distributions agree very well in shape with those of inelastic analysis. However, a shift of values - nearly uniform along each surface - causes appreciable differences in the calculated stress-intensities for the two methods and probably leads to the differences in positions of maximum creep and fatigue damage estimates,

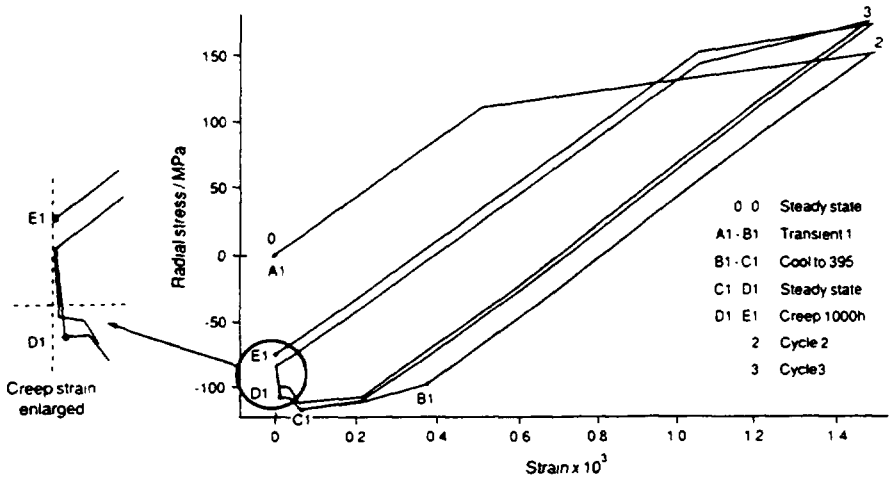

Fig. 11. Plate under thermal shock, elastic-plastic-creep calculation

5.3 Thin Plate Subject to Thermal Shock

5.3.1 Description of the Problem

This example considers a thermal transient on a stainless steel circular flat plate 20 mm thick and of large radius which is immersed in sodium at 585°C. The plate undergoes 300 thermal downshock cycles on the top and bottom surfaces with temperatures reducing to 395°C over a period of 100s. The temperature on the bottom surface reduces more quickly than the top surface giving rise to through-wall temperature differences of approximately 60°C after 4s, reducing to 22°C after 10s, followed by a slow re-heat to 585°C.

The loading cycle includes a 1000 hr creep hold period at 585°C. 2-D axisymmetric finite element elastic and elastic-plastic-creep calculations were carried out on an idealised section of the plate geometry. The inelastic analyses were performed using bi-linear approximations to the material behaviour, according to different detailed constitutive laws selected from alternatives in the RCC-MR code. A further case was investigated using an ORNL constitutive mode. The endurances of the plate were estimated from the calculated stress-strain loops for the third loading cycle. Fig. 11 shows the cyclic behaviour of a point on the lower surface using the ORNL constitutive law that gave the highest creep/fatigue damage.

5.3.2 Details of Shakedown Analysis and Damage Assessments

Convergence was found after four iterations of ADAPT. Strict shakedown was not found. There was a region of non-shakedown adjacent to the lower surface representing 7.5% of the section. This was less than 20% and therefore overall shakedown is assumed. Creep/fatigue damage estimates were made and compared with the results using RCC-MR elastic and inelastic code rules, as given in Table 3.

The table shows the creep-fatigue damage using the shakedown method, to be significantly lower than calculated using the present RCC-MR elastic code method but higher than calculated using the inelastic code route. Also because the shakedown analysis is based on elastic stress solutions the analysis steps are much simpler to perform than full inelastic analysis.

TABLE 4. COMPARISON OF CREEP-FATIGUE PREDICTION METHODS FOR THIN PLATE

Assessment Method	Creep Damage (W)	Fatigue Damage (V)
Elastic RCC-MR	174	0.2
Inelastic RCC-MR^{+}	2.25(0.1*)	0.05
Shakedown method	3.1 (0.14*)	0.13

* RCC-MR rule allowing for less damaging effects of compressive creep. (Note that this could not be used in the RCC-MR elastic assessment, since no estimate of stress components during the dwell is made).

\+ Highest value from inelastic calculations using ORNL model.

5.4 Large Diameter Plate Subjected to Thermal Transient Loadings

This example shows the application of the method to large 3-D shell type structures. The case chosen is a thin flat plate supported by a number of tubes. The plate has a number of holes drilled in it to allow sodium to pass through the plate. The study is to investigate stresses and creep/fatigue damage in the plate under thermal gradient conditions arising from temperature differentials in the sodium flow. The geometry and the resulting finite element mesh with a refined region for calculation of localised stresses is shown in Fig. 12. A

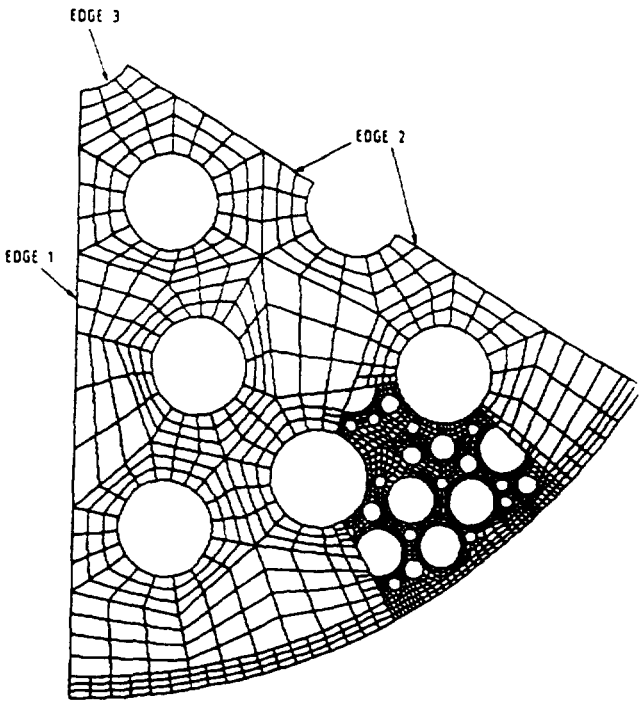

Fig. 12 Large plate - finite element model

temperature profile was applied to the complete mesh and a shakedown calculation carried out in accordance with the shakedown rules using the ADAPT post processor to estimate a constant residual stress field. A stress optimisation technique was used but a reverse application of the usual process. This was necessary since, the hot yield stress of the material was of an insufficient level to prompt the ADAPT programme to evaluate a residual stress. This in itself meant that the plate was globally within the strict shakedown limits, however, for creep/fatigue evaluation it was important to minimise the calculated plus residual stresses at the hot end of the cycle. For the plate therefore a lower yield stress (of 50 MPa) was selected initially and then this was increased until the strict shakedown limit had been achieved. The final calculation step in which shakedown was achieved in fact used a hot yield stress of 65 MPa.

Results of the subsequent creep/fatigue evaluation are shown in Table 5 for the highest stress point. Note that fatigue damage results are negligible as expected, however, creep damage estimates using the shakedown approach are lower than those predicted using the RCC-MR code elastic route.

TABLE 5. COMPARISON OF CREEP/FATIGUE ASSESSMENTS USING RCC-MR AND SHAKEDOWN METHOD

	RCC-MR Elastic Code Analysis		Shakedown Analysis	
	Top of Plate	Bottom of Plate		
Temperature	562	567	562	567
Stress range	135	110	135	110
Fatigue damage (V)	0	0	0	0
Creep damage (W)				
(Neglecting stress relaxation)	2.87	2.12	0.31	0.34
(Including stress relaxation)	1.91	1.48	-	-

5.5 Tubeplate of Heat Exchanger

Elastic methods are available which permit the modelling of the perforated regions of tubeplates under non-creep conditions as an axisymmetric continuum. American work is the basis of most of the current design methods resulting in the simplified procedures of ASME III. This approach has been developed to cover thick plates with triangular and square perforation patterns.

Work under significant creep conditions is less well established with the main emphasis in recent years coming from Japanese developments. Three studies were initiated by the European Commission DGXI, Environment, Nuclear Safety and Civil Protection, Working Group Codes and Standards, Activity Group 2[8].

The methods of assessing shakedown in high temperature structures as described above uses elastic results to indicate whether ratcheting will occur under specified loadings and to provide an estimate of the reference stress during periods of steady operation at creep temperatures. The purpose of this example (Fig. 13) was to extend the principles of shakedown to tubeplate design methods. One approach is to perform an elastic analysis using the full tubeplate geometry, however, an alternative strategy was devised based on tubeplate equivalent solid plate techniques as follows:

(i) Although not part of the shakedown method, there is a prerequisite to check that the primary stress limits are not exceeded. This would be done by following the tubeplate methods of ASME A8000 or RCC-MR for example

- If satisfied the following steps are undertaken:

- Establish the elastic stress history.

- Establish an effective yield stress for the equivalent solid plate region. This is a function of biaxiality ratio and the value used may correspond to the actual biaxiality ratio in the elastic calculations, alternatively the most pessimistic value of yield stress may be used. A further choice exists between the yield stress that corresponds to the limits of strict shakedown or that corresponding to overall shakedown. Initially the value for strict shakedown would be used.

- Determine the residual stress field which satisfies the usual self equilibrium conditions. This process is most easily carried out using the computer code ADAPT.

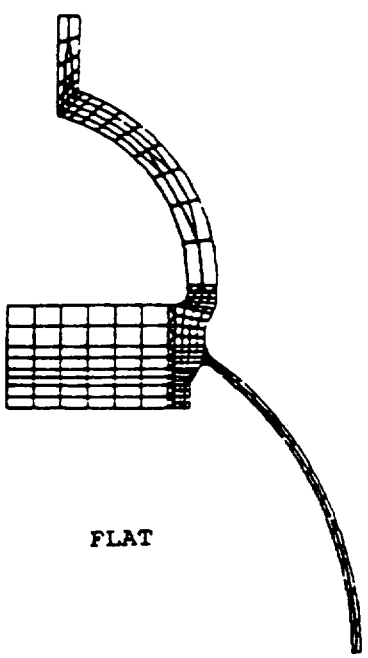

Fig. 13 Typical FBR tube plate

The determination of the yield stress was a significant part of the work performed, one approach being to carry out a shakedown calculation on a representative geometry and the other to use the stress function method. An investigation of an example case in fact showed a creep/fatigue damage prediction to be considerably lower than that of the conventional design code approach of ASME. However, this technique has not been extensively tested nor subjected to rigorous theoretical justification. At this stage in its development the technique is therefore applied with care and the results treated with caution.

5.6 Secondary Circuit Piping Structure

The work is at an early stage and involves the application of the shakedown approach to a piping structure as shown in Fig. 14. The work is funded by a European Commission DGXI, WGCS, Activity Group 2 on structural mechanics. Some preliminary calculations are underway to test the method using piping (elbow) elements in order to establish the suitability of the elements to cope with the ADAPT algorithms. A comparison of the results will be made with full inelastic analysis and with other simplified methods.

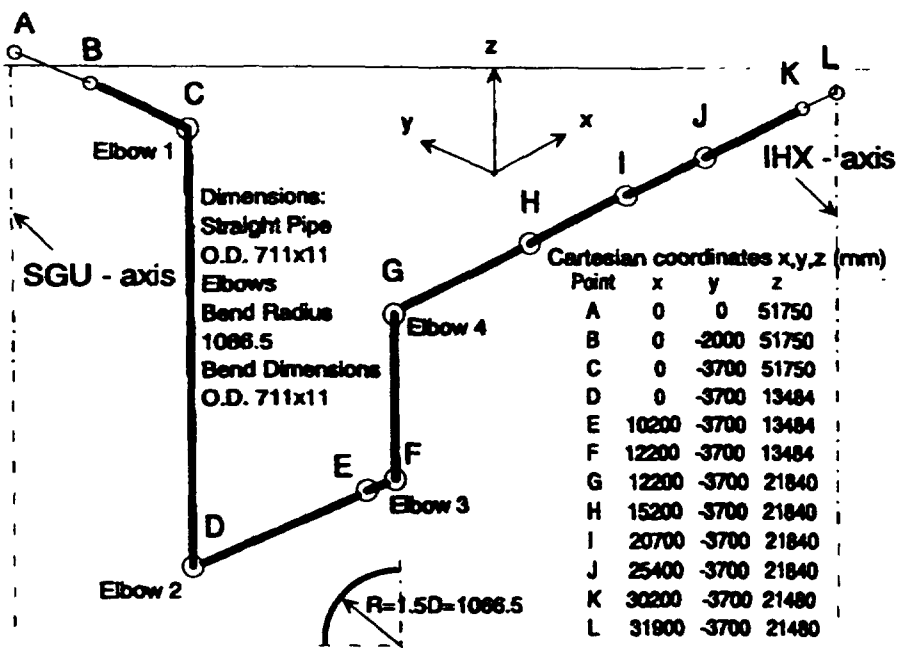

Fig. 14 Geometry of FBR secondary main circuit - pipe section IHX-SGU

6. RECENT DEVELOPMENTS

The shakedown design method has been accepted within European Fast Reactor project as a means of assessing a cyclically loaded high temperature structure against ratcheting, fatigue and creep damage. The above examples show the benefits available with respect to existing elastic and inelastic simplified methods. Despite the success further developments have been introduced particularly in the areas of creep-fatigue damage estimation.

6.1 Incorporation of Alternative Plasticity Algorithm

One such development is a modification of the ADAPT algorithm to provide a residual stress which gives a nearly symmetrical stress-trajectory in the case of overall shakedown[5]. This modification tested on performance trials, showed a slightly slower convergence but gave a higher degree of symmetrisation in areas of alternating plasticity giving a lower estimated value of elastic plus residual stress at the most severe stage of the cycle. The results were shown to be closer to those of inelastic analysis and gave a more realistic estimate of creep usage. In some cases these have led to higher estimate of stresses and higher creep damage. Incorporation of this algorithm in regions where conditions for strict shakedown are not achieved, but still within overall shakedown give results which are nearer to the condition where creep damage is minimised.

6.2 Incorporation of Elastic Follow-up and Strain Based Damage Estimates

Creep damage estimates are currently correlated using equivalent stress whereas it is desirable to allow an assessment using strain based damage rules. In order to allow this development some allowance would be required for elastic-followup effects and a value of elastic followup factor [9] was proposed[6,7] in conjunction with a suitable creep law in order to give conservative estimates of stress-reduction during hold periods for estimating stress based creep damage. For component estimates for strain based damage it was assumed that strongly creeping regions are localised at a small region on the surface and a method based on bounds for computer changes devised which enables bounds to be obtained for the creep damage increment. This extension has been developed to an initial stage but requires more work and trials in order to provide a simple assessment approach without undue pessimisms.

6.3 Inclusion of Mod 9Cr1Mo Steel

In principle there appears to be no difficulty in providing a value of K_1S_y for Mod 9Cr1Mo steel over the defined operating temperature range. However, results of tests are sparse. Work is underway within a CEC funded WGCS study contract to estimate appropriate yield stress values from creep/fatigue tests and to perform some initial benchmarks.

7. DISCUSSION AND CONCLUSIONS

7.1 Usefulness of Shakedown as a Design Tool

Significantly experience in FBR design suggests that the loading of structures must fall within the overall shakedown limit if creep and fatigue damage rates are to be acceptable over a plant lifetime of 40 years.

From the foregoing description and examples it should be clear that use of the principle of shakedown fulfils the following design purposes:

(i) It excludes ratcheting.

(ii) It limits strain accumulation

(iii) It provides a basis for creep damage calculation and

(iv) It permits strain range prediction for fatigue analysis in creep conditions

The advantages of the shakedown method with regard to implementation are first that it involves only elastic analysis in determining the shakedown state, second that this obviates the need for time-consuming and costly cyclic inelastic analysis, and third that the problem of definition of complicated constitutive laws is avoided.

The overall advantages of shakedown as a design route are that it provides a powerful physical description of structures subject to cyclic loading; it goes directly to the steady cyclic state without the need to evaluate the detailed intermediate processes; it is a procedure of general applicability and it provides conservative assessments of design suitability which are potentially less pessimistic than assessments made by traditional code routes.

Shakedown assessments can be made for a wide variety of loadings and geometries at less computational effort and complexity than complete inelastic analysis.

Comparison of creep/fatigue endurance against elastic design code methods show less conservatism and allows specialized rules that enable the less damaging effects of creep under compressive stress in stainless steel to be utilised with elastic predictions. The creep/fatigue damage estimates were shown to be conservative with respect to full elastic-plastic creep analysis, but less pessimistic than rule-based methods.

REFERENCES

[1] ROSE R T, Elastic route design based on creep modified shakedown. 2nd International seminar on Standards and Structural Analysis in Elevated Temperature Applications for Reactor Technology, Venice, October 1986

[2] ROSE R T, WHITE P S, Shakedown design methods for high temperatures. Recent advances in design procedures for high temperature plane. I. Mech. E, November 1988

[3] TOULIOS M, WHITE P S, BUCKTHORPE D E, Simplified design methods by shakedown and an algorithm for F.E. implementation. Applied Solid Mechanics 4 Conference, University of Leicester, 1991

[4] BUCKTHORPE D E, WHITE P S, Shakedown based assessment of LMFBR structures. Conference on Structural Mechanics in Reactor Technology (SMIRT) 11, Transactions, E, Paper E07/2, Tokyo, Japan 1991

[5] BUCKTHORPE D E, WHITE P S, Incorporation of alternating plasticity in the shakedown method. Conference on Structural Mechanics in Reactor Technology (SMIRT) 12 Transaction, E, Paper C04/2, Stuttgart 1993

[6] BUCKTHORPE D E, WHITE P S, Recent developments in the shakedown method. SMIRT 11, Paper E07/1, Tokyo, 1991

[7] WHITE P S, BUCKTHORPE D E, Shakedown method with strain based damage assessments, SMIRT 12, Paper D04/5, Stuttgart, 1993

[8] BUCKTHORPE D E, GUINOVART J, KASTL H, Tubeplate design under creep conditions, SMIRT 13, Brazil, 1995

CREEP-FATIGUE EVALUATION METHOD FOR TYPE 304 AND 316FR SS

Y. WADA, K. AOTO, F. UENO
Power Reactor and Nuclear Fuel Development Corporation,
Oarai Engineering Center,
Ibaraki, Japan

Abstract

For long-term creep-fatigue of Type 304SS, intergranular failure is dominant in the case of significant life reduction. It is considered that this phenomenon has its origin in the grain boundary sliding as observed in cavity-type creep-rupture. Accordingly a simplified procedure to estimate intergranular damages caused by the grain boundary sliding is presented in connection with the secondary creep.

In the conventional ductility exhaustion method, failure ductility includes plastic strain, and damage estimation is based on the primary creep strain, which is recoverable during strain cycling. Therefore the accumulated creep strain becomes a very large value, and quite different from grain boundary sliding strain. As a new concept on ductility exhaustion, the product of secondary creep rate and time to rupture (Monkman-Grant product) is applied to fracture ductility, and grain boundary sliding strain is approximately estimated using the accumulated secondary creep strain. From the new concept it was shown that the time fraction rule and the conventional ductility exhaustion method can be derived analytically

Furthermore an advanced method on cyclic stress relaxation was examined. If cyclic plastic strain hardening is softened thermally during strain hold, cyclic creep strain behavior is also softened. An unrecoverable accumulated primary creep strain causes hardening of the primary creep, and the reduction of deformation resistance to the secondary creep caused by thermal softening accelerates grain boundary sliding rate. As the results creep damages depend not on applied stress but on effective stress.

The new concept ductility exhaustion method based on the above consideration leads up to simplified time fraction estimation method only by continuous cycling fatigue and monotonic creep which was already developed in PNC for Monju design guide. This method gave good life prediction for the intergranular failure mode and is convenient for design use on the elastic analysis basis.

For 316FR ss, at the operating temperature of LMFBR main components, the dynamic strain ageing is observed and the cyclic strain hardening becomes higher with strain hold. If this effect is considered, the above simplified method gave also good life prediction.

1. INTRODUCTION

Creep-fatigue evaluation is a key technology in structural design of LMFBR components, and the linear damage rule with the life fractions of fatigue and creep lives is widely used in high temperature plant design. Though the life fraction concept is simple for practical use, it is an empirical rule and not based on the failure mechanism. So in some material test cases estimated creep damage values are too small, because creep damages are sensitive to the thermal softening effect of stress level.

Fatigue life is usually evaluated by cyclic strain range, though creep is by stress. Therefore strain basis creep damage evaluation is consistent with that in fatigue. However in pure creep conditions simplified elastic analysis results can be applied directly by using stress basis life evaluation method, so stress basis is very convenient for structural design. For long years stress basis method is used in practical structural design of high temperature plants.

Considering the above background, in this paper, the consistency between stress and strain basis creep damage estimation methods is investigated using creep-fatigue test results on Type 304 ss.

2. LONG TIME CREEP-FATIGUE FAILURE OF TYPE 304 STAINLESS STEEL

Long time creep-fatigue tests for Type 304 ss were carried out, and obtained test results are shown in FIG.1 including shorter life ones[3]. The maximum test duration was about 15,000 hours. Figure 2 shows stress-strain relationship with elastic follow-up using electro-mechanical servo-system. The displacement between two shoulders is controlled, so the strain in parallel section is not constant during strain hold.

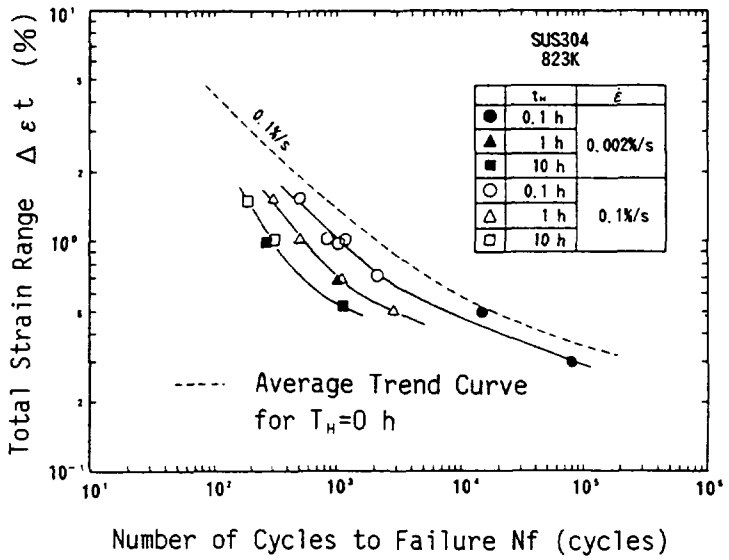

FIG.1 CREEP-FATIGUE TEST RESULTS OF TYPE 304 SS AT 827K

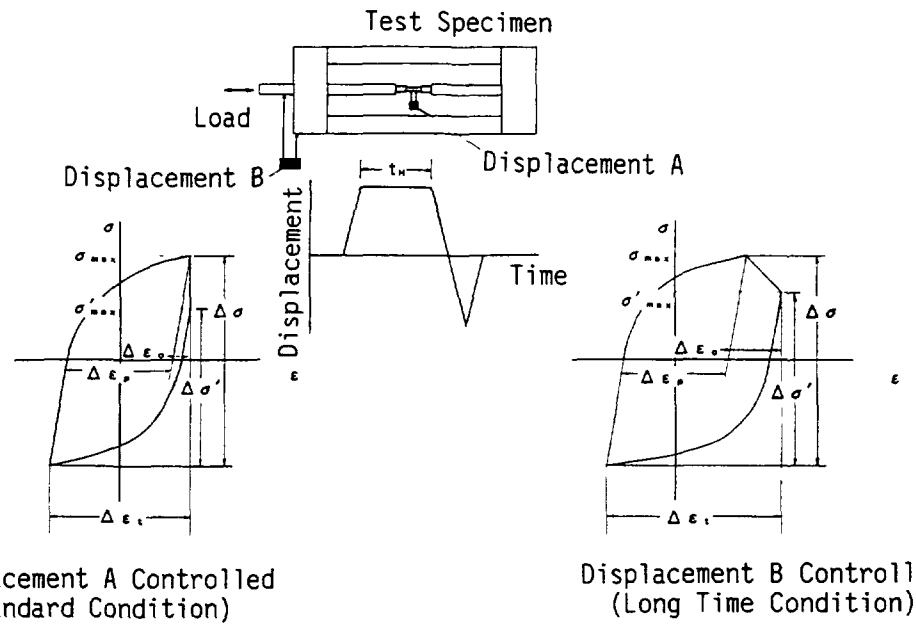

FIG.2 CYCLIC STRESS-STRAIN BEHAVIOR IN TEST WITH ELASTIC FOLLOW-UP

The difference between creep-fatigue lives with and without elastic follow-up was not large. The failure modes strongly depended on a strain hold time as shown in FIG.3. For the strain range of 0.3% and the hold time of 0.1hr, the transgranular failure occurred though time to failure was about 15,000 hrs. In the condition of longer hold time, the failure mode changed from transgranular to intergranular. In order to examine micro-structural damages at grain boundaries, creep cavities were observed by scanning electric microscope(SEM), and the area fraction of cavities was counted[3]. FIGURE 4 shows the relation of the area fraction of cavities to life fraction or failure mode. When life fraction was less than 0.2, the intergranular failure was dominant and the area fraction of cavities became larger.

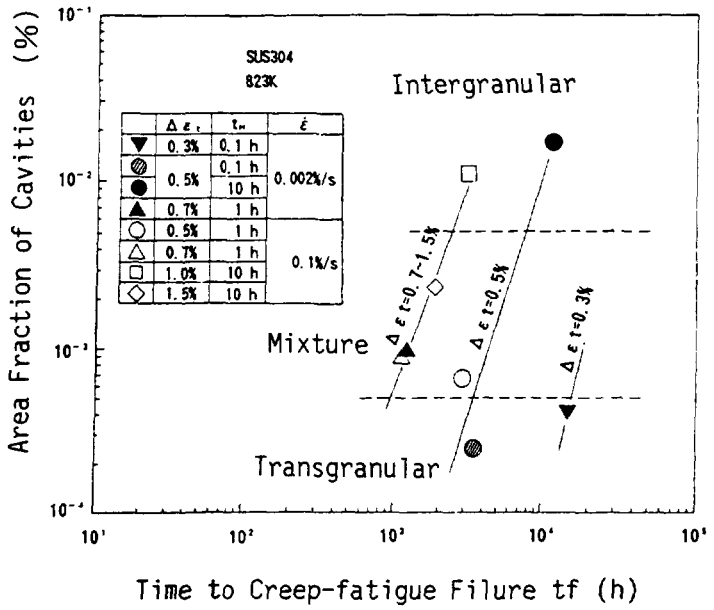

FIG.3 FAILURE MODE DEPENDENCE WITH TEST DURATION

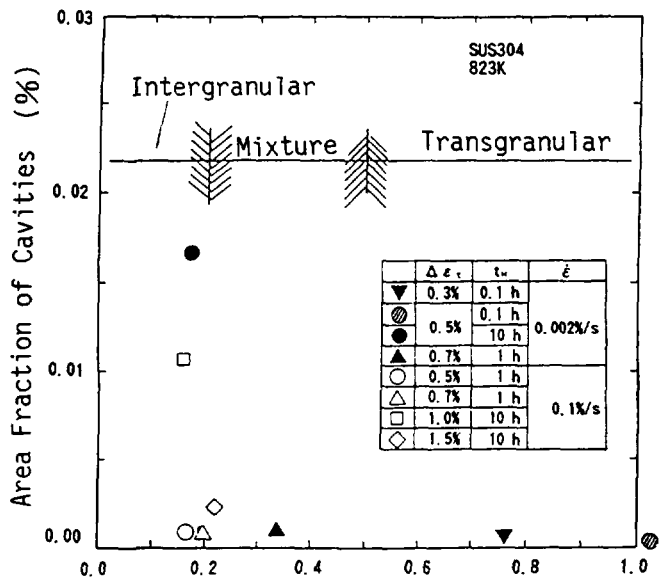

FIG.4 RELATION OF AREA FRACTION OF CAVITIES TO LIFE REDUCTION RATIO

Subsequently cavity growth behavior was analyzed destructively using interrupted damaged specimens. Creep-fatigue damaging test was carried out in the condition of 0.5% strain range and 10 hrs strain hold at 823K, because in this condition the area fraction of cavities is maximum. Interrupted number of cycles(creep-fatigue damages) are 1/50, 1/20, 1/10, and 1/5 of creep-fatigue life. FIGURE 5 shows typical observation result. Both of the cavity size and the number of cavities increased with the number of cycles. In the cavity nucleation stage cavities are distributed at random along grain boundaries, however in the micro-crack initiation stage cavities grow along grain boundaries perpendicular to loading direction.

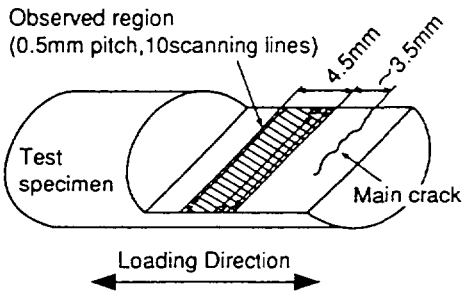

Observed region of cavity in creep-fatigue tested specimen

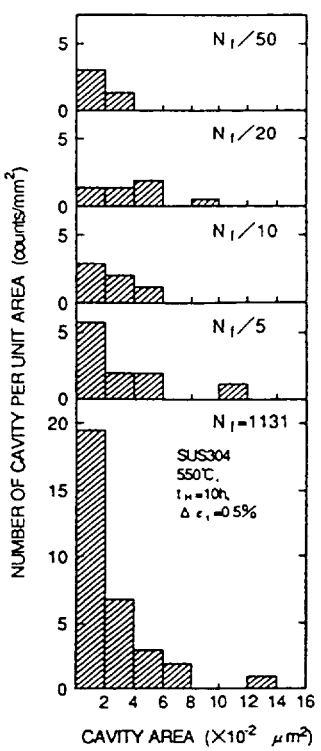

Histograms change of cavity under creep-fatigue loading

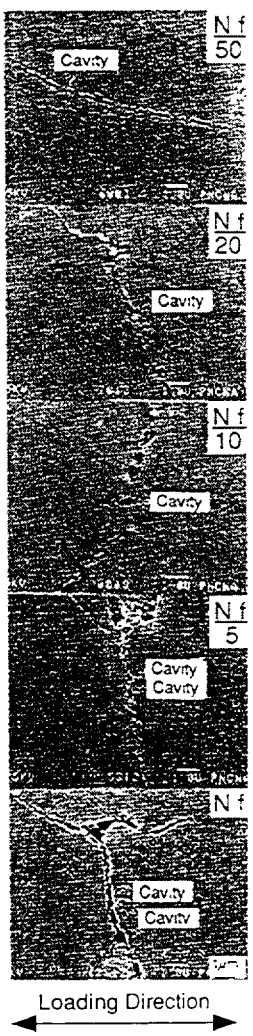

SEM photographs of cavity nucleation and growth along grain boundary (823K, 10h, 0.5%)

FIG.5 TYPICAL CREEP CAVITY OBSERVATION AND EXPERIMENTAL ANALYSIS RESULTS ON CREEP CAVITY GROWTH

3. EXAMINATION OF CREEP-FATIGUE FAILURE MECHANISM

In the case of the intergranular failure, it is considered that creep damage should be caused by grain boundary sliding, and a sliding strain limit has to be determined by the creep ductility. And in pure torsion creep-fatigue test, failure mode was different from that with tension hold in the condition of effective strain range of 1% and hold time of 1hr, and only a few small cavities were observed along a grain boundary. That is to say, the creep cavity nucleation and growth depend on the grain boundary sliding and the hydrostatic pressure. FIGURE 6 shows a schematic view of cavity growth and concept of the creep-fatigue failure. If the grain boundary sliding can be estimated by apparent creep strain, it is expected that the conventional ductility exhaustion method might be applicable. Apparent creep strain per cycle can be estimated by relaxed stress $\Delta\sigma_r$ during strain hold. However the primary creep strain which can recover during load cycling is redundantly counted in each cycle, so the estimated accumulated creep strain is too large to the grain boundary sliding.

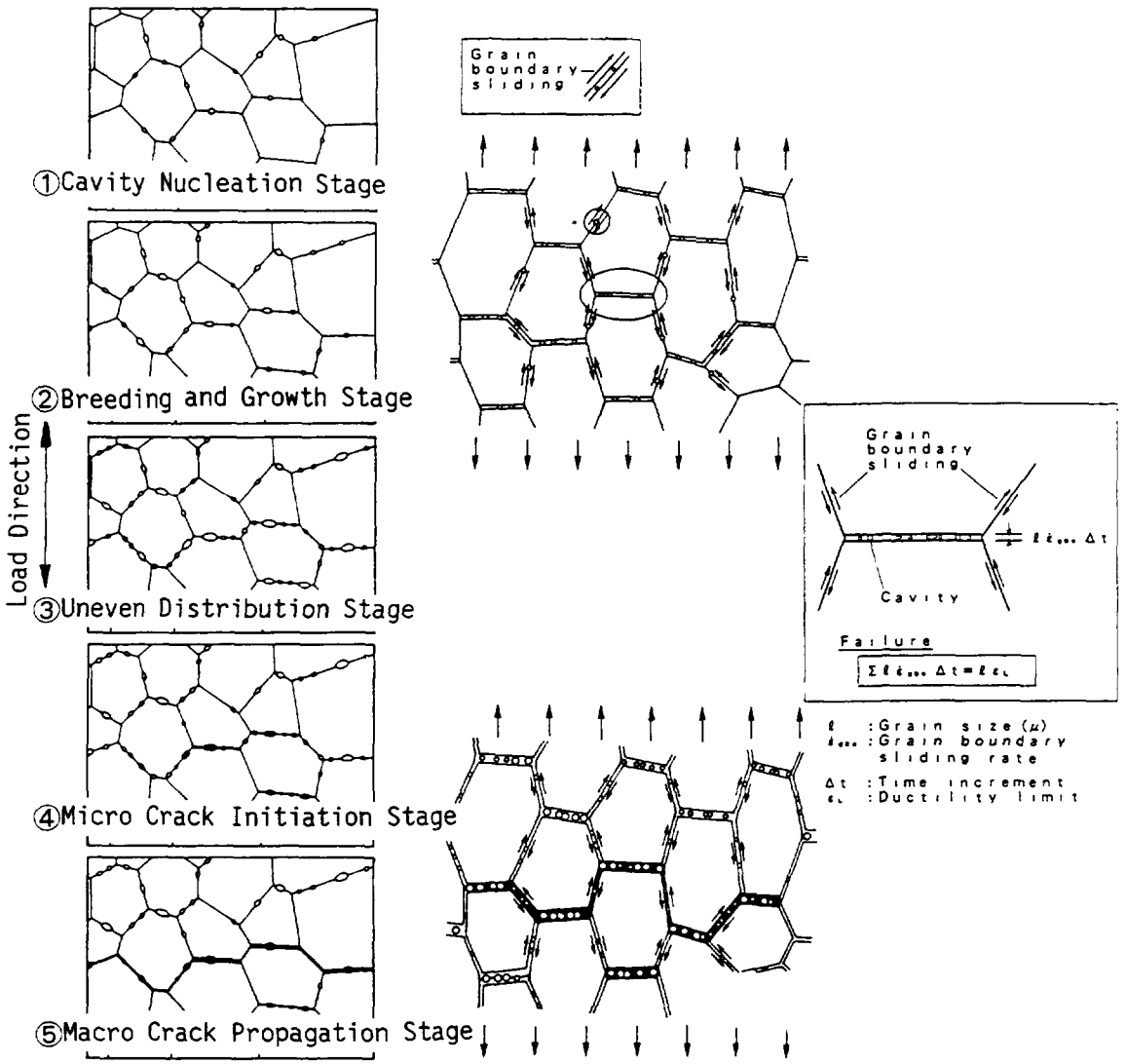

FIG.6 SCHEMATIC VIEW OF CREEP CAVITY GROWTH AND CONCEPT ON CREEP-FATIGUE MECHANISM IN CREEP DAMAGE DOMINANT CONDITION

Ductility exhaustion based on the grain boundary sliding is reasonable for the simulation of creep damage mechanism. Figure 7 shows the grain boundary sliding model composed by rigid parts(grain) and viscosity connection(grain boundary). Micro-crack initiation along grain boundaries perpendicular to loading direction can be easily simulated.

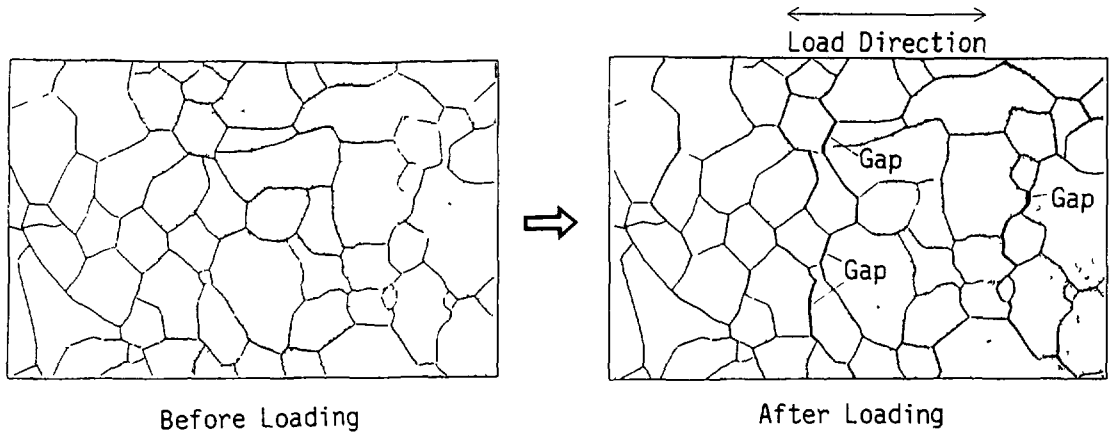

FIG.7 GRAIN BOUNDARY SLIDING MODEL AND MICRO-CRACK INITIATION

The conventional ductility using $-\ln(1-\phi)$ (ϕ:the reduction of area) is unsuitable, because this value is composed mainly of plastic strain in the stages of initial.loading, tertiary creep and necking. As the pure creep ductility Monkman-Grant product $\delta = \dot{\varepsilon}_2 \, t_R$ is a good parameter, because this value excludes recoverable primary creep. For Type 304 ss this value depends on the temperature, and it is about 5% at 823K in the condition of the time to rupture of 10,000hrs. In FIG.6 the grain boundary sliding strain; $D \, \varepsilon_c \, \Delta t/D$ (D: grain size) is not so large(less than 5%) at 823K and δ is reasonable rather than $-\ln(1-\phi)$.

Before the creep-fatigue failure is investigated, the ductility exhaustion rule in pure creep should be analyzed. The secondary creep rate $\dot{\varepsilon}_2$ is represented by the following equation.

$$\dot{\varepsilon}_2 = F \exp[-(Q-f(\sigma))/RT] \qquad (1)$$

Then the time to stress rupture can be evaluated using $\delta = \dot{\varepsilon}_2 \, t_R$.

$$t_R = \dot{\varepsilon}_2 / \delta = F \exp[-(Q-f(\sigma))/RT_K] / \delta$$

And from the above equations the following relation can be easily derived.

$$T_K \log(t_R+C) = -(Q-f(\sigma))/R, \quad \text{where } C = \log(\delta / F) \qquad (2)$$

The equation (2) is well-known as the effort by Larson and Miller. The master relationship between stress and creep life depends on eq.(1) and Monkman-Grant product $\delta = \dot{\varepsilon}_2 \, t_R$. Consequently there are two approaches for ductility exhaustion as shown in TABLE 1. One is the primary and secondary creep basis(conventional type), the other is only the secondary creep basis. The time fraction rule is induced from the latter basis.

$$\text{Creep damage} = \dot{\varepsilon}_2 \, \Delta t / \delta = \Delta t / t_R \qquad (3)$$

TABLE 1 FLOWDIAGRAM OF TWO EVALUATION APPROACHES FOR DUCTILITY EXHAUSTION METHODS

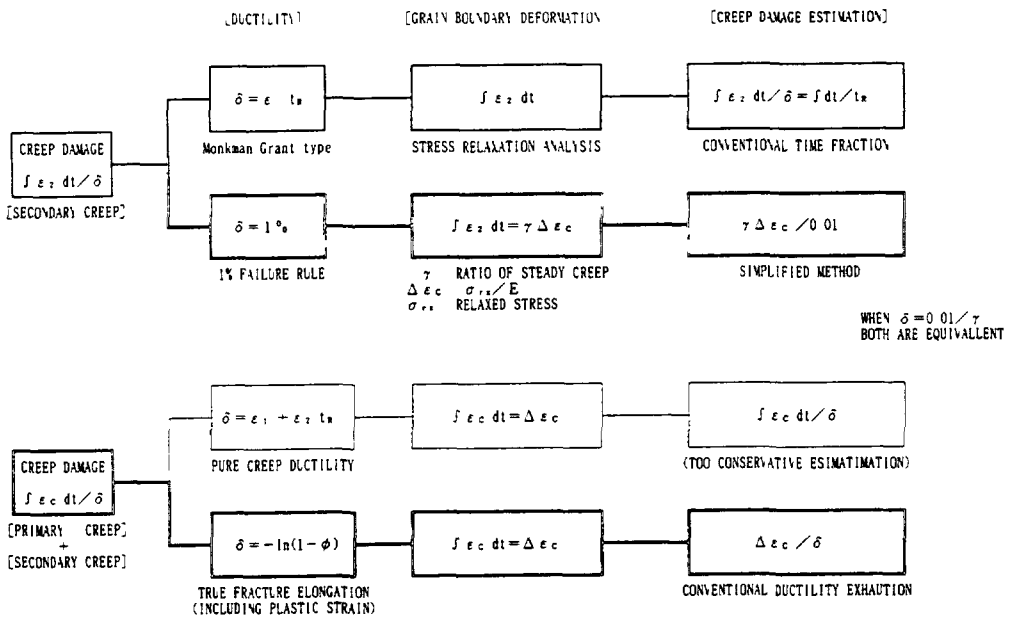

The time fraction rule is one of ductility exhaustion approaches, and there are several possibilities for estimation on ε_2 Δt and δ. In the conventional time fraction rule apparent material behavior is directly applied. In PNC presented procedure[2] as shown in FIG.8, stress relaxation behavior is analytically represented. Initial value of stress relaxation is determined by the cyclic stress-strain relation without strain hold, stress relaxation behavior during strain hold time is analyzed using the creep strain-time relation and the strain hardening rule. Creep damages are estimated using the creep rupture time-stress curves.

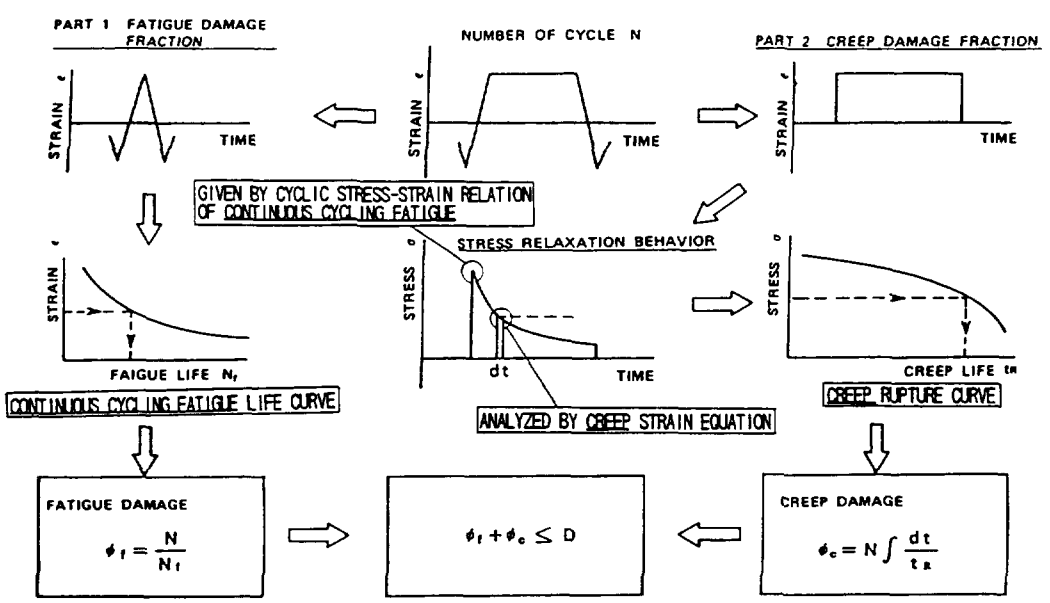

FIG 8 CONCEPT OF CREEP-FATIGUE EVALUATION PROCEDURE

As the basic mechanical properties for creep-fatigue damage evaluation, the following equations, which are obtained by continuous cycling fatigue test and monotonic creep test, are required.

- the cyclic stress-strain relation[4]
- the creep strain-time relation[5] and the strain hardening rule
- the creep rupture time-stress curves[5]
- the continuous cycling fatigue curves[6]

Therefore in PNC procedure creep-fatigue test data are used only to evaluate the estimation error, and long time extrapolation is based on the above basic mechanical properties.

Creep-fatigue life prediction based on PNC procedure and Campbell type damage diagram in ASME Code Case N-47 is good for long time extrapolation as shown in FIG.9[1]. The concept of PNC procedure is very simple, and the extrapolation to long time is justified by test data.

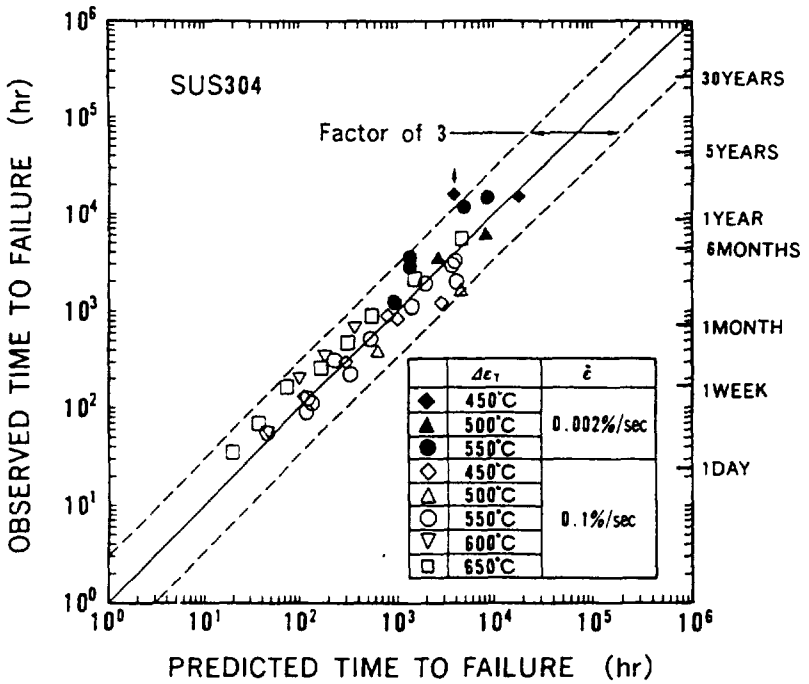

FIG.9 CORRELATION BETWEEN PREDICTED LIFE BY PNC PROCEDURE AND OBSERVED LIFE IN CREEP-FATIGUE TEST FOR TYPE 304 SS

It is clarified that PNC procedure using the time fraction rule is one of the ductility exhaustion method and gives good life prediction. While it is still important and very interesting whether the difference between two approaches(including and excluding primary creep basis) in TABLE 1 is essential for creep-fatigue failure evaluation. FIGURE 10 shows the ratio of secondary creep to relaxed strain; $\Delta\sigma_r$ /E at 823K. The ratio γ was calculated based PNC procedure. At 823K the γ value does not depend on hold time. When -log(1-ϕ) is nearly equal to δ/γ, the difference of estimated creep damages between the conventional ductility exhaustion and PNC time fraction procedure is not large, because creep damage by the conventional ductility exhaustion; $\Delta\varepsilon_c$/-log(1-ϕ) is nearly equal to $\gamma\,\Delta\varepsilon_c/\delta = \varepsilon_2\,\Delta t/\delta = \Delta t/t_R$ by PNC procedure.

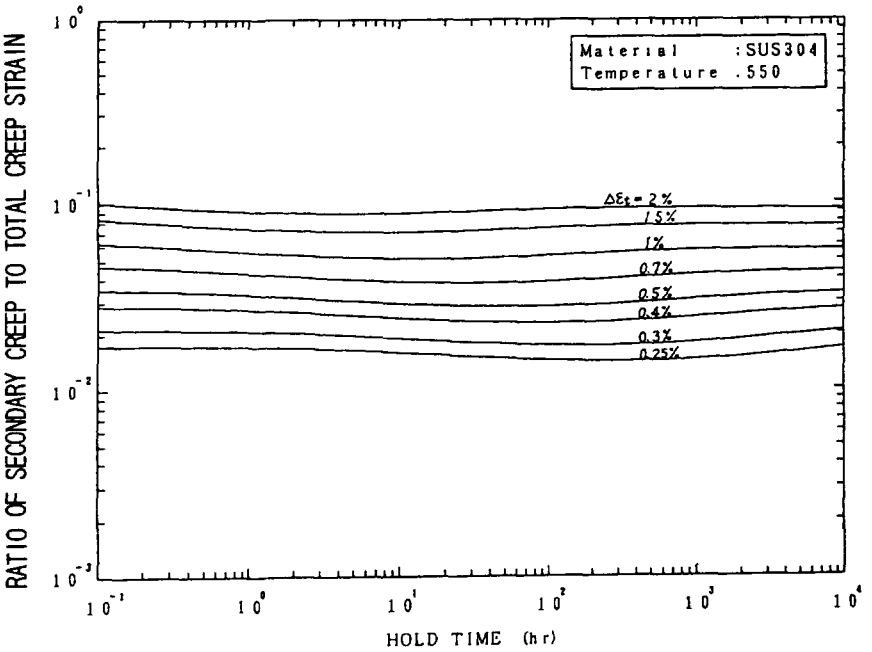

FIG.10 RATIO OF SECONDARY CREEP TO TOTAL CREEP STRAIN

The comparison of life prediction results for strain range of 0.3% at 823K is shown in FIG.11. As shown in FIG.10 the γ value depends on strain range, however in the condition interested in structural design $\Delta\varepsilon_c$/-log(1-ϕ) is nearly equal to $\gamma\,\Delta\varepsilon_c/\delta$. If the δ value is determined from pure creep ductility; $\varepsilon_1 + \varepsilon_2\ t_R$, estimated creep-fatigue life is too conservative because of accumulation of recoverable primary creep for each cycle. The value of -log(1-ϕ) is not suitable for the limit of the primary and secondary creep, but it gives good prediction due to canceling out the accumulation of recoverable primary creep for each cycle. For structural design use of the conventional ductility exhaustion rule, the estimation of $\Delta\varepsilon_c$ is required.

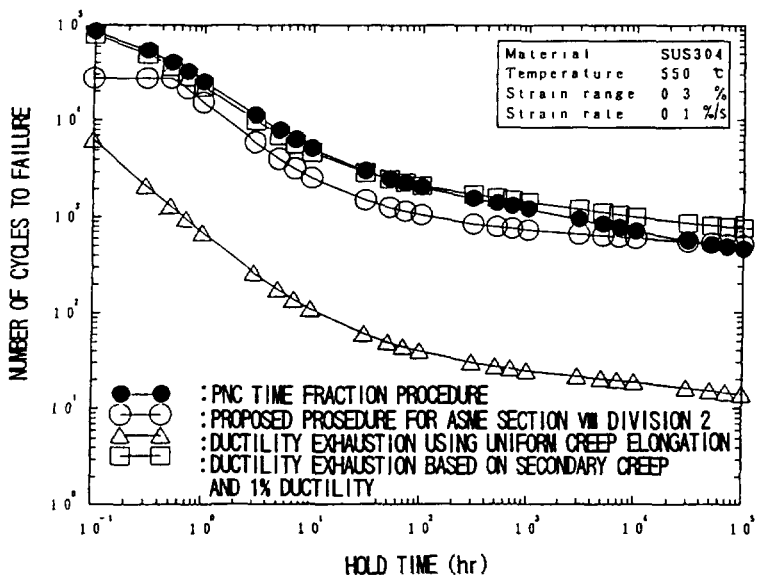

FIG.11 COMPARISON BETWEEN PNC TIME FRACTION PROCEDURE AND CONVEENTIONAL DUCTILITY EXHAUSTION

Therefore the simplicity of the ductility exhaustion rule based on total creep strain is not so different from that of the time fraction approach, if the accurate estimation of $\Delta\varepsilon_c$ is required.

As the results, for Type 304 ss, it is clarified that PNC time fraction procedure with the damage limit in ASME Code Case N-47 is one of the good evaluation methods for practical design use.

4. CREEP-FATIGUE EVALUATION ON TYPE 316 FR SS

For 316FR ss, the applicability of PNC time fraction rule is examined. FIGURE.12 shows creep-fatigue life estimation results on 316FR ss based on PNC rule. The Creep-fatigue strength of 316FR ss is much higher than that of Type 304 ss, so this material is the candidate for the next demonstration reactor in Japan. The fitness of estimated life to test data is good as for the dependence of hold time at 1% strain range at 823K. In the correlation between predicted and observed lives, as shown in FIG.13, the estimation error is below the factor of 2. It is concluded that PNC time fraction procedure could be applied for 316FR ss as one of the practical design evaluation criteria.

As for design evaluation methods, in PNC Monju design guide, creep damages are evaluated using a diagram for given strain range, temperature and operation time, and the diagram is given for Type 304, 316(conventional) and 321 ss based on PNC procedure.

For the next demonstration reactor design, now the best approach for 316FR ss is under discussion[7]. It is considered that the method in Monju design guide is better for structural design of LMFBR components considering the consistency with Type 304 ss, if the dominance (simplicity for design use, proper design margin for long time extrapolation, and so on) of the ductility exhaustion is not clear. For the ductility exhaustion, both of the estimation procedure of creep strain for each cycle and the determination method of the ductility limit have to be investigated for practical design use.

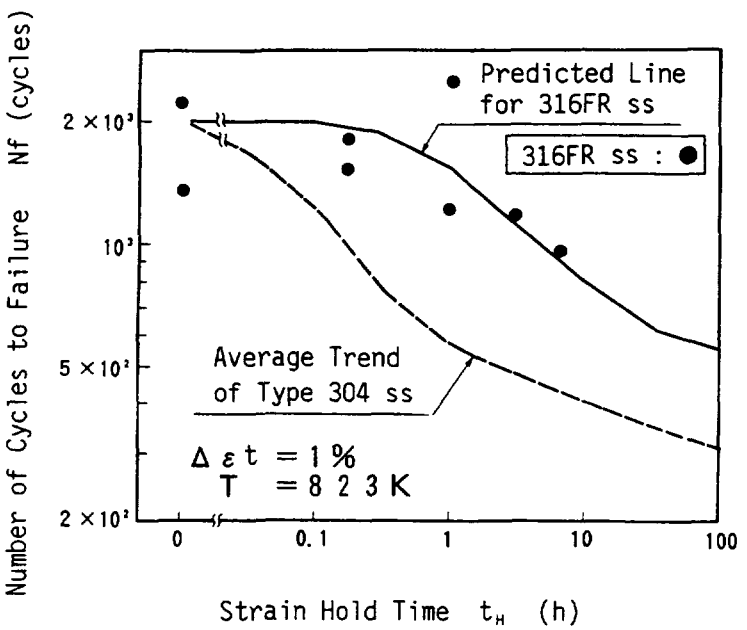

FIG.12 STRAIN HOLD TIME DEPENDENCE IN CREEP-FATIGUE FOR 316FR SS

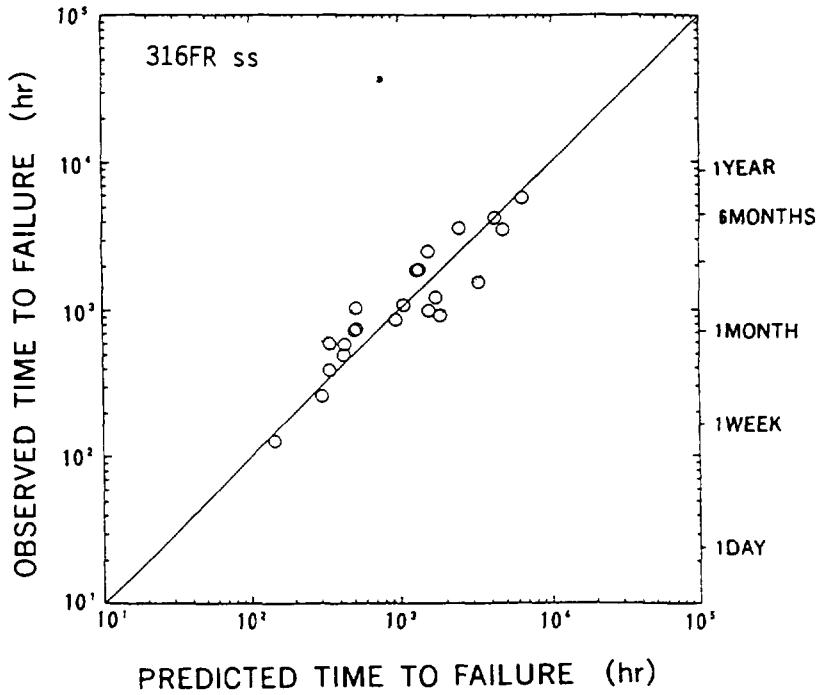

FIG.13 CORRELATION BETWEEN PREDICTED LIFE BY PNC PROCEDURE AND OBSERVED LIFE IN CREEP-FATIGUE TEST FOR 316FR SS

5. CONCLUSIVE REMARKS

1) PNC time fraction procedure give good creep-fatigue life prediction for not only Type 304 and also 316FR ss.
2) Time fraction: $\Delta t/ t_R$ is one of the ductility exhaustion, and it can be derived analytically from the secondary creep exhaustion $\varepsilon_2 \Delta t/ \varepsilon_2 t_R$. PNC time fraction procedure is analytically represented, so it is applicable easily for various effects: weldment, environmental effects, elastic follow-up and so on. It is suitable for Class 1 component design.
3) The conventional ductility exhaustion was simple for the count of creep damage, if the creep ductility and the creep strain for each cycle are easily determined by long time creep rupture test data and isochronous stress-strain diagram, respectively. However it is considered that this simplification might induce too conservative evaluation. So the simplified approach should be applied to components other than Class 1.
4) If the ductility exhaustion is modified for the accurate estimation of creep damage, stress relaxation analysis is required and its simplicity is not different from PNC time fraction procedure for design use.

REFERENCES

[1] Y.Wada, et al., "New concept on ductility exhaustion considering creep-fatigue failure mechanism of Type 304 ss," J. of Society of Materials Science, Japan, Vol.44, No.496(1995)29-34(in Japanese)
[2] K.Aoto, et al., "An analytical approach to creep-fatigue life prediction for SUS304, 316 and 321 austenitic stainless steels," ASME PVP-Vol.123(1987)43-48
[3] F.Ueno, et al., "A study on creep damage parameters in creep cavity growth dominant region under creep-fatigue loading," Proc. SMiRT-12, Vol.L(1993)L05/4

[4] Y.Wada, et al., "Analytical representation for the cyclic stress-strain hysteresis loops of Type 304 austenitic stainless steel," Proc. of Int. Conf. on Computational Mechanics (1986)IV-25-30
[5] A.Yoshitake, et al., "A statistical study of creep rupture and stress-strain behavior of structural materials under elevated temperature conditions," Proc. of Int. Conf. on Creep (1986)441
[6] Y.Wada, et al., "A statistical approach to fatigue life prediction for SUS304, 316 and 321 austenitic stainless steels," ASME PVP-Vol.123(1987)37-42
[7] M.Ueta, et al., "Creep-fatigue properties of advanced 316-steel for FBR structures," ASME PVP-313-2(1995)423-428

MULTIAXIAL CREEP-FATIGUE RULES

M.W. SPINDLER, R. HALES, R.A. AINSWORTH
Nuclear Electric plc,
Barnwood, Gloucester,
United Kingdom

Abstract

Within the UK, a comprehensive procedure, called R5, is used to assess the high temperature response of structures. One part of R5 deals with creep-fatigue initiation, and in this paper we describe developments in this part of R5 to cover multiaxial stress states. To assess creep-fatigue, damage is written as the linear sum of fatigue and creep components. Fatigue is assessed using Miner's law with the total endurance split into initiation and growth cycles. Initiation is assessed by entering the curve of initiation cycles vs strain range using a Tresca equivalent strain range. Growth is assessed by entering the curve of growth cycles vs strain range using a Rankine equivalent strain range. The number of allowable cycles is obtained by summing the initiation and growth cycles. In this way the problem of defining an equivalent strain range applicable over a range of endurance is avoided. Creep damage is calculated using ductility exhaustion methods. In this paper we address two aspects; firstly, the nature of stress relaxation and, hence, accumulated creep strain in multiaxial stress fields; secondly, the effect of multiaxial stress on creep ductility. The effect of multiaxial stress state on creep ductility has been examined using experimental data and mechanistic models. Good agreement is demonstrated between an empirical description of test data and a cavity growth model, provided a simple nucleation criterion is included. A simple scaling factor is applied to uniaxial creep ductility, defined as a function of stress state. The factor is independent of the cavity growth mechanisms and yields a value of equivalent strain which can be conveniently used in determining creep damage by ductility exhaustion.

1. INTRODUCTION

The ASME procedure for assessing creep-fatigue endurance [1] uses an elastic design route. In this method, a "slow-cycle" creep-fatigue endurance curve is used to relate the allowable number of cycles to the strain range. The effect of multiaxial loading is accounted for by reducing the changes in principal strains (the principal strain ranges) to a single equivalent value by the von Mises function and this is used to determine the number of cycles from the uniaxial endurance curve.

The inelastic route of Code Case N-47 [1] and the fast reactor design code RCC-MR [2] both assess creep and fatigue damage independently. Multiaxial effects are again accounted for by use of the von Mises function of equivalent stress and strain. Recently both procedures have adopted a slightly different equivalence due to Huddleston [3] for determining creep damage; this leads to a less pessimistic assessment when a significant component of compressive stress is present.

Within the high temperature assessment procedure, R5 [4] assessment of creep-fatigue endurance is concerned with determining the number of service cycles to initiate a defect of specified dimensions [5]. The procedure calculates fatigue damage and creep damage for each cycle type. Creep damage is assessed on the basis of accumulated strain normalized with respect to the strain rate dependent creep ductility of the material. Fatigue damage is calculated by a procedure which takes account of both the crack initiation and the crack growth stages of laboratory fatigue endurance data. In this paper we present a method for including the effect of multiaxial loading in the R5 approach.

2. CALCULATION OF FATIGUE DAMAGE

The approach to the calculation of fatigue damage in R5 has been set out in Ref. [5] for uniaxial loading. Fatigue damage D_F is simply

$$D_F = \sum_i N^{(i)}/N_o^{(i)} \quad (1)$$

where $N^{(i)}$ is the number of operational cycles of type i and $No^{(i)}$ is the corresponding endurance at the surface strain range. However, N_o is not necessarily equal to the number N_1, say, of cycles to failure in a laboratory test. Instead, N_o is the number of cycles to create a defect of a specified size a_o in the laboratory specimen. $D_F = 1$ then corresponds to the creation of a defect size a_o at the surface of the component.

In practice, the value of a_o is chosen by the assessor to be much less than the section width so that changes in the structural compliance due to the defect do not significantly influence the uncracked body stresses. Where the structural section is larger than the laboratory specimen size, the failure of the laboratory specimen can be taken to correspond to defect initiation in the structure, as in the N47 and RCC-MR codes. However, allowance for the creation of an arbitrary defect size allows crack initiation to be assessed for any size of structural section, in particular sections smaller than typical laboratory specimens.

In order to deduce N_o from the total endurance N_1 measured in the laboratory, separation of the total endurance into initiation and growth phases is performed. Initiation is taken as the production of a crack of size $a_i = 20\ \mu m$ and is described by the empirical relationship.

$$N_1 = N_1 \exp(-8.06 N_1^{-0.28}) \quad (2)$$

This has been derived from the data for austenitic steels reported by Pineau [6].

The number N'_g of cycles for a crack to grow from the initiation size $a_i = 20\ \mu m$ to the specified size a_o could, given adequate data, be deducted from fatigue crack growth equations, such as that of Tomkins [7], which depend on the plastic strain range. An alternative approach is adopted in R5 which ensures that N_o corresponds to the total endurance N_1 when a_o is equal to the crack size a_1, say, corresponding to the failure condition in the laboratory test. Then

$$N'_g = \gamma N_g \quad (3)$$

where $\gamma = 0$ for $a_o = a_i$ and $\gamma = 1$ for $a_o = a_1$. For intermediate values of a_o, the value of γ is obtained by assuming a crack growth law of the form

$$da/dN = Ba^Q \quad (4)$$

where Q is a constant and B is a function of strain range [8]. For any given value of Q, the function B may be eliminated by imposing the condition $\gamma = 1$ for $a_o = a_1$, leading to an expression for N'_g in terms of N_1, N_1 and a_o as described in [5].

A typical result of applying the above procedure to lower bound endurance data for type 316 stainless steel at 600°C is shown in Figure 1. It can be seen that the endurance is dominated by initiation at low strain ranges, and by growth at high strain ranges. The separation of data as in Figure 1 recognizes that there are two important processes which lead to fatigue failure. The first, Stage I, is the formation of an initiation site by the development of persistent slip bands in suitably oriented surface grains. This step is highly dependent on the crystallography and is controlled by the cyclic shear strain. When the Stage I defect reaches a critical size, Stage II crack growth takes over. This usually corresponds to mode I crack growth and is controlled by crack opening in the direction of the largest principal stress range.

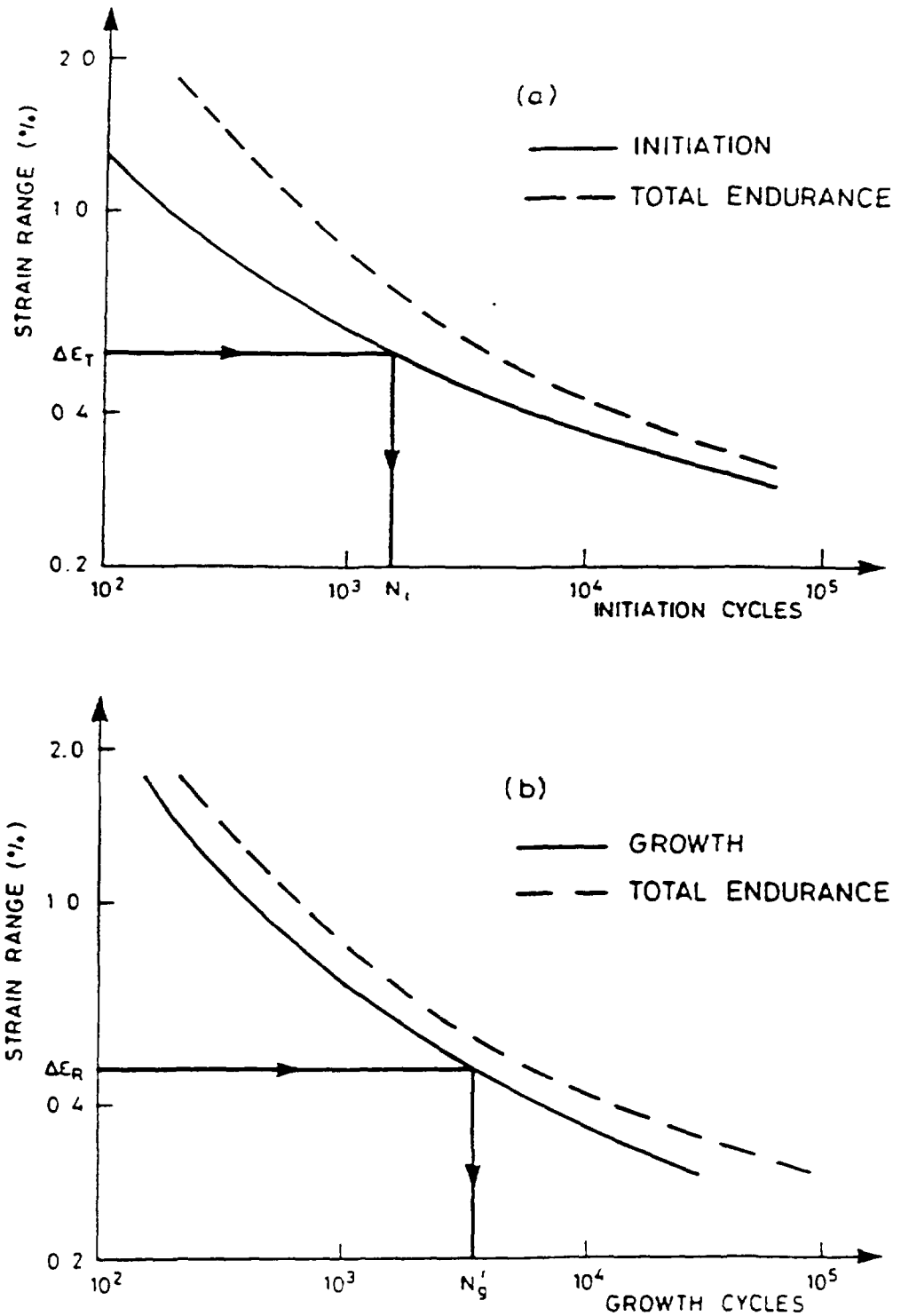

FIG. 1. Separation of the number of cycles for initiation and growth plotted against the equivalent strain ranges.

The above discussion suggests a simple method for determining the fatigue endurance under multiaxial loading: use the Tresca equivalent strain range to determine the number of cycles for initiation under multiaxial loading N_i by reference to a curve such as that in Figure 1(a); use the Rankine equivalent strain range to determine the number N'_g of cycles for growth under multiaxial loading by reference to the growth curve as shown in Figure (b); and then the number $N_o = N_i + N'_g$ of allowable cycles under multiaxial loading.

The above procedure does not yield an equivalent strain function, but rather the number of allowable cycles for a specific combination of principal strain ranges. However, it clearly corresponds to an equivalent strain function intermediate between the Rankine and Tresca forms. This is similar to the approach in Brown and Buckthorpe [9] which proposed the equivalent strain range

$$\Delta\varepsilon_{eq} = A\ \Delta\varepsilon_R + (1 - A)\ \Delta\varepsilon_T \tag{5}$$

where A is a function of strain range, and sub-scripts R and T denote Rankine and Tresca respectively. Furthermore, in Brown and Buckthorpe [9], A is interpreted as the ratio N_g/N_i so that the equivalent strain function tends towards Tresca at low strain ranges and Rankine at high strain ranges. The separation of endurance into initiation and growth, as described above could be used to define A but in that case there is little merit in recombining the contributions and using an equivalent strain range. Instead Brown and Buckthorpe [9] proposed an empirical expression for A dependent on the ratio of fatigue limits in tension and torsion. However, here the use of separate initiation and growth functions as in Fig 1 is preferred as it avoids the empirical choice of A and, more importantly, enables the fatigue data to be modified for any choice of specified defect size a_o as described earlier.

3. CALCULATION OF CREEP DAMAGE

To assess creep damage at a surface subjected to creep-fatigue loading, R5 uses the ductility exhaustion approach by Hales [10]. With this approach the creep damage is

$$D_c = \sum_i N^{(i)} \int_0^{t_h^{(i)}} [\dot{\varepsilon}_c / \varepsilon_f(\dot{\varepsilon}_c)]\, dt \tag{6}$$

where $\dot{\varepsilon}_c$ is the creep strain rate, ε_f is the ductility which depends on creep strain rate, and $t^{(i)}_h$ is the dwell time in the cycle of type i. In using Equation (6) for multiaxial conditions, it is necessary to assess the effect of stress state on both creep strain rate and on ductility. For constant stress conditions the creep strain rate depends on the von Mises equivalent stress $\bar{\sigma}$ and it is, therefore, straightforward to allow for multiaxiality. However, more generally some stress relaxation occurs and requires solution of

$$-\frac{Z}{E'}\frac{d\bar{\sigma}}{dt} = \dot{\bar{\varepsilon}}_c(\bar{\sigma},\ t) \tag{7}$$

where Z describes the degree of elastic follow-up and E′ is an effective modulus determined by the structural constrains imposed.

For strict strain control with Z = 1, solution of the full multiaxial relationships for biaxial loading leads to

$$E' = \frac{E}{2(\alpha^2 + 3\beta^2)}\left(\frac{\alpha^2}{1 - \nu} + \frac{9\beta^2}{1 + \nu}\right) \tag{8}$$

where $\alpha = \sigma_1 + \sigma_2$, $\beta = \sigma_1 - \sigma_2$, E is Young's modulus and σ_1, σ_2 are the principal stresses. As relaxation takes place, the principal stresses relax at different rates and hence α and β vary with time. However, for overall reductions of stress less than 40% of the initial value, the ratio of the principal

stresses is approximately constant [11]; hence, the instantaneous equivalent strain rate is calculated using equation (7) and the equivalent strain is simply

$$\bar{\varepsilon}_c = (\bar{\sigma}_0 - \bar{\sigma}(t_h))/E' \tag{9}$$

where $\bar{\sigma}(t_h)$ is the value of the equivalent stress at the end of the dwell period.

If the initial stress results from displacements or differential thermal expansions in parts of the structure remote from the point of interest, there is not usually total constraint on the strains in the localised region. Generally, there will be some elastic follow-up as indicated by the scalar factor Z in Equation (7). Some detailed calculations have been performed for a complex thin shell structure subjected to load-controlled bending to examine this load case [11]. The details are not discussed here, but it may be noted that none of the total strain components remained constant during stress relaxation, the degree of elastic follow-up was different in the two principal directions so that the use of a scalar factor in Equation (7) is an approximation, and stress changes were non-proportional. Therefore, it was found that creep strains could not be evaluated from Equation (7) using Equation (9) multiplied by Z because an appropriate value of E´ could not be defined. Instead, it was found that, using Equation (7) with E´ = E, estimating the principal components of the accumulated creep strain by

$$\begin{aligned} \varepsilon_{c1} &= Z(\sigma_{10} - \nu\sigma_{20})\ \Delta\bar{\sigma}/E\bar{\sigma}_0 \\ \varepsilon_{c2} &= Z(\sigma_{20} - \nu\sigma_{10})\ \Delta\bar{\sigma}/E\bar{\sigma}_0 \end{aligned} \tag{10}$$

was reasonably accurate (within about 10% provided that the stress drop was less than 20% of the initial equivalent stress.

Having evaluated the creep strain components by the approximations of Equations (9) or Equations (10) or by full analysis, it is necessary to determine both the appropriate creep strain rate and the corresponding ductility for input to Equation (6).

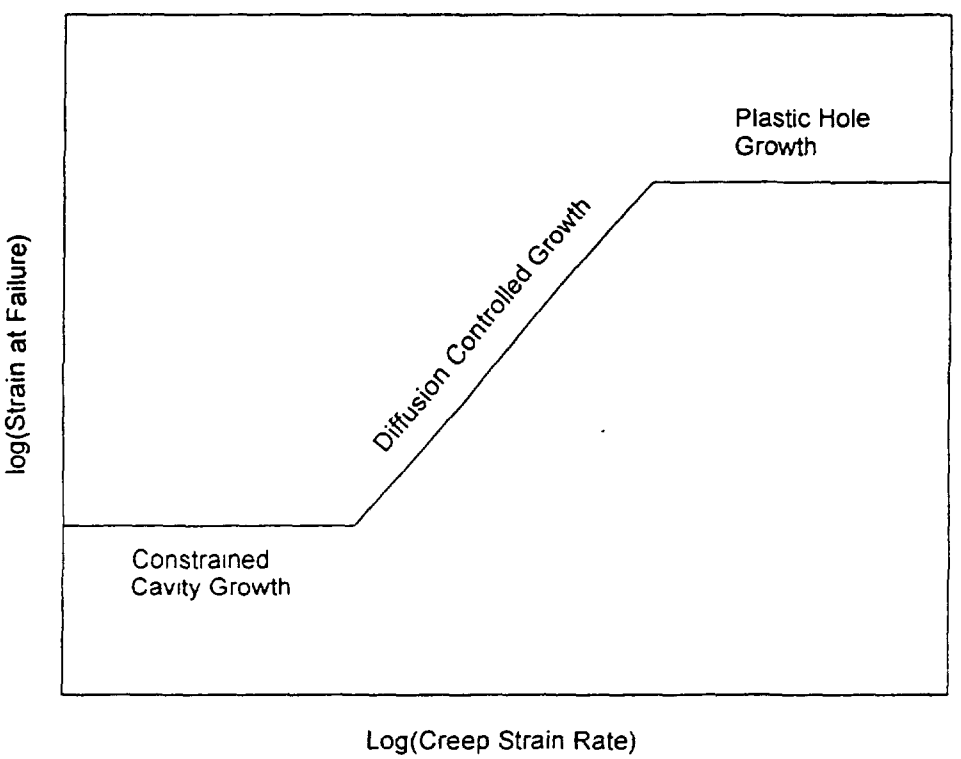

FIG. 2. Dependence of creep ductility on creep strain rate.

3.1 Multiaxial Creep Ductility

In many materials creep rupture is controlled by the growth of cavities. The precise mechanisms of growth lead to differing creep rupture ductilities as shown schematically in Figure 2. In an attempt to derive an equivalent stress for creep rupture, Hales [12] has analysed growth of creep cavities under biaxial stresses. The high, or upper shelf, ductility corresponds to failure by plastic hole growth and it was suggested by Hales [12] that the maximum principal strain at failure remains equal to that under uniaxial stress. By means of the Levy-Mises deformation relationship for constant stress conditions, the ratio of von Mises equivalent strain to failure, $\bar{\varepsilon}_f$, to the uniaxial strain to failure, ε_{uf}, is given by

$$\frac{\bar{\varepsilon}_f}{\varepsilon_{uf}} = \frac{\bar{\sigma}}{\sigma_1 - \sigma_2/2} \tag{11}$$

For diffusion controlled cavity growth it was shown that cavity growth alone predicts only modest effects of stress state on time and strain to rupture. However, if a simple nucleation law is postulated such that the mean cavity spacing is inversely proportional to σ_1^m, where m is a constant, then a stronger relationship between creep ductility and stress state is predicted

$$\frac{\bar{\varepsilon}_f}{\varepsilon_{uf}} = \frac{\bar{\sigma}^{(m+1)}}{\sigma_1} \tag{12}$$

Constrained cavity growth is controlled by the diffusion of vacancies under the influence of a tensile stress and the rate of growth is limited by the deformation rate of the surrounding material. Thus the cavity growth rate is proportional to the principal strain rate and, in the absence of nucleation effects, the principal strain at failure is constant. When nucleation effects are taken into consideration as before it can be shown that

$$\frac{\bar{\varepsilon}_f}{\varepsilon_{uf}} = \frac{\bar{\sigma}^{(m+1)}}{\sigma_1 - \sigma_2/2} \tag{13}$$

In an attempt to verify equations (11) to (13) Spindler [13] has analysed an extensive body of creep rupture data on austenitic stainless steels. This analysis led to an empirical relationship

$$\frac{\bar{\varepsilon}_f}{\varepsilon_{uf}} = \exp\left[p\left(1 - \frac{\sigma_1}{\bar{\sigma}}\right)\right] \exp\left[q\left(\frac{1}{2} - \frac{3\sigma_h}{2\bar{\sigma}}\right)\right] \tag{14}$$

where σ_h is the hydrostatic stress; p and q are constants determined by regression analysis of the data. The second term in equation (14) was derived from the plastic hole growth model of Rice and Tracey [14]. The first term being included to account for the nucleation of creep cavities, which are controlled by σ_1. Although equation (14) does not explicitly address the different cavity growth models, Spindler found that in the case of austenitic stainless steels the values of p and q differ depending on which regime, indicated in Figure 2, the creep data refer to such that: for transitional behaviour, $p \approx 2.38$ and $q \approx 1.04$ and for lower shelf behaviour, $p \approx 0.15$ and $q \approx 1.25$.

The data used to determine p and q in equation (14) also indicate that a simple yet conservative interpretation of biaxial stress state effects can be achieved by simply factoring uniaxial ductility such that

$$\begin{aligned} \bar{\varepsilon}_f &= \varepsilon_{uf}\,(1 - \sigma_2/\sigma_1) \quad \text{for } -\infty < \sigma_2/\sigma_1 < 0.5 \\ \bar{\varepsilon}_f &= \varepsilon_{uf}/2 \quad \text{for } 0.5 \le \sigma_2/\sigma_1 \le 1 \end{aligned} \tag{15}$$

for $\sigma_1 \geq \sigma_2$.

The appropriate relationships for the effect of stress state on the creep ductility in the transition region and lower shelf are compared in Figs. 3 and 4 respectively.

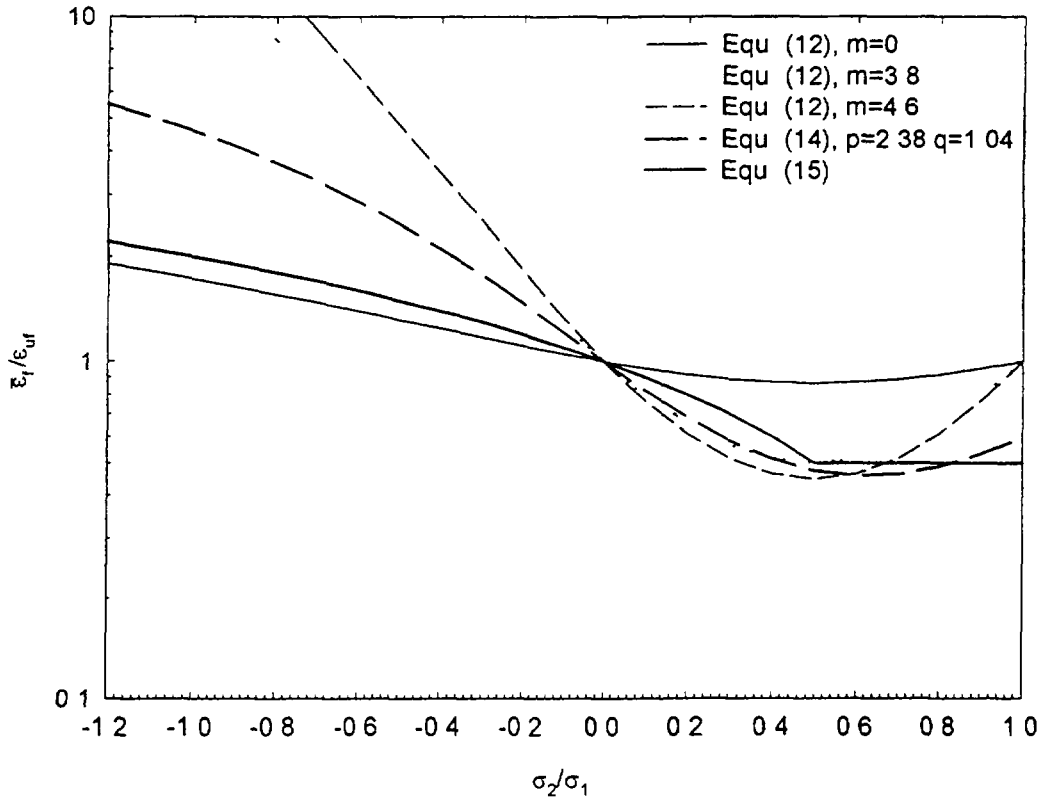

FIG 3 Influence of stress state on creep ductility in the transition region

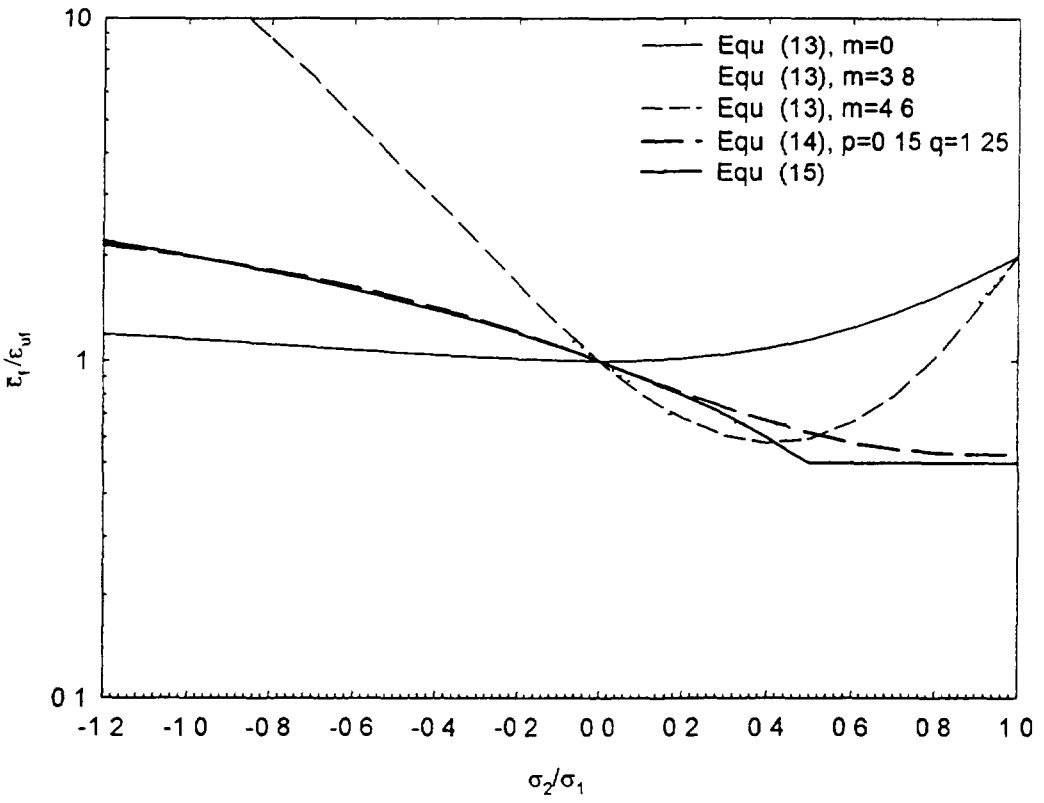

FIG 4 Influence of stress state on creep ductility at the lower shelf

4. CALCULATION OF TOTAL DAMAGE

Within R5 [4] linear damage summation is used to assess the combined effects of creep and fatigue damage. Thus, the endurance is determined by assuming that the sum

$$D_C + D_F = 1 \tag{16}$$

at failure. This approach has been validated for a range of materials and cycle types for uniaxial loading [5]. For creep-fatigue under multiaxial loading, there is little experimental evidence to provide validation for Equation (16). Therefore, the extension to multiaxial conditions has been based on current understanding of the physical processes leading to failure, noting that under multiaxial loading it is provable that the two types of damage will develop on differently oriented planes, so reducing the possibility of interaction.

5. AN ASSESSMENT PROCEDURE FOR MULTIAXIAL CREEP FATIGUE

The objective of the R5 development is to provide an assessment document which is easily used. Therefore, the principles of Sections 2-4 have been converted into a step-by-step procedure. The steps in the procedure are as follows.

(1) Determine the temperature and stress history of the component, making due allowance for the influence of structural response and elastic follow-up. It is assumed that the maximum strain range which occurs at the surface pertains throughout the cyclic plastic zone.

(2) Construct cyclic deformation stress-strain loops for each of the different service cycles, including any creep deformation occurring during the dwell.

(3) Calculate the fatigue damage D_F. Fatigue damage is calculated using fatigue endurance of smooth specimens measured as a function of strain range in conjunction with the equations given in Section 2. These take account of the acceptable size of fatigue crack a_o and stress state.

   (a) Size effect is treated by dividing the endurance into initiation and growth. The latter value is adjusted to take account of allowable crack length.

   (b) The influence of stress state on the initiation and growth stages is assessed using equivalent strain ranges as in Figure 1.

   (c) The number N_o of allowable cycles is the sum of the number of cycles for the two processes.

(4) Calculate the creep damage D_c using ductility exhaustion and the equations given in Section 3. These take account of the effect of stress state on stress relaxation and creep ductility.

   (a) Stress relaxation under multiaxial conditions is described by the von Mises equivalent stress, but taking account of the imposed structural constraints. Detailed analysis or the approximations in Section 3 may be used.

   (b) The effect of biaxial stresses on creep ductility is taken into account by a simple relationship, equation (15).

(5) Determine the total damage from the damage terms D_F and D_c using Equation (16).

(6) Perform a sensitivity analysis with respect to the input data in order to identify those parameters which are life limiting.

(7) Report the results of the assessment and provide information on the analysis methods and the materials data used in all aspects of the analysis.

ACKNOWLEDGEMENT

This paper is published with permission of Nuclear Electric Ltd.

APPENDIX A: NOMENCLATURE

A	strain range dependent factor in Equation (5)
a_o	initiation crack size required for structural assessment
a_i	initiation crack size in specimen
a_f	crack size at failure in specimen
B	function of strain range in Equation (4)
D_c	creep damage
D_F	fatigue damage
E	Young's modulus
E'	effective modulus in Equation (7)
N	Number of cycles
N_f	uniaxial fatigue endurance
N_i	number of cycles to initiate a defect size a_i
N_g	N_f-N_i
N'_g	number of cycles to grow a defect to a_o
N_o	$N_i + N'_g$
Q	constant in Equation (4)
t_h	hold time
Z	elastic follow-up coefficient
α	$\sigma_1 + \sigma_2$
β	$\sigma_1 - \sigma_2$
γ	factor in Equation (3) dependent on a_o
$\varepsilon_1, \varepsilon_2$	principal strains
$\varepsilon_{c1}, \varepsilon_{c2}$	principal creep strains
$\dot{\underline{\varepsilon}}_c, \dot{\varepsilon}_{c1}$	creep strain rate, principal creep strain rate
$\bar{\varepsilon}_c$	von Mises equivalent creep strain rate
$\varepsilon_f, \varepsilon_{1f}$	uniaxial creep ductility, principal cree strain to failure
$\Delta\varepsilon_R$	Rankine strain range
$\Delta\varepsilon_T$	Tresca strain range
$\Delta\varepsilon_{eq}$	equivalent strain range of Equation (5)
ν	Poisson's ratio
σ_1, σ_2	principal stresses
σ_{10}, σ_{20}	principal stresses at start of hold time
$\bar{\sigma}$	von Mises equivalent stress
$\bar{\sigma}_o$	von Mises equivalent stress at start of dwell
$\Delta\bar{\sigma}$	change in von Mises equivalent stress during dwell

REFERENCES

[1] ASME, Boiler and Pressure Vessel Code, Case N-47-23, Class 1 Components in Elevated Temperature Service, Section III, Division 1, ASME, New York, (1986).

[2] AFCEN, RCC-MR, Design and Construction Rules for Mechanical Components of FBR Nuclear Islands, Section 1, Subsection B, AFCEN, Paris, (1985).

[3] Huddleston, R. L., An improved creep-rupture strength criterion, J Pressure Vessel Technol. **107** (1985) 421-430.

[4] Ainsworth, R. A., Hales, R., Budden, P. J., Martin, D. C., (eds), Assessment procedure for the high temperature response of structures, Nuclear Electric Rep. R5, Issue 2, (1995).

[5] Ainsworth, R. A., Defect assessment procedures at high temperature, (Proc SMiRT 10 Conf., Anaheim, C. A., 1989, Vol. L, pp 79-90) Nucl. Eng. Des. **130** (1991) 211-219.

[6] Pineau, A., High temperature fatigue behaviour of engineering materials in relation to microstructure, in Skelton R. P., (ed), Fatigue at High Temperature, Applied Science, London, (1983) 305-364.
[7] Tomkins, B., Fatigue crack propagation - an analysis, Philos. Mag. **115** (1968) 1041.
[8] Skelton, R. P., Growth of short cracks during high strain fatigue and thermal cycling, ASTM Spec. Tech. Publ. **770**, (1983), 337-380.
[9] Brown, M. W., Buckthorpe, D., A crack propagation based effective strain criterion, in Brown, M. W., Miller, K. J., (eds), Biaxial and Multiaxial Fatigue, Mechanical Engineering Publications, London, (1989) 499-501.
[10] Hales, R., A method of creep damage summation based on the accumulated strain for the assessment of creep fatigue endurance, Fatigue Eng. Mater. Struct. **6** (1983) 121-135.
[11] Goodman, A. M., Creep relaxation from an initial biaxial stress state, personal communication, (1990).
[12] Hales, R., The role of cavity growth mechanisms in determining creep-rupture under multiaxial stresses, Fatigue Eng. Mater. Struct. **17** (1994) 579-591.
[13] Spindler, M. W., The Multiaxial Creep of Austenitic Stainless Steels, Nuclear Electric Rep. TIGM/REP/0014/94, (1994).
[14] Rice, J. R., Tracey, D. M., On ductile enlargement of voids in triaxial stress fields, J. Mech. Phys. Solids, **17** (1969) 201-217.

CREEP FATIGUE DESIGN OF FBR COMPONENTS

S.B. BHOJE, P. CHELLAPANDI
Indira Gandhi Centre for Atomic Research,
Kalpakkam, Tamil Nadu, India

Presented by R. Ramesh

Abstract

This paper deals with the characteristic features of Fast Breeder Reactor (FBR) with reference to creepfatigue, current creepfatigue design approach in compliance with RCCMR (1987) design code, material data, effects of weld nents and neutron irradiation, material constitutive models employed, structural analysis and further R&D required for achieving maturity in creepfatigue design of FBR components. For the analysis reported in this paper, material constitutive models developed based on ORNIb (Oak Ridge National Laboratory) and Chaboche viscoplasic theories are employed to demonstrate the potential of FBR components for higher plant temperatures and/or longer life. The results are presented for the studies carried out towards life predition of Prototype Fast Breeder Reactor(PFBR) components.

1. INTRODUCTION

Nuclear energy is an important source of electricity in the world and it has been established to be economically competitive, dependable and the clean source of energy. The basis for the energy production in the nuclear reactors, either thermal or fast. is nuclear fission chain reaction. While in a thermal reactor chain reaction is sustained by low energy thermal neutrons, in an FBR chain reaction is maintained by high energy neutrons. FBR is being developed in some countries because of its ability to extract 60 times more energy from a given mass of U than in thermal reactors. Considering the demand for energy and available resources, nuclear energy through FBR is essential for India. After successfully commissioning 40 MWt Fast Breeder Test Reactor (FBTR), design work on 500 MWe PFBR has been taken up. Towards detailed analysis, many advanced investigations particularly in the field of thermal hydraulics and structural mechanics have been carried out. Creepfatigue design is one such area in the structural mechanics domain where a high level of confidence has been achieved.

Since the boiling point of sodium is about 1200 K, the operating temperature for an FBR can be as high as 870 K even after providing sufficient margin betveen boiling point and operating temperature. The existing FBRs in the world operate at high temperature (about 820 K) wherein creep effects are important to be included in the design. Although design and operation of components in this temperature range is not new to aircraft and rocket engines, steam turbines, etc., direct technology transfer from these industrial practices is not feasible because they have characteristics such as short life times, easy inspection and maintenance (may not be true for rocket engines), etc. The FBR must operate safely and reliably for 30 to 40 years. Inservice inspection is more difficult due to radioactivity and use of sodium. Hence more emphasis is being placed upon analytical design techniques in conjunction with experimental validations.

Since a large tonnage of structural material (~10 t/MWe for NSSS) is needed for FBR components, use of the costly high temperature materials, like nickel based super alloys, are not preferred. Hence for the requirement of operating temperature less than 870 K. less costly and easily available materials like austenitic stainless steels (ASS) for sodium components and ferritic steels, specifically 9CrlMo steel for steam generator are used. These materials have sufficient creepfatigue strength at the temperature of interest and the required material data for the stress/strain analysis and creep fatigue damage assessment.

The design and construction codes basically deal with the stringent rules to ensure a safety factor against structural failures by perceived materialfailure processes which have to be respected for ensuring the long term structural integrity of a specific component at high temperature. The US code ASME Section III, Code Case N47 (1992), French Code RCCMR(1987) and Japanese code ETSDG (1984) are currently used for the design of out of core components. These codes provide design methodology for the FBR applications for the operating temperatures upto at least 900 K. Out of these, RCCMR is preferred because it is more relevant to FBR system, in terms of geometrical characteristics of structures, loading and structural materials. As regards to core components, special rules are recommended based on experience to take into account the neutron irradiation effects.

All the design codes are based upon a designbyanalysis concept. This means, in meeting these code rules, it is required to perform detailed inelastic analysis for predicting accurately the stress/strain history taking into account both time independent and time dependent material deformation behaviour. Earlier inelastic analysis was performed using widely semiclassical theories, viz. Linear Kinematic Hardening (LKH) and ORNL models. But currently, constitutive models based on unified creepplasticity, also called viscoplastic theory, have been employed. Among various viscoplastic models, the 'Chaboche viscoplastic model' is found to be superior for FBR applications because of its ability to simulate, with reasonable accuracy, all the essential mechanical behaviour of ASS in the temperature range 300900 K under monotonic and cyclic loading conditions.

Finally it can be summarised that for the creepfatigue design of FBR components, good understanding is needed about various aspects, viz. the characteristic features of FBR components, material data, effects of weldments and neutron irradiation, material constitutive models, structural analysis methodology and design codes. All these aspects are briefed in this paper with examples to illustrate the creepfatigue design of FBR components.

2. CHARACTERISTICS OF FBR COMPONENTS

The critical high temperature components of NSSS in a pool type FBR are core components, viz. fuel clad and hexcane in the core, CRDM and out of core components, viz. control plug (CP), inner vessel (IV), Intermediate Heat Exchanger (IHX), hot secondary sodium pipe and steam generator (SG) (Fig 1). The overall layout of piping is designed to minimise thermal expansion stresses in the secondary circuit but these are nevertheless significant. Thermal transients lead to the need for relatively thin walled piping to minimise the thermal transient stresses which is adequate to withstand thc internal pressure (<1 MPa). I However, tile thennal expansion stresses concentrate at bends and lead to potential problems of creep buckling. For CRDM, the primary stresses and steady state thermal stresses are low and the skin stresses which are developed during the reactor scram will not be critical. Further, these components are replaceable.

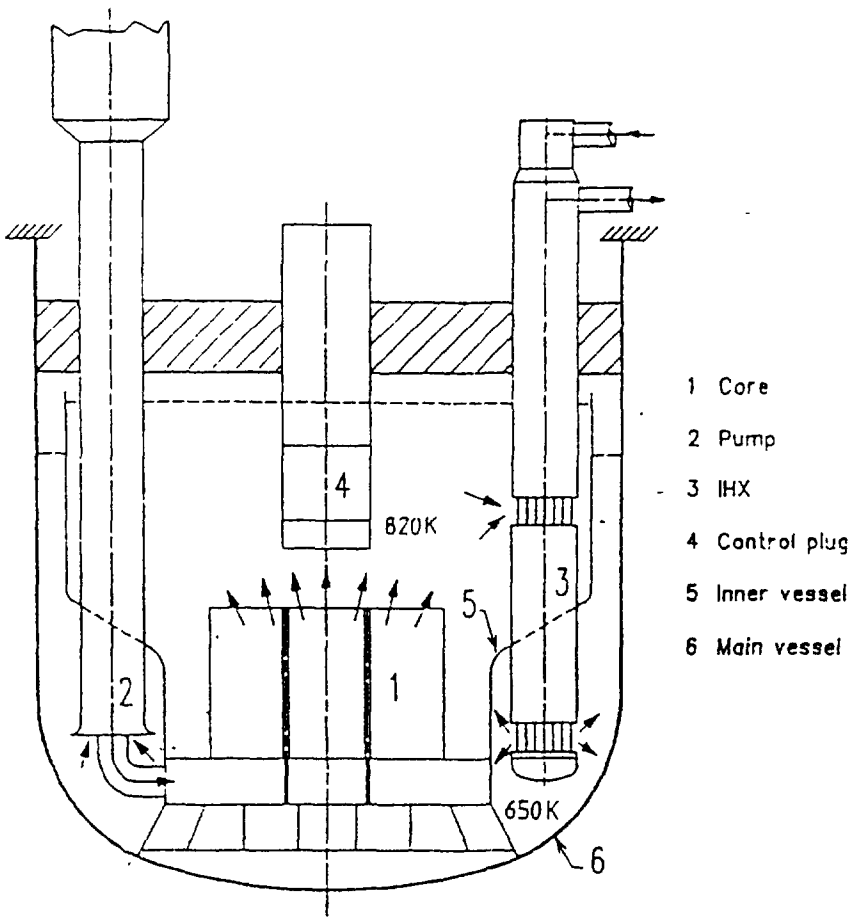

FIG. 1. Schematic sketch of FBR vertical section

TABLE I

Parameter	PWR	FBR
Reactor inlet/outlet (K)	566/601	670/820
ΔT across core (K)	35	150
Structural material	carbon steel	SS 316 LN
Coolant	water	Sodium
Heat Transfer Coeff, h (W/m^2-K)	5,000	10,000
wall thickness S (mm)	40	20
Biot Number hS/K (Bi)	5	12.5
Duration of shock Δt (s)	30	40
Fourier Number ($a.\Delta t/S^2$)	0.17	0.47
Fritz factor f^1	0 5	0.56
Maximum skin stress (MPa) (= $f.E.\alpha.\Delta T/[1-\gamma]$)	75	420

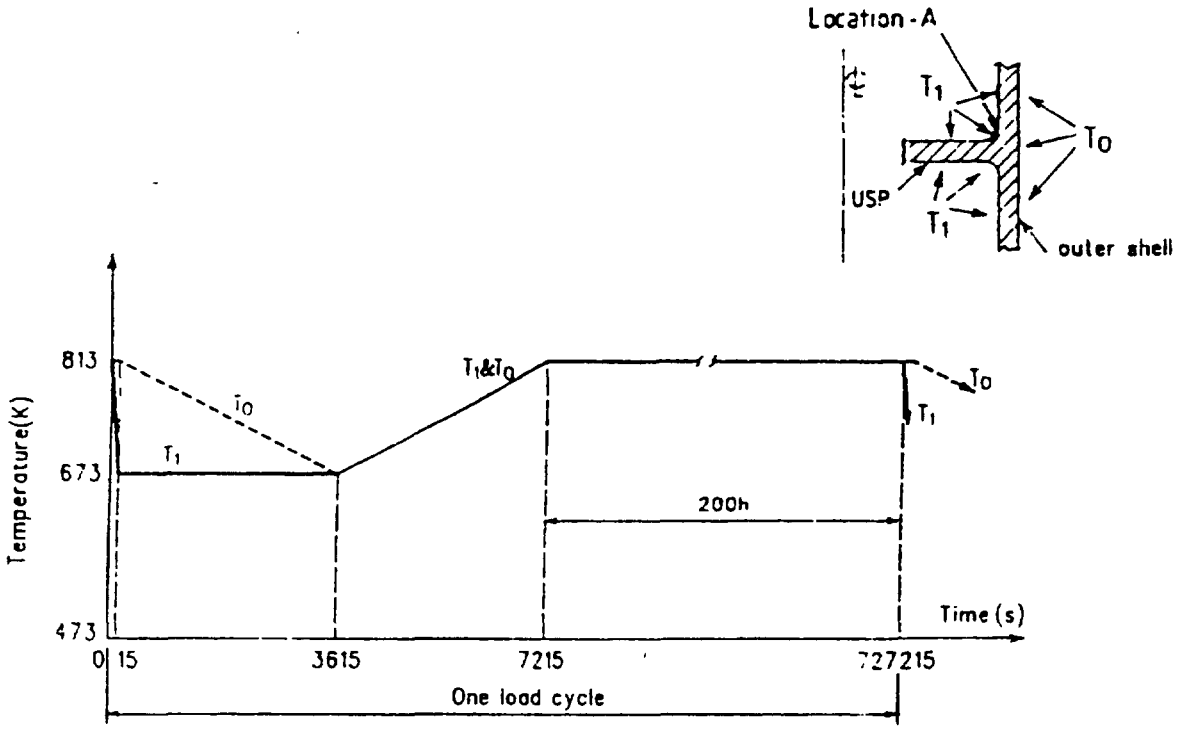

Idealised thermal load cycle for control plug - USP junction analysis.

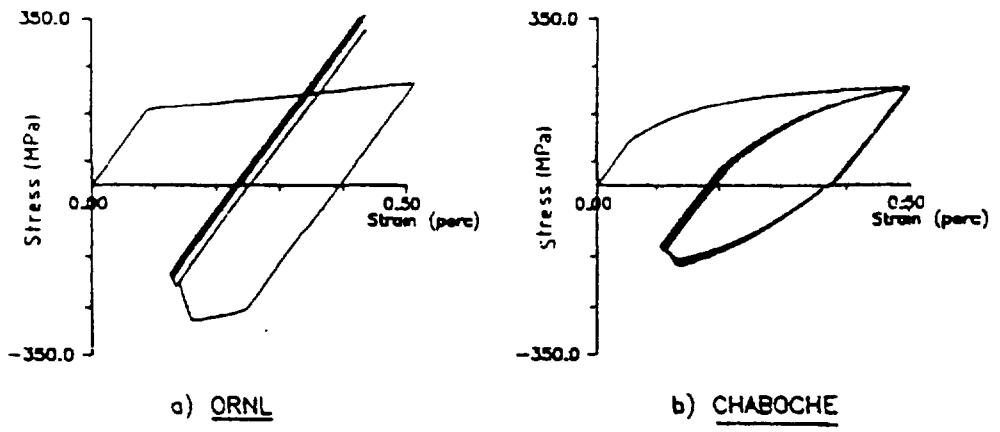

FIG. 2. Hysteresis loop at the location - A

2.1 Geometrical charactcristics

The high temperature components in the primary sodium circuit are generally of thin walled shell structures with radius lo thickness ratio rangnig from 60 to 500. I thin components are preferable not only for economical use of material but also to reduce cyclic thermal stresses due to severe thermal transients and temperature fluctuations.

2.2 Structural materials

For in core components, D9 material improved ASS with respect lo resistence to neutron irradiation) is used. ASS type 316 LN, is used as the main structural material for out of core components except for SG. Since SG is a barrier between sodium and water, 9 Cr I Mo type ferritic steel, particularly grade T 91 is preferred. Tile maximum operating temperatures arc selected as high as these material can permit.

2.3 Loadings

The use of sodium as coolant is a major factor responsible for low pressure and high thermal induced stresses at the temperature limits in tile creep range of the structural materials. This is mainly due to, (i) high boiling point of sodium and (ii) high thermal conductivity of sodium (about 100 times higher than that of water) and high temperature differentials across the reactor core (150-160 K), leading to high through wall temperature gradient even under normal operating condition. l'he main event which severely affects the high temperature components, is the reactor scram, during which hot pool components are subjected to severe thermal transient with the shock rate ranging from 5 to 10 K/s along with a through wall temperature gradient of about 100120 K at the critical locations. For the design purpose, 1000 reactor scrams are conservatively assumed during the reactor life. The associated strain range due to above transients rarely exceeds 0.5%. Severity of a thermal shock on an FBR component as compared lo PWR is illustrated in Table.l.

2.4 Failure modes

A major threat to structural integrity of the high temperature components is posed by thermal stress origin. The possible failure modes under this condition are the accumulation of inelastic strain and associated creepfatigue damage. For example, in the case of control plug, the thermal transient due to a reactor scram causes local yielding at the plateshell junctions, a subsequent dwell period at elevated temperature (at normal operation) leads to a stress relaxation, during which creep deformation as well as creep damage get accumulated (Fig 2). Repeated thermal loading during the life of the plant can lead to fatigue damage and in addition, exacerbates the accumulated creep damage during the dwell periods. Besides, these fatigue loadings can also create many complexities in the subsequent creep relaxation processes due to cyclic hardening nature of solution annealed ASS. The analysis of whole phenomenon is very complex and calls for detailed inelastic analysis using a constitutive material model. 'Ultirnately, the wmulative creepfatigue damage and accumulated inelastic strains at the end of the reactor life, predicted through the analysis, should be within the design code limits for assuring the long term structural integrity of the component.

3. DESIGN CODES

The normal practice in the design of nuclear power plant components is to follow the rules of Section III Division I of Ihe ASME Boiler and Pressure Vessel code2, in the temperature range, less than 700 K for ASS and 650 K for carbon and ferritic steels. It may be noted that this code can

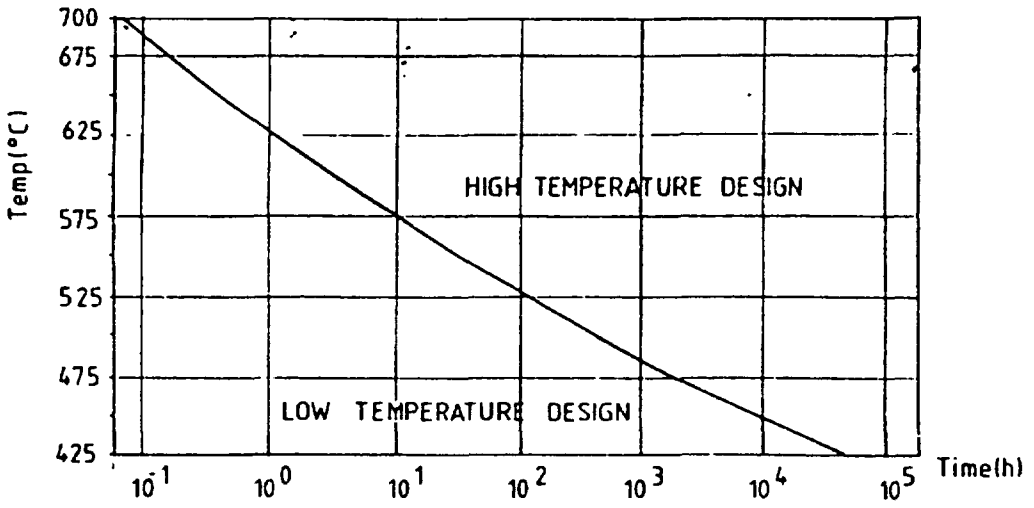

FIG. 3. RCC-MR creep cross over curve

also be used even if the temperatures are higher, provided that the associated duration is limited not to introduce any significant creep effects (Fig 3). But for the desig,n of high temperature components, these code rules are not directly applicable because Section III does not consider the failure modes due to creep and relaxation of metals at high temperatures. The design and construction criteria given in ASME CC N473 are used to assure the longterm elevated temperature structural integrity of FBR components. However, the French code RCCMR4 and Japanese code ETSG5 can be used directly for high temperature design. In the creepfatigue damage evaluation procedures given in the design code, distinction is made between loadcontrolled and deformation-controlled quantities. The codes also categorize applied load conditions as Normal (level A), Upset (level B), Emergency (level C) and Faulted (level D) and accordingly set different limits. Creep-fatigue damage assessment is not required for level C and level D loadings. Recent opinion of design code developers is that the damage under level C should also be considered

3.1 Creepfatigue design Criteria

Design codes specify appropriate limits on creep fatigue damage. The steps involved are as follows.

Stress and strain, the number of cycles, and time durations are the primary parameters that are used to predict and control the creepfatigue damage. These informations are extracted from analysis results.

Fatigue damage is computed using Miner's cumulative fatigue damage rule and creep damage is by Robinson's 'time fraction' damage rule. To account for the creep and fatigue interaction, a cumulative creep and fatigue damage assessment is used. The design limit is given by

$$\Sigma (n/Nd)_i + \Sigma (t/Td)_k < D$$

where, n =number of applied cycles of loading condition i, Nd =number of designallowable cycles of loading condition i Nd is read from the fatigue curves corresponding to the maximum metal temperature during the cycles tor the equivalent strain range $\Delta\varepsilon i$. t time duration of load at the condition k, Td =allowable time for a given effective stress from load k, Td values are obtained by entering the stress;orupture curve at a stress value equal to the effective stress σeq (from load K)

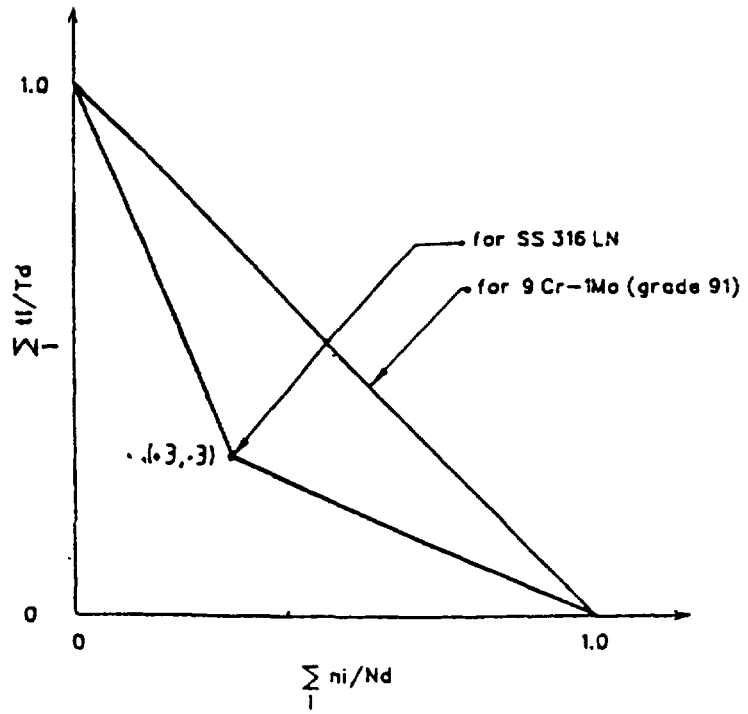

FIG. 4. Creep-fatigue interaction limit

divided by the factor K' 0.9. D =allowable cumulative damage limit which is a function of the cycle or time fraction sum (Fig 4). An equivalent strain range approach to multiaxial stressstrain effects is used. Rules for determining the equivalent strain range are intended to be applicable whether principal strains change directions during the cycle or not. The equivalent strain range is given by,

$$\varepsilon_{eq} = \{2/3\ [(\Delta\varepsilon x - \Delta\varepsilon y)^2 + (\Delta\varepsilon y - \Delta\varepsilon z)^2 + (\Delta\varepsilon z - \Delta\varepsilon x)^2 + 6(\Delta\varepsilon xy^2 + \Delta\varepsilon yz^2 + \Delta\varepsilon zx^2)^{1/2}]\}^{1/2}$$

The multiaxial creep rupture criteria based on ORNL model is used for defining the equivalent stress needed for the computation of creep damage in ASME CC N47. As per this,

$\sigma_{eq} = \sigma_{vm} \exp[c(J1/Ss-1)]$
where
$J1 = \sigma_1 + \sigma_2 + \sigma_3$
$Ss = [\sigma_1^2 + \sigma_2^2 + \sigma_3^2]^{1/2}$
σ_i are principal stresses. c = 0.24 for ASS and 0.0 for ferritic steels

3.2 Codified Materials

ASME CC N47 deals with SS 316 which has slightly different composition than SS 316LN. However, SS 316 LN has been codified in RCCMR and hence more appropriate for PFBR. For SG material modified 9CrlMo (91), properties are not codified presently in the nuclear codes (ASME Sec VIII codifies this material) and it is expected that this material data will be included in the nuclear code in the near future6. However sufficient material data is available in literature for this material' and also for D9 material8.

3.3 Design rules for welds

Weldments can be the life limiting feature of a componenet and therefore specific rules are needed for the design of welded joints. Although numbers are small, the weld failures that have occured in FBRs have, neverthless, proved costly. Often they have caused a long shut down time. They have al.so led to expensive programmes of inspection and repair9. One aspect which is of particular concern is that a significant proportion of the weld failures have occured long before the design life of the plant. The reason for this lies in the design procedures used earlier for welds. There was an implicit assumption that, provided creep rupture strength of the weld metal matches that of the parent metal, the life of the weld will be same as that of the parent material. According to the currently recommended weld design rules for the European Fast Reactor10, the stress and strain analysis is carried out as if the structures were made of humogeneous material, and factors (fatigue and creep strength reduction factors) are then applied to the parent rnaterial failure properties to allow for any weakening effect of the welds. Though factors are separately applied for creep and fatigue, the reduction factors under creepfatigue interaction effects need to be considered. Comprehensive creep strength reduction factors are provided in RCCMR, and are likely to be adopted for the EFR. Table II indicates the essence of the recommendations.

TABLE II

	Parent material	Weld metal and welding procedure	Type of weld and inspection
Creep damage	Sr	JrSr	nJrSr
Fatigue damage	$\Delta\mathfrak{E}$ - > N	$\Delta\varepsilon$/Jf - > N	f.$\Delta\varepsilon$/Jf - > N

The factors J are to account for weld material differences with respect to parent material behaviour. The factor n covers the possibility of defect being present in the weldments and is related to the type of inspection performed. The factor f is used as a fatigue strain reduction factor and is dependent on the type of weldment. RCCMR recommends a value Jf = I . For full penetration weldments with full volumetric inspection n = 1, f=l. For weldments with partial penetration or with reduced inspection n = 0. 5, f = 4. These values are chosen to penalize such weldments so that they are avoided in critical parts of the structure. Jr is time and temperature dependent; 0.8<Jr<l.0. The UK design procedures for assessment of structural integrity at high temperatures, called CEGBR511 has also given an explicit treatment for weldments in volumes 6 and 7. Volume 6 uses a simplified reference stress technique to assess the behaviour of dissimilar metal weldments. An appropriate multiaxial definition of the reference stress in the region of the transition joint is evaluated and used in conjunction with laboratory data on crossweld specimens to estimate the creep damage fraction in the transition joint. This is then added to fatigue damage fractions, allowing for strains induced during temperature changes as a result of the different thermal expansion coefficients of the materials in the joint, to give the total damage fraction. Volume 7 addresses the behaviour of dissimilar welds. In particular, factors are given for modifying the homogeneous reference stress to allow for the stress redistributions which occur in weldments as a result of offloading of stress from the weaker constituent materials to the stronger ones.

3.4 Effect of irradiation

The main vessel and inner vessel are exposed to relatively low neutron dose levels less than I dpal2. The thermal neutron irradiation produces helium, mainly by the reaction with boron present in the steel. Helium affects creep rupture strength and ductility of ASS in the creep regime The interim recommendation for design activities'3 is to apply a stress reduction factor which varies as a function of helium content.

3.5 Effect of sodium

The effects of reactor quality sodium on the mechanical properties for SS 316 LN and modified 9 Cr 1 Mo (T91) steel base matel are negligible. Hence material data generated in air could be safely applied for the design of components with wall thiclcness larger than 2 mml4.

4. FUEL SUBASSEMBLY DESIGN

Two components that are subject to severe operating conditions are fuel cladding tube and the hexagonal sheath called 'hexcan'. Typical details of a fuel subassembly are shown in Fig 5. While both clad tube and hexcan are subject to same level of neutron irradiation, their operating temperatures and environments are significantly different. Fuel cladding tube operates at temperatures upto 970 K at which damage due to thermal creep is important while operating temperature of hexcan is atleast 100 K less. Therefore, only irradiation creep and void swelling are important for hexcan from deformation considerations. Moreover, hexcan is subject to moderate internal pressure of 0.5 MPa due to coolant temperature while fuel clad is subject to internal pressure upto 6 MPa due to accumulated fission gases. Fuel clad is subject to fuel side corrosion in addition to that due to sodium. Therefore, design of clad tube is complex and involves various phenomena due to neutron irradiation and high temperature. While the steady state clad midwall hotspot temperature is as high as 970 K, under transients like LOFA and TOPA it can go up to about 1150 K. The neutron fluence seen by clad in its residence time inpile is more than 100 dpa. Apart from thermal creep due to high temperature operation, it is also necessary to consider irradiation induced creep and the embrittlement of material due to neutron irradiation. ASS is the current choice for fuel clad and it is used in 20 % CW condition to improve its resistance to irradiation induced deformations like swelling and creep, it is also necessary to consider the cold work recovery when the material is subject to temperature transients In this regard the rate of temperature rise becomes important. It has also been reported that there is additional phenomenon of liquid metal embrittlement under high temperature transients due to fission products collecting on the inner surface of cladding tube.

Early designs of fuel concerned with limiting thermal creep calculated using correlations obtained on unirradiated material to the outpile creep mpture elongation exhibited by irradiated material. When data on outpile mpture life on irradiated material was available it was sought to be used on a lifefraction rule concept. This practice of using only therrnal creep in assessing damage was on the premise that irradiation induced creep is structurally nondamaging. The stress exponent in the irradiation creep equation being unity unlike in thermal creep expression is also a pointer to this fact. Thus irradiation induced creep in fuel subassembly components is important only from deformation considerations. One of the deformations that is lifelimiting is the dilation of fuel subassembly hexagonal sheath due to irradiation induced creep by coolant pressure. Another instance of significance of irradiation induced creep is bowing of subassembly under thermal and neutron flux gradients.

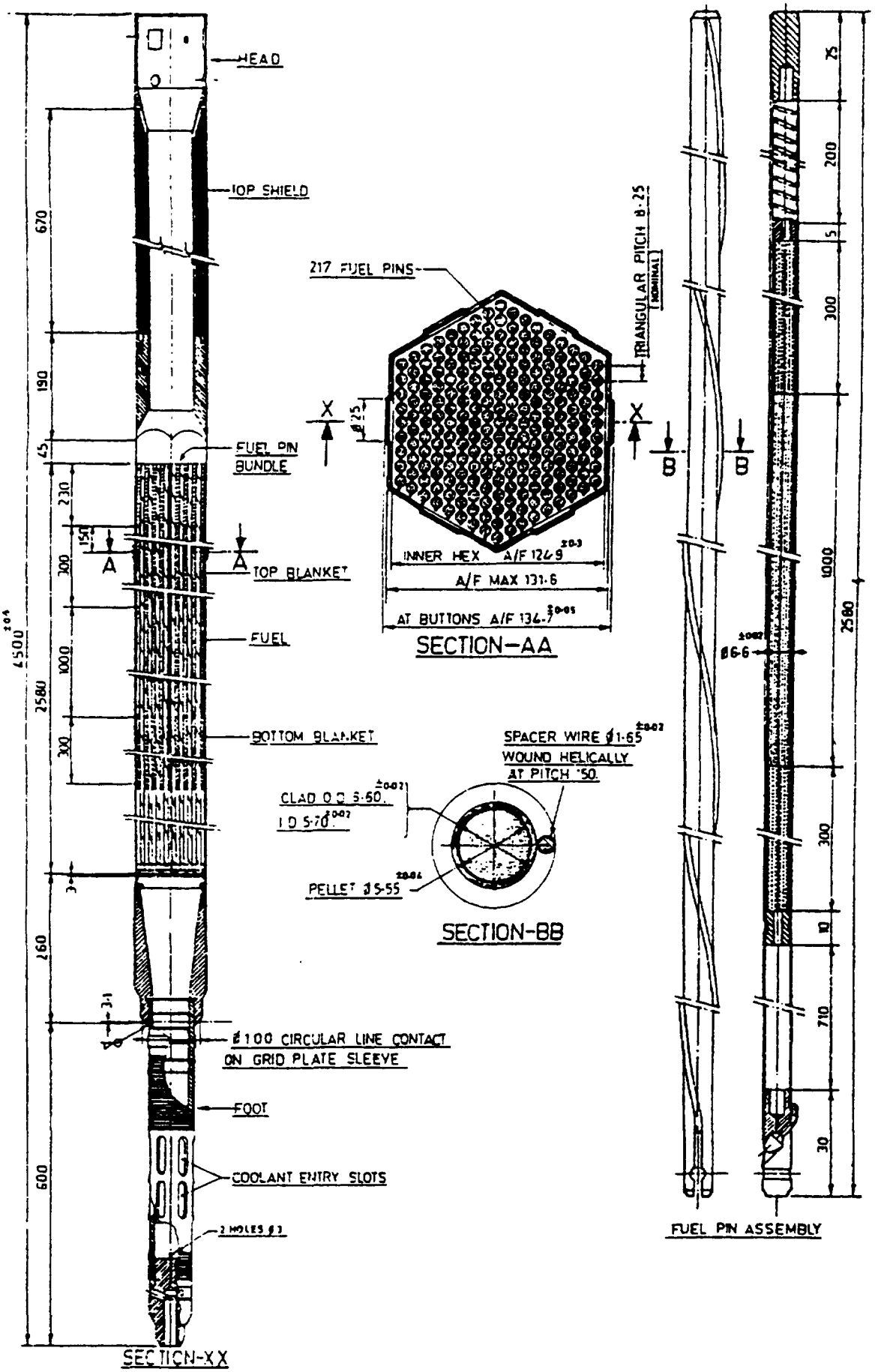

FIG. 5. Fuel subassembly

TABLE III

	Categories 1 & 2 (Normal operation & upset)	Category 3 (emergency)
1	Pm $< 0.6 \times \sigma u$	Pm $< 0.7 \times \sigma u$
2	(Pm+Pb) $< 0.6 \times K \times \sigma u$	(Pm+Pb) $< 0.7 \times K \times \sigma u$
3	(Pm+Pb+Q)max $< \sigma y$	
4	$1/2 \times \sigma$max $< 2/3 \times \sigma y$	
5.	Σ (ti/td) < 0.25 for category 1, < 0.5 for category 1 & 2	
6	Σ (ti/td) < 1 for category 1,2 & One category 3 incident	

With data on inpile rupture life becoming available, it was found that inpile creep rupture life is as good as unirradiated material rupture life and using creep rupture correlations obtained by out-pile testing on irradiated material would be overly conservative. Recent experiments indicate that rupture life is reduced only beyond a threshold fluence. This inpile rupture life data is presently utilised along with a lifefraction rule as the stress in the clad tube varies with fuel burnup.

For assessing the damage due to temperature transients, tests have been conducted on irradiated material by simulating transient by induction heating. Heating rates upto 1 10 K/s have been achieved. Correlations on rupture life as a function of heating rate, temperature, sbress, fluence etc. have been derived for use in analysis. It has been found that ASS are subject to enhanced embrittlement due to low melting point fission products under transients. This phenomenon has been terrned as ' fuel adjacency effect'. Fatigue damage is negligible for .fuel clad. A typical set of structural design criteria for irradiated components in PFBR is presented in Table III.

5. STRUCTURAL ANALYSIS METHODOLOGY

The creep fatigue damage assessment in compliance with the design codes, are based on the sbain and stress history. Hence the analysis to evaluate stress and strain in critical regions of a component from the loading history is the main stage of design. Depending on the design stage of a component, stresses and strains to expected during operation need to be known more or less accurately. Accordingly, the necessary computational effort varies. Some inelastic considerations are possible on the basis of fictitiously elastic analyses along with correction factors. The most important prerequisite of a rigorous inelastic analysis is the material model. It describes the stress-straintimetemperature response of a material in a homogeneous process by a set of constitutive equations. They are solved simultaneously along with equlibrium and continuity equations. The constitutive equations are derived empirically using a phenomenological approach to correlate the test data. They are the weak link in the structural analysis. Such a situation is emphasised in Fig 4.

Since the stress/strain response of the components is closely related to life prediction, the reliability of life prediction depends strongly on the adequacy of the constitutive models employed in the analysis. To illustrate this, the results of a parametric study on a bar subjected to a through wall temperature gradient by using a 'linear kinematic hardening' and 'Chaboche plastic' models performed by European Fast Reactor (EFR) design groupl5 are presented. The study indicates that the maximum and minimum stress levels predicted by the models (212 and 16 MPa by linear

kinematic hardening model, 145 and 118 MPa by Chaboche model), are quite different while the stress ranges amount to closely similar values. Accordingly, fatigue damage predictions differ by a factor up to 10, whereas the creep damage is over predicted by a factor up to 300 by the elastic analysis route of RCCMR. Hence it is necessary to employ more realistic constitutive equations to perform inelastic analysis of critical components of FBR.

5.1 Constitutive Equations

Selection of a 'good' constitutive model is the most important and difficult step in the inelastic analysis. A 'good' constitutive model is the one, the application of which gives realistic stresses and strains, taking into account rate dependent effect (sometimes called viscous), time dependent behaviour (rheological), history dependent effects (plastic), etc. Towards this, the most important requirement demanded from a constitutive model is its ability to simulate with reasonable accuracy, all the essential mechanical behaviour at high temperature like, creep, plasticity, creep-plasticity interaction, rate effects, cyclic hardening, strain memory, time recovery or thermal ageing, under monotonic and cyclic loading conditions. With reference to FBR application, broadly two forms of constitutive equations are currently being used. The first is based on traditional classical theories of plasticity and creep and the second form of equations are based on the unified creep-plasticity theory (also called viscoplastic theory).

5.1.1 Semilassical theory

Semiclassical theory is based upon the fundamental assumption that the total inelastic strain is regarded as the sum of time independent ('plastic') and time dependent ('creep') quantities. These time independent and time dependent quantities are evaluated from the classical theories of plasticity and creep respectively. However, certain interactions between these two types of processes are introduced by ~ad hocb mles such that the plasticity has some ratedependence and the creep is influenced by a rateindependent term. These interactions have the nature of empirical modifications of the classical laws. They allow some account to be taken of the real complexities of material behaviour in restricted circumstances but are unlikely to be fundamentally accurate. Models are not many in this category and the difference between them is mainly in the methodology adopted to model the cyclic hardening or softening behaviour with the hold time effectsl0. The 'ORNL' model developed by Oak Ridge National Laboratories, is probably a complete model based on the semi-classical theoryl6. The salient features of ORNL model are dealt in ref[17].

5.1.2 Viscoplastic theory

In the theory of materials, the materials are generally classified based on their rate-independent (elasticity or plasticity) and ratedependent behaviour (viscoelasticity or viscoplasticity) The intrinsic phenomena of viscoelasticity are relaxation, creep and rate dependent energy dissipation. A general feature of viscoelasticity is the 'fading memory' property, i.e., all past histories are completely forgotten after sufficiently long time. Generally, the rate independent plasticity is characterised by a perfect memory',i.e., the influence of the input history on the response remains valid irrespective of the time between past events and the present. Viscoplasticity mimics both rate independent (elastoplastic) as well as rate dependent (viscoplastic) occur simultaneously.

The viscoplastic behaviour is seen in certain metal alloys, especially under extreme thermomechanical loadings. To illustrate this, with reference to FBR situation, a deformation mechanism map (interrelationship between temperature, stress, strain rate and possible deformation mechanism) developed by Asbyl8 for SS 316, is reproduced in Fig 6 highlighting only the relevant

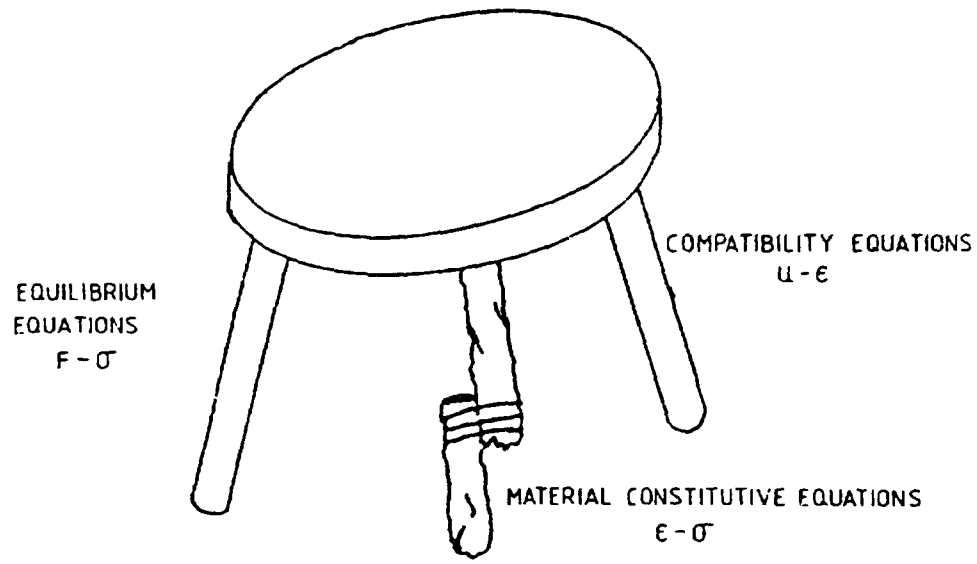

FIG. 6. The three bases of structural analysis

aspects. Basically there are three regions marked in the figure, which are separated by two solid lines, corresponding to infinitely small strain rates and extremely high strain rates respectively. In region I and region II, time independent deformation mechanisms, viz. elasticity and plasticity, occur. When rate of loading is very small (region I), the asymptotic state is attained during the loading stage itself and hence further response after loading is negligible, thus justifying the absence of viscous effects. If the rate of loading is extremely fast (region II), then, there is no time available for viscous deformation to occur and hence under this condition also, viscous effects are absent. The region III is the domain of viscoplasticity wherein material response is function time i.e., the response continues even after loading/unloading. For metals loaded at temperatures lower than about 0.3 times of their absolute melting temperature (Tm), the viscoplastic region III in between the above two lines are absent. But for the temperatures higher than about 0.3Tm> the width of this region (represents the viscous stress) increases significantly with the temperature. For the given temperature, the total internal stress developed may be decomposed into elastic, plastic and viscous contributions. At the higher temperatures (> 0.6Tm), the elastic contribution is even absent and so the viscous flow starts at zero stress itself. It is to be emphasised that the viscous stress is responsible for the subsequent time dependent behaviour.

Many viscoplastic theories have been developed to model these complex processes in a constitutive model. Among them, a '23parameter Chaboche model'19 is found to be suitabie one for FBR applications because of its ability to simulate accurately all the essential material behaviour in the temperature range of 300-900 K.

Since a lot of expensive material data is needed to identify all the 23 material parameters and the identification of these constants from these experimental data itself is very difficult, the complete 23parameter Chaboche viscoplastic model is simplified and a 'Reduced Chaboche Model' has been: derived with only 13 material parameters. These 13 parameters have been identified from very few experimental data based on physical interpretations attached to each of the material parameters. Out of these 13, only 6 parameters are found to be temperature dependent. Using Reduced Chaboche Model, the key components of PFBR namely inner vessel and control plug have been analysed and

results are compared with those obtained using ORNL model. From the analysis the maximum operating temperature for the required design life for PFBR has been arrived at. More details of application viscoplasticity theory to the high temperature design can be found in ref[17].

6. VALIDATIONS

An example is presented here to illustrate the validity of design code procedures in conjunction with detailed inelastic analysis with Reduced Chaboche Model. This example which is given in detail in ref[20] deals with life prediction of Ubend specimen subjected to loads equivalent to those of FBR's structures and designed to study simultaneously creep under tension and compression. The details of the geometry is given in Fig 7 along with loading details. The material constants for SS 316 LN at 873 K used in the analysis are given in ref[17]. Experiments indicated that the number of load cycles to produce 0.1 mm crack size in the internal surface (which is under tensile stress) is 1280, whereas 1365 load cycles were needed to produce the same size crack on the outer surface which is under compressive stress. The corresponding theoretical predictions are 648 and 803 load cycles, which shows that the currently used life prediction approach in compliance with RCCMR seems to be conservative. It may be worth to note that the corresponding load cycles according to elastic analysis are 241 and 293. Thus the present investigation indicates that the full inelastic analysis brought the benefit of a factor of 2.7 on number of cycles to failure when compared with elastic analysis.

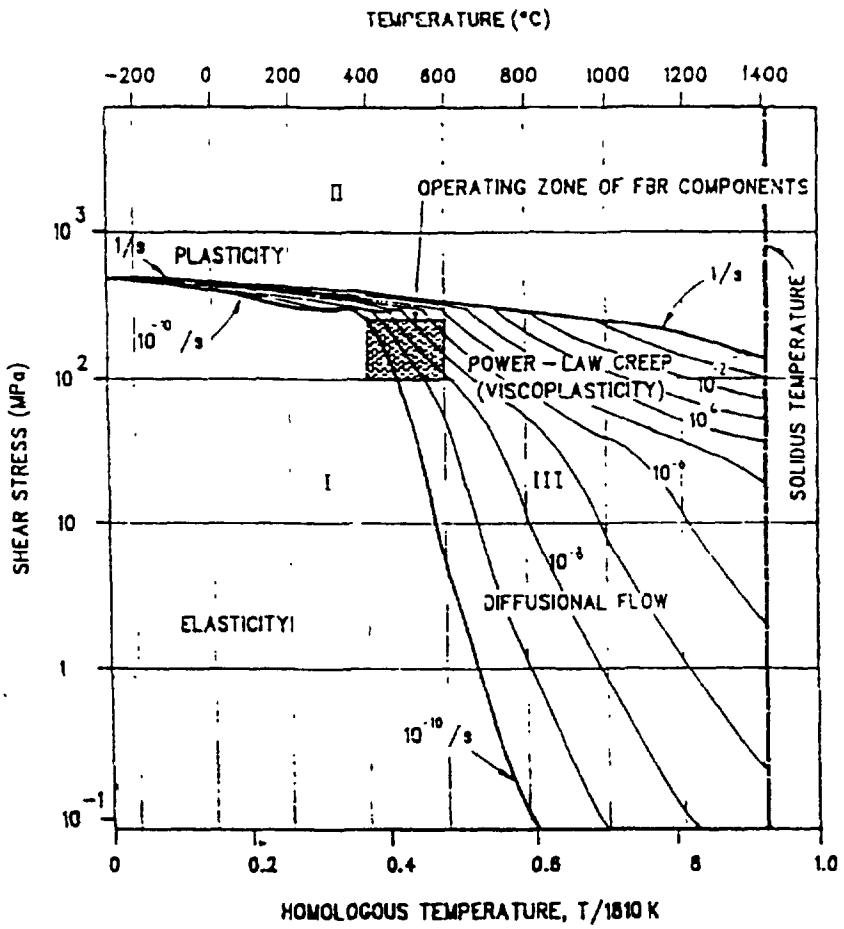

FIG. 7. Deformation mechanism map for SS 316

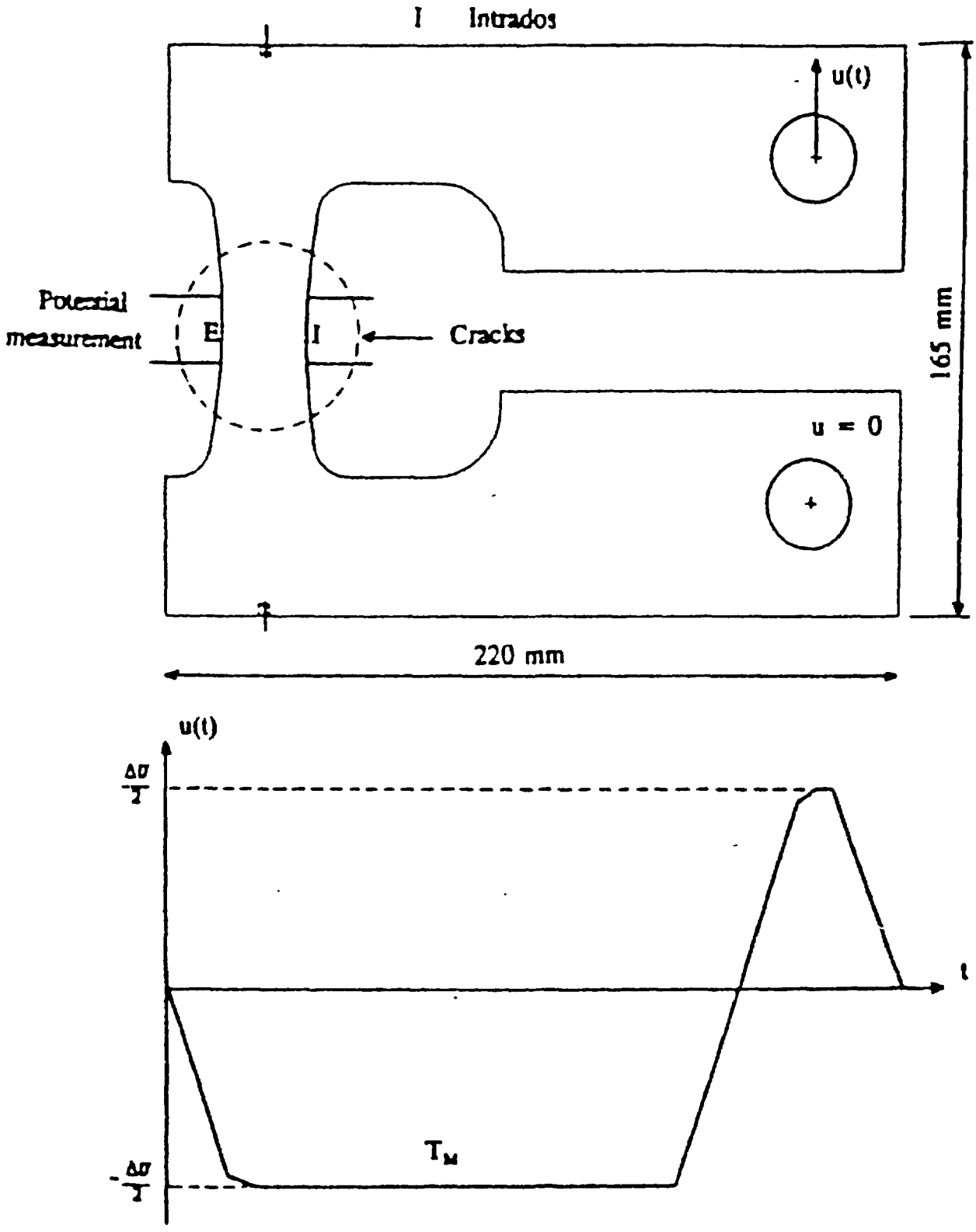

FIG. 8. Description of geometry and loads on U bend specimens

TABLE IV

component	thermal transients	critical locations
CP	reactor scram	the junction of upper stay plate - outer shell
Inner vessel	reactor scram	hot side of connection of redan with IHX stand pipes.
Main vessel	DHR operation	straight portion near Na free level.
IHX	reactorscram and reactor shut down	top tubesheet - shell junction
SG	reactor shut down	top tube sheet and Na inlet nozzle.
Piping	reactor shut down	elbows

TABLE V

Primary outlet Temp (K)	Elastic analysis			Inelastic (ORNL)			Viscoplastic (CHAB)	
	CP	IV	IHX	CP	IV	IHX	CP	IV
793	285	1033	8716	3028	5466	48092	4095	18395
803	177	427	3398	2000	7592	18906	2647	11867
813	108	208	1490	1217	4717	7700	1633	7472
823	68	106	718	728	2890	3523	1048	4508
833	42	58	365	500	1670	1670	773	2907

7. PFBR ANALYSIS

The critical out of core components, viz. CP, IV, IHX have been analysed for estimating their life at various operating temperatures in compliance with RCCMR. The governing thermal transients and the critical locations for each of these components are given in Table IV.

For the inelastic analysis the neccessary material data for ORNL model has been taken from RCCMR appendix Z and for viscoplastic analysis, the Reduced Chaboche Model is used. In identifying material parameters, material data generated at Material Development Division was used. Analysis is in progress for SG and main vessel. Viscoplastic analysis has been done for CP and IV. For IHX, considering the convenient safety margins with inelastic analysis using ORNL model itself (ORNL gives conservative result), viscoplastic analysis is not required.The summary of results of analysis for CP, IV and IHX are depicted in Table V. Details of analysis can be found in ref[21-23].

CP and Inner vessel can not meet RCCMR 87 code rules by elastic analysis route for temperatures above 775 K. CP is the most critical component. For the design requirement of 1000 cycles which corresponds to the reactor design life of 30 years, maximum permissible reactor outlet terr;perature can be 823 K. This corresponds to a steam temperature of 763 to 773 K. Thus by way of performing a detailed analysis with realistic material model, it is demonstrated that 50 K increase is possible in the steam temperature which in turn results in 1% increase in plant efficiency. This increase in efficiency represents an additional energy of 12.5 MWe during entire service life of the plant. This is the benefit of performing detailed inelastic analysis. More details on operating temperature for an FBR can be found in ref[24].

8. FURTHER STUDIES

8.1 Material data

For PFBR material SS 316 LN, relaxation curves with starting strains 0.30.5 % for temperatures 770 870 K and cyclic consolidation curves (maximum stress vs number of cycles) for different hold times should be generated in order to define all the 13 material parameters that are associated with Reduced Chaboche model. For modified 9 Cr 1 Mo (91 grade), stress strain hysteresis loops, creep, relaxation and cyclic consolidation curves need to be generated in order to define material constants for SG analysis. It may be worth to note that the effect of heat to heat variation should be taken to account in generating the material data.

8.2 Design rules for weld

Sufficient material data to validate the currently recommended RCCMR design rules for welds need to be generated by including the effects of weld metal, welding procedure, type of weld and inspection creep fatigue damage assessment. Emphasis should be given on the validation of weld strength reduction factors in case of creep fatigue interaction.

8.3 Validations

In order to validate creep fatigue damage methodology with particular reference to PFBR situation taking into account possible scattering in the material data, idealisation procedure for geometry, boundary conditions, loading and material modelling in the finite element analysis1 experiments should be conducted on simple benchmark geometries involving multiaxiality, weldments, stress concentrations etc. at high temperature.

8.4. Collaboration

There is a good case for settlement some form of collaboration to pool the existing information on the material data and benchmark validation results towards establishing confidence on the creep fatigue design methodology.

9. CONCLUSIONS

Various aspects involved in creep fatigue design of FBR components including the characteristic features of FBR, current creepfatigue design approach in compliance with RCCMR (1987) design code, material data, effects of weldments and neutron irradiation, material constitutive models employed, structural analysis and further R&D required for achieving maturity in creep-fatigue design of FBR components were discussed.

One typical validation study and an example for PFBR analysis for creep fatigue damage assessment have been dealt in this paper. The benefits of detailed viscoplastic analysis with Reduced Chaboche and ORNL material models in demonstrating higher operating temperature and longer design life have also been brought out. Finally, further R&D required in this field have also been discussed.

ACKNOWLEDGEMENTS

Authors sincerely acknowledge the technical infonnations supplied by Shri S.C. Chetal, Head, Nuclear Systems Division and Shri S. Govindarajan, Head, Core Engineering Section, towards preparing this paper.

REFERENCES

1. Lang,W. 'Transient thermal stresses in a plane wall', A report KFK Feb (1965).
2. ASME Boiler and pressure vessel code, Rules of construction of nuclear power plant components, Sec.III, Div. l, American Society of Mechanical Engineers, NewYork (1992).
3. ASME Boiler and pressure vessel code case N47, Class I components in elevated temperature service, Sec.III, Div. l, American Society of Mechanical Engineers, NewYork, (1992).
4. Design and construction rules for mechanical components of FBR Nuclear Islands (RCCMR), AFCEN, Paris, France, with addendaNov.1987
5. Elevated temperature structural design guide for class 1 components of Prototype Fast Breeder Reactor, PNC N241 84 08 (1), Power Reactor and Nuclear Fuel Development Co, Sep (1984).
6. Recommended practices in elevated temperature design: A compendium of breeder reactor experiences (19701987), Volume I Current status and future directions, Edited by A.K.Dhalla, WRC Bulletin No.362, April (1991).
7. S.L.Mannan, et al . 'Mechanical properties of modified 9 Cr 1 Mo (T91) steel', a report under preparation.
8. Gopal, S. et al. 'Design data for 20% CW D9 material' Internal report No. PFBR/31100/DN/10171RA, June 1994.
9. Martin, L. et al. 'Leak before break operating experience from European Fast Reactors', Proc. Int. Conf. Fast Reator and Related Fuel Cycles (FR91), Kyoto, Japan, Paper No5.4, (1991).
10. Escaravage, M. et al. 'Weldment design rules for the European fast Reactor', Seminar on High Temperature Weldments, Institution of Mechanical Engineers, London, (1990).
11. R5, An Assessment Procedure for the High Temperature Response of Structures, Berkely Nuclear Laboratories Report R5 Issue 1, Nuclear Electric plc, UK, (1990).
12. Private communication with Reactor Physics Division
13. Tavassoli, et al. 'EFR Structural materials Highlights and progress', Proc. Int. Conference on Fast Reactor and related fuel cycles (FR91), Kyoto, Japan, (1991).
14. Recommendations made in the concluding session of IWGFR/IAEA Specialists Meeting on Properties of Structural Materials in Liquid Metal Fast Breeder Reactor, Karlsruhe, Germany, Jan (1991).
15. AGT-98 from EFR Newsletter, Ed.W.Worth and D.Bammann and G.Muhling Nol, June (1990).
16. Pugh, C.E. et al. 'Currently recommended constitutive equations for inelastic design on FFTF components', 0RNLTM3602, (1972).
17. Chellapandi, P. 'Application of viscoplastic theory to high temperature design of fast breeder reactor components' PhD thesis, Dec (1994).
18. Frost, H.J. and Ashby, M.F 'DeformationMechanism maps. The plasticity and creep of metals and ceramics', Pergaman Press, (1982).

19. Chaboche, J.L and Nouailhas, D. 'A unified constitutive model for cyclic viscoplasticity and its applications to various stainless steels', ASME Journal of Enginnering Materials and TechnologyX Vol. 111, (1989).
20. Riou, B and Waeckel, N. 'Validation of a viscoplastic model in creep regime', proc. fifth international conference on creep of materials, Lake Buena Vista, Florida, USA, May (1992).
21. Alwar, R.S, Chellapandi, P. and Bhoje, S.B 'Assessment of inner vessel for a pool type fast breeder reactor based on inelastic and viscoplastic deformations', ASME Journal of Pressure Vessel Technology, Vol 115, (1993).
22. Chellapandi, P., Chetal, S.C. and Bhoje, S.B. 'Structuml design of the IHX for PFBR', Trans. IOth Int. Conference on Structural Mechanics in Reactor Technology (SMIRT10), Vol.E., Anaheim, California, Aug (1989).
23. Chellapandi, P., Chetal, S.C. and Bhoje, S.B. Creep fatigue damage assessment of PFBR control plug', a companion paper in this seminar (1995).
24. Bhoje, S.B. and Chellapandi, P. 'Operating temperature for an LMFBR' (in press). Parameter Reactor inlet/outlet (K) AT across core (K) Strucalral material Coolant PWRFBR

CREEP-FATIGUE CRACK INITIATION ASSESSMENT ON THICK CIRCUMFERENTIALLY NOTCHED 316L TUBES UNDER CYCLIC THERMAL SHOCKS AND UNIFORM TENSION WITH THE σ_d APPROACH

B. MICHEL, C. POETTE
Commissariat à l'énergie atomique,
CEN Cadarache,
Saint-Paul-lez-Durance,
France

Abstract

For crack initiation assessment under creep fatigue loading, in high temperature Fast Reactor's components, specific approaches based on fracture mechanics analysis had to be developed. In the present paper the crack initiation assessment method proposed in the A16 document is presented. The so called "σ_d method" is also validated on experimental results for tubular specimens with internal axisymetric surface cracks. Experimental data are extracted from the TERFIS program carried out on a sodium test device at the CEA cadarache.

Metallurgical examinations on TERFIS specimens confirm that the initiation assessment of the "σ_d" approach is conservative even for a different geometry than the CT specimen on which the method was set up. However, the conservatism is reduced when the creep residual stress field is relaxed during the hold time. An investigation concerning this last point is needed in order to know if relaxing the stress, when using a lower bound of the mechanical properties, always keeps a safety margin.

1 Introduction:

The design of some weldment joints can lead to geometrical singularities. Creep-Fatigue damage rules often propose to use a joint coefficient for the analysis of such singularities. As this approach can be too conservative, an alternative method can be proposed with the initiation time assessment of these flaws. For this a creep fatigue damage approach, initially devoted to the analysis of uncracked structures, has been extended to the fracture mechanics domain, where the elastic stress-train field can reach infinity around the crack tip. This method, called the "σ_d approach" is proposed in the A16 document [1], which gather up a wide range of tools necessary for fracture mechanics analyses. The specificity of this approach is to define an intrinsic distance "d" from the crack tip, where the results of an elastic analysis of the cracked body can be used, and sensitivity of the stress-strain field to the computation method is avoided. Cyclic and constant inelastic loading at the distance "d" are estimated with a simplified method. These inelastic loads give a fatigue and a creep damage with respectively a Manson Coffin and a Katchanov criteria, both identified for an uncracked specimen. The analysis is finally completed with an initiation assessment curve based on a Creep-Fatigue damage interaction diagram.

In the first part of the paper, after a brief historical aspect introducing the so called "σ_d method", the whole initiation assessment procedure is presented according the A16 document. Then, an experimental validation of the "σ_d method" is proposed for tubular specimens with internal axisymetric surface cracks. Experimental results are extracted from the TERFIS program carried out at Cadarache. In this program crack initiation and crack growth are

observed for the 316L stainless steel under mechanical and thermal creep-fatigue loading at 600° C on a sodium test device. The "σ_d method" initiation assessment is compared with the metallurgical examinations for the TERFIS specimens dedicated to the initiation analysis.

2 The σ_d method:

2-1 Distance d:

In fracture mechanics the elastic stress-strain field is infinite at the crack tip according the WESTERGAARD [2] solution, such results can't be used in an initiation criteria unless they are observed at an intrinsic distance "d" from the crack tip. In 1980 D'ESCATHA et al. [3] proposed to compute the distance "d" for a cracked specimen under a fatigue loading with an elastic approach and the CREAGER formula. Then many authors [4][5][6] extended this method to the austenitic stainless steel, with an elastoplastic estimation of the cyclic stress based on the NEUBER's rule. These previous studies showed that it exists an intrinsic distance "d" for initiation assessment approximately equal to the average of the material grain size. More recently a procedure to introduce the elastoplastic stress-strain field at the distance "d" in an initiation criteria (the σ_d method) was proposed by ROCHE [7], MOULIN et al. [8][9] and AUTRUSSON et al. [10] for a fatigue and a creep-fatigue loading. In these approaches fatigue and creep damages (V and W) for initiation assessment are respectively computed with a Manson Coffin and a Katchanov criteria, both identified on an uncracked tensile specimen. Then the creep fatigue interaction diagram of the RCC-MR is used as an initiation assessment curve of the considered flaw.

Since, the σ_d method has been validated by LAIARINANDRASANA [11] on a wide range of experimental results for CT specimens under creep-fatigue loading; moreover applications have been made for tubular notched specimens under complex thermal loading by POETTE [12].

2-2 Creep-fatigue crack initiation assessment with the σ_d method

As it is mentioned above in this approach the cumulated damage due to the creep-fatigue loading is separated in two parts :

- V is the fatigue damage due to the cyclic loading
- W is the creep damage due to the constant loading

The procedure to compute V and W according the A16 document is the following.

2-2-1 Cyclic loading :

After an elastic analysis of the strain-stress field applied to the structure, parameters to compute are :

- ΔK_I: the mode one stress intensity factor range applied to the crack during a characteristic creep-fatigue cycle. Elastic stress intensity factors can be computed with weight functions or a Finite Element analysis.
- $\Delta\sigma_d$: the maximal elastic main stress range in the crack plane at the distance d, it is calculated with the CREAGER formula :

$$\Delta\sigma_d = \frac{\Delta K_I.(1+\frac{\rho}{2.r})}{\sqrt{2.\pi.r}} \qquad (1)$$

where r=d + ρ/2, d = 50 µm for the 316L stainless steel and ρ is the crack tip radius

- $\Delta\sigma_{ref}$: the reference stress range for the cracked body, due to a primary load range ΔP

$$\Delta\sigma_{ref} = \frac{\Delta P}{P_L}.\sigma_y \qquad (2)$$

where ΔP is the primary load range norm, according the limit load sense, P_L is the limit load of the cracked body, and σ_y the hield stress.

- $\Delta\varepsilon^{ep}$: the elasto-plastic strain range at the distance d from the crack tip under $\Delta\sigma_d$, with the cyclic curve at the highest temperature of the creep-fatigue cycle. To compute this parameter a simplified method based on the NEUBER's rule is used, like described on figure 1.

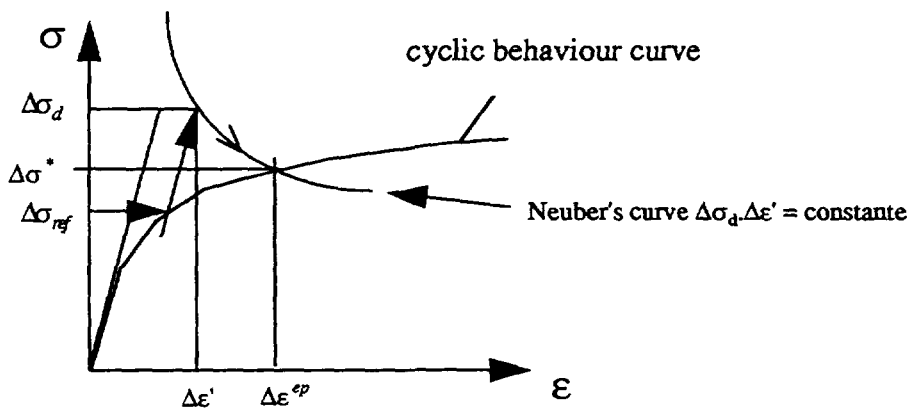

Figure 1 : Elastoplastic strain range at the distance d

2-2-2 Constant loading :

For the creep damage due to the constant loading during the hold time parameters to compute are :

- σ_{kd} : the elastoplastic stress at the distance d at the beginning of the hold time.

$$\sigma_{kd} = 0{,}5.\Delta\sigma^* \qquad (3)$$

where Δσ* is the elastoplastic stress range on figure 1, and 0,5 the symetrisation factor of the stabilised cyclic curve.

- $\Delta\varepsilon_f$: the creep strain range during the hold time.

$$\Delta\varepsilon_f = \int_0^{t^{cycle}} \dot{\varepsilon}_f(\sigma_{kd}(t),t).dt \qquad (4)$$

where t^{cycle} is the hold time length and ε_f the creep strain rate according the material creep law

2-2-3 Creep and fatigue damages :

The fatigue damage V is coming with :

$$V = N/N_R$$

where N_R is the number of cycles to failure at $(\Delta\varepsilon^{cp} + \Delta\varepsilon_t)/1.5$, evaluated on a fatigue failure assessment diagram based on the Manson Coffin criteria, and N the number of creep-fatigue cycles.

The creep damage W is computed as :

$$W = N.\int_0^{t^{cycle}} \frac{dt}{T_R(\sigma_{kd}(t))}$$

where $T_R(\sigma_{kd})$ is the creep time to failure under the stress σ_{kd}, , computed on a creep failure assessment curve based on the Katchanov criteria.

2-2-4 Creep-fatigue interaction diagram:

The creep-fatigue interaction diagram from the RCC-MR is used as an initiation assessment curve. So, initiation occurs when the representative damage point (V,W) is located outside the safe domain represented on figure 2.

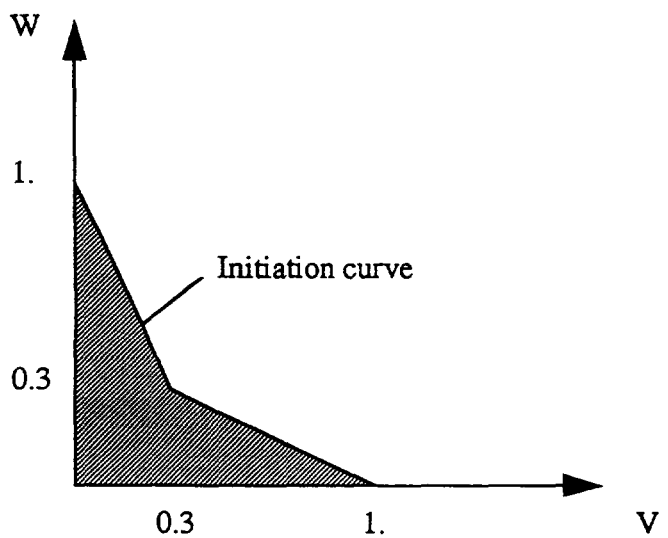

Figure 2 : creep-fatigue interaction diagram

3 TERFIS program :

The TERFIS program is carried out on an experimental sodium loop. The goal is to give quantitative estimations of crack initiation times and subsequent crack growth of flaws, for tubular geometry in representative creep-fatigue conditions of the LMFBR structures (i.e. low primary stress and high secondary stress).A lot of specimens have been tested since the beginning of this program; in the present study, experimental results are initiation times of axisymetric inner wall electroeroded notches.

3-1 Test device description :

The test specimens, shown on figure 3, are thick 316L(N) tubes with axisymetric inner wall electroeroded notches. Geometrical characteristics are the followings:

- internal radius Ri = 18 mm
- thickness t = 12 mm
- crack depths a = 0.5 mm, a = 1 mm, a = 2 mm, a = 4 mm
- specimen length L = 120 mm

The primary load is applied with a pneumatic jack and is equivalent to an axial nominal stress Pm = 29 MPa. The secondary load is a residual stress state due to an outside cold thermal sodium shock from 600°C to 350 °C applied outside the tube. This residual stress field is hold at an homogeneous temperature of 600°C and every two hours a new shock is made in order to get a periodic creep-fatigue cycle.

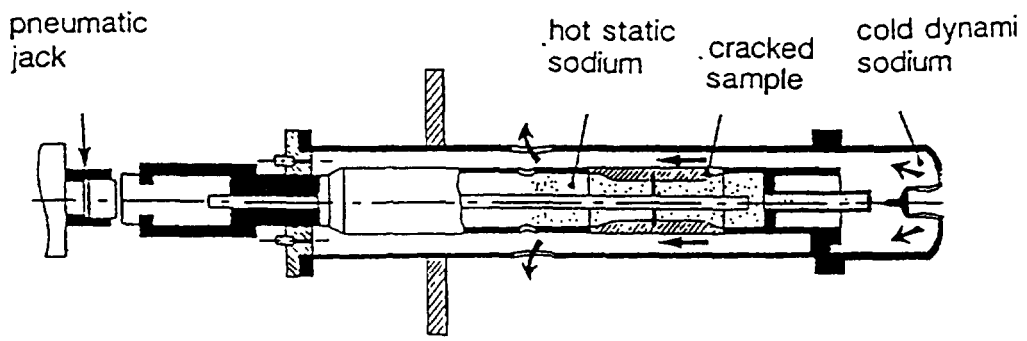

Figure 3 : Technical scheme of the TERFIS bench test.

3-2 Loading identification

The thermal loading during the cold shock is shown on figure 4, the linear part of the temperature distribution through the thickness has been identified and reach a maximum of 180°C four second after the beginning of the shock. A simulation of the stress state during the thermal shock on figure 5 shows that plasticity lead to a tension residual stress field around the crack tip when the temperature is back to 600°C.

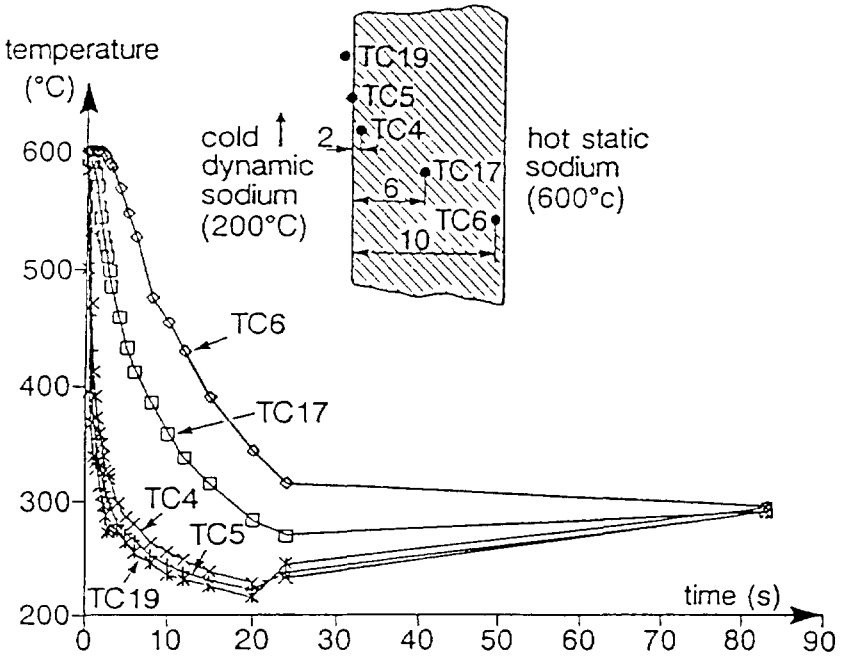

Figure 4 : Temperature-time distribution through the thickness during the thermal shock

T . Tension
C : Compression

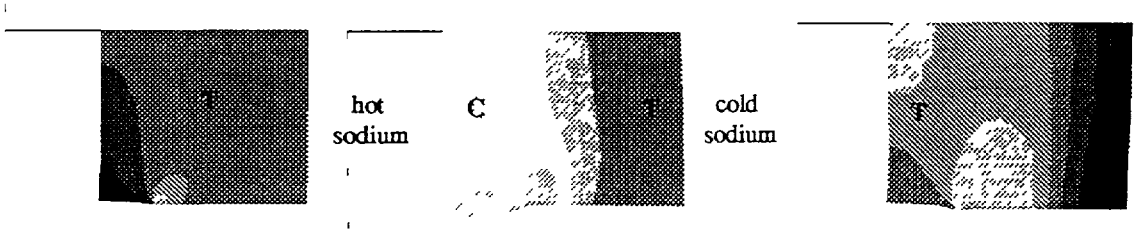

Tension Pm = 29 MPa

Tension Pm = 29 MPa
Thermal shock ΔT1 = 180°C

Residual stress field at an homogeneous temperature of 600°C

Figure 5 · Axial stress field σ_{zz} in the TERFIS specimen during a creep fatigue cycle.

The strain-stress path during the creep fatigue cycle is illustrated on a mono-dimensionnal example on figure 6, and shows that plasticity lead to a residual stress state when an elastic behaviour doesn't. To evaluate the magnitude of this residual stress state we use a monotonic equivalent load based on the remark that the stabilised cycle tend to be symmetric. So the creep tension level (σ_{kd} in paragraph 2-2-2) is half of the whole fatigue elasto-plastic stress range ($\Delta\sigma^*$ in paragraph 2-2-2).

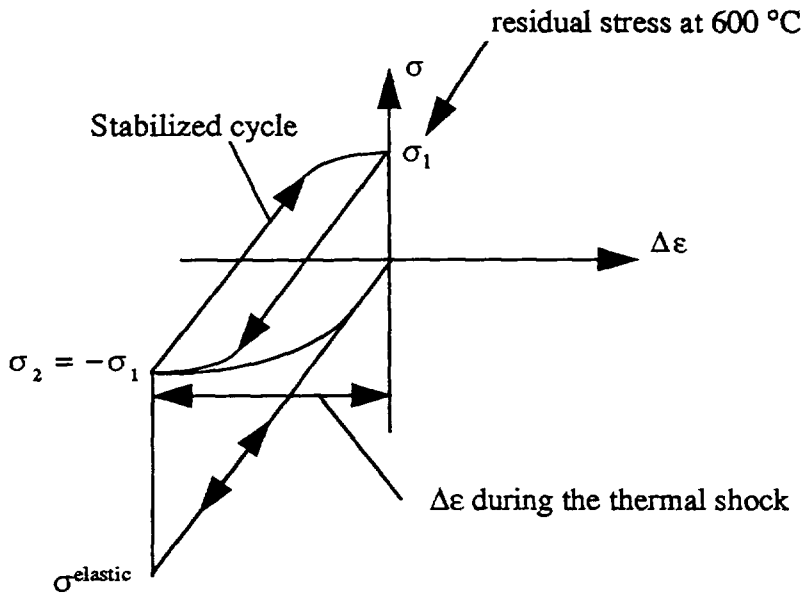

Figure 6 : Strain stress path for an elastic and an elastoplastic behaviour during the thermal shock

3-3 Experimental results

Experimental results for initiation are summarised in the following table :

Table 1 : TERFIS experimental results for crack initiation

Specimen	Initial crack depth (mm)	Final crack depth (mm)	Number of cycles
1	4	4.05	10
2	0.5	~0.5	10
	1.	~1.05	10
	2.	~2.05	10

Detail of the crack tip after ten cycles for the specimen 1 is shown on figure 7. According to the metallurgical examinations we can consider that initiation under ten creep-fatigue cycles is significant for the specimens with an initial crack depth of 1, 2 and 4 mm.

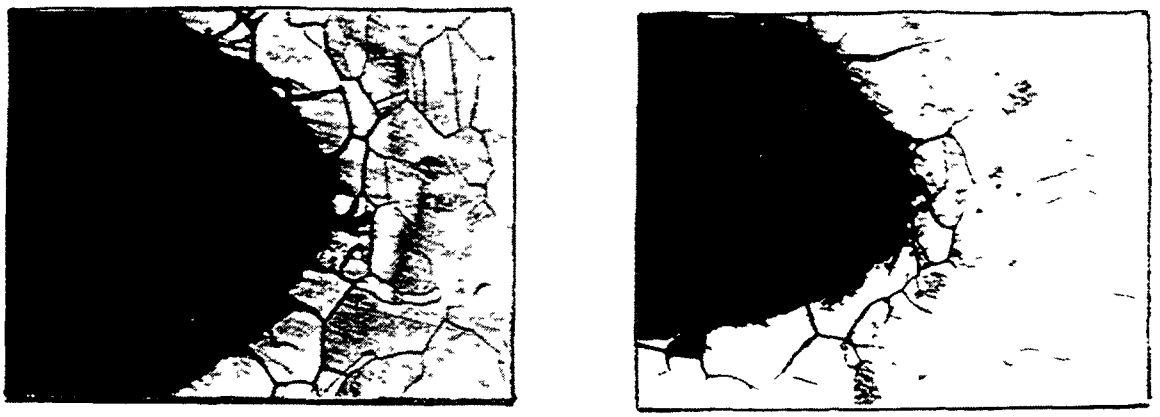

Figure 7 : Detail of the specimen 1 crack tip after 10 creep-fatigue cycles.

4 Validation of the σ_d method :

The validation consists in comparing the σ_d crack initiation assessment with experimental remarks of the paragraph 3-3

4-1 Cyclic loading :

The elastic stress intensity factors in mode I have been computed with the Finite Element code CASTEM 2000; the range is deduced from :

- K_{MAX} : only the primary tension load is applied (Pm = 29 MPa)
- K_{MIN} : the thermal bending ($\Delta T1$ = 180 °C), with compression for the inner wall, is superposed to the tension load

Table 2 : Stress intensity factor range versus crack depth

crack depth a (mm)	a/t	K_{MIN} (MPa.m$^{0.5}$)	K_{MAX} (MPa m$^{0.5}$)	ΔK_I (MPa.m$^{0.5}$)
0.5	0.042	-13.5	1.2	14.7
1	0.083	-18.5	1.7	20.2
2	0.167	-23.2	2.5	25.7
4	0.333	-26.2	3.7	29.9

Elastic properties at 500°C are:

- Young Modulus : E = 153000 MPa
- thermal expansion : $\alpha = 18{,}3.10^{-6}$ °C^{-1}
- Poisson ratio : $\nu = 0.3$

Other parameters are computed according the σ_d method described in section 2-2-1

Table 3 : Elastoplastic stress-strain range at the distance d with tensile cyclic curve at 500°C (A3-1S of the RCC-MR [13])

a/t	$\Delta\sigma_d$ (MPa)	$\Delta\varepsilon^{vp}$ (%)	$\Delta\sigma^*$(MPa)	$\Delta\sigma_{ref}$ —
0.042	819	0.7	538	0
0.083	1126	1.08	660	0
0.167	1432	1.51	765	0
0.333	1666	1.87	837	0

4-2 Creep loading :

4-2-1 Stress relaxation

The influence of the stress relaxation on the creep damage has been tested. The hold stress σ_{kd} is relaxed according the RCC-MR RB3200 [14] rule described bellow.

During the relaxation the stress-strain path is given by the elastic follow up equation :

$$\Delta\varepsilon_f(t) = \frac{C_R}{E}.(\sigma_{kd} - \sigma_R(t)) \qquad (5)$$

where $\Delta\varepsilon_f$ is the cumulated equivalent creep strain during the hold time, C_R the elastic follow up ratio (C_R =3), E the Young modulus at 600°C (E = 145000 MPa), σ_{kd} the stress at t=0 and σ_R the relaxed stress.

In order to compute the relaxed stress versus the time we also need the primary or the secondary creep law; the second one is used when the primary creep strain rate is smaller than the secondary creep strain rate for the same stress level $\sigma_R(t)$.

- Primary creep law $\dot{\varepsilon}_f(t) = K.\Delta\varepsilon_f^x(t).\sigma_R^y(t)$ (6)
- Secondary creep law $\dot{\varepsilon}_f(t) = 100.C.\sigma_R^n(t)$ (7)

where $\dot{\varepsilon}_f$ is the creep strain rate and K, x, y, C and n are the creep law parameters at 600°C :

$K = 2.2812.10^{-24}$
x = -0.9478
y = 9.0425
$C = 2.268.10^{-24}$
n = 8.2

These parameters are given for $\dot{\varepsilon}_f$ (%.h^{-1}), $\Delta\varepsilon_f$ (%) and σ_R (MPa).

The relaxed stress $\sigma_R(t)$ and the cumulated creep strain $\Delta\varepsilon_f$ are the solutions of a first order non-linear differential equation established with (5),(6) and (7). They are given in the following table :

Table 3 : Relaxed stress and cumulated creep strain during the hold time.

a/t	σ_{kd} (MPa)	σ_R (t=2h) (MPa)	$\Delta\varepsilon_t$(t=2h) (%)
0.042	269	209	0.12
0.083	330	228	0.21
0.167	382	240	0.29
0.333	418	246	0.35

4-3 Fatigue and creep damages :

The creep and fatigue failure assessment curves are shown on figure 8 and 9, and are extracted from the reference [13]. The fatigue damage V and the creep damage W are computed according the section 2-2-3 and are summarised in the following table :

Table 4 : Creep and fatigue damages

	without relaxation		with relaxation	
a/t	V	W	V	W
0.5/12	0.71	0.76	0.59	0.11
1/12	1.32	7.87	0.94	0.4
2/12	2.21	58.	1.33	0.98
4/12	3.09	201	1.65	1.72

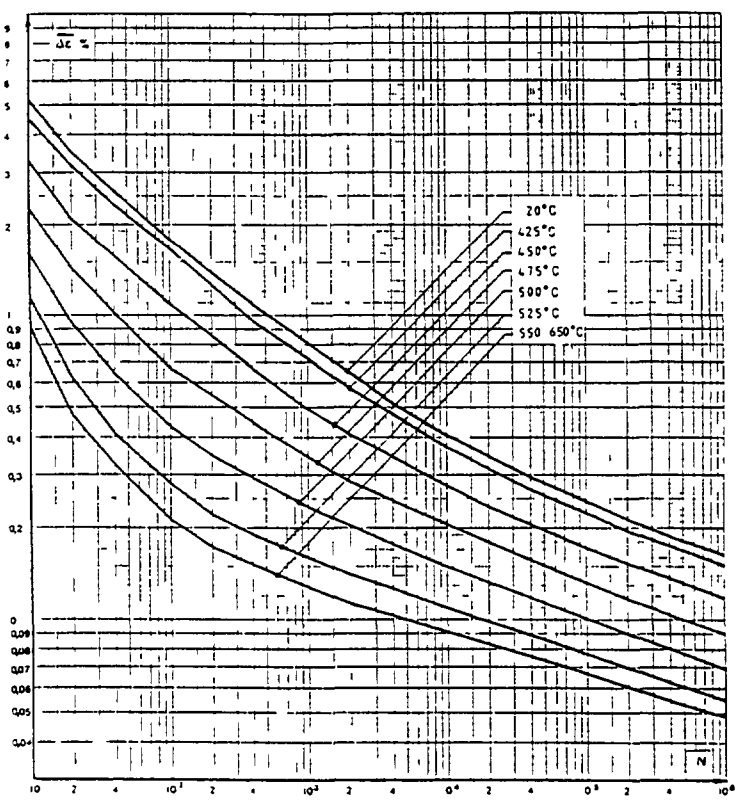

Figure 8 : Number of cycles to failure for a fatigue strain range $\Delta\varepsilon$

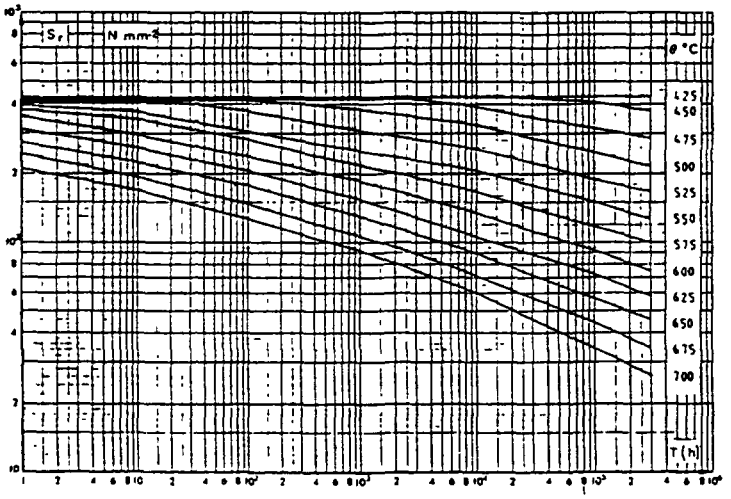

Figure 9 : Time to failure for a creep stress Sr

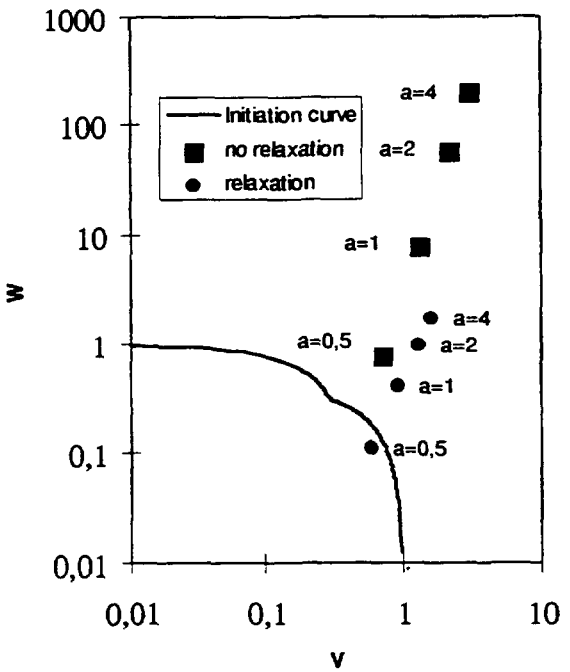

Figure 10 : σ_d initiation assessment in the creep-fatigue interaction diagram

In some cases the creep failure assessment curve of figure 9 had to be extrapolated for stresses greater than 353 MPa, and the fatigue failure assessment curve of figure 8 had to be extrapolated for strain ranges greater than 0.915 %.

The figure 10 represents the localisation of each cracks in the logscale creep fatigue initiation assessment diagram. We can see that the hypothesis of a non relaxed stress during the hold time always give a conservative initiation assessment compared to experimental observations of section 3-3. However, this conservatism is reduced when the stress is relaxed and lead to assess that the crack with an initial depth of 0.5 mm will not initiate although it is very close to the initiation curve. As the 1 mm crack initiated, we can think that the 0.5 one

was not so far from initiation after 10 cycles; so it seems that in this case the σ_d method, used with a lower bound of the creep and fatigue failure assessment curves, should assess initiation for the 0.5 mm crack.

Concerning the thermal residual stress relaxation, an investigation should be done in order to analyse the sensitivity of the initiation assessment to the mechanical properties, when the representative damage point is close to the initiation curve.

5 Conclusions :

Initiation assessment for design singularities requires a specific approach like the σ_d method presented above. The fundamental concept of this method is to consider that the singular strain-stress field around the crack is characterised by its magnitude at a distance d from the tip, where the computation of a creep-fatigue damage can be used to assess crack initiation. In the σ_d method, creep damage and fatigue damage are calculated separately with respectively a stress criteria (Katchanov) and a strain criteria (Manson Coffin). Moreover the method used an elastic analysis coupled with a simplified approach to compute stress and strain at the distance d.

The σ_d approach has been formatted as a procedure in the A16 document and a validation on a tubular geometry with an internal axisymetric surface crack is proposed. Experimental crack initiation data are coming from the TERFIS program carried out at Cadarache. The sensitivity of the σ_d crack initiation assessment to the stress relaxation has been tested. For this last point it appears that an investigation is needed to know if relaxing the stress, when using a lower bound of the creep and fatigue failure assessment curves, always assess initiation with a safety margin. However the method is always conservative, compared to the present experimental data, when the thermal residual creep stress is kept constant during the hold time.

REFERENCES

[1] A16 : "Guide pour l'analyse de la nocivité des défauts et la fuite avant rupture", Rapport DMT 95/659, troisième version préliminaire, 1995.

[2] WESTERGAARD, HM, "Bearing Pressures and Cracks." Journal of Applied Mechanics, Vol 6, 1939, pp. 49-53

[3] Y.C. D'ESCATHA, J.C. DEVAUX, J.L. BERNARD, A. PELISSIER-TANON : "A criterion for analysing fatigue crack initiation in geometrical singularities", IMechE, 1980.

[4] C. AMZALLAG, P. RABBE : "Etude de l'amorçage des fissures et de la vitesse de fissuration par fatigue de quelques aciers austénitiques", 13ème journée des aciers spéciaux, Revue de Métalurgie Décembre 1974.

[5] K. SAANOUNI, C. BATHIAS : "Study of fatigue crack initiation in the vicinity of notches" Engng. Fract. Mech., Vol.16, pp 695-706, 1982.

[6] F. BILLON : "Calcul de structures en plasticité cyclique et amorçage de fissures", Thèse de docteur-Ingénieur à l'Université de Paris VI, 1980.

[7] R. ROCHE : "The use of elastic computation for analysing fatigue damage", 9th SMIRT Lausanne, 1987.

[8] D. MOULIN, B. AUTRUSSON, B. BARRACHIN : "Fatigue analysis methods of crack like defects : strain range evaluation" 9th SMIRT Lausanne, 1987.

[9] D. MOULIN, B. DRUBAY D. ACKER : "A pratical method based on stress evaluation (σ_d criterion) to predict initiation of crack under creep and creep fatigue conditions"

Pressure Vessel Fracture, Fatigue and Life Management, ASME 1992, PVP VOL.233, pp 19-25.

[10] B. AUTRUSSON, D. MOULIN, B. BARRACHIN : "Fatigue analysis of crack like defects : experimental verification of practical rules to predict initiation" 6th ICPVT Beijing China, 1988.

[11] L. LAIARINANDRASANA : "Amorçage de fissure à haute temperature dans un acier inoxydable austenitique", Thèse de doctorat au CEA/DER/DMT Saclay, Rapport CEA-R-5692, 1995.

[12] C. POETTE, S. ALBALADEJO : "Creep-Fatigue crack initiation and growth on thick circumferentially notched 316L tubes under cyclic thermal shocks and uniform tension", 12th SMIRT Stuttgart, FG15/2, 1993.

[13] RCC-MR : "Règles de conception et de construction des matériels mécaniques des îlots nucléaires RNR", Tome I, Vol.Z : Annexe technique A3, AFCEN.

[14] RCC-MR : "Règles de conception et de construction des matériels mécaniques des îlots nucléaires RNR", Tome I, Vol.B : Materiels de Niveau 1 (Modificatif 1er Nov. 1987), AFCEN.

UK DEVELOPMENT OF A STRAIN BASED CREEP-FATIGUE ASSESSMENT PROCEDURE FOR FAST REACTOR DESIGN

C. PICKER
AEA Technology,
Risley, Warrington,Cheshire,
United Kingdom

Abstract

For some time, there has been an awareness that the creep-fatigue tests on which the ASME creep fatigue assessment procedure of the high temperature code N47, and as a consequence similar procedures that are based on it, such as RCC-MR, were performed using relatively high strain ranges and short hold periods. Long hold time, low strain range tests, more representative of service in fast reactors, have shown predominantly creep-dominated failures and these could be predicted successfully using a ductility exhaustion approach for the creep damage. The tests on which the procedures of N47 were developed, however, showed a predominantly fatigue dominated failure.

As a result of these observations, a strain-based creep-fatigue procedure was developed within the UK fast reactor programme, over a period of several years, in the late 1980s and early 1990s. This effort involved the collaboration of staff from AEA Technology, NNC Ltd and CEGB/Nuclear Electric. The aim was to produce a more mechanistically-based procedure which, it was hoped, would provide a safe but less over-conservative assessment than the stress based procedures. Because of the interaction of AEA Technology and CEGB/Nuclear Electric staff there are quite close parallels between the methodology of this procedure and those of the R5 procedure developed by the latter, although there are some differences in detail.

The procedure was developed first for application to Type 316 steel at temperatures up to 650°C, including thermal striping, and was subsequently extended to cover Mod 9Cr1Mo steel, weldments and vibration. In its present form it is limited to application with inelastic analysis methods.

This paper outlines the procedure and its background philosophies. The ductility exhaustion approach is used to assess creep damage and a short crack growth concept is used to assess fatigue damage. The fatigue cycles are assessed using the Rankine strain range, rather than the von Mises equivalent strain range. Use of a crack growth concept to assess fatigue damage permits the extension of the methodology to cover the effects of thermal striping, which are treated by consideration of fatigue crack growth thresholds. The overall procedure also employs a L-shaped creep-fatigue interaction diagram that differs from those used in other procedures. This is based on an understanding of the interaction of creep and fatigue damage mechanisms and the results of creep fatigue endurance tests covering a range of conditions.

1. INTRODUCTION

Thermal shock is a key factor that has to be taken into account in fast reactor structural design because of the high thermal conductivity of the liquid sodium coolant and the large coefficient of expansion of the austenitic stainless steels commonly used for structural components. Thermal shock can occur during reactor trips or other disturbances to steady state operation. Thermal shocks that are sufficiently acute as to cause local plasticity give rise to residual stresses. These may relax during subsequent high temperature operation, converting elastic strain into creep strain and, consequently, creep damage. Repeated cycling by thermal shocks can therefore result in creep-fatigue damage.

In the design rules of ASME Code Case N47 [1] and RCC-MR [2], the creep damage is assessed by a rupture strength time fraction rule, in which the hold times at a given load

condition are summed over the lifetime and divided by the allowable time at that load condition. This allowable time is derived from the minimum stress-to-rupture curve at a stress calculated from the given load condition divided by a factor K'. The factor K' provides a design margin relative to that data. The cumulative creep damage is the sum of creep damages from different load conditions. The Addendum to the RCC-MR Code [3] takes account of the less damaging effect of compressive stresses in creep-fatigue.

The fatigue damage in the N47 and RCC-MR design codes is based on a cycle fraction in which the number of applied cycles at a given loading condition is divided by the design allowable cycles at the loading condition. The design allowable cycles are derived, on the basis of an equivalent strain range, from fatigue data factored by a suitable margin (2 on strain range at high cycles and 20 on life at low cycles) to prevent the initiation of cracks. This margin is also sufficient to provide for uncertainties, such as surface finish, section size, residual stress, mild environmental attack plus material and loading variability [4]. The cumulative fatigue damage is the sum of fatigue damages arising from different load cycles.

The total creep-fatigue damage in the N47 and RCC-MR design codes is obtained by a linear summation of the cumulative creep damage and cumulative fatigue damage. This total creep-fatigue damage is compared with a total allowable creep-fatigue damage, D. The allowable damage, D, was based on data from high temperature uniaxial strain-controlled fatigue tests with hold periods at constant strain. These tests were generally of a short duration relative to a plant life of, typically, 200,000 hours and extrapolation to the plant life introduces a large degree of uncertainty [5].

More recently, creep-fatigue tests made at lower strain ranges and longer hold times have indicated that the failure mechanism may change under these conditions in austenitic stainless steels. At high strain ranges, failure takes place by a creep-modified fatigue mechanism in which rapid crack growth occurs through the interlinking of creep cavities by the crack tip stress/strain field of the fatigue cycle [6]. This tends to produce a fracture surface showing both fatigue striations and intergranular cracking [7]. At lower strain ranges, it is possible, particularly in low ductility material, for bulk creep cavity nucleation to take place more rapidly than the fatigue crack initiation and growth process and a totally intergranular creep-type failure will then occur [7].

These findings emphasise the importance of performing tests under conditions that produce failures representative of the low strain range, very long hold time conditions likely to occur in fast reactor components. In the UK, a design code based on a mechanistic understanding of the damage processes in creep-fatigue has been evolved [8][9]. This has subsequently been written as a damage assessment procedure for trial use and has been applied to benchmark experiments and design examples to gain experience in practical application and to examine the performance against actual failures. This procedure includes assessment of thermal striping (the rapid surface temperature variation on components exposed to the mixing zone of coolant streams of different temperature, causing strain controlled high cycle fatigue loading).

Initially, this UK-developed procedure was limited in application to Types 316 and 316L(N) austenitic stainless steels at temperatures up to 625°C and thicknesses of at least 4 mm. However, the method was later extended to cover Mod 9Cr1Mo steel, weldments and vibrational loading. In its present form, it can only be used with inelastic analysis, since its adaptation to simplified methods was precluded by the withdrawal of UK Government funding for fast reactor research and development in 1993. This paper describes the philosophies behind the procedure and outlines the rules employed to assess creep-fatigue damage.

2. BASIS OF PROCEDURE

2.1. Creep damage

The view in the UK has been that the creep and fatigue damage estimation methods used in the N47 [1] and RCC-MR [2] design codes do not provide a true representation of the

mechanisms of failure and do not place sufficient emphasis on the importance of high ductility in providing resistance to failure. The evidence indicates that creep damage resulting from repeated hold periods imposed on fatigue cycles is related more to ductility than to creep rupture strength. The idea of summing creep strain to result in failure when the ductility is reached was suggested first for ferritic steels [10] and was later extended to austenitic stainless steels [6].

In the procedure, creep fracture is assumed to be associated with the formation and growth of grain boundary cavities. It is further assumed that the material is in the minimum ductility condition, so that creep cavities grow by diffusional mechanisms [11]. Then, by a theoretical treatment of cavity growth, based on work by Dyson [12] and Cane [13], a relationship between creep strain and creep damage can be derived (see Appendix 1).

It is assumed that all casts of Type 316 and Type 316L(N) steel have the same value of minimum ductility. Whilst creep ductility varies significantly with strain rate and temperature, there is no evidence to suggest that the minimum creep ductility for Type 316 steel is dependent on either of these parameters [14]. The minimum creep ductility for Type 316 and Type 316L(N) steel is assumed to be 10%. This is based on data from a large number of tests on Type 316 steel in the temperature range 500°C to 700°C [14].

An important factor in the summing of creep strain for comparison with the ductility is that tensile creep strain in one direction can be compensated by compressive creep strain in the opposite direction, which sinters the cavities.

In multiaxial loading, the theory of constrained cavity growth suggests that the strain in the direction of the maximum principal stress appears to be the most appropriate for the calculation of creep damage. If the axes of principal stress and strain coincide, the required strain component is the maximum principal strain. To ensure conservatism, the maximum principal strain is used in all cases to calculate the creep damage.

At this stage of development of the strain-based creep-fatigue procedure, it has been necessary to distinguish between creep strain (which arises during periods of steady state operation by stress relaxation, elastic follow-up and forward strain caused by primary loading) and strain which may occur at slow strain rates during a transient. The latter is shown to be damaging by reduced endurance in high temperature fatigue tests with unbalanced cycles having slow tensile strain rates and fast compressive strain rates, compared with cycles with equal tensile and compressive ramp rates [15]. In the UK creep fatigue procedure, the distinction between creep strain occurring during steady states and that occurring during slow transients is made because there is no experimental evidence to confirm that damage from tensile creep strains, due for example to relaxation, could be reversed by sintering from slow compressive strains during transients. It is hoped that evidence will be forthcoming to enable this to be established at a later date.

At present, total (elastic and inelastic) strains occurring in parts of the operational cycle, other than the operational steady state, are termed quasi-creep strains. These quasi-creep strains are summed separately from the creep strains occurring during operational steady states and quasi-creep damage is assessed as the ratio of quasi-creep strain to the ductility.

2.2. Fatigue damage

The N47 [1] design curve for fatigue was based on continuous-cycling strain-controlled data from un-notched cylindrical specimens factored, as noted earlier, to prevent crack initiation. The majority of these data came from tests at relatively high total strain ranges, generally at least 0.6%. Under these conditions, the initiation of cracking generally occurs quite rapidly and most of the endurance is taken up in the process of crack growth. At lower strain ranges, closer to that for design conditions, the endurance becomes increasingly dominated by the cycles necessary to cause crack initiation. If, however, tensile or compressive dwell periods are introduced into the fatigue cycle, crack initiation will occur early in life and the initiation phase will be eliminated and the endurance substantially reduced [3].

In the UK creep fatigue design procedure, account is taken of the elimination of the crack initiation phase in creep fatigue and the fatigue design curve is based on a model in which a surface crack of one grain depth (conservatively assumed to be 0.1 mm) grows to a final crack depth of 0.5 mm [9]. This final depth is one which would not significantly affect the stiffness of structures of at least 4 mm thick and at which the cracks could not be readily detected. This limits the applicability of the procedure to thickness of 4 mm or greater. The crack growth model used to derive the UK fatigue design curve assumes a semi-elliptical surface crack of a depth/half length ratio of 0.2, consistent with those produced by thermal shock tests on components [9]. The number of cycles to grow a crack from 0.1 mm to 0.5 mm deep is calculated from equations developed by Tomkins [16], modified to take account of the crack shape:

$$\frac{da}{dN} = Y^2 \Delta\varepsilon_p \left[\sec\left(\frac{\pi\sigma}{2T}\right) - 1\right]a \qquad (1)$$

where

da/dN is the crack growth per cycle,
Y is a compliance factor,
$\Delta\varepsilon_p$ is the plastic strain range of the cycle,
σ is, here, the maximum tensile stress range of the cycle,
T is the material flow stress (i.e. the cyclic UTS),
a is the crack depth.

Because Y is dependent on crack depth, integration of this equation over a series of small intervals of crack growth, during which Y is assumed to be constant, is necessary.

The UK fatigue design curve, derived from the assumption of growth of surface-cracks from 0.1 mm deep to a limiting size of 0.5 mm deep, is compared with the N47 continuous cycling curve in Fig 1. At present, it has been necessary to use high cycle fatigue data factored by two on strain for total strain ranges below 0.35%, where the crack growth data are less reliable.

The N47 [1] and RCC-MR [2] design codes use the von Mises equivalent strain range $\Delta\bar{\varepsilon}$ for plastic materials to relate uniaxial fatigue data to multiaxial stress/strain conditions on components. Clayton [9] has indicated previously that the Rankine equivalent strain range provides a better correlation of multiaxial fatigue performance than the von Mises equivalent strain range (Fig 2). The Rankine strain range, as used in the UK creep fatigue procedure, is given by:

$$\Delta\varepsilon^R = \left(\frac{\Delta\sigma_1}{\Delta\bar{\sigma}}\right)\Delta\bar{\varepsilon} \qquad (2)$$

where

$\Delta\sigma_1$ is the maximum principal stress range,

$\Delta\bar{\sigma}$ is the von Mises equivalent stress range,

$\Delta\bar{\varepsilon}$ is the von Mises equivalent strain range.

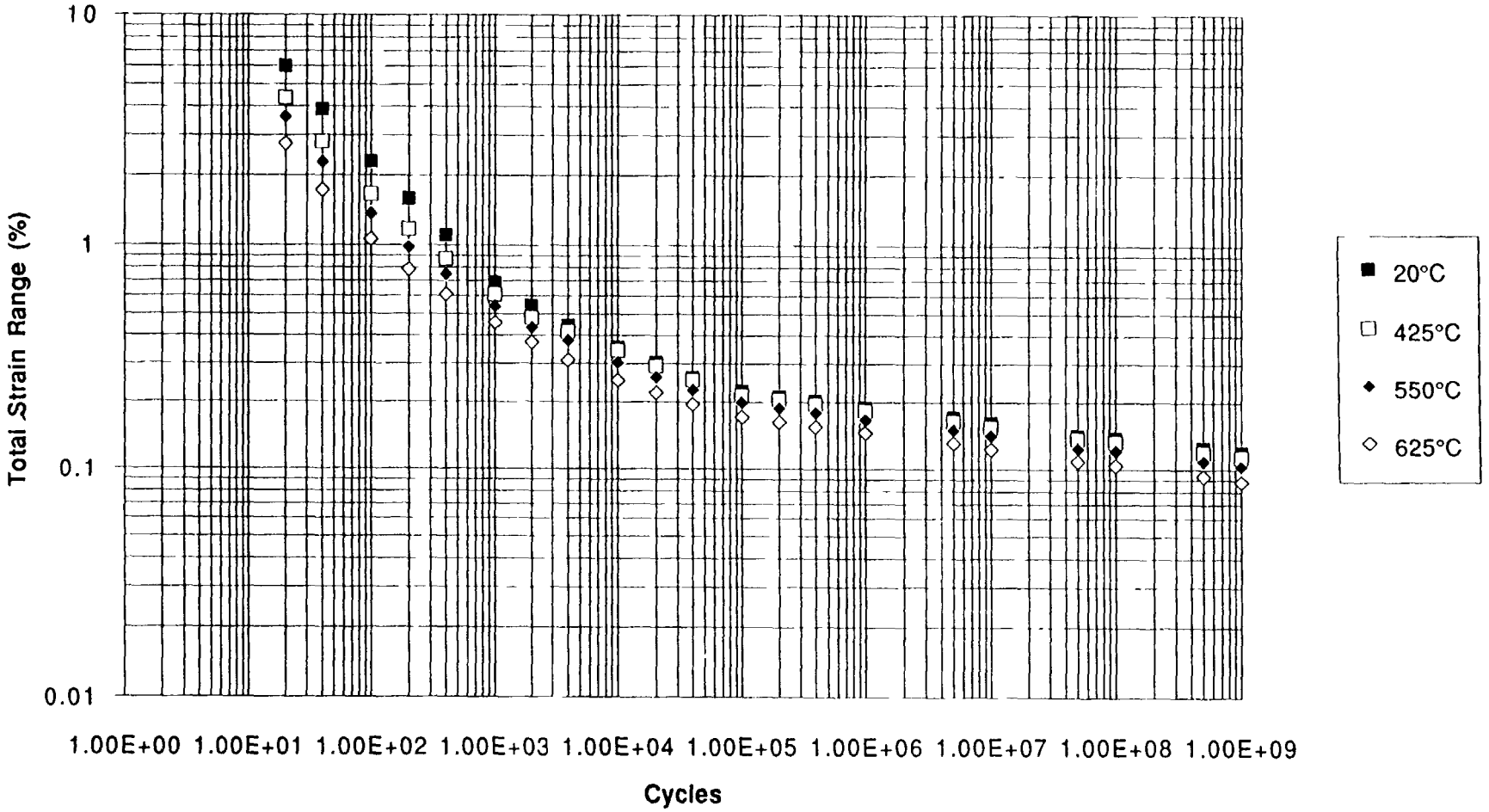

FIG. 1. Fatigue design curve for Types 316 and 316L(N) steel.

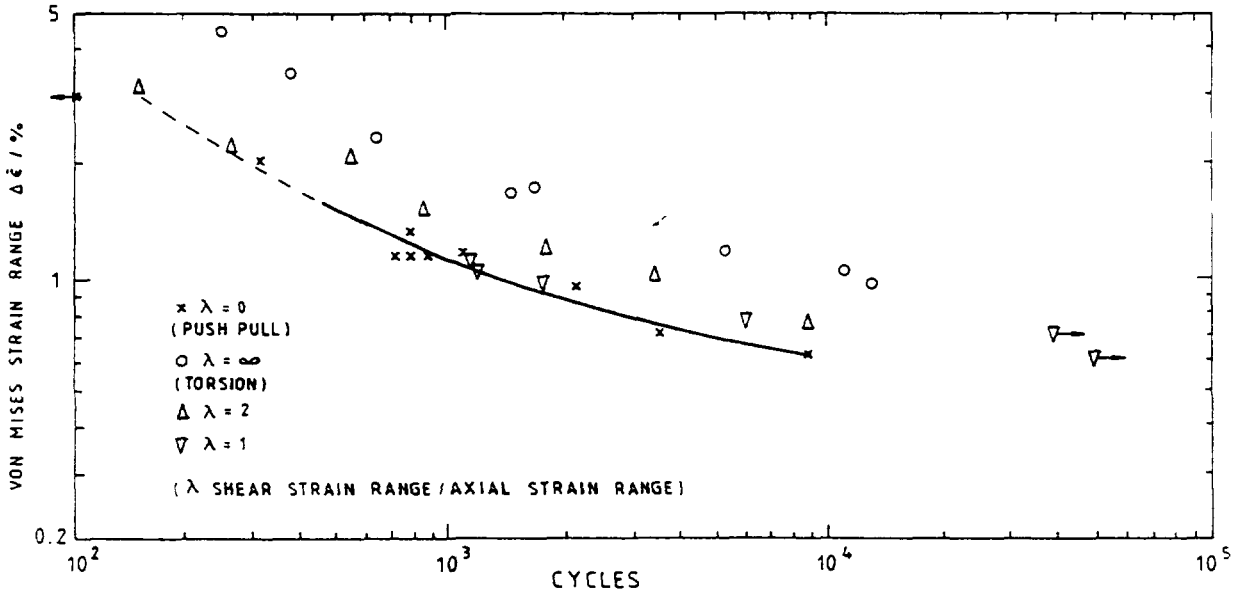

FIG. 2(a) TENSION TORSION DATA 316 AT 550°C ON BASIS OF VON MISES STRAIN RANGE (DATA FROM REFS. 10 & 11)

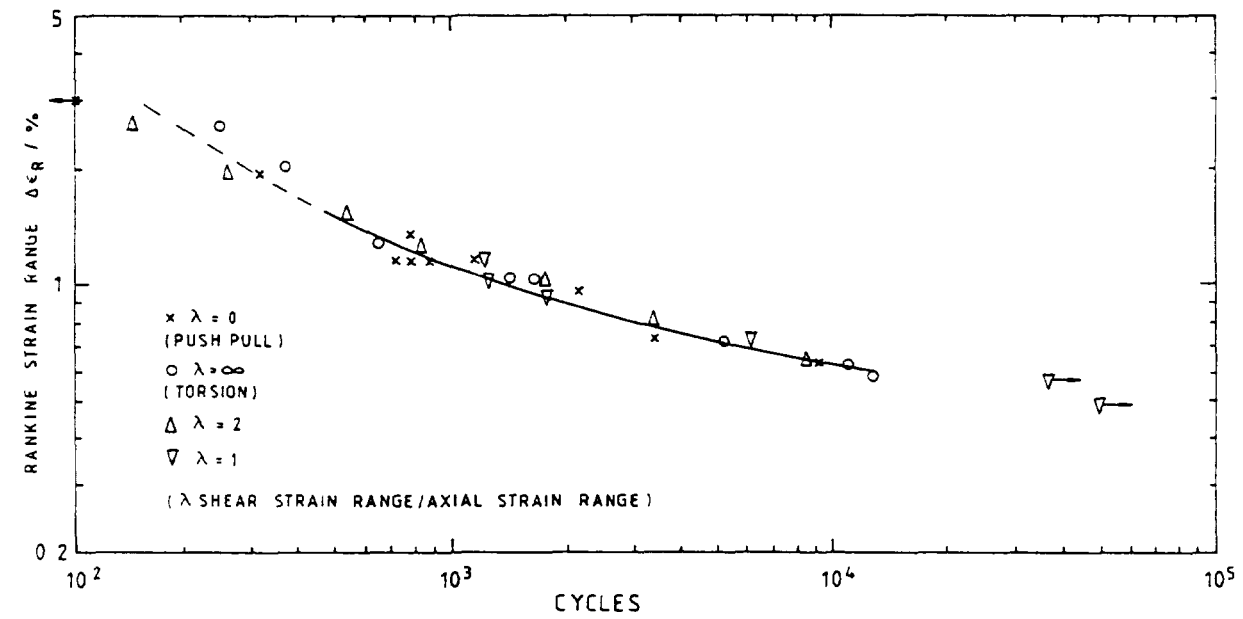

FIG 2(b) TENSION TORSION DATA 316 AT 550°C ON BASIS OF RANKINE STRAIN RANGE

FIG. 2. Comparison of tension/torsion data using the von Mises equivalent strain range and the Rankine strain range.

In the UK procedure, a correction to the von Mises equivalent strain range, $\Delta\bar{\varepsilon}$, is made prior to the evaluation of the Rankine strain range, to allow for the increase in the inelastic strain in the fatigue cycle due to creep relaxation, as suggested by Angerbauer [17]. The corrected value of the von Mises equivalent strain range, $\Delta\bar{\varepsilon}'$, is given by:

$$\Delta\bar{\varepsilon}' = \Delta\bar{\varepsilon} + \Sigma \left| \frac{\Delta\bar{\sigma}_h}{E_h} \right| \tag{3}$$

where

$\Delta\bar{\sigma}_h$ is the change in the von Mises stress between the start and end of each hold period,
E_h is the Young's Modulus at the maximum temperature in the hold period.

Relaxation in both compression and tension contributes to the increased inelastic strain in the fatigue cycle. The approach is conservative when hold periods do not occur at the extreme of the fatigue cycle.

It should be noted that the definition of von Mises strain range is, strictly speaking, applicable only to plastic strains. The UK design fatigue curve has been adjusted to compensate for the underestimation of the Rankine strain range when elastic strains are a significant proportion of the total strain range.

Thermal striping is a random rapid surface temperature variation of broad frequency content, occurring in the mixing zone of coolant streams of different temperature. When thermal striping is superimposed on major cycles, it is possible for the strain range to be increased over that of the major cycles above. The maximum possible strain range is then the maximum strain range within the major cycles plus the thermal striping strain range. Consequently, to provide a conservative assessment in the UK procedure, using Rainflow [18] cycle counting, the strain range of the major cycle with the largest Rankine strain range is corrected by adding the thermal striping strain range $\Delta\bar{\varepsilon}_s$ as defined in Section 2.3.

Fatigue damage for a given cycle type is assessed as the ratio of the number of cycles at the given total strain range to the allowable cycles at that total strain range, read from the design curve. The cumulative fatigue damage, V, over all cycles is then given by:

$$V = \sum_{0}^{j} \frac{n_j}{N_j} \tag{4}$$

where

n_j is the number of cycles at the j th strain range,
N_j is the allowable number of cycles at the j th strain range.

Clayton [9] points out that the use of Miner's law is likely to be most accurate for the conditions to which it is applied in the UK procedure.

2.3. Thermal striping

The equivalent Rankine strain range $\Delta\bar{\varepsilon}_s$, resulting from restraint of the maximum surface temperature range $\Delta\theta_p$ over a period of continuous thermal striping, is given by:

$$\Delta\bar{\varepsilon}_s = \frac{\alpha \Delta\theta_p}{1-\nu} \quad (5)$$

where

α is the instantaneous coefficient of thermal expansion at the mean of the temperature range $\Delta\theta_p$

ν is the elastic Poisson's Ratio

The elastic Poisson's Ratio is assumed because thermal striping is a high cycle phenomenon.

A simplified and conservative approach is provided in the UK creep-fatigue procedure to assess the effects of thermal striping. It is assumed, for conservatism, that all major cycles occur before any thermal striping. The crack depth resulting from application of these major cycle to an initial crack 0.1 mm deep can then be calculated.

From the crack growth Equation (1), the number of cycles, N, to grow from an initial depth a_o to a final depth a can be simplified as:

$$N = k \ln (a/a_o) \quad (6)$$

where

k is dependent on material properties and loading conditions.

The fatigue damage V, given that $a_o = 0.1$ mm, is then:

$$V = \frac{\ln\left(\frac{a}{0.1}\right)}{\ln\left(\frac{0.5}{0.1}\right)} = 0.621 \ln\left(\frac{a}{0.1}\right) \quad (7)$$

If the major cycles have propagated a crack to a depth a, it is then necessary to show that thermal striping will not propagate the crack further. This is achieved by calculating the stress intensity factor range resulting from thermal striping and comparing it with a crack growth threshold. Assuming an elastic stress range $E\Delta\bar{\varepsilon}_s$, where E is the Young's Modulus, the stress intensity factor range ΔK is given for a shallow semi-elliptical surface crack by:

$$\Delta K = 1.12\, E\Delta\bar{\varepsilon}_s \frac{\sqrt{\pi a}}{E(k)} \quad (8)$$

where

E(k) is a crack geometry factor = 1.05

Using suitable values for E and threshold ΔK enables an allowable value of $\Delta\bar{\varepsilon}_s$ to be obtained from a previously calculated value of V by the equation:

$$V = 0.621 \ln\left\{\frac{0.01774}{(\Delta\bar{\varepsilon}_s)^2}\right\} \quad (9)$$

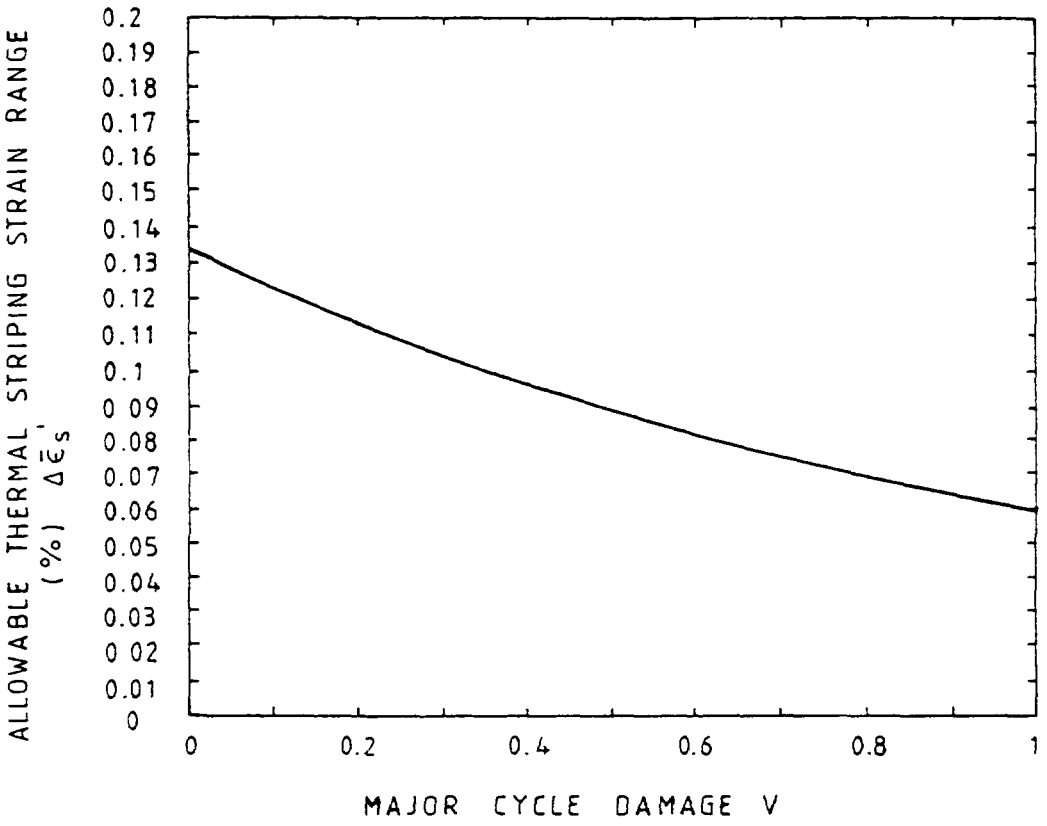

FIG. 3. Allowable thermal striping strain range as a function of major cycle strain range.

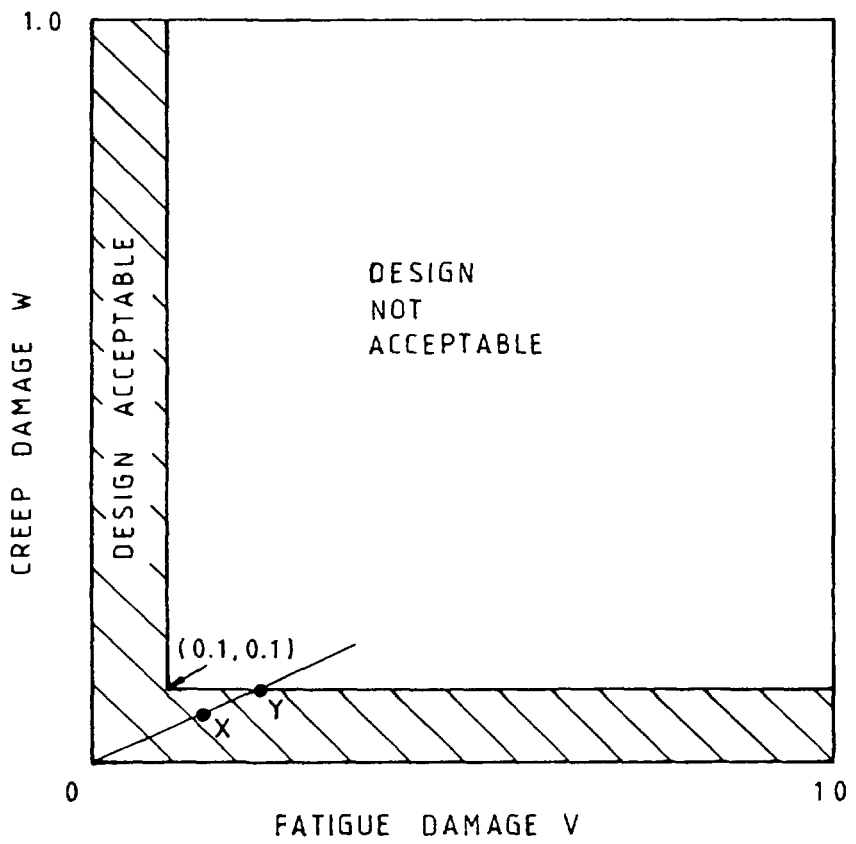

FIG. 4. Creep-fatigue assessment diagram.

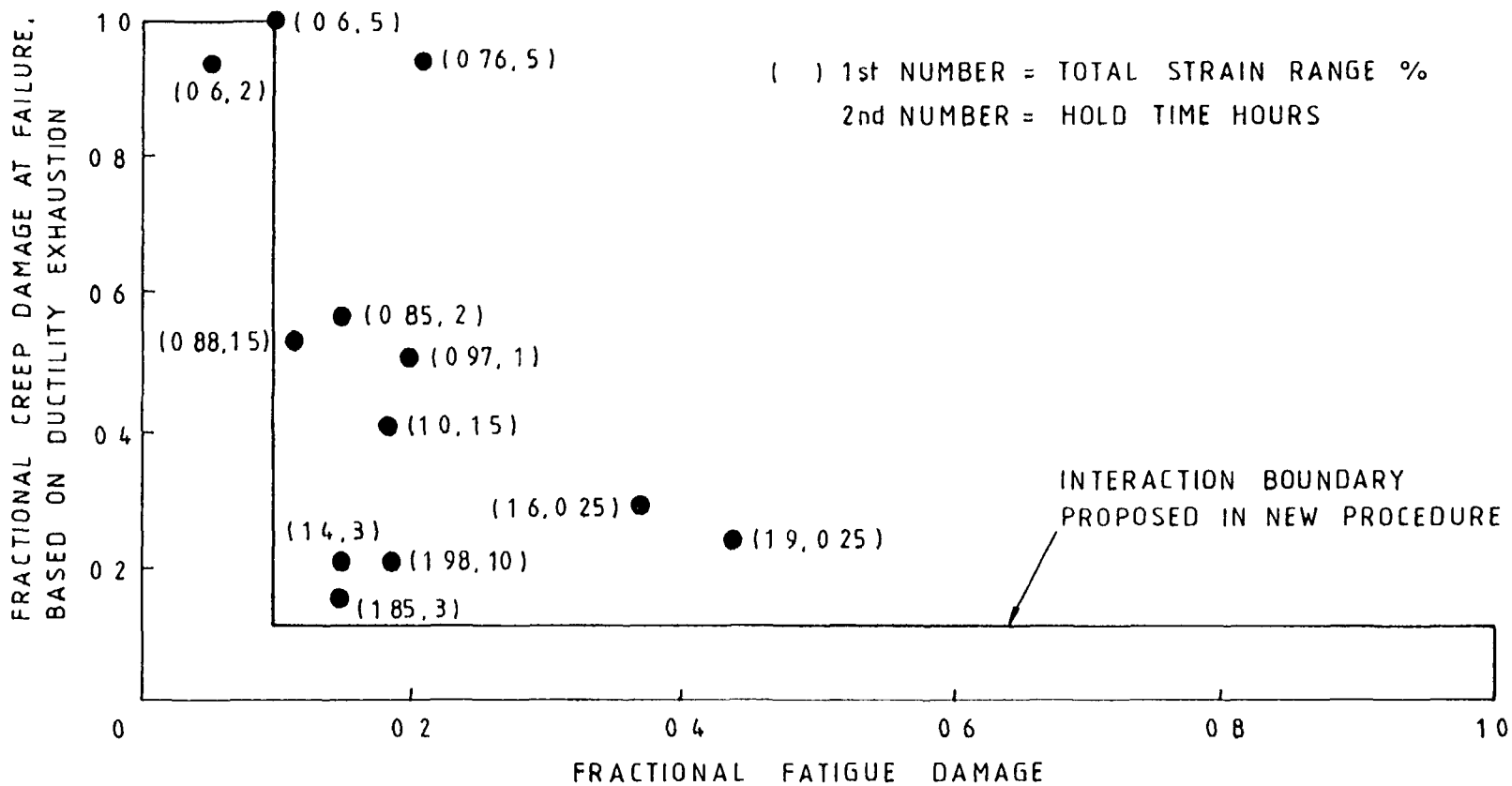

FIG. 5. Plot of fractional fatigue damage against fractional creep damage for tensile hold period cycling tests on Type 316 steel on the UK procedure diagram.

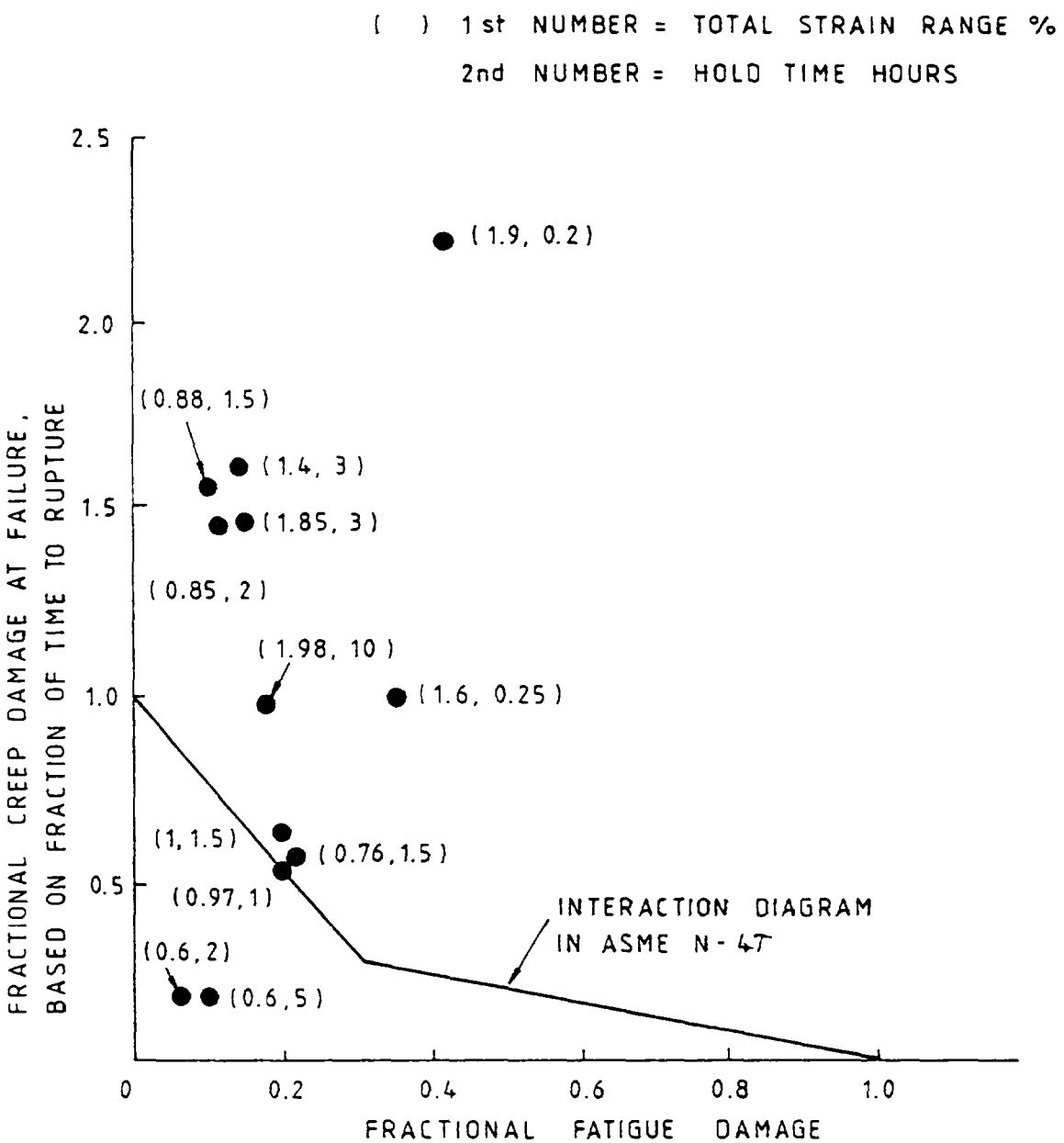

FIG. 6. Plot of fractional fatigue damage against fractional creep damage for tensile hold period cycling tests on Type 316 steel on the ASME N47/RCC-MR interaction diagram.

This relationship is shown in Fig 3. The allowable thermal striping strain range of 0.133% in the absence of major cycles corresponds to a maximum thermal striping temperature range of about 45°C and the minimum value of 0.06% at V = 1 is equivalent to a maximum temperature range of about 20°C. If the calculated value of $\Delta\bar{\varepsilon}_s$ is less than the allowable value, the thermal striping can be regarded as acceptable. If the thermal striping strain range is unacceptable, or if a less conservative treatment is required, it would be necessary to treat the thermal striping as part of the major cycle using Rainflow [18] cycle counting. This requires extension of the fatigue design curve to higher cycle numbers (up to 10^{10} cycles).

2.4. Creep-fatigue damage

In the UK creep-fatigue damage assessment procedure, an L-shaped diagram (Fig 4) has been developed to assess creep fatigue interaction. This diagram has the same axes as the N47/RCC-MR diagram. It is based on observations from a number of uniaxial creep fatigue tests on Type 316 steel in which creep damage has been assessed in terms of ductility exhaustion and fatigue damage in terms of crack growth from one grain depth to 0.5 mm deep. Creep cavities form at creep damage levels as low as 10% of that required to cause failure and creep-fatigue interaction becomes possible at creep damages as low as 0.1.

Clayton [9] noted that work by Wareing et al [19] had been successful in unifying data from high and low strain ranges and showed comparisons of the assessment of data on the UK L-shaped creep-fatigue interaction diagram and that from N47 (Figs 5 and 6). The tests at lower strain range (0.6% total strain range) and long hold times showed accumulated strains of the same order as the ductility (Fig 5) and failure was by fully intergranular fracture [20]. The N47 assessment route, however, showed low calculated creep damages for these tests (Fig 6). Similarly the higher strain range tests showed mixed fatigue striation and intergranular fracture, consistent with the low creep damage calculated by the UK assessment method (Fig 5). The N47 assessment method gave high creep damages for these tests (Fig 6). Similar observations to these have been made by Wood [5].

3. OUTLINE OF ASSESSMENT PROCEDURES

Application of the procedure requires the definition of load cycles. For the evaluation of creep damage, it is convenient to consider operational cycles, which are defined as sequences of events which start and end at the same operational steady state. This could be, for example, the shutdown state or the full power steady state. The transitions between these steady states involve transients and it is necessary to be able to characterise the stress and strain values and temperatures during transients as a function of time.

The net creep strain is evaluated over the operational cycle. From the definitions of creep and quasi-creep used, creep strains are evaluated during operational steady states where the temperature is in the range 480°C to 625°C for Type 316 and Type 316L(N) steel. Quasi-creep strains are evaluated during all other parts of the operational cycle, when the temperature is in this range, but not during the steady states. Once the cycle is completed, it is assumed that further cycles do not cause sintering of creep cavities which were formed in that cycle.

The definition of stress/strain cycles for the evaluation of fatigue damage is that used for cycle counting by the Rainflow method [18], i.e. a cycle in any stress-strain loop which returns to an initial condition. The strain range of any cycle is calculated as the maximum difference in strain between any two times in the cycle.

The use of different damage concepts and consequent different treatment of multiaxial loading from that of N47 [1] or the RCC-MR [2] design codes leads to greater complications where rotation of principal axes may occur during operation. For many fast reactor components, the principal axes of stress and strain remain essentially fixed and coincident during the operational cycles. For convenience, two alternative procedures have been drawn up, one covering this

case and the other the more general case in which the principal axes may rotate during the operational cycle. Provision for a combination of operational cycles of both types is also made. The second step after determining the loading conditions is to select the appropriate (i.e. fixed and coincident principal axes of stress and strain or rotating principal axes) procedure. These procedures are outlined in Appendices 2 and 3.

TABLE I. MATERIALS DATA FOR CREEP DAMAGE ASSESSMENT

Material	Temp. (°C)	Minimum Creep Ductility ε_f	$\dot{\varepsilon}_{CRIT}$ (h^{-1})	$(\dot{\varepsilon}/\sigma)_{CRIT}$ $(hMPa)^{-1}$	φ_i^o
WROUGHT TYPE 316 / 316L(N) STEEL (unirradiated or irradiated to < 10^{-4} appm He)	480-625	0.1	3.6×10^{-3}	9×10^{-6}	0.1
WROUGHT TYPE 316 / 316L(N) STEEL (irradiated to > 5 appm He)	480-625	0.02	Not yet specified	Not yet specified	Not yet specified
WROUGHT TYPE 316 / 316L(N) STEEL (irradiated to between 10^{-4} appm and 5 appm He)	480-625	See Fig 8	Not yet specified	Not yet specified	Not yet specified
WROUGHT Mod 9Cr1Mo STEEL (unirradiated)	425-550	0.14	4×10^{-5}	1.1×10^{-7}	0.001

4. EXTENSION FOR MOD 9Cr1Mo, WELDMENTS AND VIBRATION

4.1. Mod 9Cr1Mo steel

The extension of the strain-based creep-fatigue assessment procedure to Mod 9Cr1Mo steel was made at a time when the data base on this material was sparse and so represents an interim position. It is hoped that additional data may allow a less conservative approach to be developed in future.

The data base on which the procedure was founded contained results for tensile and compressive dwell tests, both of which resulted in a modest reduction in cycles to failure. These reductions were believed to be mainly related to enhanced fatigue crack nucleation due to creep processes and are taken into account via the fatigue design curve. Although there is no strong evidence to support a creep-fatigue interaction for tensile dwells, it has been assumed, for conservatism, that such a mechanism could occur in longer term tests.

The creep-fatigue interaction procedure has been developed in a manner consistent with that used for Types 316 and 316L(N) steel, including the use of the same L-shaped creep-fatigue interaction diagram (Fig 4). This has allowed a consistent procedure to be used, but employing material specific constants for Type 316/16L(N) and Mod 9Cr1Mo steels.

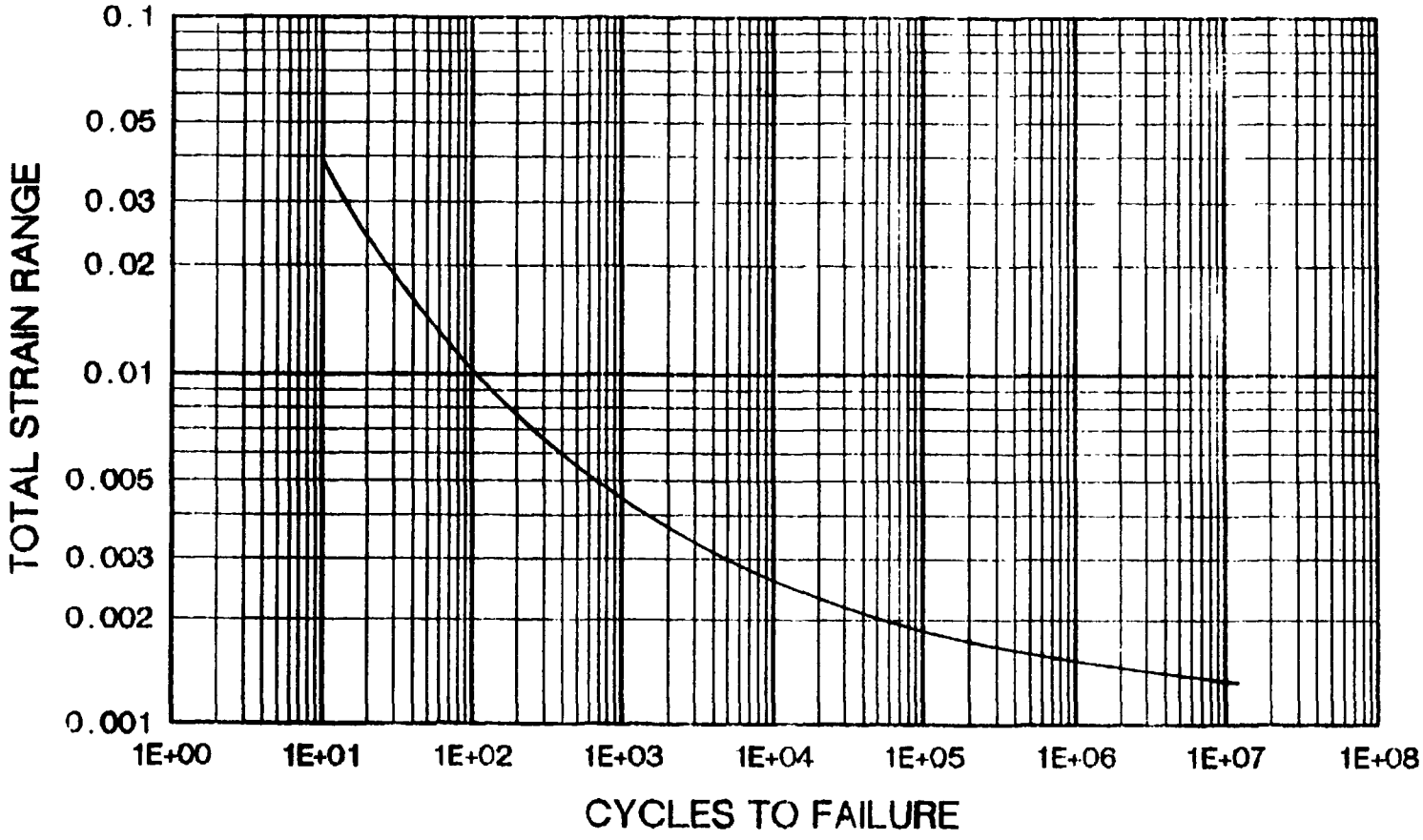

FIG. 7. Fatigue design curve for Mod 9Cr1Mo steel.

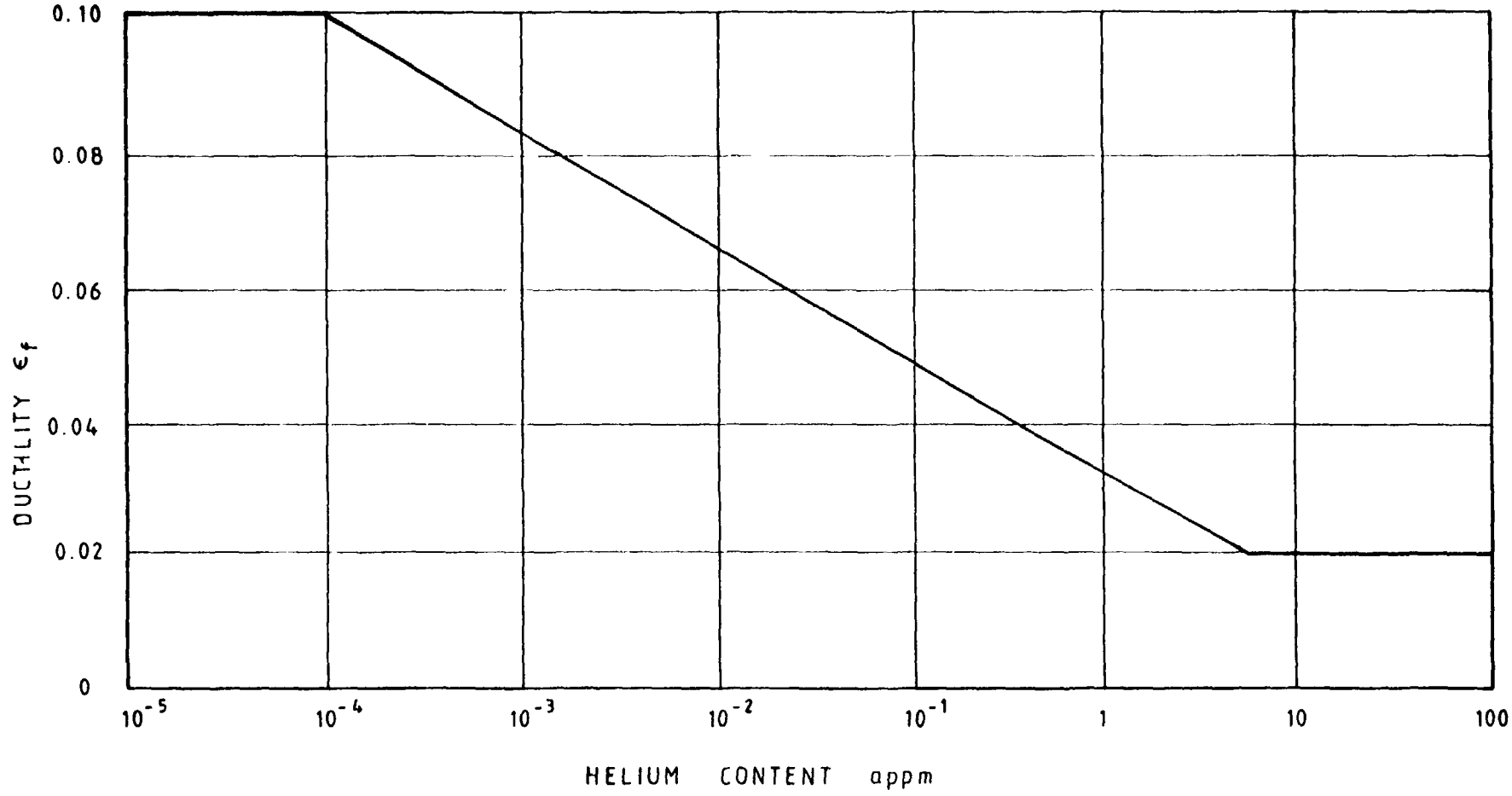

FIG. 8. Variation of minimum creep ductility of Type 316 steel with helium content.

The maximum temperature of application of the strain based creep-fatigue procedure for Mod 9Cr1Mo steel is 550°C.

The materials data recommended for use in creep damage assessment are given in Table I and an interim fatigue design curve for Mod 9Cr1Mo steel is given in Fig 7.

The value of 14% for the minimum creep ductility of Mod 9Cr1Mo steel is based on data for a large number of tests in the temperature range 480 to 600°C. It represents both the lowest value measured in long term (>30,000 hour) tests at 593°C and the lower 95% confidence limit to a data base compiled by the Commission of the European Community. The critical strain rate of 1.1×10^{-8} s^{-1} is based on an examination of the available data. The transition strain rate is, conservatively, 5.5×10^{-9} s^{-1} and it has been assumed (following the procedure used for Type 316 steel) that the critical strain rate is twice this value.

4.2. Weldments

In order to apply the rules to weldments, it is necessary to limit the effects of:

(a) Departures in weldment geometry from that of the model used for analysis.
(b) Weld defects
(c) Mismatches in properties between the weld metal and base material.

These requirements are recognised in the RCC-MR rules [2], as modified by the EFR Design Companies Rules Committee.

The components of stress and strain in the welded assembly are calculated taking into account the weldment geometry, but using the physical and mechanical properties of the base material throughout. The evaluation of creep, fatigue and creep-fatigue is modified by the use of weldment factors K_F, K_Z and K_D applied to a region comprising the weld metal plus one half the thickness of the base material on either side of the weld metal.

- K_F is an elastic-plastic strain enhancement factor equal to the fatigue strength reduction factor.
- K_Z is a creep strain enhancement factor.
- K_D is a creep ductility reduction factor.

The creep weldment factors are required to cover two effects which may modify the response to a given loading of the weld metal, or heat affected zone (HAZ):

- Strain rates may be higher than calculated using base material properties. There may be consequential effects on stress levels and on stress state, but these cannot be estimated simply. It is therefore assumed that the base material calculation can be used for stress levels but the creep strain enhancement factor K_Z is used to allow for strain rate enhancement.
- The minimum creep ductility ε_f for welds may be less than that for base material. The creep ductility reduction factor K_D is used to allow for this effect.

TABLE II. LOWER BOUND DUCTILITY VALUES FOR TYPES 316 / 316L(N) STEEL AND WELD METAL

Temperature	ε_f (base material)	ε_f weld metal
550	0.10	0.04
600	0.10	0.04
625	0.10	0.02

For Type 316L(N) steel K_Z may be taken as unity but K_D is significant for austenitic weld metal. Lower bound values of ductility for Type 316 / 316L(N) base material and weld metal are given in Table II:

Based on the values in Table II, K_D is taken as 2.5 for welds in Types 316 and 316L(N) steel at temperatures up to 600°C. For 600-625°C, a linear temperature dependence is assumed i.e.:

$$K_D = 0.10\,\Theta - 57.5$$

where

Θ is the temperature in °C.

It is necessary to take into account the effects of irradiation on weldment ductility. The UK recommendations on this subject have been incorporated in the rules for base material. These recommendations state that the combined effects of irradiation and weldments should not result in a ductility below 0.02. This recommendation is incorporated into the weldment rules by specifying that K_D/ε_f need not be taken as greater than 50.

For Mod 9Cr1Mo steel, accelerated creep rates in the HAZ leading to Type IV cracking dominate long term cross-weld rupture behaviour and are therefore the major concern in creep-fatigue assessment. There are no relevant creep-fatigue data but the nature of Type IV cracking implies that the problem can be treated conservatively by taking $K_D = 1$ and basing the value of K_Z on the ratio of rupture time for base material to that for weldments in iso-stress rupture tests. Data from such tests imply K_Z values of up to 10 at temperatures around 600°C. However, at lower temperatures the effects of Type IV cracking appear to be less severe and a value of $K_Z = 5$ has been used to bound the estimates at 525°C.

Fatigue weldment factors are required to cover, for weld metal and HAZ, enhancement of the strain range and/or reductions in endurance for a given strain range. Both of these effects can be covered by a single factor since, unlike the analogous creep case, only a single quantity (the strain range) has to be calculated for entry into the base material fatigue curve. This fatigue strength reduction factor (K_F) has exactly the same basis as J_F in the RCC-MR [2] rules. The value of 1.25 has been used for both Type 316/316L(N) steel and Mod 9Cr1Mo steel, on the basis of test data.

Values of K_F, K_Z, K_D are given in Table III.

For the case of fixed and coincident principal axes, K_Z has two effects: on the strain rate and ductility factors in creep and on the strain increment in fatigue.

With fixed and coincident principal axes of stress and strain:

a) Equation (A2.1) becomes:

$$(\varphi_i)_k = \left(\frac{\sigma_i}{K_Z \delta\varepsilon_i} \cdot \delta t\right)_k \cdot \left(\frac{\dot{\varepsilon}}{\sigma}\right)_{crit} \qquad (10)$$

where the value of $\left(\frac{\dot{\varepsilon}}{\sigma}\right)_{crit}$ is that given for base material in Table 1 and the value of φ_i^o is $1/K_Z$ times that given in Table I.

TABLE III. VALUE OF WELDMENT FACTORS K_F, K_Z AND K_D

Base Material	K_F	K_Z	K_D
Types 316 & 316L(N)	1.25	1	2.5 ($\theta_{min} \leq \theta \leq 600°C$) 0.10 θ - 57.5 ($600 \leq \theta \leq 625°C$)
Irradiated 316 & 316L(N) (See Note)	1.25	1	2.5 ($\theta_{min} \leq \theta \leq 600°C$) 0.10 θ - 57.5 ($600 \leq \theta \leq 625°C$)
Mod 9Cr1Mo	1.25	5	1

Note that, for irradiated 316L(N) weldments, K_D/ε_f need never be taken as greater than 50.

b) The creep and quasi-creep damage fractions calculated from Equation (A2.2) become:

$$W_i = K_Z K_D \sum_{k=0}^{k=j} \left(\frac{\delta\varepsilon_i . \beta_i}{\varepsilon_f} \right)_k \qquad (11)$$

The value of ε_f is that given for base material in Table 1.

c) The effective strain range for fatigue assessment is calculated from:

$$\Delta\varepsilon_t{}^R = \left| \frac{\Delta\sigma_i}{\Delta\bar{\sigma}} \right| \left(K_F \Delta\bar{\varepsilon} + K_Z \sum_{1}^{r} \left| \frac{\Delta\bar{\sigma}_h}{\bar{E}_h} \right|_r \right) \qquad (12)$$

In the case of rotating principal axes these become:

a) $$W = \sum_{\text{all operational cycles}} (\varepsilon_c + \varepsilon_q) \frac{K_Z K_D}{\varepsilon_f} \qquad (13)$$

The value of ε_f is again that given for base material in Table 1.

b) The effective (Rankine) strain range for each cycle is the maximum value for all time pairs of the quantities $\Delta\varepsilon^R$ given by:

$$\Delta\varepsilon^R = \left|\frac{\Delta\sigma_1}{\Delta\bar{\sigma}}\right| \left(K_F \Delta\bar{\varepsilon} + K_Z \sum_1^r \left|\frac{\Delta\bar{\sigma}_h}{E_h}\right|_r \right) \quad (14)$$

The overall effect of the provisions for creep is illustrated in Figure 9, in terms of a dimensionless plot of the effective weldment ductility ε^* (normalised with respect to the minimum ductility of base material) against the effective value of $\dot{\varepsilon}/\sigma$, (i.e. $\dot{\varepsilon}^*/\sigma$), normalised with respect to the critical value for base material. In fact, K_Z has no effect at high strain rates, but reduces both the critical value of $\dot{\varepsilon}/\sigma$ and the minimum ductility. Fig 9 also shows the effect of K_D which reduces the effective ductility at all strain rates.

For the case of rotating principal axes, the effect of K_D is unchanged but K_Z will have a greater effect on creep damage because it is used to enhance all creep and quasi-creep strains. The effect of K_Z on strain rates is considered for quasi-creep but not for creep. The procedure may therefore be highly conservative in some cases.

4.3. Vibration

Vibration is treated in a similar way to thermal striping, by limiting the maximum strain amplitude to below the threshold stress intensity factor for the assumed surface crack.

For vibration, there is no equivalent limiting stress to that corresponding to the source temperature difference in thermal striping, but for sinusoidal loading, the maximum vibration strain can be determined. For random vibration, a Rayleigh or Gaussian distribution has to be assumed for the vibrational amplitude and a probability of the amplitude not exceeding a certain value then used.

For the Rayleigh distribution, the probability, P, that the peak-to-peak amplitude, $\Delta\sigma_v$,is greater than $\lambda\sigma_{rms}$ (where σ_{rms} is the time averaged root mean square stress) is given by:

$$P(\Delta\sigma_v > \lambda\sigma_{rms}) = \exp[-\lambda^2/8] \quad (15)$$

such that $\lambda = 6$ for $P(\Delta\sigma_v > \lambda\sigma_{rms}) = 1.1\%$. A crest factor $\lambda = 6$ is recommended for most situations. The assumption of a Rayleigh distribution is generally considered to be conservative.

The vibration strain range is given by:

$$\Delta\bar{\varepsilon}_a = \frac{\Delta\sigma_v}{E} \quad (16)$$

For simultaneous vibration and thermal striping, the thermal striping strain range is enhanced by the vibration strain, i.e.:

$$\Delta\bar{\varepsilon}_a = \Delta\bar{\varepsilon}_s + \frac{\Delta\sigma_v}{E} \quad (17)$$

FIG. 9. 'Effective' ductility strain rate relstionship.

4.3.1. Vibration Correction

In the presence of vibration and thermal striping, the main fatigue cycle is enhanced by the maximum strain range of thermal striping and vibration, so Equation (A2.3) becomes:

$$\Delta\bar{\varepsilon}_i{}^t = \Delta\varepsilon_i{}^R + \Delta\bar{\varepsilon}_s + \frac{\Delta\sigma_v}{E} \qquad (18)$$

4.3.2. Allowable vibration strain range

The allowable thermal striping and vibration equivalent strain range $\Delta\bar{\varepsilon}_a'$ is obtained from Fig 3 by inputting the value of fatigue damage V from Equation (4). In the absence of any major cycles (V = 0), the maximum value of $\Delta\bar{\varepsilon}_a' = 0.133\%$.

The design is acceptable if $\Delta\bar{\varepsilon}_a' > \Delta\bar{\varepsilon}_a$

5. CONCLUSIONS

A method has been developed in the UK for assessing creep-fatigue damage for fast reactor components, based on what is believed to be a sound mechanistic understanding of the failure behaviour under creep-fatigue conditions.

The method is based on ductility exhaustion for creep damage and, for fatigue damage, on a model of crack growth from an assumed initial crack depth equivalent to one grain size (taken as 0.1 mm for conservatism) to a final depth of 0.5 mm. The use of this crack growth model for fatigue damage allows thermal striping and vibration to be taken into account by the use of fatigue crack thresholds.

Because of the different multiaxial criteria made necessary by the use of this method, it has proven convenient to provide separate procedures to cover instances where the principal axes of stress and strain remain essentially fixed and coincident throughout all operational cycles and a more general procedure to cover instances where rotation of principal axes occurs during some operational cycles.

While the method was initially written for use on unwelded Type 316 and Type 316L(N) steel at temperatures up to 625°C, it has been possible to extend its use to Mod 9Cr1Mo steel by the use of suitable data. Treatment of weldments has been accomplished by the introduction of suitable weldment factors for creep and fatigue.

At the present time the method can only be used with inelastic analysis. Its status is such that it has been approved for trial use within the European Fast Reactor collaboration, with a view to identifying shortcomings in application.

ACKNOWLEDGEMENTS

The procedures described are the result of contributions by a group of individuals, taking into account work by many of the people quoted in the references and others. The contributions of A M Clayton, N M Irvine, V B Livesey and M W J Lewis of AEA Technology and R D W Bestwick of National Nuclear Corporation in the drafting of the procedures are particularly acknowledged.

REFERENCES

[1] AMERICAN SOCIETY OF MECHANICAL ENGINEERS. Boiler and Pressure Vessel Code Case N47, Class 1 Components in Elevated Temperature Service, Section III, Division 1.

[2] AFCEN. Design and Construction Rules for Mechanical Components of FBR Nuclear Islands (RCC-MR) June 1985 Edition.

[3] AFCEN. RCC-MR Addendum No.1, (November 1987).

[4] MANJOINE M J. Contribution to discussion: ASME Symposium on Critical Factors in Materials and Mechanical Engineering, (1980).

[5] WOOD D S. The interpretation of some long term creep-fatigue tests results in relation to design code rules. 3rd International Post-SMIRT Seminar on Construction Codes and Engineering Mechanics, Anaheim, California, 21-22 August 1989.

[6] HALES R and TOMKINS B. Creep-fatigue failure in austenitic stainless steels relevant to structural performance. ASME PVRC Meeting, Orlando, USA (1982) Paper 82-PVP-70.

[7] TOMKINS B and WAREING J. Elevated temperature fatigue interactions in engineering materials. Metal Science. **11** (1977) 414.

[8] BESTWICK R D W and CLAYTON A M. "Design methodology for creep-fatigue assessment using creep ductility criteria". SMIRT 8, Inelastic Analysis and Life Prediction in High Temperature Environment (Proc. 5th Int. Seminar, Paris, 1985).

[9] CLAYTON A M. "Creep-fatigue assessment procedures for fast reactors". Recent Advances in Design Procedures for High Temperature Plant (Proc. I.Mech.E Conf. Risley, UK 1988 4954).

[10] PRIEST R H and ELLISON E G. Materials Science and Engineering. **49** (1981) 7.

[11] ASHBY M F and DYSON B F. Creep damage mechanics and micromechanisms. ICF 6.

[12] DYSON B F. Can. Met. Quarterly. **18** (1979) 31.

[13] CANE B J. Creep fracture of dispersion strengthened low alloy ferritic steels. Acta Met. **29** (1981) 1518.

[14] HALES R. Unpublished work (1987).

[15] LIVESEY V B and WAREING J. Influence of slow strain rate tensile deformation on creep fatigue endurance of 20Cr 25Ni Nb stainless steel at 593°C. Metal Science **17** (1983) 297-303.

[16] TOMKINS B. Fatigue crack propagation - an analysis. Phil. Mag. **18**-155 (1968) 1041.

[17] ANGERBAUER A. "Elastic creep-fatigue damage evaluation: less restrictive design rules for SNR-2 components". Reactor Technology (Proc. 8th Int. Conf. Brussels, August 1985) Paper E5/3.

[18] MATSUISHI M and ENDO T. Fatigue of metals subject to varying stress. Japan. Soc. of Mech. Engineers (1968).

[19] WAREING J, BRETHERTON I and HALES R. "Failure criteria during elevated temperature creep fatigue cycling of austenitic stainless steel". Inelastic Analysis and Life Prediction in High Temperature Environment. (5th Int. Seminar, EdF, Paris, August 1985).

[20] WAREING J, BRETHERTON I and LIVESEY V B. "Life prediction for elevated temperature components subjected to cyclic deformation". Engineering Materials and Structures (Proc. I.Mech.E. Conf. Sheffield) 147-164.

APPENDIX 1. DERIVATION OF CREEP DAMAGE/CREEP STRAIN RELATIONSHIP FROM THEORETICAL CAVITY GROWTH EQUATIONS

Cavities are initiated early in life on grain boundaries normal to principal planes. The growth of these cavities can be described by:

$$\dot{v} = A\sigma \tag{A1.1}$$

where v is the volume of a cavity growing on a boundary normal to the principal stress σ and A is a constant.

This equation is valid only if the principal strain rate $\dot{\varepsilon}$, corresponding to σ is sufficient to accommodate the dilatation associated with cavity growth, that is:

$$\dot{v} < \dot{\varepsilon} .h^2.d \tag{A1.2}$$

where

h is the radius of grain boundary associated with the cavity,

d is the spacing of cavitating boundaries in the direction of $\dot{\varepsilon}$ (taken as the grain size) .

Where this inequality is not met, the cavity growth is geometrically constrained and the maximum cavity growth rate is given by:

$$\dot{v} = \dot{\varepsilon} .h^2.d \tag{A1.3}$$

Expressing the growth rate in terms of strain rather than time, Equation (A1.1) gives:

$$\frac{dv}{d\varepsilon} = A\left(\frac{\sigma}{\dot{\varepsilon}}\right) \tag{A1.4}$$

and Equation (A1.3) gives:

$$\frac{dv}{d\varepsilon} = h^2.d \tag{A1.5}$$

Integrating Equations (A1.4) and (A1.5) for constant σ and $\dot{\varepsilon}$ and assuming that the volume of a cavity at coalescence v_c and the principal strain ε_f at cavity coalescence are much greater than these values at initiation, Equations (A1.4) and (A1.5) give, respectively:

$$\varepsilon_f = \frac{v_c}{A}\left(\frac{\dot{\varepsilon}}{\sigma}\right) \tag{A1.6}$$

and $$\varepsilon_{f\,min} = \frac{v_c}{h^2\ d} \tag{A1.7}$$

The relationship between ductility and $\dot{\varepsilon}/\sigma$ represented by Equations (A1.6) and (A1.7) is given in Fig A1.1.

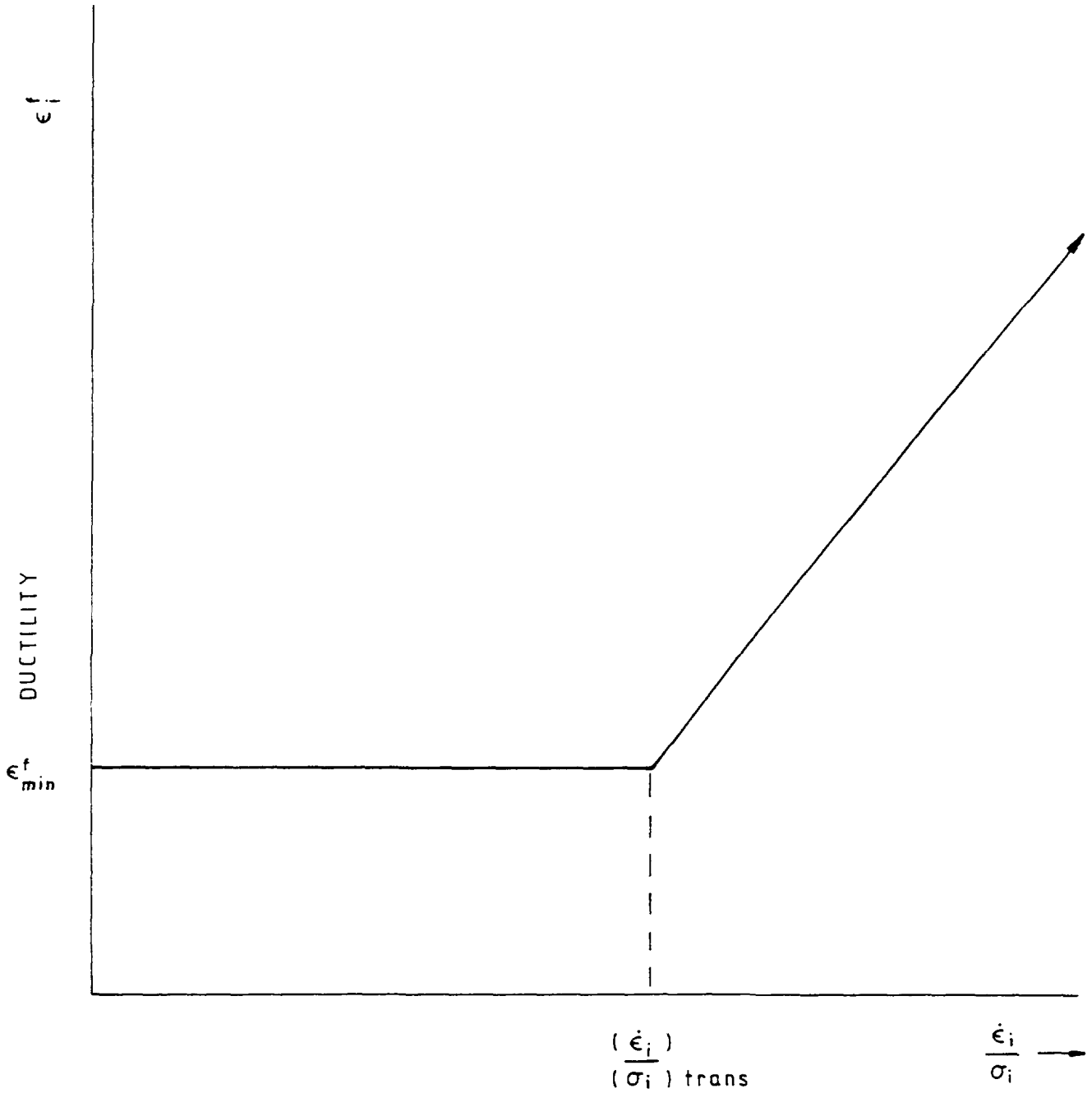

FIG. A1.1. Theoretical relationship between ductility and $(\dot{\epsilon}/\sigma)$.

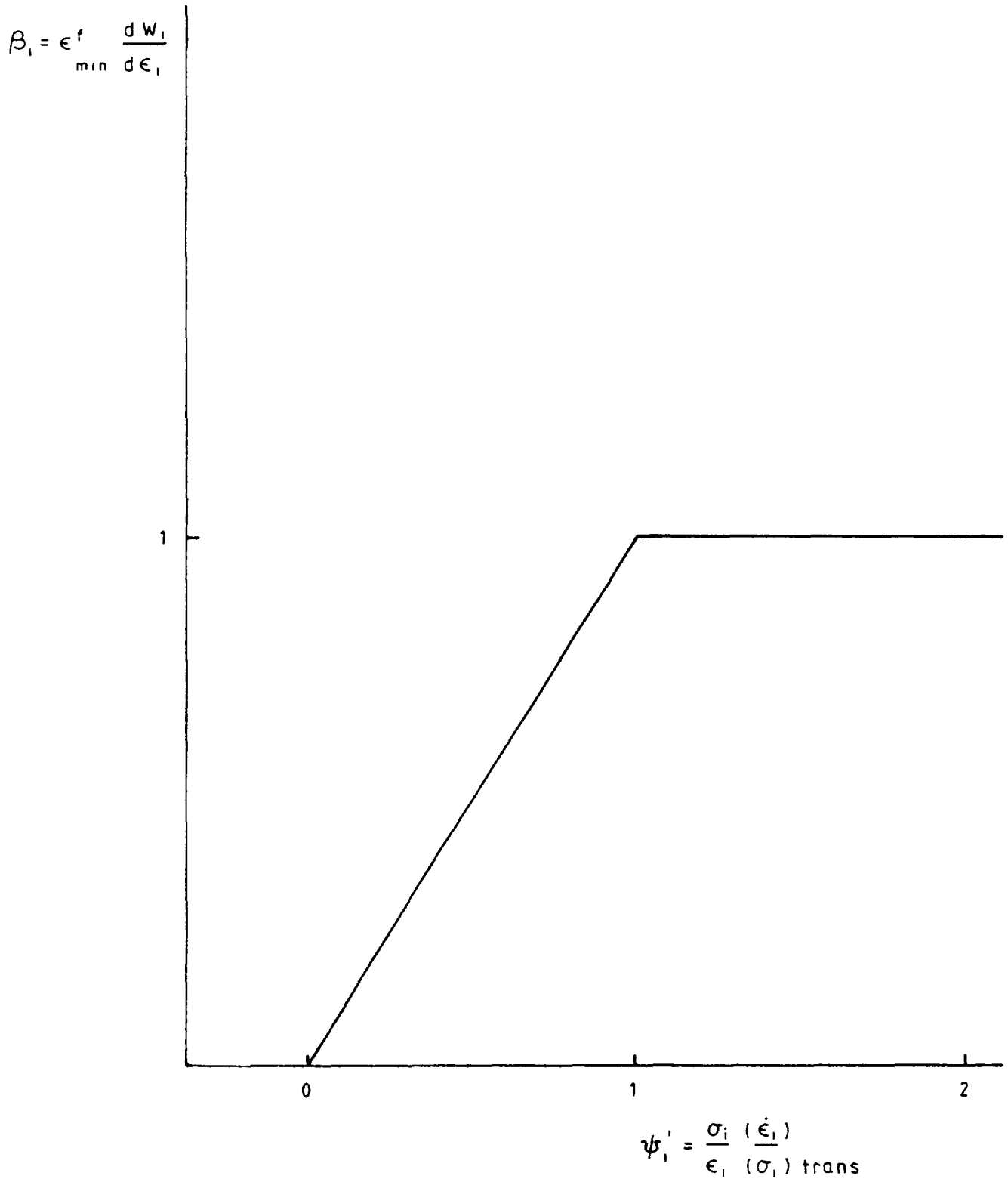

FIG. A1.2. Theoretical creep damage relationship.

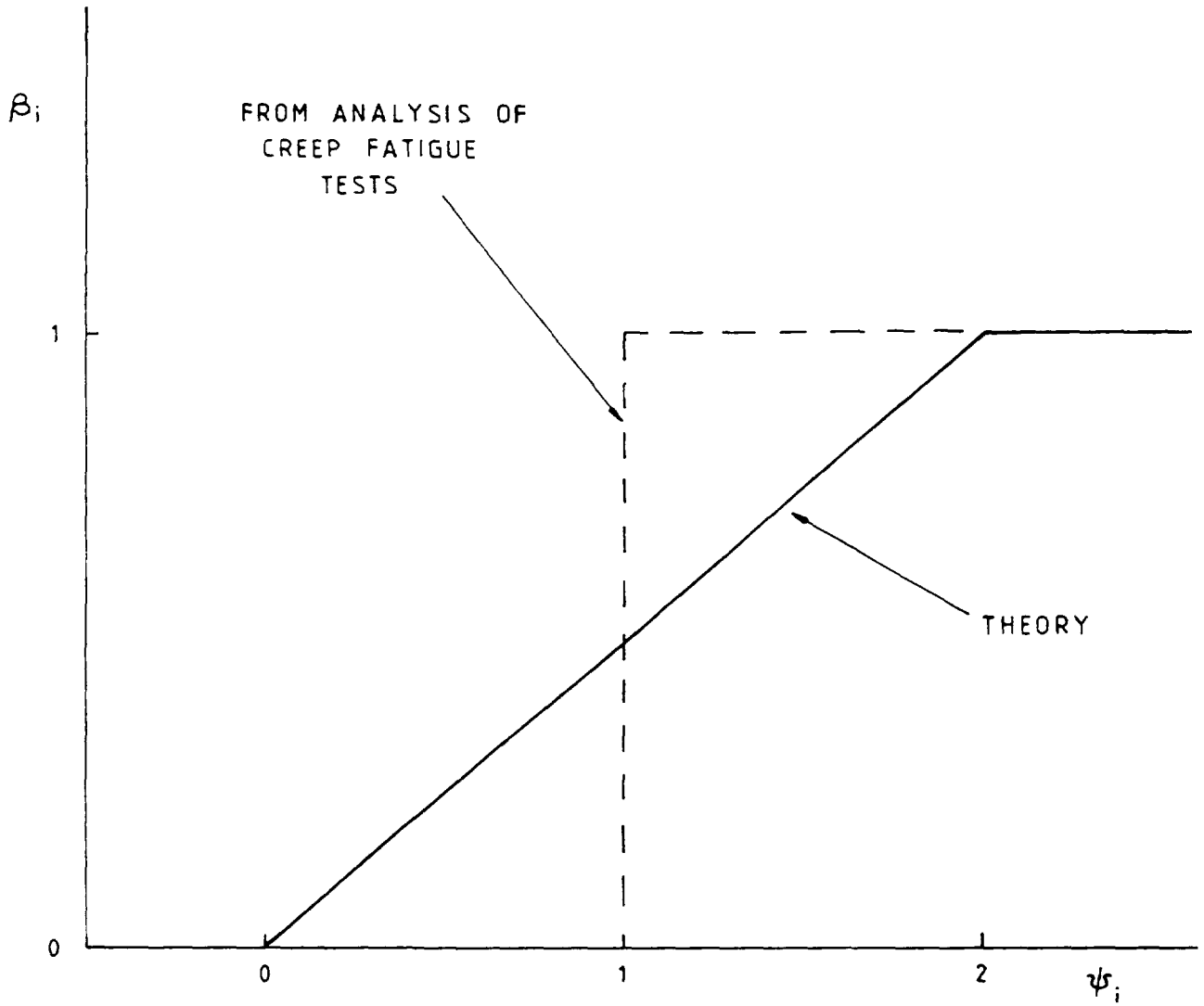

FIG. A1.3. 'Step change' and theoretical creep damage relationships.

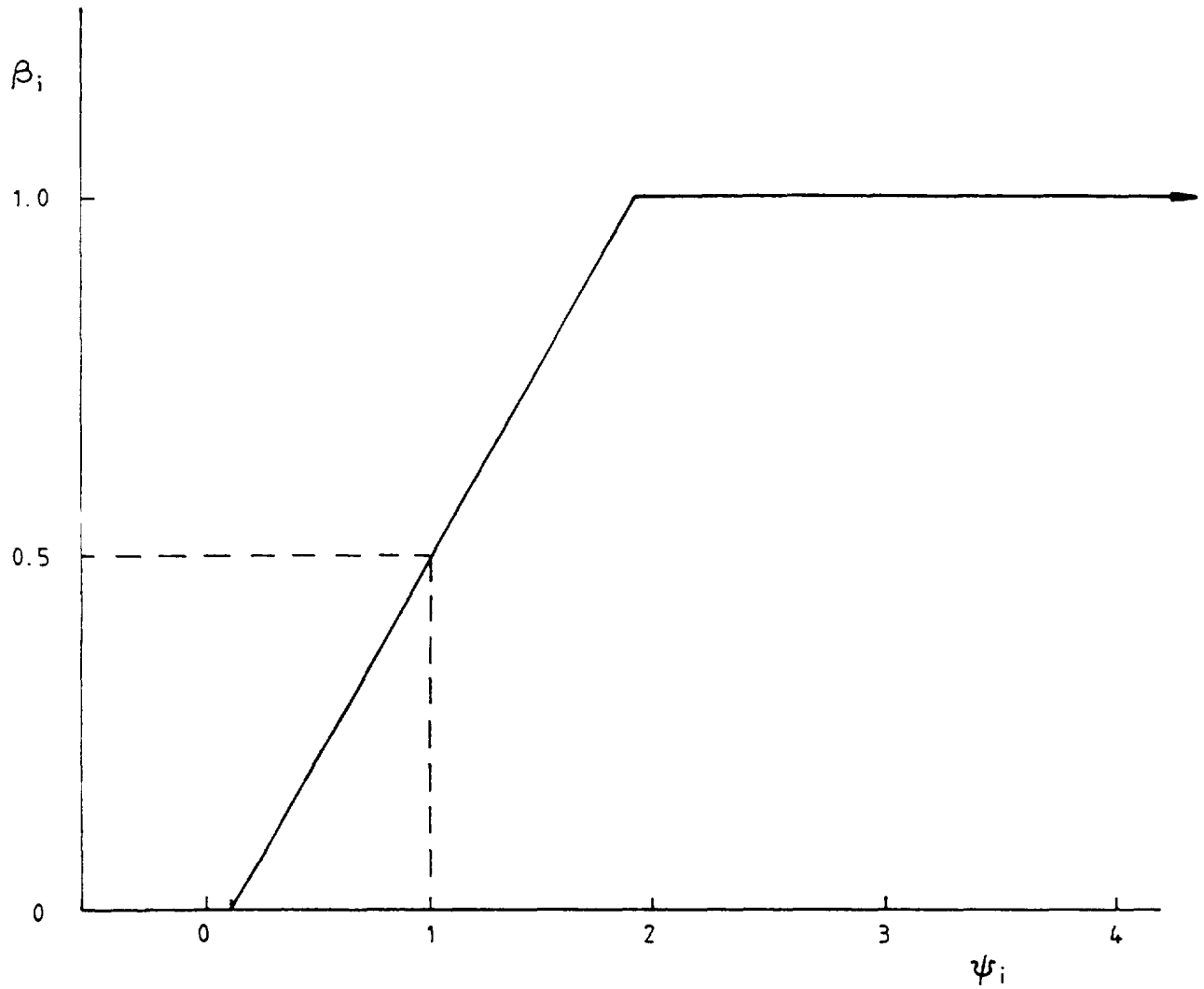

FIG. A1.4. General form of relationship between β and ψ.

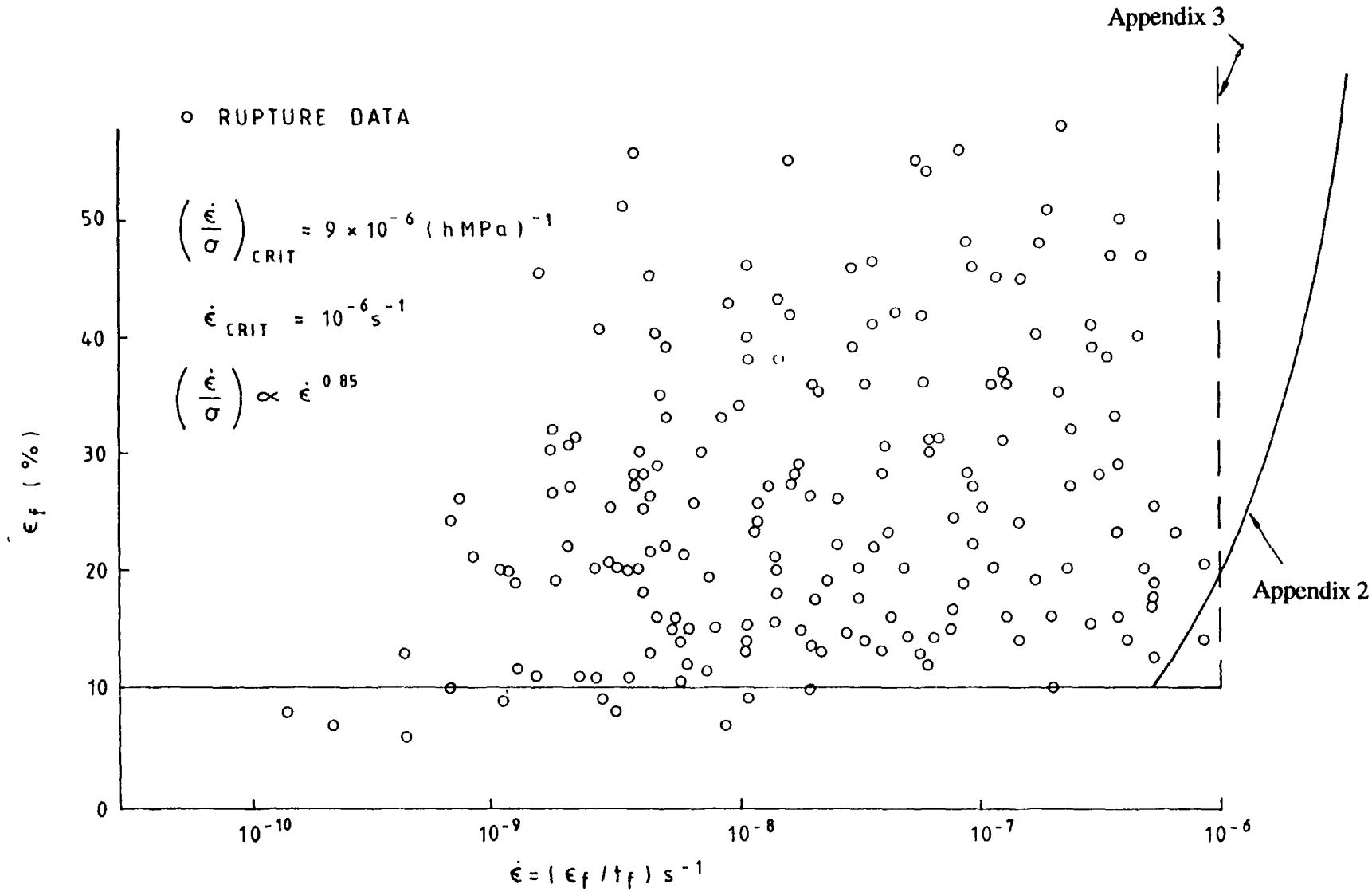

FIG. A1.5. Ductility/strain rate relationship used in UK rules compared with stress rupture data for Type 316 steel at 600°C

Then

$$\varepsilon_f = \varepsilon_{f\,min}\left(\frac{\dot{\varepsilon}}{\sigma}\right)\left(\frac{\sigma}{\dot{\varepsilon}}\right)_{trans} \tag{A1.8}$$

where the subscript 'trans' denotes a transition rate.

For the range of strain rates in a plant component, cavity growth and hence creep damage is related to the accumulation of creep strain in the material. The creep damage is then given by the creep strain divided by the ductility.

Considering an incremental definition of damage W associated with a principal direction:

$$dW = \frac{dv}{v_c} \tag{A1.9}$$

For unconstrained cavity growth, Equations (A1.4), (A1.6) and (A1.9) give:

$$dW = \frac{d\varepsilon}{\varepsilon_f} = \frac{d\varepsilon}{\varepsilon_{f\,min}}\left(\frac{\sigma}{\dot{\varepsilon}}\right)\left(\frac{\dot{\varepsilon}}{\sigma}\right)_{trans} \tag{A1.10}$$

and for constrained cavity growth, Equations (A1.5), (A1.7) and (A1.9) give:

$$dW = \frac{d\varepsilon}{\varepsilon_{f\,min}} \tag{A1.11}$$

Equations (A1.10) and (A1.11) provide strain based definitions of damage with the same physical meaning in the regimes of constrained and unconstrained cavity growth. These can be expressed in the form of a general equation:

$$dW = \frac{\beta\, d\varepsilon}{\varepsilon_{f\,min}} \tag{A1.12}$$

where β is also related to the principal direction and depends on:

$$\varphi' = \left(\frac{\sigma}{\dot{\varepsilon}}\right)\left(\frac{\dot{\varepsilon}}{\sigma}\right)_{trans} \tag{A1.13}$$

The relationship between β and φ' is given in Fig A1.2.

The equations have been modified to simplify application in the procedure. The first modification involves redefining φ in terms of $(\dot{\varepsilon}/\sigma)_{crit}$ instead of $(\dot{\varepsilon}/\sigma)_{trans}$ where the subscript 'crit' denotes a critical rate. Fig A1.3 shows that $(\dot{\varepsilon}/\sigma)_{crit}$ corresponds to a change from damaging to non-damaging strain. The modification is introduced because analysis of creep fatigue tests using the step relationship allow both $(\dot{\varepsilon}/\sigma)_{crit}$ and $\varepsilon_{f\,min}$ to be determined [14]. For pure relaxation, it can be shown that:

$$\left(\frac{\dot{\varepsilon}}{\sigma}\right)_{crit} > 2\left(\frac{\dot{\varepsilon}}{\sigma}\right)_{trans}$$

To avoid a large number of redundant creep damage calculations for those parts of an operational cycle where the strain rate is high, a second modification is used, in which a linear relationship of the form shown in Fig A1.4 is used. This relationship is based on two assumptions:

i. $$\left(\frac{\dot{\varepsilon}}{\sigma}\right)_{crit} = 2\left(\frac{\dot{\varepsilon}}{\sigma}\right)_{trans}$$

(This is conservative for pure relaxation)

ii. a value of φ can be defined (φ_o) below which damage is, in effect, negligible.

A value of $(\dot{\varepsilon}/\sigma)_{crit} = 9 \times 10^{-6}$ (h MPa)$^{-1}$ has been used in the creep-fatigue procedure on the basis of an analysis of creep-fatigue tests on Type 316 steel at 550°C to 600°C by Hales [14] and a value of $\varphi_o = 0.1$ has been judged appropriate from the data at 550°C to 600°C, where $\dot{\varepsilon}_{crit} = 10^{-6}$ s^{-1}. The value $\varphi_o = 0.1$ corresponds to a strain rate of approximately 1.5×10^{-5} s^{-1} and a ductility of $10\varepsilon_{f\,min}$. The assumed relationship between strain rate and ductility is compared with data for Type 316 steel in Fig A1.5.

It should be noted that the damage increment takes on the sign of the strain increment as sintering of the cavities in Type 316 steel can occur under compressive loading.

The factors φ and β depend on the strain rate and stress state, and the damage formulation takes on the following effects:

i. No damage occurs when σ_i, the principal stress, is zero as, for example, in the plane of the surface of axisymmetric components.

ii. Damage is ameliorated for stress states which are mainly compressive, but which have one or two small positive principal stresses.

iii. When $(\sigma_i/\dot{\varepsilon}_i)$ is negative, creep damage is zero. Growth of cavities cannot occur under a positive principal stress because the negative principal strain rate cannot accommodate the dilatation necessary for cavity growth. Similarly cavity growth cannot occur when the principal stress is negative, even if the principal strain rate is positive.

APPENDIX A2. RULES FOR DAMAGE ASSESSMENT: FIXED AND COINCIDENT PRINCIPAL AXES OF STRESS AND STRAIN.

A2.1. General comments

In this case it is possible to characterise the cycle, for both creep and fatigue damage assessment, on the basis of principal stresses and strains. Both creep damage and fatigue damage can be associated with principal planes. The three principal directions i = 1, 2, 3 must be identified by their direction cosines with respect to the co-ordinate used, not by the usual convention $\sigma_1 \geq \sigma_2 \geq \sigma_3$.

A2.2. Creep damage assessment

Creep damage is assessed incrementally. The operational cycle is divided into j time increments k of duration $(\delta t)_k$. Then the following quantities are calculated for each principal plane:

a. Strain rate factor $(\varphi_i)_k$

Where the temperature is less than 480°C, for Types 316 and 316L(N) steel, this is zero. Where the temperature is between 480°C and 625°C, the strain rate factor is calculated for creep during all operational steady states in the operational cycle as:

$$(\varphi_i)_k = \left(\frac{\sigma_i}{\delta\varepsilon_i} . \delta t\right)_k . \left(\frac{\dot{\varepsilon}}{\sigma}\right)_{crit} \qquad \text{(A2.1)}$$

where

$(\sigma_i)_k$ is the mean value of the principal stress over the time increment k

$(\delta\varepsilon_i)_k$ is the change in principal inelastic strain over the time increment k

$\left(\frac{\dot{\varepsilon}}{\sigma}\right)_{crit} = 9 \times 10^{-6}$ (h MPa)$^{-1}$

Similarly, for all other parts of the operational cycle, a similar strain rate factor is calculated for quasi-creep, except that $(\delta\varepsilon_i)_k$ is now the change in total principal strain over the time increment k.

b. Ductility factors $(\beta_i)_k$

These are calculated separately for creep and quasi creep where:

$(\beta_i)_k = 0$ for $(\varphi_i)_k \leq 0.1$

$1.8(\beta_i)_k = (\varphi_i)_k - 0.1$ for $0.1 < (\varphi_i)_k \leq 1.9$

$(\beta_i)_k = 1$ for $(\varphi_i)_k > 1.9$

(see Appendix 1)

c. Creep damage fractions

The three principal creep damage fractions W_i are calculated separately for creep and quasi-creep from:

$$W_i = \sum_{k=0}^{k=j} \left(\frac{\delta\varepsilon_i . \beta_i}{\varepsilon_f} \right)_k \qquad \text{(A2.2)}$$

d. Cumulative creep damage fraction

The cumulative principal creep damage ΣW_i^c and cumulative quasi-creep damage ΣW_i^q are calculated for each principal plane for different types of operational cycle.

e. Total creep damage fraction

The total principal creep damage fraction W_i^t from all operational cycles is calculated as the largest of ΣW_i^c, ΣW_i^q and $(\Sigma W_i^c + \Sigma W_i^q)$. (That is, creep and quasi-creep damage are combined only if the resulting damage is greater than that due to creep or quasi-creep alone).

The creep damage W is then the largest of the three principal quantities W_i^t, where $W \not< 0$. If $W \geq 1$ the design is unacceptable.

A2.3. Fatigue damage

The history of the total (elastic + plastic + creep) value of principal stress and strain is calculated for each stress-strain cycle and the change in each principal stress $\Delta\sigma_i$ and each principal strain $\Delta\varepsilon_i$ (where i = 1, 2, 3) is calculated for all available pairs (t_m, t_n).

a. For each of these time pairs, the von Mises stress range, $\Delta\bar{\sigma}$, and von Mises strain range $\Delta\bar{\varepsilon}$ are calculated.

b. Correction for relaxation - Correction is made for stress relaxation by identifying all hold periods in the operational cycle and obtaining the changes in principal stress $\Delta\sigma_{1h}$, $\Delta\sigma_{2h}$, $\Delta\sigma_{3h}$ between the start and end of each hold period. From these, the change in von Mises stress is obtained for each hold period and the von Mises strain range $\Delta\bar{\varepsilon}$ is corrected for relaxation using Equation (3). The effective (Rankine) strain range, $\Delta\varepsilon_i^R$, is then calculated for each principal plane using Equation (2).

c. Thermal striping correction - A thermal striping correction is then applied to the major cycle with the largest Rankine strain range which occurs in any group of major cycles between consecutive periods of thermal striping:

$$\Delta\bar{\varepsilon}_i^t = \Delta\varepsilon_i^R + \Delta\bar{\varepsilon}_s \qquad \text{(A2.3)}$$

where $\Delta\bar{\varepsilon}_s$ is obtained from Equation (5).

No enhancement is made to other major cycles in the group.

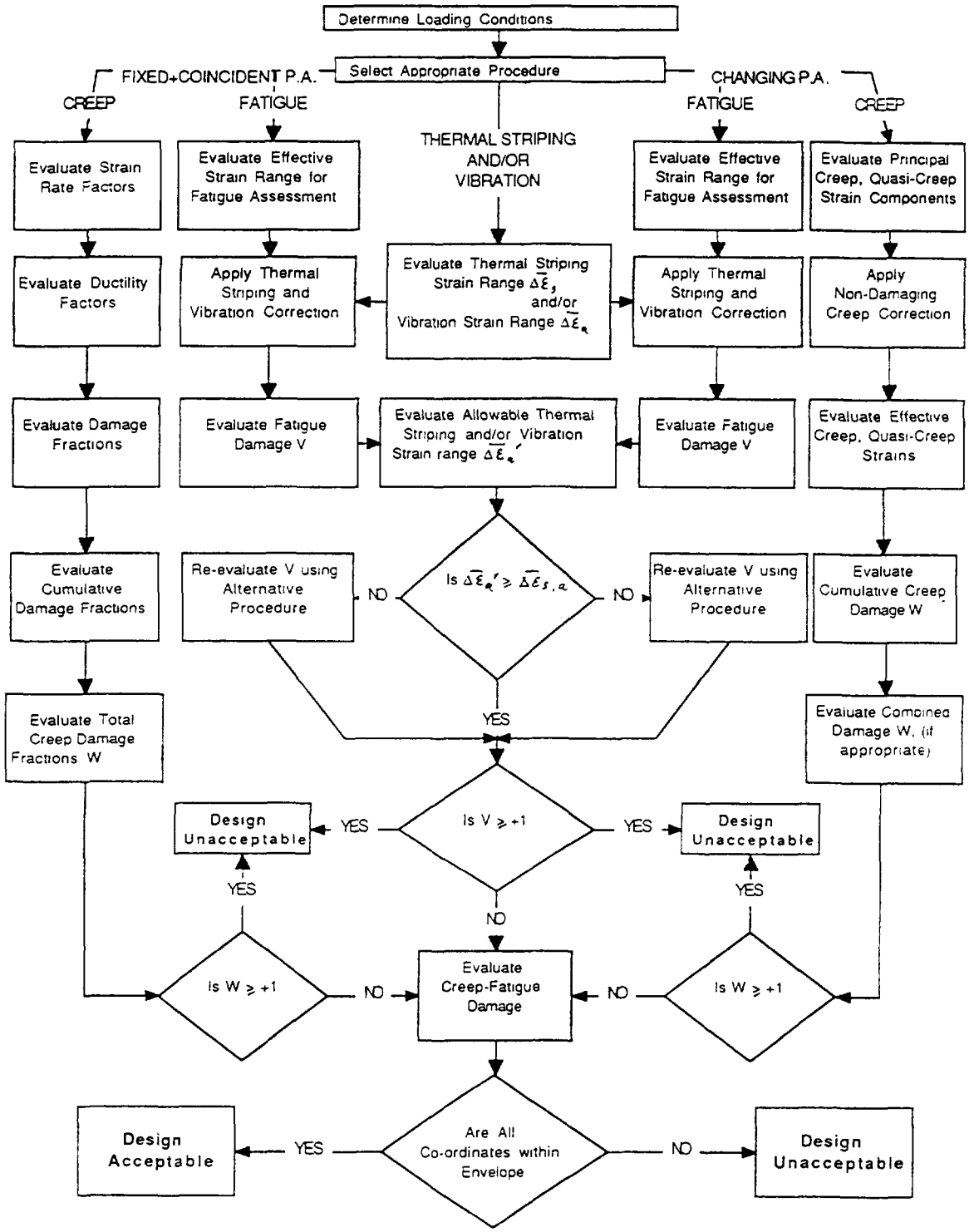

FIG. A2.1. Sequence of assessment stages for creep damage evaluation.

d. Fatigue damage evaluation - The fatigue damage associated with each principal plane, i, is obtained from:

$$V_i = \sum_{\text{all major cycles}} \left(\frac{n}{N_i^g}\right) \qquad \text{(A2.4)}$$

where

n is the number of applications of each major cycle

N_i^g is the allowable number of cycles obtained from Fig 1 at a strain range $\Delta\bar{\varepsilon}_i^t$.

The fatigue damage V is the largest of the three values V_i. If $V \geq 1$, the design is unacceptable.

A2.4. Evaluation of thermal striping

If the thermal striping is unacceptable by the simplified method (Section 2.3), then V must be re-assessed, calculating the thermal striping as part of the major cycles without applying the correction for thermal striping in Section A2.3 c.

A2.5. Creep-fatigue evaluation

The co-ordinates (V, W) are plotted on the interaction diagram (Fig 4). The design is acceptable if all co-ordinates fall within the shaded area.

A creep-fatigue usage factor Q can be evaluated by constructing a line through the point X of co-ordinates (V, W) to meet the envelope of the L-shaped diagram at Y. The usage factor Q is then given by:

$$Q = \frac{OX}{OY}$$

Note that all creep damages and all fatigue damages should be separately summed before entering the diagram. The usage factors Q from different cycles cannot be added.

The steps in assessing creep fatigue damage for the case of fixed and coincident principal axes of stress and strain are shown in Fig A2.1.

APPENDIX 3. RULES FOR DAMAGE ASSESSMENT: ROTATING PRINCIPAL AXES OF STRESS AND STRAIN

A3.1. General comments

These rules are used when rotation of principal axes occurs during some or all operational cycles. It is then necessary to characterise the operational cycle on the basis of the six components of stress and strain. Damage has then to be evaluated for notional 'principal planes' defined from the changes in the six components of stress and strain. When comparing damage from more than one type of cycle, it cannot be assumed that the 'principal' planes coincide and the worst combination is taken for conservatism.

A3.2. Creep damage assessment

Where the axes of principal stress and strain remain fixed and coincident throughout some operational cycles, the creep damage can be assessed using the rules outlined in Section A2.2. Provision is made for adding the damage in those cycles to damage from cycles in which the principal axes of stress and strain rotate in sub-section A3.2 i below.

The incremental damage assessment described in Section A2.2 relies on the existence of fixed principal planes for which damage calculations could be made. For rotating principal axes, it is necessary to identify the axes associated with maximum damage. For constrained cavity growth, these axes will be those for which the net normal creep and quasi-creep strain over the operational cycle is a maximum.

The procedure requires the separate evaluation of the net change in the six components of creep strain and quasi-creep strain for the operational cycle. From these, the net changes in the three components of principal creep strain and principal quasi-creep strain are evaluated separately. The creep ductility is assumed to be constant with strain rate and temperature, so the net creep damage can be evaluated from the net changes in principal creep and quasi-creep strain. No allowance is made for the possibility that damage introduced in one operational cycle may be reversed by succeeding operational cycles, since the plane of maximum creep damage could change for the two cycles.

Since the strain rate factors φ_i used for fixed and coincident principal axes of stress and strain cannot be evaluated for rotating principal axes, conservative provisions are made. Firstly all creep strain is included in the assessment of net component strain changes regardless of strain rate. Secondly, time increments during which quasi-creep strains occur are identified on the basis of a von Mises strain rate criterion, using a critical strain rate of 10^{-6} s^{-1} (see Appendix 1).

Consideration is taken of the possibility that part of the creep or quasi-creep strain may be non-damaging to reduce over-conservatism. The criteria for creep strain to be non-damaging are:

i. Positive net principal creep strains or quasi-creep strains are non-damaging if the corresponding resolved normal stress is zero or compressive at relevant times, since cavities cannot then grow.

ii. If the net creep strain for a cycle is negative, i.e. compressive, in an operational cycle, then this creep strain is taken as non-damaging.

To assess creep damage for the case of rotating principal axes of stress and strain, the following steps are taken:

a. Divide the operational cycle into time increments. Then, using a set of orthogonal axes x, y, z:

b. Evaluate the net creep strain components. These are the net changes in each of the six components of inelastic strain $\Delta\varepsilon_{cx}$, $\Delta\varepsilon_{cy}$, $\Delta\varepsilon_{cz}$, $\Delta\gamma_{cxy}$, $\Delta\gamma_{cyz}$, $\Delta\gamma_{czx}$ over all operational steady states in the operational cycle.

c. Evaluate quasi-creep time increments; for each time increment of the operational cycle which falls outside the operational steady state, evaluate the changes in total strain components $\delta\varepsilon_x$, $\delta\varepsilon_y$, $\delta\varepsilon_z$, $\delta\gamma_{xy}$, $\delta\gamma_{yz}$, $\delta\gamma_{zx}$ during the time increment δt.

From these, the increment in total von Mises strain $\delta\bar{\varepsilon}$ is obtained. Time increments during which quasi-creep strains occur are then those in which the temperature, for Types 316 and 316L(N) steel, is over 480°C and $\delta\bar{\varepsilon}/\delta t < 10^{-6}\ s^{-1}$.

d. Evaluate the quasi-creep strain components. These are the net change of the six components of quasi-creep strain $\Delta\varepsilon_{qx}$, $\Delta\varepsilon_{qy}$, $\Delta\varepsilon_{qz}$, $\Delta\gamma_{qxy}$, $\Delta\gamma_{qyz}$, $\Delta\gamma_{qzx}$, which are the net change in the total strain components over all the quasi-creep time increments in the operational cycle, identified in c.

e. Evaluate, separately, the net principal creep and quasi-creep strains. These are the net principal creep strains ε_{c1}', ε_{c2}', ε_{c3}' and net principal quasi-creep strains ε_{q1}', ε_{q2}', ε_{q3}'.

f. Correct the net principal creep and quasi-creep strains for non-damaging creep.

The principal creep and quasi-creep strains ε_{ci} and ε_{qi} are equal to the net principal creep and quasi-creep strains ε_{ci}' and ε_{qi}' respectively, except where at least one of the following conditions apply:

i. where the resolved normal stress in the direction of ε_{ci}' is zero or compressive for all time increments contributing to ε_{ci}' then $\varepsilon_{ci} = 0$.

ii. where the resolved normal stress in the direction of ε_{qi}' is zero or compressive for all time increments contributing to ε_{qi}', then $\varepsilon_{qi} = 0$.

iii. where $\varepsilon_{ci}' < 0$, then $\varepsilon_{ci} = 0$
where $\varepsilon_{qi}' < 0$, then $\varepsilon_{qi} = 0$

g. Evaluate the effective creep and quasi-creep strains. The effective creep strain ε_c for each operational cycle is the greatest corrected principal creep strain ε_{ci} from f.

The effective quasi-creep strain ε_q for each operational cycle is the greatest corrected principal quasi-creep strain ε_{qi} from f.

h. Evaluate the cumulative creep damage W, given by:

$$W = \sum_{\text{all operational cycles}} \left(\frac{\varepsilon_c + \varepsilon_q}{\varepsilon_f} \right) \qquad \text{(A3.1)}$$

where ε_f is the minimum creep ductility of 10% for Types 316 and 316L(N) steel.

If $W \geq +1$, the design is unacceptable.

i. Evaluate combined damage.

If some operational cycles (a, b, ...) are assessed by the rules for fixed and coincident principal axes of stress and strain (Section A2.2) and others (c, d, ...) are assessed by the rules for rotating principal axes, then the combined damage is given by:

$$W = (W)_{a+b+....} + (W)_{c+d+....}$$

If $W \geq +1$, the design is unacceptable.

A3.3. Fatigue damage assessment

For those operational cycles in which the axes of principal stress and strain remain fixed and coincident throughout the operational cycle, the fatigue damage can be evaluated using Section A2.3. For the other operational cycles, where rotation of principal axes occurs, the principles are the same as those outlined in Section A2.3. The quantities required to evaluate the Rankine strain range for the case of rotating principal axes are given in terms of the six components of stress and strain. Only the maximum principal stress range needs to be determined. A single maximum value for fatigue damage is obtained for each major cycle and these maximum values are summed over all cycle types.

a. Evaluation of the effective strain range.

Calculate for each stress-strain cycle, the history of the total (elastic + plastic + creep) value of each component of stress and strain as a function of time using a set of orthogonal axes x, y, z.

Calculate the change in each of the six components of stress $\Delta\sigma$ and strain ($\Delta\varepsilon$ or $\Delta\gamma$) for all available pairs of times (t_m, t_n).

Calculate the following quantities for each pair of times (t_m, t_n)

i. von Mises stress range, $\Delta\bar{\sigma}$

ii. von Mises strain range, $\Delta\bar{\varepsilon}$

iii. principal stress range $\Delta\sigma_1$.

b. Correction for relaxation.

The quantity $\bar{\sigma}_h$ is calculated from the changes in stress components i.e. $\Delta\sigma_{xh}$, $\Delta\sigma_{yh}$, $\Delta\sigma_{zh}$.... between the start and end of each hold period. The corrected value of the von Mises stress range $\Delta\bar{\varepsilon}$ is then calculated using Equation (3).

c. Evaluation of effective strain range.

The effective (Rankine) strain range for each cycle is calculated as the maximum value for all time pairs (t_m, t_n) using Equation (2).

d. Correction for thermal striping

The Rankine strain range is corrected as in Section A2.3 c, using the equation:

$$\Delta\bar{\varepsilon}^{\,t} = \Delta\varepsilon^{R} + \Delta\bar{\varepsilon}_{s} \qquad \text{(A3.2)}$$

e. Fatigue damage evaluation.

The fatigue damage, V, is evaluated from:

$$V = \sum_{\text{all major cycles}} \left(\frac{n}{N_g}\right)$$

where

n is the number of cycles at each major cycle Rankine strain range corrected for thermal striping

N_g is the allowable number of cycles obtained from Fig 1 at a strain range $\Delta\bar{\varepsilon}^{\,t}$.

If $V \geq 1$, the design is unacceptable.

f. Evaluation of combined damage.

If some operational cycles (a, b, ...) are assessed by the rules for fixed and coincident principal axes of stress and strain and others (c, d, ...) are assessed by the rules for rotating principal axes, then the combined damage is given by:

$$V = (V)_{a+b+....} + (V)_{c+d+....}$$

If $V \geq 1$ then the design is unacceptable.

A3.4. Thermal striping evaluation

If the thermal striping is unacceptable by the simplified method (Section 2.3) then V must be re-assessed, calculating the thermal striping as part of the major cycles without applying the correction for thermal striping as in Section A3.3 d.

A3.5. Creep-fatigue evaluation

Creep fatigue damage is evaluated in the same way as in Section A2.5. The steps in assessing creep-fatigue damage for the case of rotating principal axes are shown in Fig A2.1.

CREEP-FATIGUE EVALUATION METHOD FOR MODIFIED 9Cr-1Mo STEEL

Y. WADA, K. AOTO
Power Reactor and Nuclear Fuel Development Corporation,
Oarai Engineering Center,
Ibaraki, Japan

Abstract

As creep-fatigue evaluation methods on normalized and tempered Modified 9Cr-1Mo steel for design use, the time fraction rule and the simplified conventional ductility exhaustion rule are investigated for the prediction of tension strain hold creep-fatigue damage of this material.

For the above investigation, stress relaxation behavior during strain hold has to be analyzed using stress-strain-time relation. The initial value of stress relaxation was determined by cyclic stress-strain curves in continuous cycling fatigue tests. Cyclic stress-strain behavior of Mod.9Cr-1Mo(NT) steel is different from that of austenitic stainless steels, so this effect was considered. Stress relaxation analysis was performed using static creep strain-time relation and conventional hardening rule. The time fraction by using the above stress relaxation analysis results can give good prediction for creep-fatigue life of Mod.9Cr-1Mo(NT) steel. For design use it is practical to be able to estimate creep damages conservatively by both strain behavior of cyclic plastic(in continuous cycling fatigue tests) and monotonic creep(in standard creep tests).

The life reduction by strain hold at the minimum peak of compressive stress in creep-fatigue tests was examined, and this effects can be evaluated by the relationship between the location of oxidation and the effective deformation at crack tip. In an accelerated oxidation environment, for example in high temperature and high pressure steam, a different approach for life reduction should be developed based on the mechanism of growth of oxide and crack growth with oxidation. However, in the creep damage dominant region, its effect is saturated and the effect of cavity growth along grain boundary becomes dominant for long-term strain hold in the high temperature conditions.

1. INTRODUCTION

The analytical procedure(PNC procedure) using the time fraction approach to evaluate creep damage has been already developed for Type 304 ss[1], and as the physical background of the time fraction the grain boundary sliding was connected with the secondary creep deformation[2]. For 316FR ss PNC procedure gave good life estimation[3]. In structural design of LMFBR components long time extrapolation has to be evaluated considering the intergranular failure mode which leads to severe life reduction. Therefore PNC procedure for Type 304 ss and Type 316FR ss is good for design use.

For normalized and tempered modified 9Cr-1Mo steel it is interesting whether the procedure for austenitic stainless steel can be applied. As the first consideration point the cyclic strain softening is observed in modified 9Cr-1Mo steel, and determination of cyclic stress level is important to evaluate the time fraction. And the second point is an environmental effect(oxidation). The strain hold effect at the compression side of each strain cycle induces fatigue life reduction. For long time extrapolation it has to be clarified which interaction effect of creep damage or oxidation is more severe for the fatigue life reduction.

2. CREEP-FATIGUE LIFE EVALUATION IN TENSILE STRAIN HOLD CONDITION

2.1 PNC TIME FRACTION PROCEDURE FOR CREEP-FATIGUE EVALUATION

PNC time fraction procedure is investigated based on creep-fatigue test results on Type 304 ss[1]. The time fraction is one of the ductility exhaustion, and it can be derived from secondary creep strain fraction: $\varepsilon_m \Delta t / \varepsilon_m t_R$.

For austenitic stainless steels this procedure was applied not only for Type 304 ss and also for Type 316 and 321 ss as Monju structural design guide[1], and furthermore it is applicable for 316FR ss from recent study[3]. The general schema of PNC creep-fatigue evaluation procedure based on time fraction is shown in FIG.1. In PNC procedure, creep strain-time relation is expressed using time to rupture and secondary creep rate. For normalized and tempered $2^1/_4$Cr-1Mo steel, which shows cyclic strain softening, the initial value of stress relaxation in FIG.1 is estimated using tensile stress-strain relation(the first cycle behavior) in Monju structural design guide. In higher strain range this estimation is too conservative[4], however in lower one(interested in design) it gives suitable margin for practical design use. Therefore for normalized and tempered modified 9 Cr-1Mo steel, the applicability of PNC procedure is investigated using mechanical properties of this material and creep-fatigue test data with tensile strain hold.

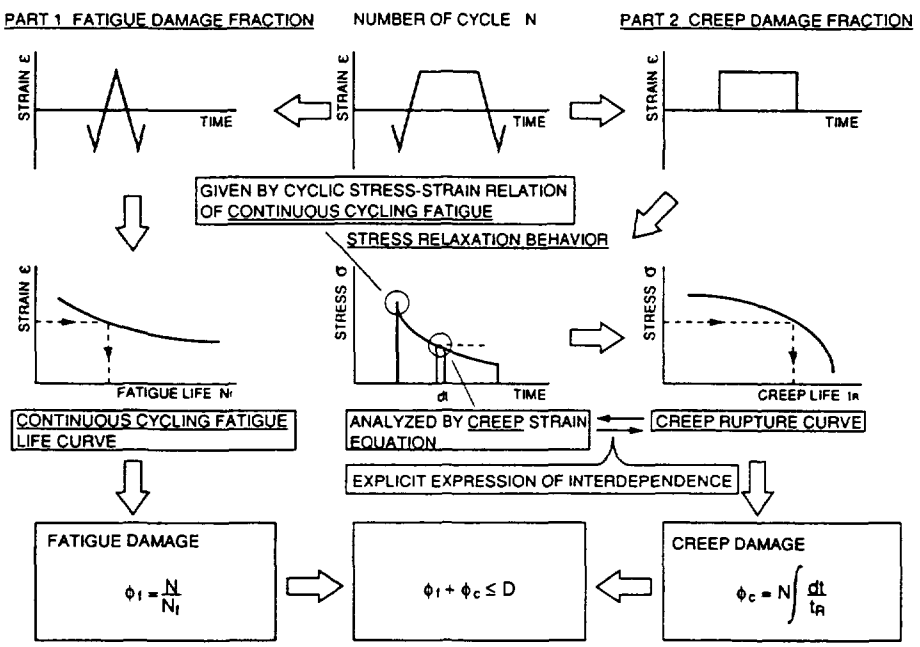

FIG 1 CONCEPT OF CREEP-FATIGUE EVALUATION PROCEDURE OF PNC TIME FRACTION PROCEDURE

2.2 MATERIAL PROPERTIES USED FOR CREEP-FATIGUE EVALUATION

2.2.1 CREEP STRAIN-TIME RELATION AND TIME TO RUPTURE CURVE

The creep strain of modified 9Cr-1Mo steel (normalized and tempered) is expressed by the following equation[5], of which type was already examined for Type 304 ss in Japan.

$$\varepsilon_c = C_1[1-\exp(-r_1 t)] + C_2[1-\exp(-r_2 t)] + \dot{\varepsilon}_m t \qquad (1)$$

where,

$C_1 r_1 = \alpha_1 \dot{\varepsilon}_m^{a1}$

$C_2 r_2 = \alpha_2 \dot{\varepsilon}_m^{a2}$

$r_1 = \beta_1 t_R^{b1}$

$r_2 = \beta_2 t_R^{b2}$

and $\dot{\varepsilon}_m$ is secondary creep strain rate and t_R is time to rupture. In the above equation it is the distinctive feature that creep strain-time relation is represented using $\dot{\varepsilon}_m$ and t_R instead of stress. At the same stress level, creep strain behavior is scattered in response to the difference of time to rupture. If stress relaxation rate is high, then creep rupture strength is weak. Therefore in the time fraction rule, higher stress relaxation rate is not connected to lower creep damage.

Secondary creep strain rate $\dot{\varepsilon}_m$ related to time to rupture t_R is expressed in the following Monkman-Grant type equation[5],

$$\dot{\varepsilon}_m = F \exp(-Q/RT_K)\, t_R^{-\lambda} \qquad (2)$$

and time to rupture t_R is expressed as follows[5] using Larson-Miller type time-temperature parameter.

$$T_K(\log_{10} t_R + C) = A_0 + A_1 \log_{10}\sigma + A_2 (\log_{10}\sigma)^2 \qquad (3)$$

where σ is stress, and T_K is absolute(Kelvin) temperature.

2.2.2 CYCLIC STRESS-STRAIN RELATION AND LOW CYCLE FATIGUE CURVE

The cyclic stress range $\Delta\sigma$-strain range $\Delta\varepsilon_t$ relation of modified 9Cr-1Mo is analytically represented using Ludwik type equation as follows:

$$\text{for } \Delta\sigma \leqq \sigma_P, \quad \Delta\sigma = E\,\Delta\varepsilon_t$$
$$\text{for } \Delta\sigma > \sigma_P, \quad \log_{10}(\Delta\sigma - 2\sigma_P) = G_0 + G_1 \log_{10}(\Delta\varepsilon_t - \Delta\sigma / E) \qquad (4)$$

where σ_P is the proportional limit, E is Young's Modulus, and G_0, G_1 are parameters of temperature. In eq.(4) materials constants were determined from experimental results on continuous cycling fatigue at the strain rate of 0.001 mm/mm/sec[5].

The average trend of low cycle fatigue life of modified 9Cr-1Mo steel is determined using an analogous technique between analysis results on $2^1/_4$Cr-1Mo steel(widely compiled data base) and test results on modified 9Cr-1Mo steel. The effects of temperature and strain rate is considered based on the above analogy. Obtained equation is as follows:

$$\begin{aligned}(\log_{10} N_f) = {} & D_0 + D_1 \log_{10}\Delta\varepsilon_t + D_2(\log_{10}\Delta\varepsilon_t)^2 + D_3(\log_{10}\Delta\varepsilon_t)^4 \\ & + D_4\, T^2 \log_{10}\dot{\varepsilon} + D_5\, T(\log_{10}\Delta\varepsilon_t)^4 + D_6 T \log_{10}\dot{\varepsilon}\,(\log_{10}\Delta\varepsilon_t)^4 \end{aligned} \qquad (5)$$

where N_f is number of cycles to failure, $\dot{\varepsilon}$ is strain rate(mm/mm/sec) and T is temperature(℃). The coefficients D_0 to D_6 are constants[5].

2.2.3 DIAGRAM OF CREP-FATIGUE DAMAGE LIMIT

As for $2^1/_4$Cr-1Mo steel Campbell type diagram in ASME Code Case N-47 for stainless steels was applied, and life prediction result was conservative using tensile stress-strain relation (same as cyclic one for the first cycle)[4]. Therefore on the basis of the analogy to $2^1/_4$Cr-1Mo steel the examination whether estimated life using cyclic relation of eq.(4) and Campbell type diagram is conservative or not is performed for modified 9Cr-1Mo steel.

2.2.4 CREEP-FATIGUE LIFE ESTIMATION RESULTS

FIGURE.2(a)-(c) show creep-fatigue life prediction results by PNC time fraction procedure using cyclic stress-strain relation without strain hold , and they are compared with test results.

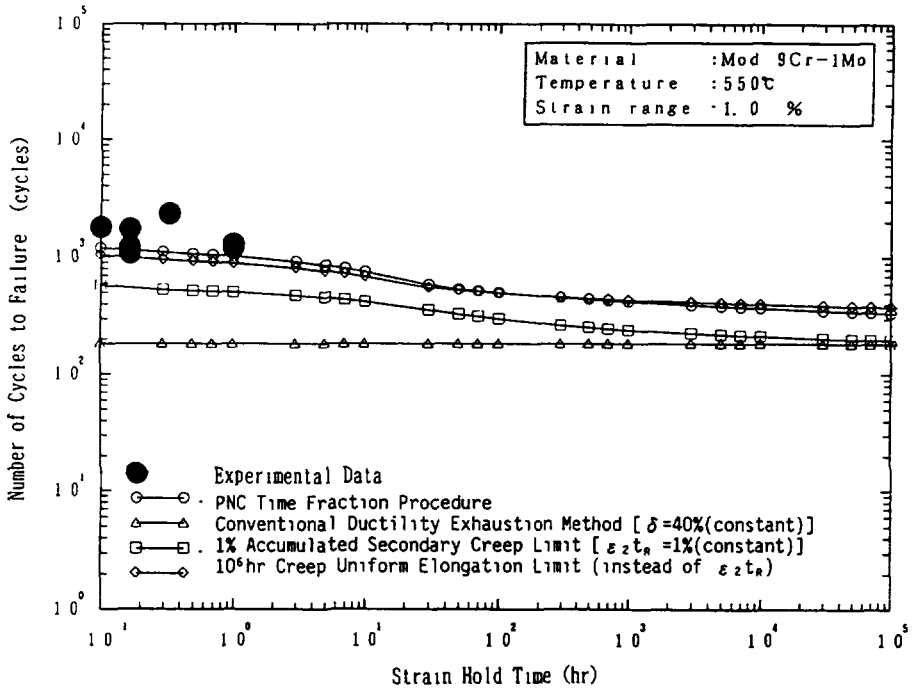

FIG 2(a) COMPARISON OF CREEP-FATIGUE EVALUATION METHODS ON THE PREDICTABILITY AND TIME EXTRAPOLATION(823K, $\Delta\varepsilon_t$=1%)

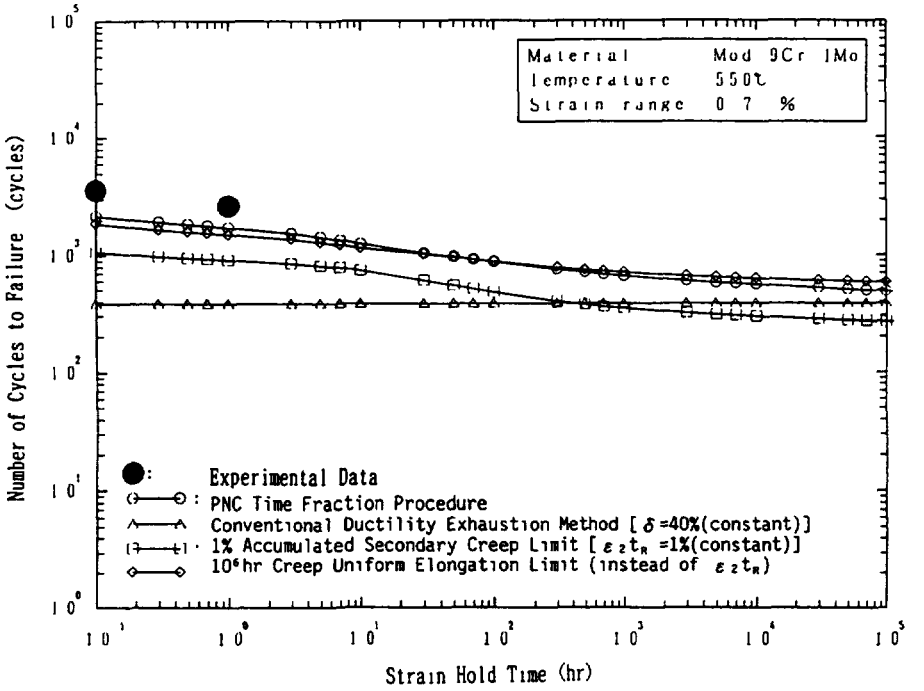

FIG 2(b) COMPARISON OF CREEP-FATIGUE EVALUATION METHODS ON THE PREDICTABILITY AND TIME EXTRAPOLATION(823K, $\Delta\varepsilon_t$=0.7%)

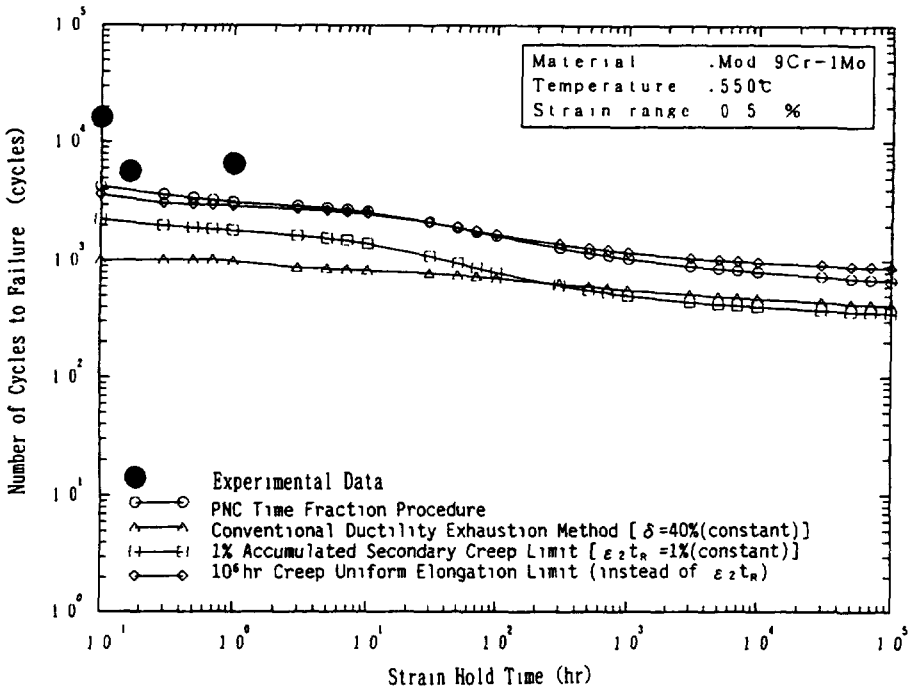

FIG 2(c) COMPARISON OF CREEP-FATIGUE EVALUATION METHODS ON THE PREDICTABILITY AND TIME EXTRAPOLATION(823K, $\Delta\varepsilon_t$=0 5%)

In FIG.2 predicted lives using the conventional ductility exhaustion rule, in which the ductility limit is determined from the reduction of area: ϕ obtained by creep rupture tests for more than 20,000 hrs. The value of ϕ is about 80% up to less than 20,000 hrs, and it is expected that it decreases steeply for longer rupture time like $2^1/_4$Cr-1Mo steel as shown in FIG.3[6].

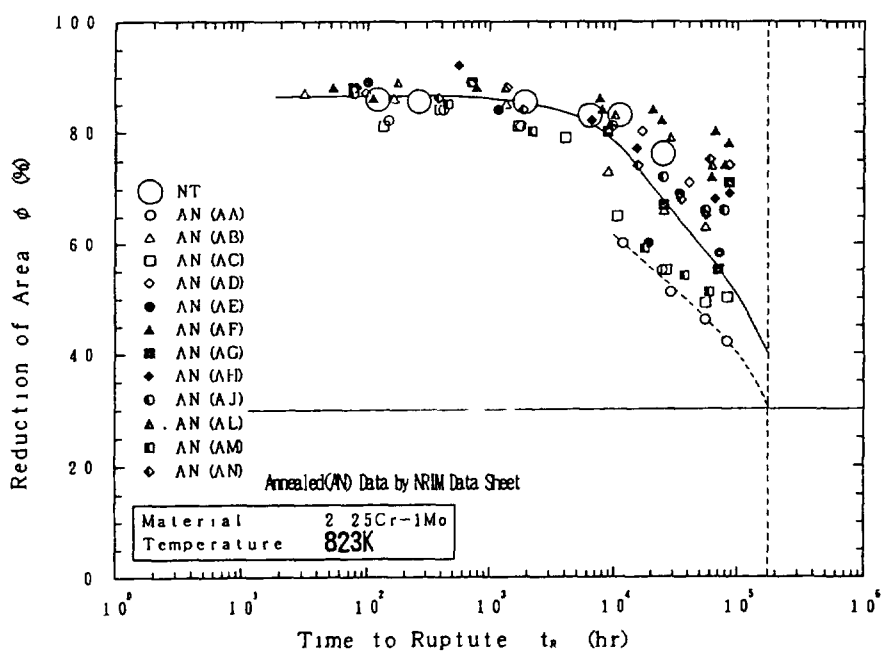

FIG 3 REDUTION OF AREA OF $2^1/_4$Cr-1Mo STEEL(823K)

For simplified application it is better that the value of ductility is constant, so 40% is given for the analysis considering the analogy to $2^1/_4$Cr-1Mo steel in FIG.3. Predicted life is conservative compared with PNC time fraction procedure for short tome strain hold. This tendency is almost same as that in $2^1/_4$Cr-1Mo steel as shown FIG.4. For long time strain hold for more than 1,000 hrs the conventional ductility exhaustion is still conservative for modified 9 Cr-1Mo steel, and it becomes more conservative if the ductility is less than 40% in very slow strain rate condition.

PNC time fraction procedure using the cyclic stress-strain relation gives reasonable life prediction as shown in FIG.2 compared with the conventional ductility exhaustion rule. And when the tensile stress-strain relation is applied it gives surely conservative life estimation. In the next demonstration reactor design the evaluation method is still under investigation, however PNC time fraction procedure using the tensile stress-strain relation procedure is probable one because of the consistency with $2^1/_4$Cr-1Mo steel, simplicity, suitable margin in lower strain and so on.

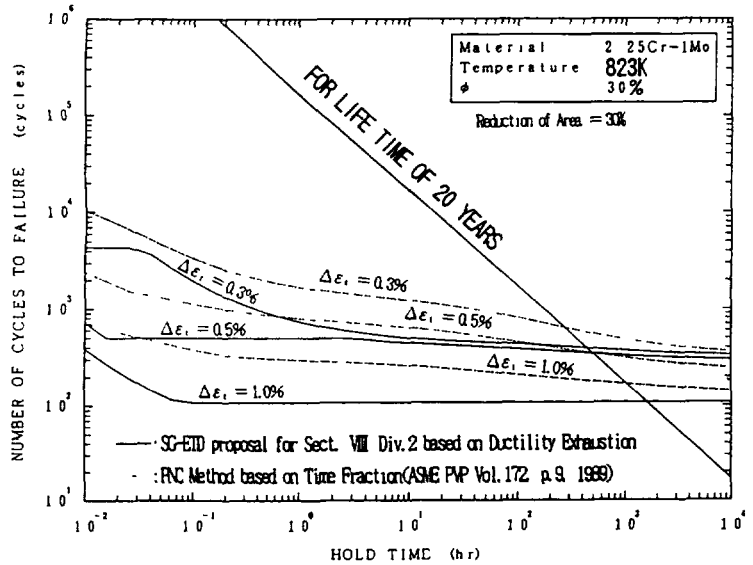

FIG 4 COMPARISON BETRWEEN TWO ESTIMATED CREEP-FATIGUE LIVES BY DUCTILITY EXHAUSTION AND PNC TIME FRACTION PROCEDURE(823K)

3. CREEP-FATIGUE LIFE EVALUATION IN COMPRESSION STRAIN HOLD CONDITION

Creep cavities along grain boundaries were observed for Type 304 ss[2], however no cavities were observed for modified 9Cr-1Mo steel under the same conditions. This fact indicates that the process of creep damage accumulation of this material is different from Type 304 ss. For modified 9Cr-1Mo steel an incubation time has to be necessary to structure grain boundary(or pseudo grain boundary) by the precipitation before the cavity nucleation. Nevertheless in the creep damage dominant condition, the failure mechanism of this material could be same as that of Type 304 ss, and the cavity growth dominates the life of material. FIGURE.4 shows creep cavities observed in a fractured specimen of which test duration time is about one year. Consequently in the design condition PNC time fraction procedure is applicable for tensile strain hold(creep damage dominant).

The failure mode of compression strain hold is quite different from that of tensile one. FIGURE.5(a) shows the shape of the crack on the cross section in the case of compression hold. The crack tip was very sharp and grew from the surface of oxide to matrix of fractured test specimen. The shape of crack tip of tension hold is filled with oxide as shown in FIG.5(b). The oxidation effect due to strain hold time is saturated, and the life reduction caused by creep damage accumulation during tensile strain hold is more severe as shown in FIG.6[5].

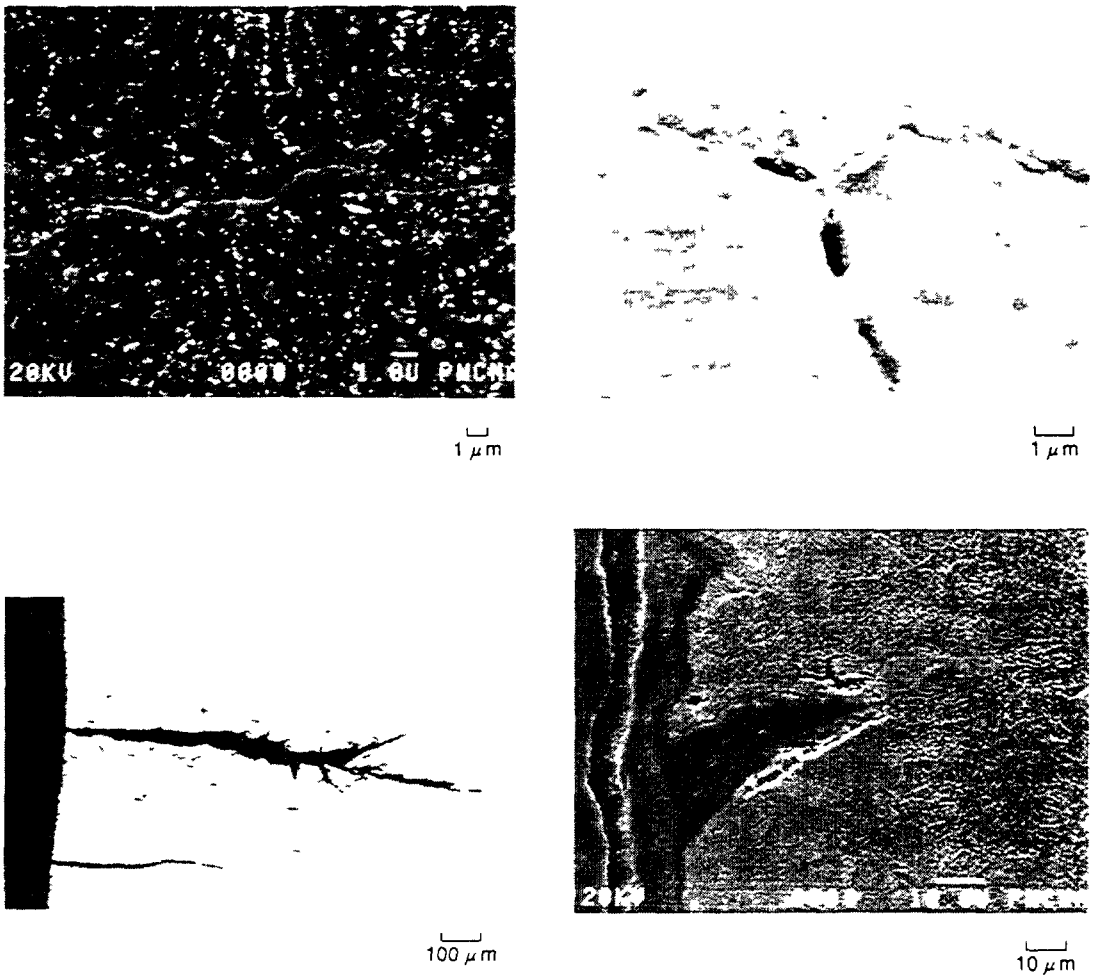

(a) COMPRESION HOLD (b) TENSION HOLD

FIG 5 CREEP CAVITIES ON GRAUIN BOUNDARY OF CREEP-FATIGUE FAILURE SPECIMEN (823K, $\Delta\varepsilon_t$=0 5% STRAIN HOLD TIME=1HR)

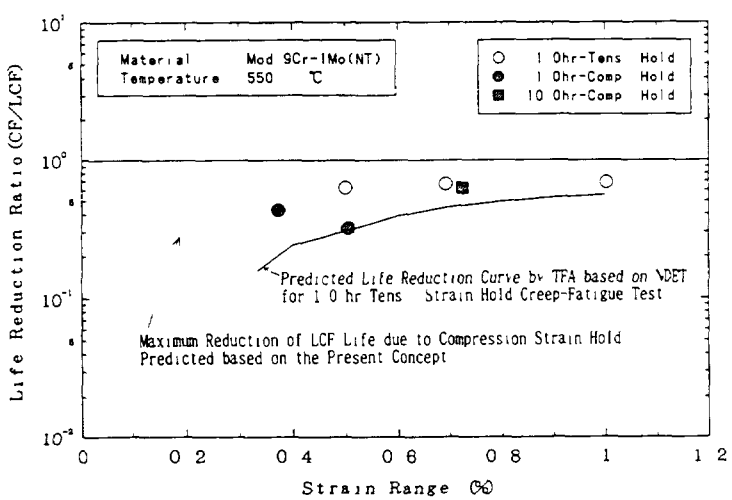

FIG 6 LIFE REDUTION DUE TO STRAIN HOLD POSSITION FOR MODIFIED 9CR-1MO

4. CONCLUSIVE REMARKS

(1) PNC time fraction procedure is applicable to creep-fatigue life evaluation of modified 9Cr-1Mo steel in the creep damage dominant (tension hold) condition.

(2) In the oxidation dominant(compression hold) condition, PNC procedure cannot be applied. However, for long time strain hold, the creep damage effect is severe rather than the oxidation effect, because the latter one is saturated. Therefore if the strain hold effect is evaluated in the condition of tension hold, as the results the oxidation effect is also evaluated conservatively.

(3) For structural design using modified 9Cr-1Mo steel PNC time fraction procedure using tensile stress-strain relation is practical, because it is simple concept, conservative, analytically represented and so on.

REFERENCES

[1] K.Aoto, et al., "An analytical approach to creep-fatigue life prediction for SUS304, 316 and 321 austenitic stainless steel," ASME PVP-Vol.123(1987)43-48

[2] F.Ueno, et al., "A study on creep damage parameters in creep cavity growth dominant region under creep-fatigue loading," Proc. SMiRT-12, Vol.L(1993)L05/4

[3] M.Ueta, et al., "Creep-fatigue properties of advanced 316-steel for FBR structures," ASME PVP-Vol.313-2(1995)423-428

[4] K.Aoto, et al., "Analytical study on correlationship between stress relaxation and creep deformation behavior of ferritic steels," ASME PVP-Vol.172(1989)9-14

[5] K.Aoto, et al., "Creep-fatigue evaluation of normalized and tempered modified 9Cr-1Mo," Nuclear Engineering & Design, Vol.153(1994)97-110

[6] NRIM CREEP DATA SHEET, No.3B, "Data sheet on the elevated-temperature properties of 2.25Cr-1Mo steel for boiler and heat exchanger seamless tubes(STBA24)," National Research Institute for Metals(1986)

APPLICATION OF CHABOCHE VISCOPLASTIC THEORY FOR PREDICTING THE CYCLIC BEHAVIOUR OF MODIFIED 9Cr-1Mo (T91)

P. CHELLAPANDI, R. RAMESH, S.C. CHETAL, S.B. BHOJE
Indira Gandhi Centre for Atomic Research,
Kalpakkam, Tamil Nadu,
India

XA9743961

Abstract

Modified 9Cr 1Mo (grade 91) is the structural material for the SG of 500 MWe Prototype Fast Breeder Reactor. This material is codified in RCC-MR (1993). SG top tubesheet and its connecting shell see the hot sodium temperature of about 800 K. The steam temperature is about 770 K at 17 MPa. It is envisaged that this component can meet the creep fatigue damage rules of RCC-MR with 'elastic route' itself. One of the important material data needed to use the simplified rules given in RCC-MR (1993) is `symmetrisation coefficient' (Ks) which is not yet included in RCC-MR. Ks values are established from numerous stress strain cyclic data generated theoretically by using Chaboche viscoplastic model and recommended for the inclusion in the RCC-MR. The Chaboche model for grade 91 material has 20 material parameters which are identified based on the uniaxial monotonic and cyclic data available in RCC-MR (1993) as well as the published data and many uniaxial monotonic, cyclic, creep data are compared well with the predictions.

1. INTRODUCTION

The high temperature out of core components in an FBR are hot sodium pool components, hot secondary sodium piping, SG and turbine. Turbine being a standard equipment, analysis is not done. Detailed elastic, inelastic and viscoplastic analysis have been done for hot pool components other than SG for 500 MWe Prototype Fast Breeder Reactor (PFBR), being designed at Indira Centre for Atomic Research Kalpakkam [1]. The creep fatigue damage assessment of this component is yet to be evaluated in accordance with design rules of RCC-MR (1993) towards checking its structural integrity at its operating temperatures (hot sodium temperature is 798 K and steam temperature is 766 K at 17 MPa pressure).

SG is an important component in the NSSS because it decides the capacity factor of an FBR plant. The structural material chosen for SG is modified 9Cr-1Mo steel (grade 91) because of its adequate mechanical strength, freedom from the risk of stress corrosion cracking and also decarburisation. For the structural analysis of SG, material properties viz. monotonic and cyclic stress strain curves, creep curves, creep and relaxation curves are required in case 'inelastic route' of design code is followed. However, in the design stage, it is felt that the SG should meet the creep fatigue damage rules of RCC-MR through 'elastic route'. This also needs some minimum inelastic properties like saturation fatigue curve, isochronous stress strain curve, creep data, symmetrisation coefficient (Ks) and creep fatigue interaction curve. All the required material data for calculating

damage are not available in the Appendix-Z of RCC-MR. The important properties which are yet to be included are saturation fatigue curve, isochronous stress strain curve data, symmetrisation coefficient (Ks) and creep fatigue interaction curve. Except Ks, other data are available in the literature [2]. Hence it is required to develop Ks either numerically or experimentally so that creep-fatigue assessment can be done using the `elastic route' of RCC-MR.

The symmetrisation coefficient is evaluated by generating required cyclic stress strain data theoretically by using Chaboche viscoplastic theory. The methodology adopted to establish Ks values have been verified by comparing the Ks values for SS 316 LN (S1 material) given in RCC-MR which have been obtained from the cyclic stress strain data generated at EDF. Such methodology is repeated for grade 91 material for the use of damage assessment of SG tubesheet in accordance with RCC-MR.

In this paper, the aspects, viz. development of Chaboche model for modified 9Cr-1-Mo (grade 91) material, identification of material constants, methodology of computing Ks and symmetrisation curve which is recommended by the authors for the inclusion in RCC-MR are presented.

2. SALIENT FEATURES OF MODIFIED 9Cr-1Mo (GRADE 91) STEEL

- The material exhibits marked strain-rate sensitivity at elevated temperature. The strain-rate sensitivity increases with increasing temperature.
- The material displays strain softening at larger strains in elevated temperature, during monotonic tests. However, under lower temperature monotonic loading, the material primarily strain hardens. The temperature over which monotonic hardening / softening behaviour changes abruptly lies in the range of 650-750 K.
- The material cyclically softens in strain-controlled cyclic tests. The amount of cyclic softening appears to be independent of temperature.
- Under constant stress loading, the material exhibits an apparently very low primary creep stage in the 750-900 K temperature range. Though the amount of primary creep is insignificant, it increases with increasing temperature. Secondary creep rates also increase with increasing temperature and stress

3. CHABOCHE VISCOPLASTIC THEORY FOR GRADE 91 MATERIAL

The '23 parameter Chaboche viscoplastic model' essentially developed for SS 316 LN has been modified to model the mechanical behaviour of grade 91 steel at high temperature. The major

modifications are: elimination of (1) an exponential term which is to simulate the strain insensitivity in the intermediate temperature range, (2) coupling between kinematic and isotropic hardening and (3) plastic strain memorisation effects and inclusion of (1) third term in the kinematic hardening variable to account for the large strain range effects, (2) two terms in the isotropic softening variable and (3) effect of isotropic hardening in the viscous stress. With these, the model for grade 91 steel now involves only 3 kinematic hardening tensorial variables ($\mathbf{X_1}$ $\mathbf{X_2}$ & $\mathbf{X_3}$) and 2 isotropic softening scalar variables ($\mathbf{R_1}$, $\mathbf{R_2}$). Totally 20 material parameters are used to define the material behaviour. The constitutive equations are stated as follows.

$$\varepsilon = \sqrt{3/2}.p.\mathbf{n}$$

$$p = \langle \sigma_v / K(R) \rangle^n$$

$$\mathbf{n} = (\mathbf{S} - \mathbf{X}) / |\mathbf{S}-\mathbf{X}|$$

$$\sigma_v = J(\sigma - \mathbf{X}) - k$$

$$K(R) = Ko + \alpha R \quad R = R_1 + R_2 \text{ Isotropic hardening variables}$$

$$\mathbf{S} = \sigma - 1/3.\sigma_{kk}\mathbf{I}$$

$$\mathbf{X} = \mathbf{X_1} + \mathbf{X_2} + \mathbf{X_3} \quad \text{(kinematic hardening variables)}$$

$$J(\sigma - \mathbf{X}) = \sqrt{3/2}.\ |\mathbf{S}-\mathbf{X}|$$

$$|\mathbf{S}-\mathbf{X}| = [(S_{ij} - X_{ij}).(S_{ij} - X_{ij})]^{1/2}$$

$$p = \sqrt{2/3}.\ |\varepsilon| \quad \text{(effective strain rate)}$$

$$\mathbf{X_i} = 2/3.a_i.c_i.\varepsilon_i + c_i.p + \beta_i.\ I(\mathbf{X_i})^{(m_i-1)}\mathbf{X_i}$$

$$R_i = b_i.(Q_i - R_i).p$$

$$J(\mathbf{X}) = \sqrt{2/3}.\ |\mathbf{X}|$$

The material parameters viz. n, k, Ko, α, a_1, c_1, a_2, c_2, a_3, c_3, β_1, m_1, β_2, m_2, β_3, m_3, b_1, Q_1, b_2 and Q_2 are temperature dependent constants.

4. IDENTIFICATION OF MATERIAL PARAMETERS

Moosbrugger [3] has developed a non-isothermal constitutive model based on Chaboche viscoplastic theory for the small strain behaviour of modified 9Cr-1Mo. Accordingly material parameters are identified by Moosbrugger as a coupled function of temperature over the temperature

Table 1

Relationship between parameters of Chaboche and Moosbrugger models

Chaboche model	Moosbrugger [3]
n	1/m
k	k
Ko	$(1/\Theta)^m$
α	$(p_1)^{-m}$
a_i	$\sqrt{3/2}b_i$
c_i	c_i
$ß_i$	$(ci.bi/Ki).(3/2)^{(1/m-0.5)}.\Theta$
m_i	1/m - 0.5
b_i	μ_i
Q_i	χ_i

range of 298 to 873 K. A systematic approach by which the material parameters that are associated with Moosbrugger model are correlated with those of Chaboche model is made. The table 1 shows one to one correspondence between parameters of Chaboche and Moosebrugger models by understanding the physical meaning of each of the parameters. The mathematical expressions of the Moosbrugger model can be found [3]. Table 2 shows the identified material properties at various temperatures.

5. NUMERICAL SIMULATION OF UNIAXIAL MECHANICAL BEHAVIOUR

Fig 1 shows the monotonic stress strain curves in the temperature range 723 - 873 K.up to 12 % strain. It is seen in this figure that the monotonic hardening decreases with increasing temperature. Above 823 K, slight monotonic softening can be noted. The strain rate sensitivity of this material can be seen in Figs 2-3 for 773 K and 873 K respectively. At 873 K, monotonic softening is higher at higher strain rate. Some creep curves of FBR interest are shown in the Fig 4. The cyclic stress strain hysterisis loops are plotted in the Figs 5-8 for various temperatures (298-873 K) under strain controlled cycling of ±1%. at the constant strain rate of 6.7×10^{-4} 1/s. Cyclic consolidation curves which are shown in Fig 9 depicts clearly the cyclic softening behaviour of T91 material. The softening behaviour is more or less independent of temperature.

It is worth mentioning that the simulation of the above curves matches satisfactorily with the uniaxial data published [2].

Table 2

Values of material parameters of Chaboche model for grade 91 steel

Constants	Temperature (K)				
	298	673	773	823	873
n	0.0	0.0	0.0	0.0	0.0
k	41.7	41.7	10.5	6.2	4.5
Ko	369.9	306.0	514.0	783.4	1076.6
α	1.3	1.3	2.5	4.7	8.5
a_1	150.0	150.0	146.5	141.1	105.0
c_1	7000.0	7000.0	7000.0	7000.0	7000.0
$ß_1$	41.7	41.7	10.5	6.2	4.5
m_1	0.0	0.0	0.44E-25	0.61E-15	0.76206E-11
a_2	117.5	117.5	64.8	48.9	27.9
c_2	500.0	500.0	500.0	500.0	500.0
$ß_2$	41.7	41.7	10.5	6.2	4.5
m_2	0.0	0.0	0.92E-25	0.1E-14	0.96319E-11
a_3	266.6	173.4	120.7	82.4	83.6
c_3	37.5	37.5	37.5	37.5	37.5
$ß_3$	41.7	41.7	10.5	6.2	4.5
m_3	0.0	0.0	0.96E-24	0.95E-14	0.16254E-09
b_1	30.0	30.0	30.0	30.0	30.0
Q_1	-65.0	-65.0	-65.0	-65.0	-65.0
b_2	0.3	0.3	0.3	0.3	0.3
Q_2	-15.0	-15.0	-15.0	-15.0	-15.0

6. ESTABLISHING SYMMETRISATION COEFFICIENT

When long hold times and elevated temperatures are involved in the considered loading cycles, creep effects are considered in RCC-MR as follows:

- In the assessment of fatigue damage fraction, addition of creep strain ($\Delta\varepsilon_c$) contribution at end of each cycle to the equivalent elastoplastic strain range.
- In the assessment of creep damage fraction, the maximum stress generated (σ_R) during the hold period of the cycle.

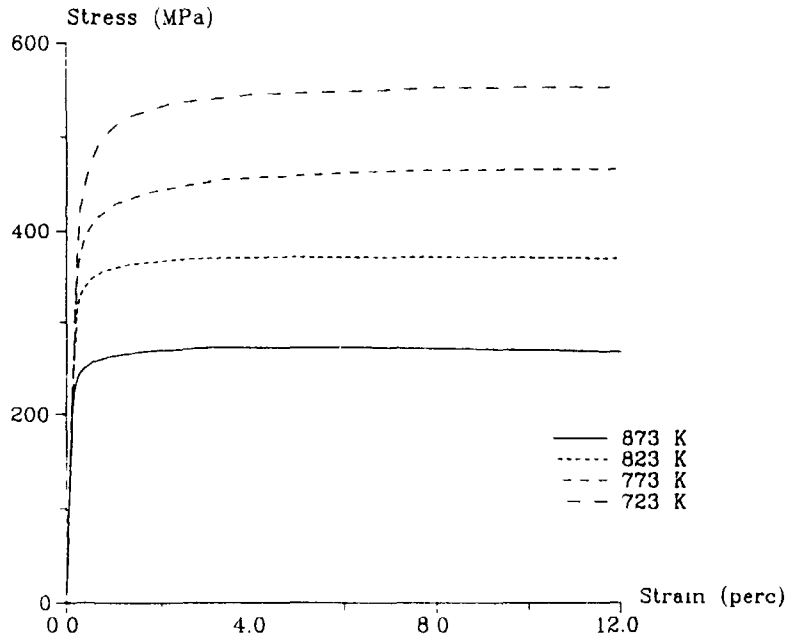

Monotonic stress strain curves for T91 material
(strain rate 6.7×10^{-5} 1/s)

Fig _ 1

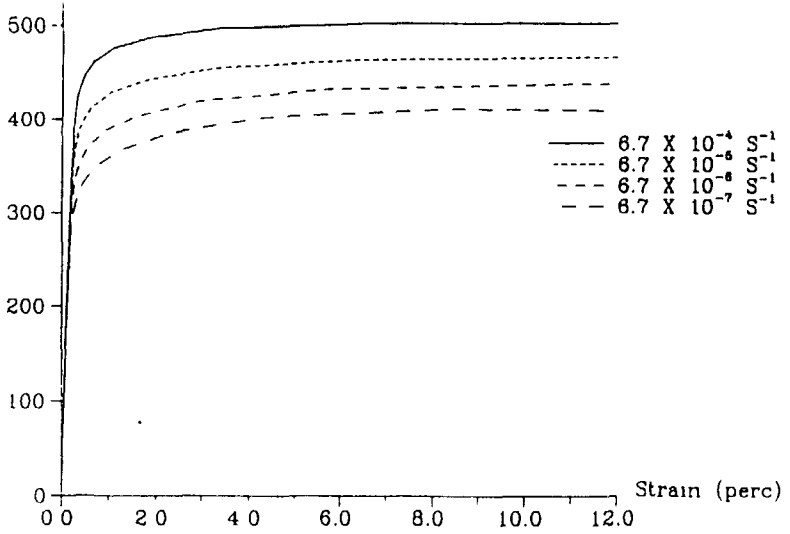

Simulation of monotonic stress strain curve at 773 K
(Mod. 9Cr 1 Mo)

Fig _ 3

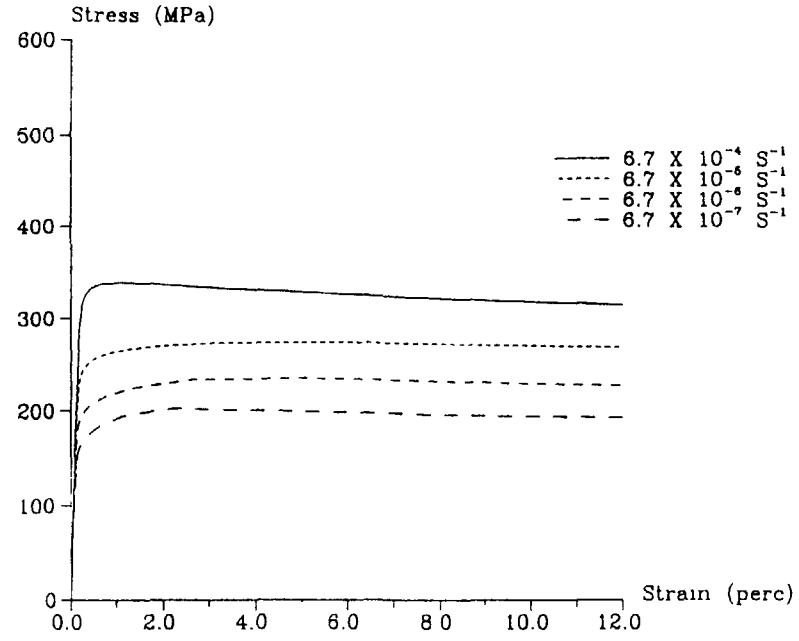

Simulation of monotonic stress strain curve at 873 K
(Mod. 9Cr 1 Mo)

Fig _ 2

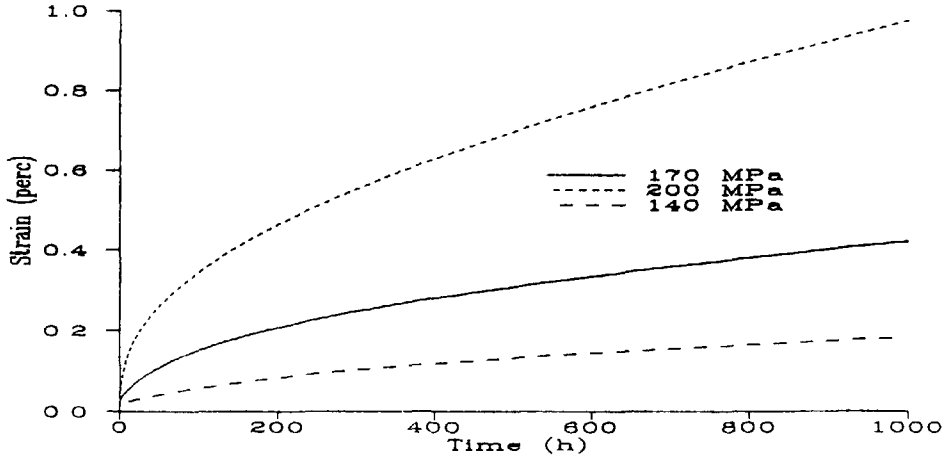

Simulation of creep curves at 873 K for T91

Fig _ 4

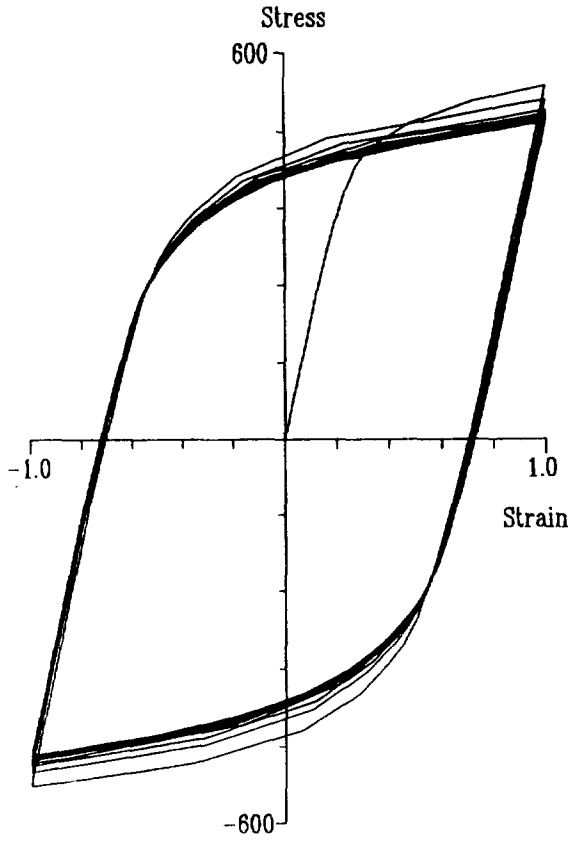

Simulation of strain controlled cycling at 298 K (Mod. 9Cr 1 Mo)

Fig _ 5

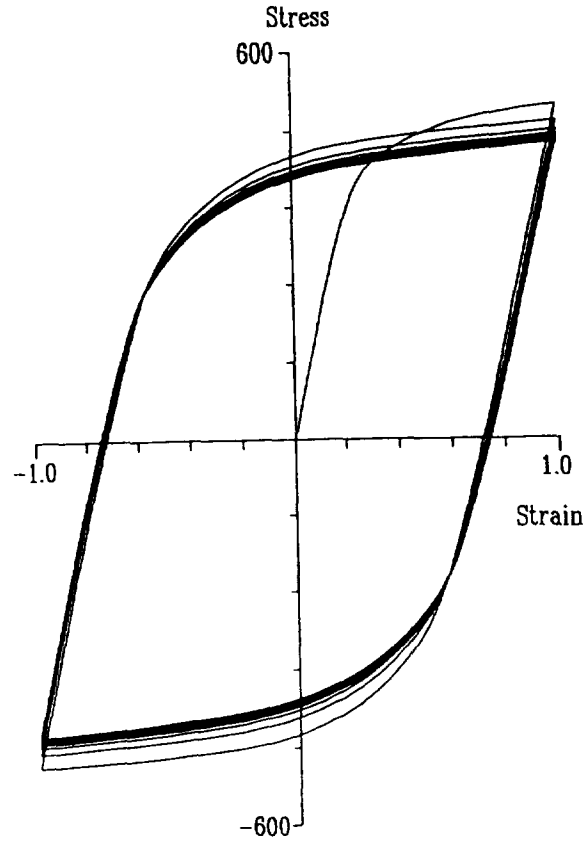

Simulation of strain controlled cycling at 473 K (Mod. 9Cr 1 Mo)

Fig _ 6

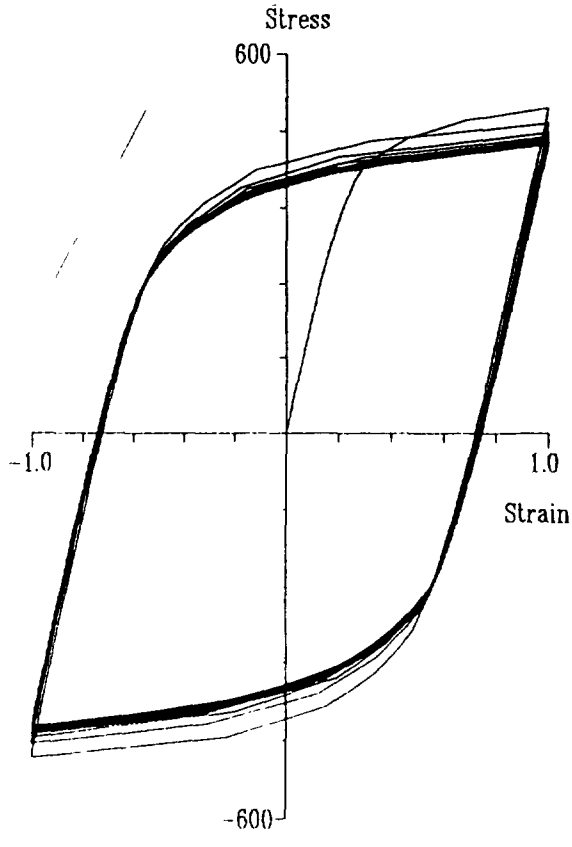

Simulation of strain controlled cycling at 723 K (Mod. 9Cr 1 Mo)

Fig _ 7

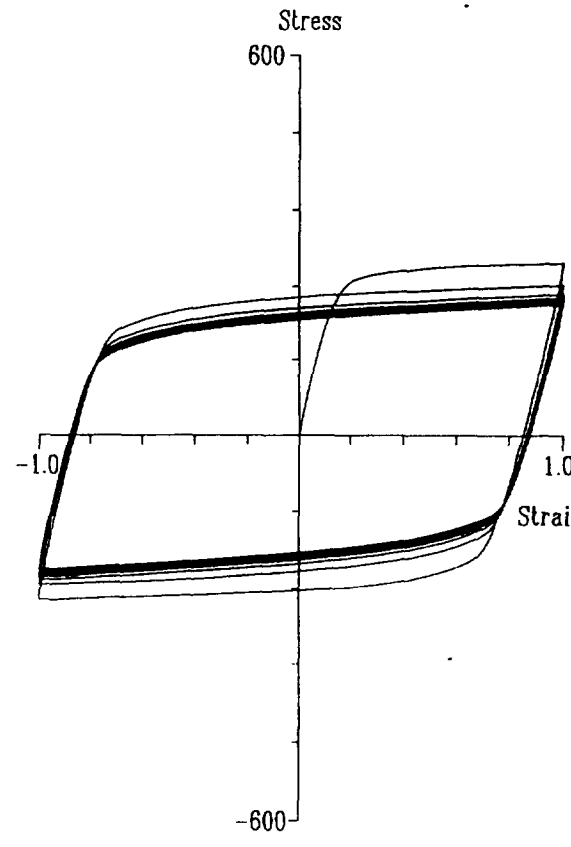

Simulation of strain controlled cycling at 873 K (Mod. 9Cr 1 Mo)

Fig _ 8

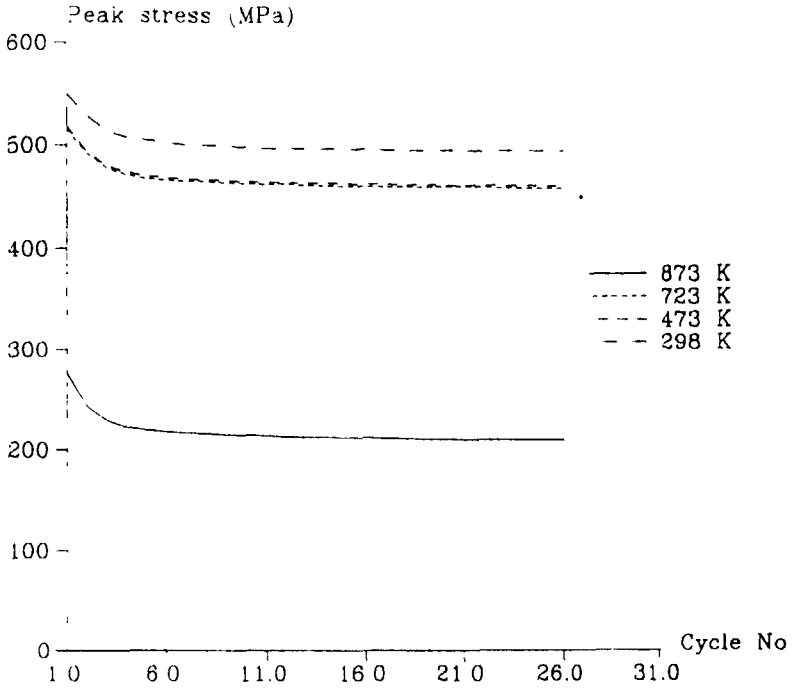

Cyclic softening behaviour of T91 material
(strain range + 1 and strain rate 6.7×10^{-5})

Fig _ 9

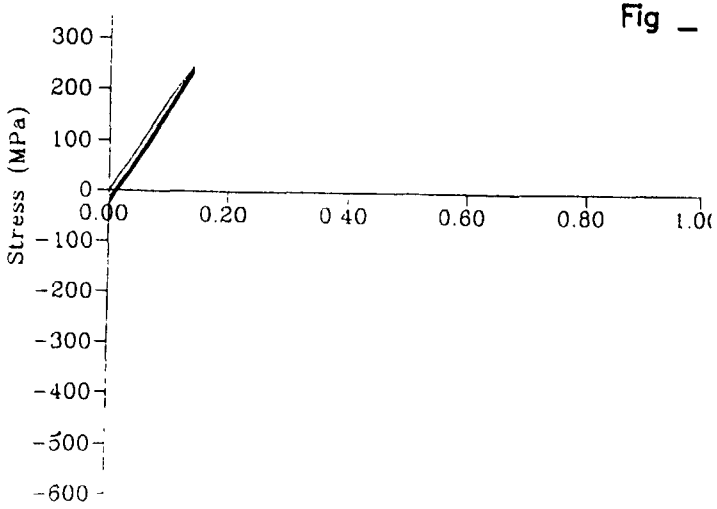

Stress cycling under repeated strain cycling
(strain range 0.14 at 773 K)

Fig _ 11

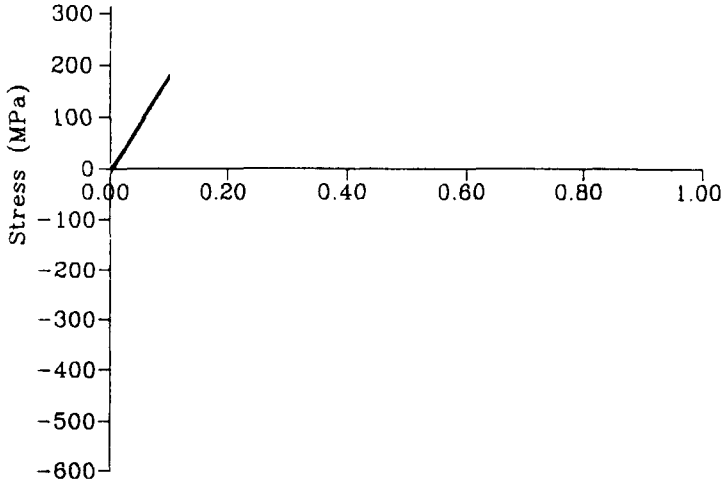

Stress cycling under repeated strain cycling
(strain range 0.1 at 773 K)

Fig _ 10

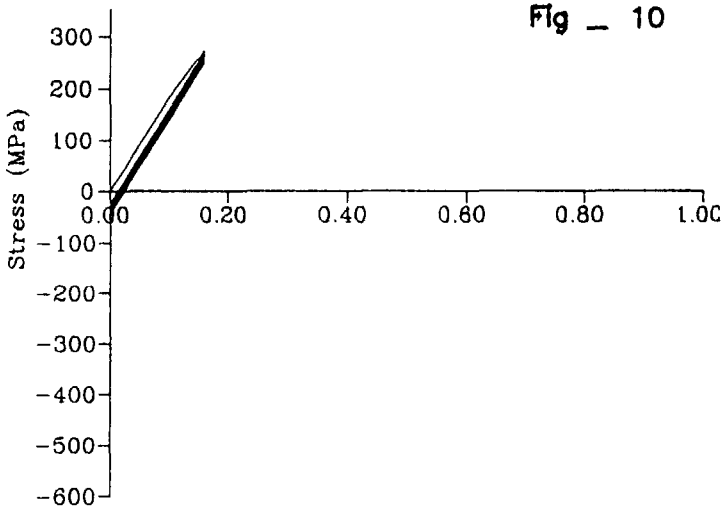

Stress cycling under repeated strain cycling
(strain range 0.1593 at 773 K)

Fig _ 12

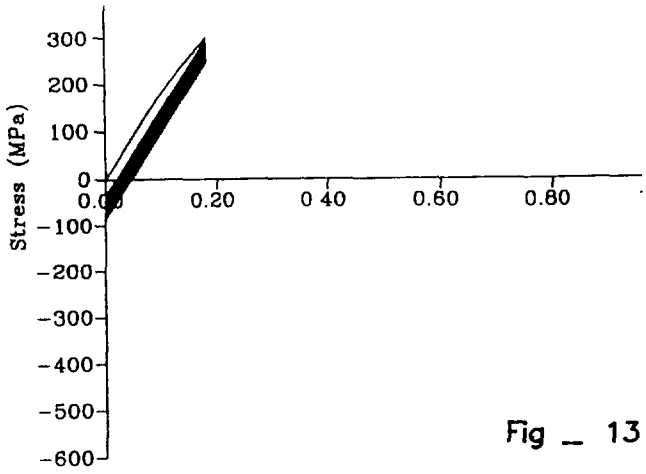

Fig _ 13

Stress cycling under repeated strain cycling
(strain range 0 1811 at 773 K)

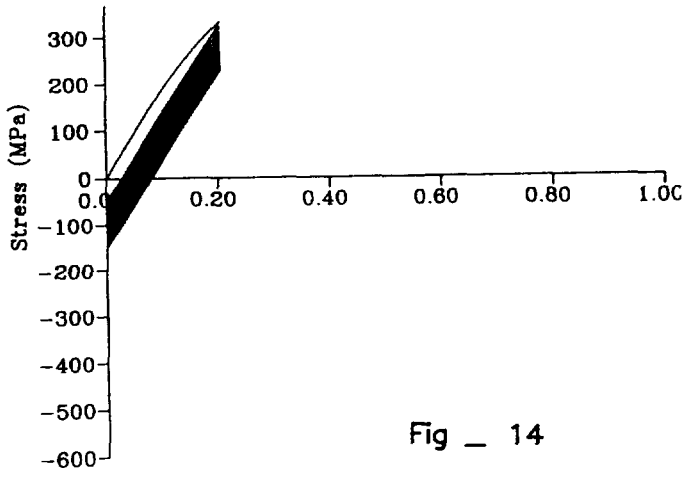

Fig _ 14

Stress cycling under repeated strain cycling
(strain range 0.2068 at 873 K)

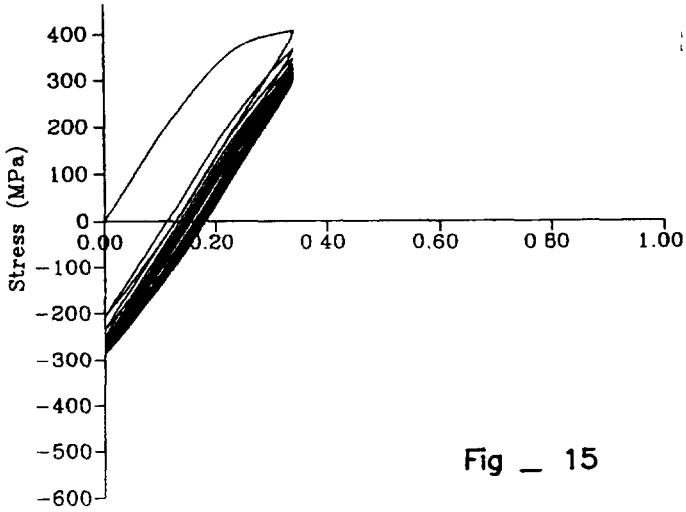

Fig _ 15

Stress cycling under repeated strain cycling
(strain range 0 3414 at 873 K)

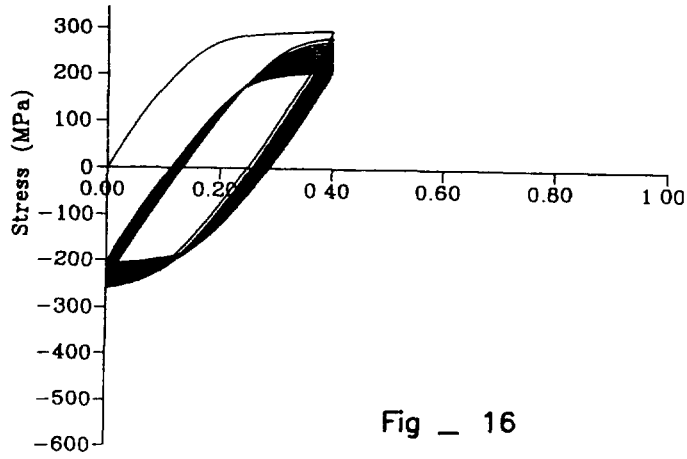

Fig _ 16

Stress cycling under repeated strain cycling
(strain range 0 4 perc at 873 K)

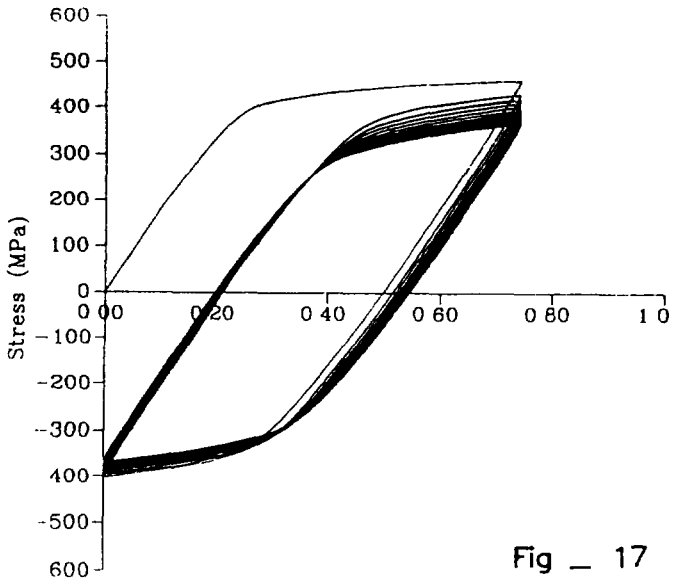

Fig _ 17

Stress cycling under repeated strain cycling
(strain range 0 7432 at 873 K)

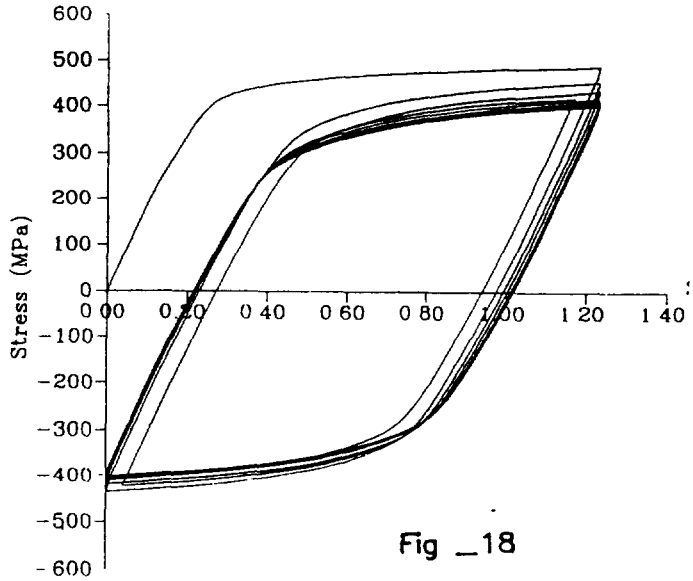

Fig _18

Stress cycling under repeated strain cycling
(strain range 1 233 at 773 K)

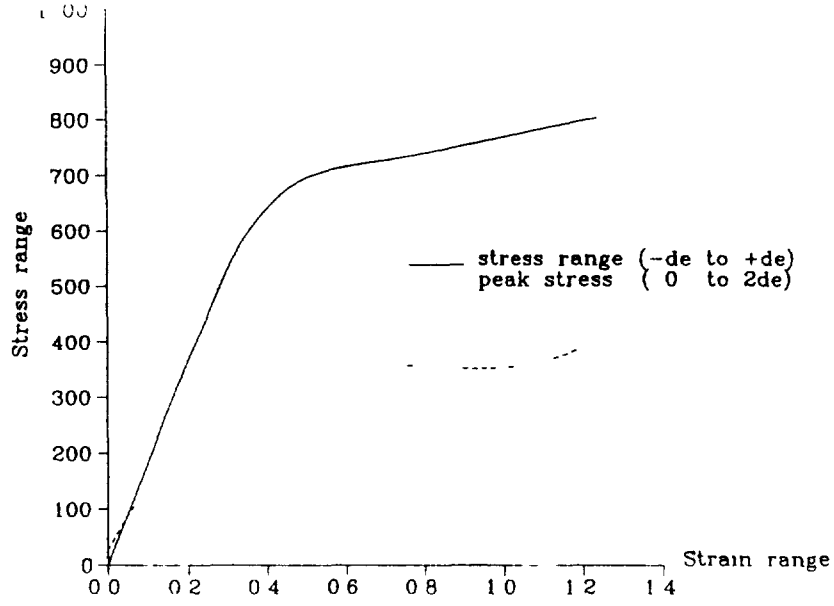

Stress range and peak stress under strain cycling
(for T91 material at 773 K)

Fig-19

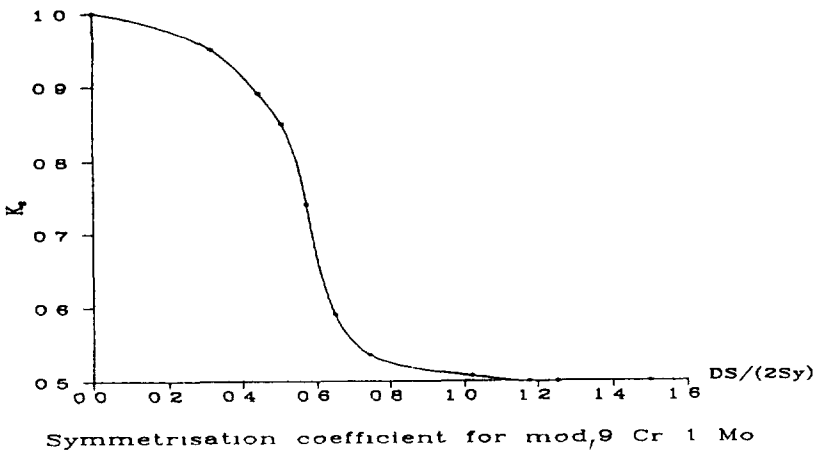

Symmetrisation coefficient for mod,9 Cr 1 Mo

Fig-20

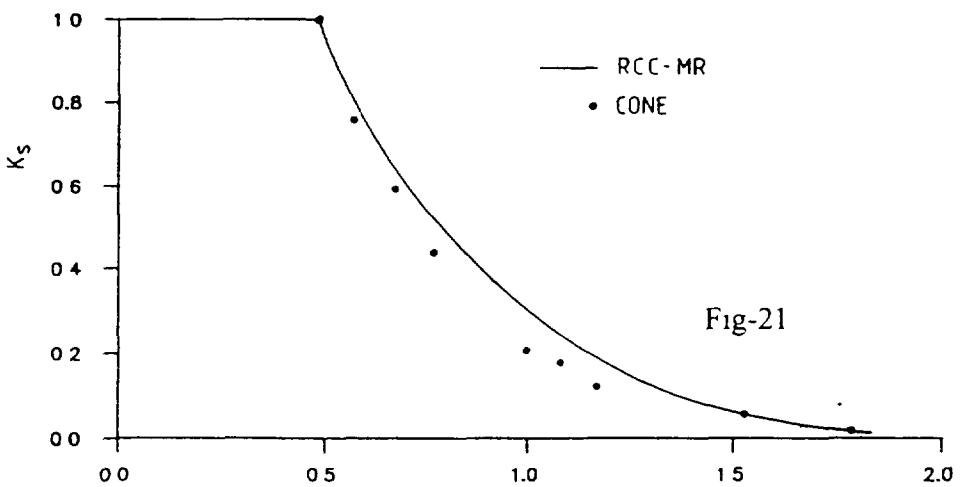

Fig-21

Symmetrisation coefficient

$\Delta\varepsilon_c$ depends upon σ_R. The value of σ_R is obtained as the sum of primary stress intensity encountered during hold time and the contribution due to secondary stress range($K_S\ \Delta\sigma_S$). $\Delta\sigma_S$ is the stress range corresponding to elastoplastic strain range $\Delta\mathcal{E}$. The K_S is the symmetrisation coefficient which accounts for the symmetrisation of the stress strain loop under large loadings. It is given as the function of ratio R (= $0.5\ \Delta\sigma_S/\sigma_Y$) . σ_Y is the minimum yield stress at the maximum temperature during hold period. For the small amplitude cycles, no plasticity arises and there is no symmetrisation and K_S is equal to 1. For large amplitude cycles full symmetrisation is possible and K_S is equal to 0.5. This function is usually determined by numerous strain controlled tests. In the absence of sufficient experimental data, required material data is generated numerically using Chaboche viscoplastic model.

The methodology adopted to generate K_S is as follows:

- Select the temperature and strain rate.
- Select the strain ranges of interest ($\Delta\mathcal{E}$).
- Determine stress cycling under repeated strain ranges (zero to maximum $\Delta\mathcal{E}$) by numerical solution of uniaxial formulation of Chaboche model (Fig 10-18 show the stress cycling under repeated strain cycling imposed in the range 0.1 % to 1.233 % at 773 K)
- Extract the stabilised peak stresses (σ_P) corresponding to various strain ranges + $\Delta\mathcal{E}$ (Fig 19).
- Determine the stabilished stress range ($\Delta\sigma_S$) corresponding to strain range ($-\Delta\mathcal{E}/2$ to + $\Delta\mathcal{E}/2$) either by analysis or by using RCC-MR Appendix-Z data (Fig 19).
- Plot a curve X (= 0.5. $\Delta\sigma_S/\sigma y$) vs Y (= $2.\sigma p/\Delta\sigma_S$) which is the required curve for determining K_S. (Fig 20).

7. DISCUSSION ON Ks

Following the aforementioned procedure, symmetrisation coefficients are determined for SS 316 LN material which is compared with the curve given in RCC-MR (1993) appendix Z corresponding to S1 material. The numerical analysis is done with 23 parameter chaboche model [4]. The results are compared well (Fig 21) and thus demonstrates the adequacy of analytical methodology of establishing Ks values. Hence the symmetrisation coefficient established by this procedure for

grade 91 material is recommended for the inclusion in the RCC-MR code for facilitating the computation of creep-fatigue damage values by 'elastic route' for modified 9 Cr 1 Mo (grade 91).

It is also worth mentioning the difference between the Ks values for SS 316 LN and grade 91. In the case of grade 91, the symmetrisation occurs at relatively low secondary stress ranges.

8. CONCLUSION

Towards establishing Ks values which are essential in the creep-fatigue damage computation as per 'elastic route' of RCC-MR for the material modified 9 Cr 1 Mo, '20 parameter Chaboche viscoplastivc model' has been identified. All the essential uniaxial data for establishing Ks values have been generated theoretically by solving uniaxial form of Chaboche model. Predicted behaviour have compared satisfactorily with the experimental data. Methodology has been established to determine Ks values in the form given in RCC-MR. Thus established curve has been recommended for the inclusion in RCC-MR in its future edition. For the sake of getting confidence in the analysis methodology, Ks values are determined for SS 316 LN also and compared with the one given in RCC-MR for S1 material. The symmetrisation coefficient Ks for grade 91 symmetrises under relatively lower secondary strain ranges during cycling loadings, as compared to SS 316 LN.

REFERENCES

1. S B Bhoje and P Chellapandi, 'Operating temperature for an FBR', Nuclear Engineering and Design, 158 (1995).
2. G.Guntz et al. 'The T91 book on Ferritic tubes and pipe for high temperature use in boilers'.
3. J C Moosbrugger, 'Nonisothermal constitutive model for the small strain behaviour of 9Cr-1Mo-V-Nb pressure vessel steel', ASME Jl. Engineering Materials and Technology, 114(1992).
4. J L Chaboche and D Nouailhas, 'A unified constitutive model for cyclic viscoplasticity and its applications to various stainless steels', ASME Jl. Engineering Materials and Technology, 111(1989).

CREEP-FATIGUE EVALUATION ON BUTT WELDED JOINTS OF TYPE 304 SS

Y. WADA, T. ASAYAMA,
S. HASEBE, N. KASAHARA
Power Reactor and Nuclear Fuel Development Corporation,
Oarai Engineering Center,
Ibaraki, Japan

Abstract

In high temperature plant systems such as thermal power generation and petro-chemical complexes, various weldments are used for pressure vessels and piping. Usually in structural design methods for weldment of conventional pressure vessels and piping systems, load controlled stresses are dominant, and to protect early failure in weldments tensile and creep strengths of each welded joint have not to be lower than the standard values of base metal. While under cyclic deformation controlled stress such as thermal loading in LMFBR, creep-fatigue phenomenon caused by reversal loading and residual stress relaxation is dominant. Therefore, a creep-fatigue evaluation method of Type 304 ss butt welded joints has to be investigated under cyclic thermal loading.

For a study of this effect, the strain concentration factor K_ε;
$K_\varepsilon = \mathrm{Max.}\,[\,1+(\,q_w q-1\,)(\,1-2\,\gamma_y\sigma_y/E\,\varepsilon_n\,),\,K_{\varepsilon 0}]$,
which is derived from the generalized elastic follow-up concept[1,2] as the plastic strain re-distribution, was applied, and in the K_ε factor the metallurgical discontinuity effects; q_w and γ_y were considered. The elastic follow-up increment factor for weldment; q_w is equal to 2 under uni-axial mechanical loading. And under bi-axial thermal loading in shell-type structures, it is clarified that 1.5 as the q_w value can be applied. As the yield ratio γ_y, the value of 0.8 is the best for Type 304 ss weldment.

As for the creep damage estimation, the simplified procedure based on the time fraction rule is discussed, and it is investigated how the creep damage of weldment can be evaluated by using mechanical properties of base metal(design standard values). The initial value of stress relaxation is determined by the cyclic stress-strain relation of base metal and the above K_ε value. Stress relaxation during strain hold can be analyzed by using creep strain behavior of base metal. Finally the allowable creep-fatigue life can be estimated by using the design curves.

1. METALLUGICAL DISCONTINUITY INDUCED STRAIN CONCENTRATION UNDER UNIAXIAL MECHANICAL LOADING

1.1 FATIGUE LIFE REDUCTION MECHANISM IN WELDED JOINT

In fatigue and creep-fatigue tests of Type 304 ss, the cyclic strain hardening for solution annealed base metal and the cyclic softening for weld metal are observed as shown in FIG.1 [3]. Stress range in weld metal becomes smaller than that in base metal. As shown in FIG.2, the former value is about 80% of the latter one at half of life, in the condition of same plastic strain range. The difference of cyclic plastic deformation properties between base and weld metals leads up to strain redistribution in welded joint, and strain increases in weld metal with strain cycling. This mechanism is conceptually shown in FIG.3 as two elements model. If the ratio of weld metal width to the gauge length is defined as the value of r, then the following relationship can be derived.

$$\Delta\varepsilon_{GL} = (1-r)\,\Delta\varepsilon_{BM} + r\,\Delta\varepsilon_{WM} \qquad (1)$$

where, $\Delta\varepsilon_{GL}$, $\Delta\varepsilon_{BM}$ and $\Delta\varepsilon_{WM}$ are strain ranges in gauge length, base metal and weld metal, respectively. In stable strain cycling $\Delta\varepsilon_{WM}$ is larger than $\Delta\varepsilon_{BM}$, and consequently the strain concentration of $\Delta\varepsilon_{WM}/\Delta\varepsilon_{GL}$ occurs.

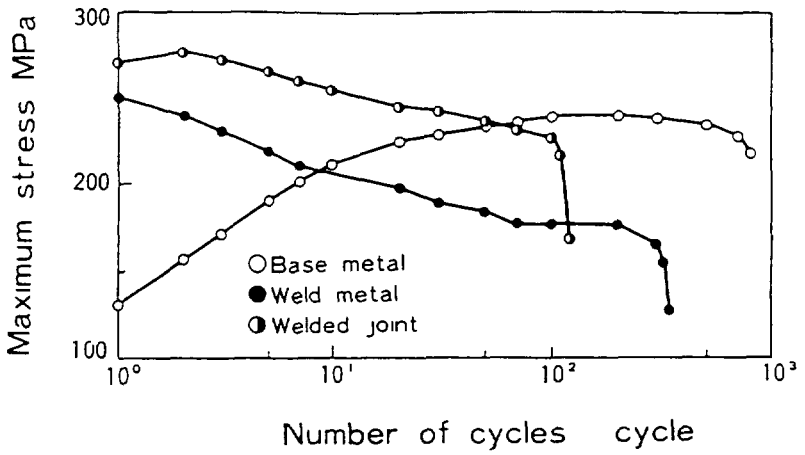

FIG.1 MAXIMUM STRESS BEHAVIOR WITH STRAIN CYCLING

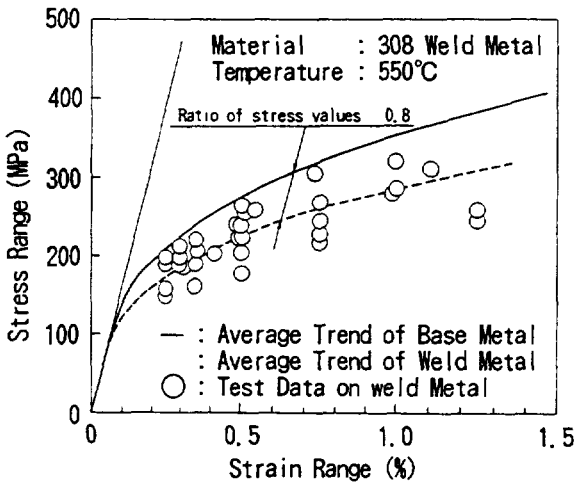

FIG 2 CYCLIC STRESS-STRAIN RELATION OF WELD METAL

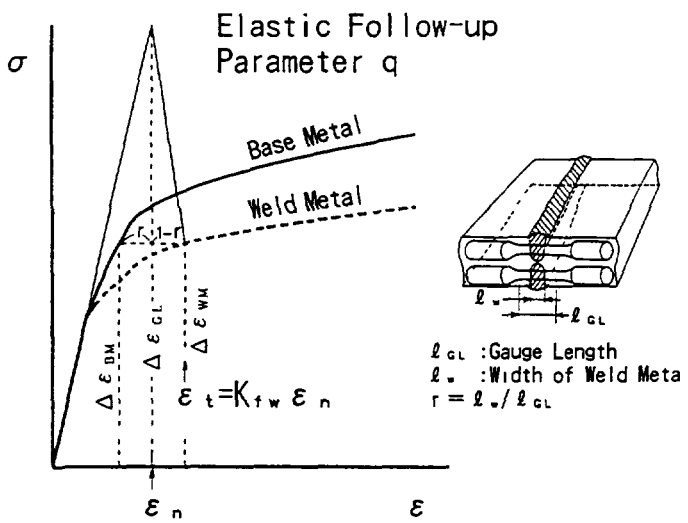

FIG 3 CONCEPT OF WELDED JOINT MODEL

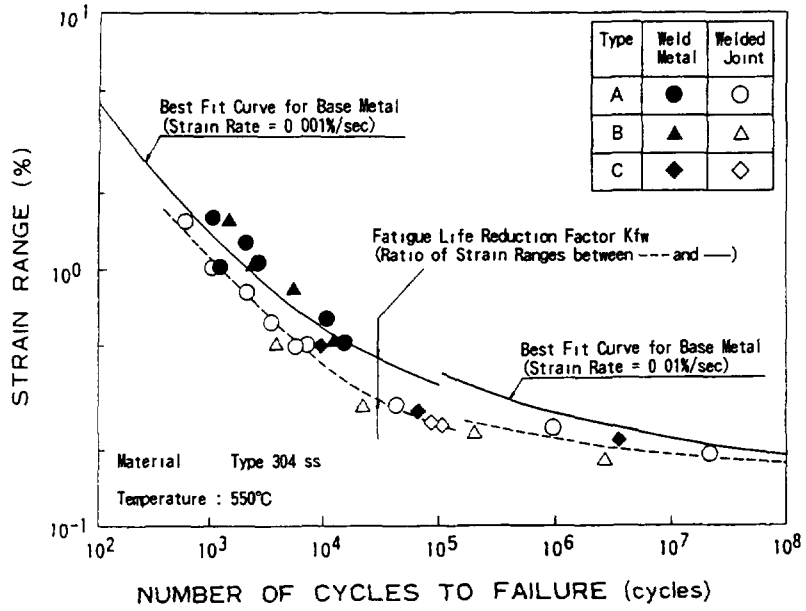

FIG.4 FATIGUE CURVE OF WELD METALS AND WELDED JOINTS

FIGURE 4 shows fatigue test data on three kinds of welded joints and their weld metals[3]. Fatigue life of weld metal is almost same as that of base metal in higher strain range region, while in welded joint it becomes shorter. The fatigue life reduction factor K_{fw} , which is defined in FIG.4, has to be estimated for the transverse type joint as shown in FIG.3. FIGURE 5 shows the relationship between the K_{fw} value and the nominal strain range $\Delta \varepsilon_{GL}$, which are determined by fatigue tests. The dashed lines are the trend of test data, and the solid line is estimated by a simplified method based on the generalized elastic follow-up concept as shown in FIG.3. This approach is different from the model using one-dimensional elements which leads up to eq.(1). In fatigue test by large-size specimen with 100mm of the gauge length and 30mm of diameter, the r value in eq.(1) is about 0.1(the width of bead is about 10mm for GTAW with narrow gap) , which is different from about 0.5 in small size specimen. However fatigue life of large specimen is almost same as that of small one. For welded joints of large thickness structures the constraint of plastic deformation of weld metal by the surrounding heat affected hardening zone of base metal is dominant.

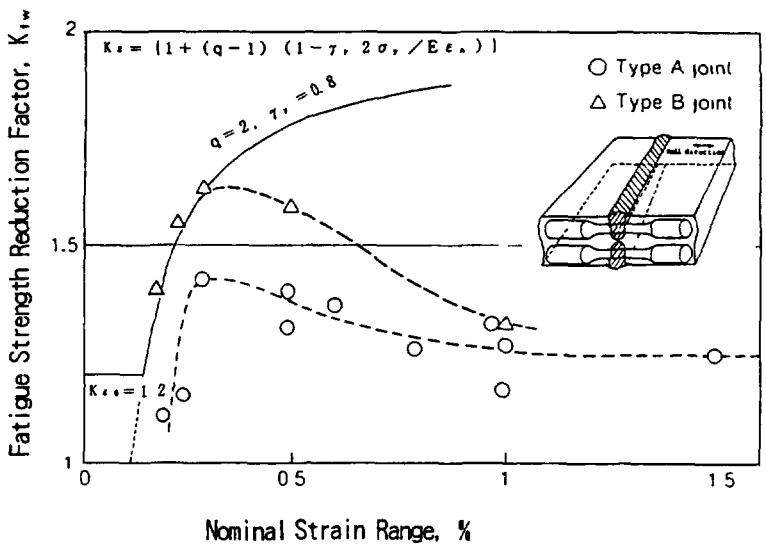

FIG.5 RELATIONSHIP BETWEEN K_{fw} AND NOMINAL STRAIN RANGE

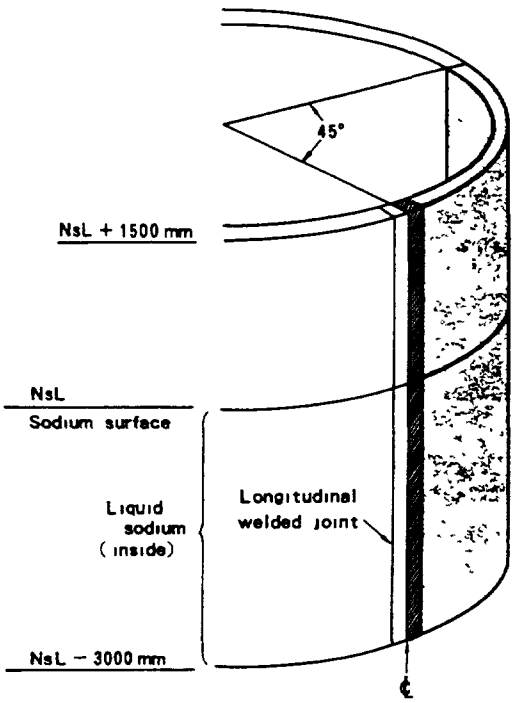

FIG 6 LONGITUDINAL WELDED JOINT OF REACTOR VESSEL

Tanigawa studied the strain concentration factor K_ε in longitudinal welded joints of reactor vessel of LMFBR as shown in FIG.6[4] In this analysis elastic-perfectly plastic behavior was assumed, and the yield stress ratio of weld metal to base metal: γ_y was 0.8 from FIG.2. Typical analysis result is shown in FIG.7, and the relation: y-0.8=q(x-0.8) is obtained for weld metal part of welded joint, where $x= E\ \varepsilon_n/2\sigma_y$ and $y=E\,\varepsilon_t/2\sigma_y$. This relation can be transformed into y/x=1+(q-1)(1-0.8/x), and the following equation is derived.

$$K_\varepsilon=[1+(q-1)(1-2\gamma_y\ \sigma_y/E\ \varepsilon_n)] \qquad (2)$$

Where q is equal to 3 in the case of FIG.7 and γ_y= 0.8. In Tanigawa's study the value of q is evaluated as the product of the elastic follow-up parameter in structures without the metallurgical discontinuity of weldment: q_T (=2) and the elastic follow-up increment factor for weldment: q_W(=1.5). In FIG.5 the solid line is determined by eq.(2) in which q_T =1 (for straight bar) and q_W=2 are applied. For transverse welded joints under uni-axial loading eq.(2) with q= $q_T\ q_W$=2 gives good prediction. In lower strain range region $K_{\varepsilon 0}$=1.2 is used as the minimum value with taking into conservative consideration of metallurgical uncertain effects such as discontinuities and residual stresses among welding passes. Consequently the K_ε value is determined as follows.

$$K_\varepsilon=\mathrm{Max}[1+(q_T\ q_W-1)(1-2\gamma_y\ \sigma_y/E\ \varepsilon_n),\ K_{\varepsilon 0}] \qquad (3)$$

For longitudinal welded joints under uni-axial loading, in which the loading direction is parallel to bead line, the strain concentration is not significant($q_W \fallingdotseq 1$), so the $K_{\varepsilon 0}$ =1.2 is dominant in eq.(3).

From the above consideration on both the transverse and longitudinal welded joint tests using small specimens under push-pull loading, eq.(3) with q_T=1and q_W=2 gives conservative life prediction.

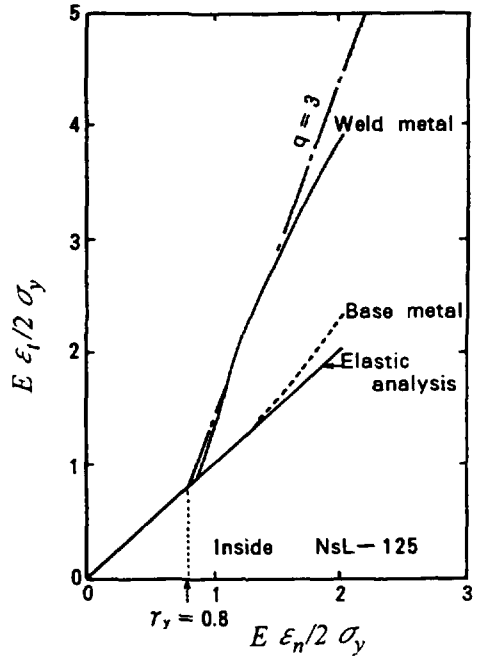

FIG.7 RELATIONSHIP BETWEEN E $\varepsilon_n/2\ \sigma_y$ and E $\varepsilon_t/2\ \sigma_y$

1.2 CREEP-FATIGUE LIFE REDUCTION IN SMALL SPECIMEN OF WELDED JOINTS

Creep rupture test results on Type 308 weld metals are shown in FIG.8. Creep strength of type A is almost same as that of base metal, while time to rupture: t_R of type B weld metal is shifted to the left side by the time factor of 6(α_R=6) compared with the average curve (α_R=1).

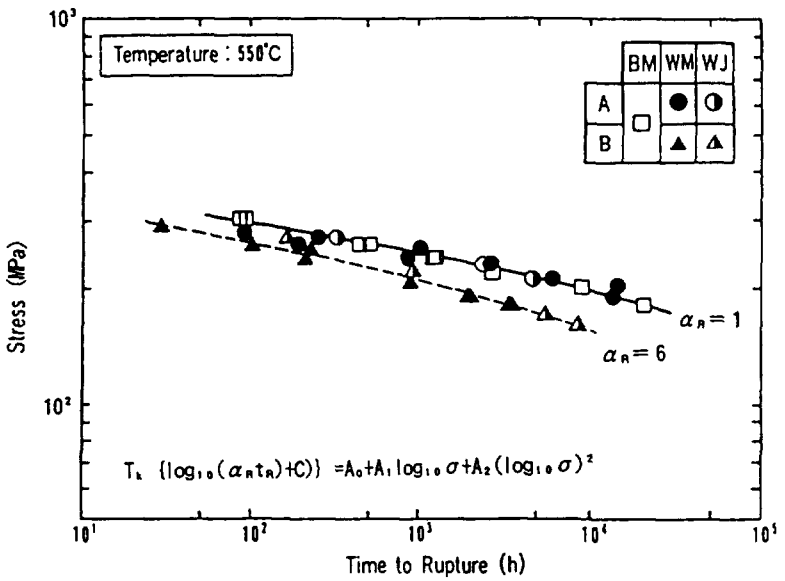

FIG.8 CREEP RUPTURE STRENGTH OF WELD METAL

FIGURE 9 shows creep-fatigue test results on base metal, weld metals and welded joints. Creep-fatigue life of weld metal shows not so large difference from that of base metal in the case of 1% strain range with 1hr hold. The initial value of stress relaxation of weld metal is about 80% of base metal as shown in FIG.2. However cyclic stress range of welded joint is almost same as base metal in the steady cycling as shown in FIG.1, because of the constraint of plastic deformation.

If the initial value of stress relaxation and creep strain behavior of weld metal during strain hold are same as base metal, creep damage of type A weld metal has to be equal to base metal. Another point is why small difference of creep-fatigue lives between two types weld metals, though there is large difference in creep rupture time. This phenomenon can be explained as the difference in relaxation stress level. The initial stress value of type B weld metal is about 15% smaller than that of type A as shown in FIG.10. While for welded joints creep-fatigue life of type B is about 6 times shorter than that of type A as shown in FIG.9[5]. This value of 6 corresponds to α_R=6. It is considered that cyclic stress range of welded joint is almost same as base metal because of the constraint of plastic deformation and the difference of creep rupture strength is dominant.

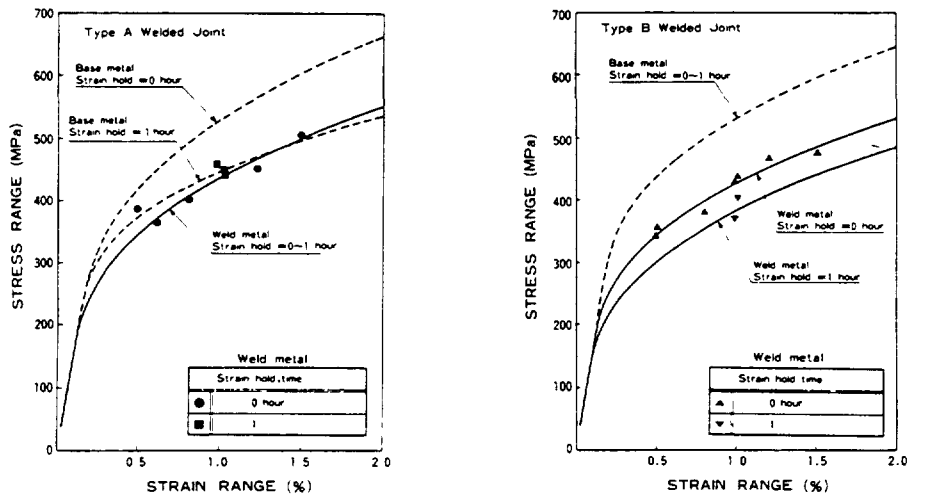

(A) Type A weld metal (B)Type B weld metal

FIG.9 CYCLIC STRESS-STRAIN RELATION OF WELD METALS

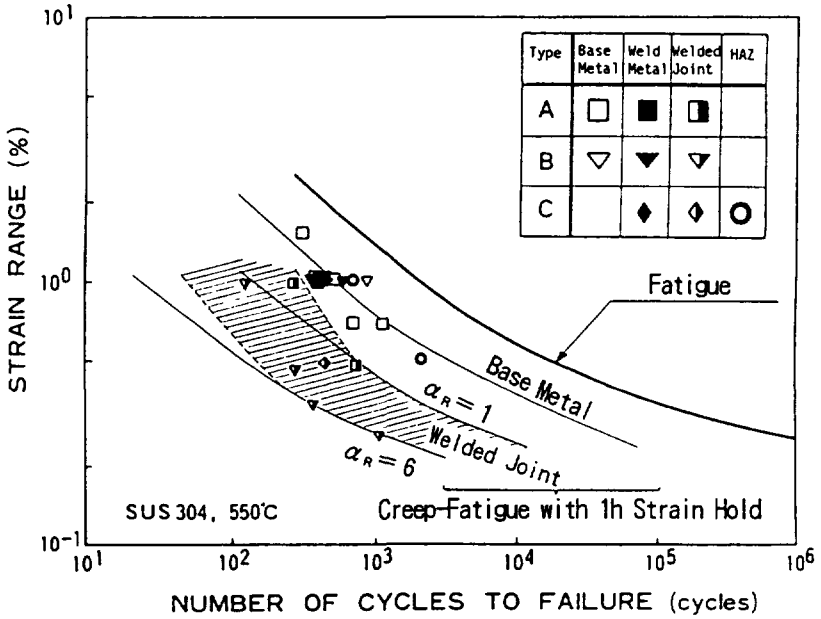

FIG.10 CREEP-FATIGUE STRENGTH OF WELDED JOINTS

Consequently creep-fatigue life of welded joints can be estimated based on the following procedure.

- Estimation of the nominal strain range; ε_n
- Calculation of the strain range; ε_t using eq. (3)
- Fatigue damage evaluation from the design fatigue curve
- Determination of the initial value of stress relaxation from the cyclic stress-strain curve using the value of ε_t in the above
- Creep damage evaluation using the design diagram estimated from stress relaxation analysis and creep rupture curve.

2. LONG TIME EXTRAPOLATION CONSIDERING CREEP DUCTILITY REDUCTION OF WELD METAL

The creep-fatigue failure mode of Type 304 ss base metal is intergranular in the creep damage dominant condition, and creep cavities along grain boundaries are observed[6]. Cavity growth is dominant in the case that the life reduction factor is more than 5. In weld metal σ phase formation induced from δ ferrite causes stress concentration around σ phase, and leads up to earlier crack initiation as shown in FIG.11. Creep rupture elongation becomes lower beyond about 500 hr as shown in FIG.12. For a long duration time it is expected that σ phase precipitation should be saturated and the ductility reduction caused by σ phase formation might not affect significantly on the creep-fatigue life. As the fact in the case of σ phase precipitation, PNC time fraction procedure for weldment gives good creep-fatigue life prediction as shown in FIG.9. When the conventional ductility exhaustion rule is applied to creep-fatigue life prediction of welded joints using the ductility in FIG.12, the difference of creep-fatigue lives between two types of joints in FIG.9 cannot be evaluated.

In higher strain range the margin of eq.(3) as shown in FIG.5 cover degradation of weld metal. In lower strain the $K_{\varepsilon 0}$ value plays a role to maintain the margin for the thermal ageing effect on weld metal. Therefore PNC creep-fatigue life evaluation procedure for weldment keeps the margin for long time extrapolation.

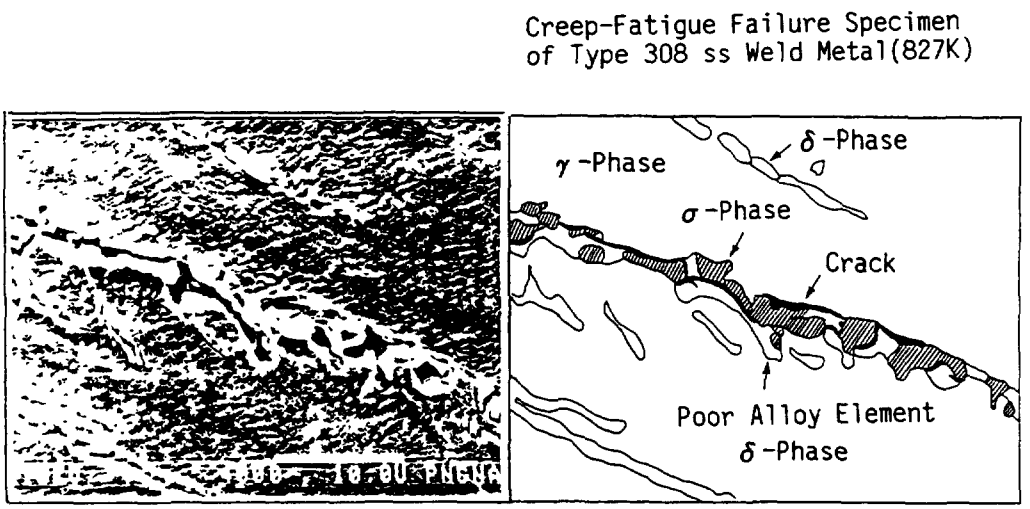

FIG.11 MICRO-CRACK INITIATION NEAR σ PHASE

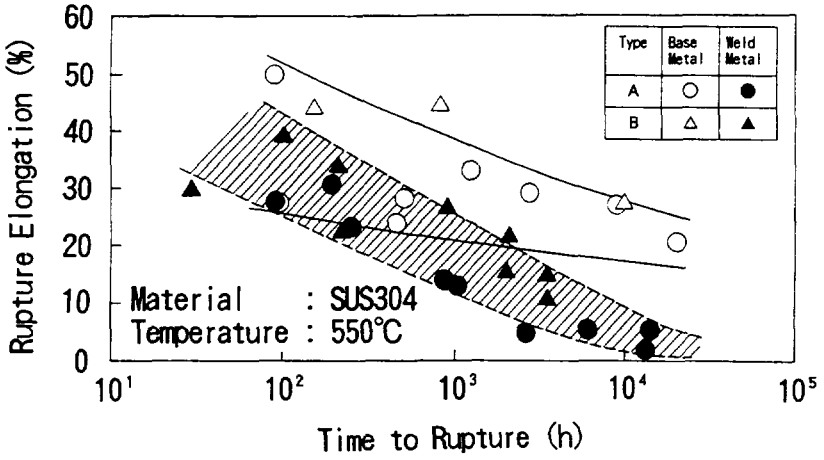

FIG.12 CREEP RUPTURE ELONGATION OF WELD METAL

3. EXAMINATION ON CREEP-FATIGUE STRENGTH OF WELDMENT IN TYPICAL SHELL STRUCTURES UNDER THERMAL LOADING

3.1 LONGITUDINAL WELDED JOINTS OF REACTOR VESSEL

For vessel type structures as shown in FIG.6 with the axi-synmetric temperature gradient along the longitudinal direction, biaxial stress condition of the longitudinal direction; σ_Z and the circumferential direction; σ_T has to be considered, and strain concentration by the metallurgical discontinuity is dominant only to the circumferential direction which is perpendicular to bead line. As for the transverse welded joints under uniaxial loading(σ_Z),

if $\varepsilon_Z{}^W = \beta\ \varepsilon_Z{}^B$, then $\varepsilon_T{}^W = \beta\ \varepsilon_T{}^B$,

where the superscripts W and B show weld and base metal parts, respectively. However as for the longitudinal welded joints under thermal loading(σ_Z and σ_T),

if $\varepsilon_Z{}^W = \varepsilon_Z{}^B$ and $\varepsilon_T{}^W = \beta\ \varepsilon_T{}^B$, then $\varepsilon_{eq}{}^W = \kappa\ \varepsilon_{eq}{}^B \quad (1<\kappa<\beta)$,

where the superscript eq means the equivalent value. The factor q_W is estimated by the following equation;

$$q_W=(\varepsilon_{eq}{}^W-2\gamma_y\ \sigma_y/E)/(\varepsilon_{eq}{}^B-2\sigma_y/E)=(\kappa\ \varepsilon_{eq}{}^B-2\gamma_y\ \sigma_y/E)/(\varepsilon_{eq}{}^B-2\sigma_y/E) \tag{4}$$

When $2\sigma_y=3S_m=285$Mpa, E=154000Mpa and $\varepsilon_{eq}{}^B=0.25\%$, then $q_W=1.5$ corresponds to $\kappa=1.2$, and $q_W=2$ to 1.4. On the other hand the value of κ is shown as follows.

$$\begin{aligned}\kappa &= \varepsilon_{eq}{}^W/\varepsilon_{eq}{}^B=[(\varepsilon_Z{}^W)^2+\varepsilon_Z{}^W\ \varepsilon_T{}^W+(\varepsilon_T{}^W)^2]^{1/2}/[(\varepsilon_Z{}^B)^2+\varepsilon_Z{}^B\ \varepsilon_T{}^B+(\varepsilon_T{}^B)^2]^{1/2}\\ &= [(\varepsilon_Z{}^B)^2+\beta\varepsilon_Z{}^B\ \varepsilon_T{}^B+\beta^2(\varepsilon_T{}^B)^2]^{1/2}/[(\varepsilon_Z{}^B)^2+\varepsilon_Z{}^B\ \varepsilon_T{}^B+(\varepsilon_T{}^B)^2]^{1/2}\end{aligned} \tag{5}$$

Under uni-axial loading when q_W is equal to 2, then $\beta \fallingdotseq 1.4$. Therefore the strain concentration factor; β, due to the metallurgical discontinuity along the perpendicular direction to bead line, is about 1.4. If $\varepsilon_T{}^B = \varepsilon_Z{}^B$ and $\beta=1.4$, then $\kappa=1.2$ from eq.(5) and $q_W=1.5$ from eq.(4). As the results the q_W value is about 1.5 in the case of $\varepsilon_T{}^B = \varepsilon_Z{}^B$ under thermal loading. In detailed inelastic analysis results on a reactor vessel as shown in FIG.12, eq.(3) with $q_W=1.5$ and q_T $q_W=3$ was proposed[4], so the concept of the strain concentration factor; β and its value of 1.4(which leads to $q_W=2$ under uni-axial loading) are applicable for design.

3.2 CIRCUMFERENTIAL WELDED JOINTS OF VESSEL TYPE STRUCTURE

In creep-fatigue failure test results on a vessel type structure under thermal gradient along thickness direction[7], four types of circumferential welded joints in a cylindrical shell structure and one welded joint of sodium inlet nozzle were investigated. The strain concentration factor of each welded joint can be compared with that from eq.(3) with q_T q_W=2, and the results are shown in FIG.13. Estimated the q_T values are within 1.31 to 1.49, and the q_W values are within 1.07 to 1.34. As for the circumferential welded joints under thermal loading, eq.(3) with q_W=1.5 is conservative.

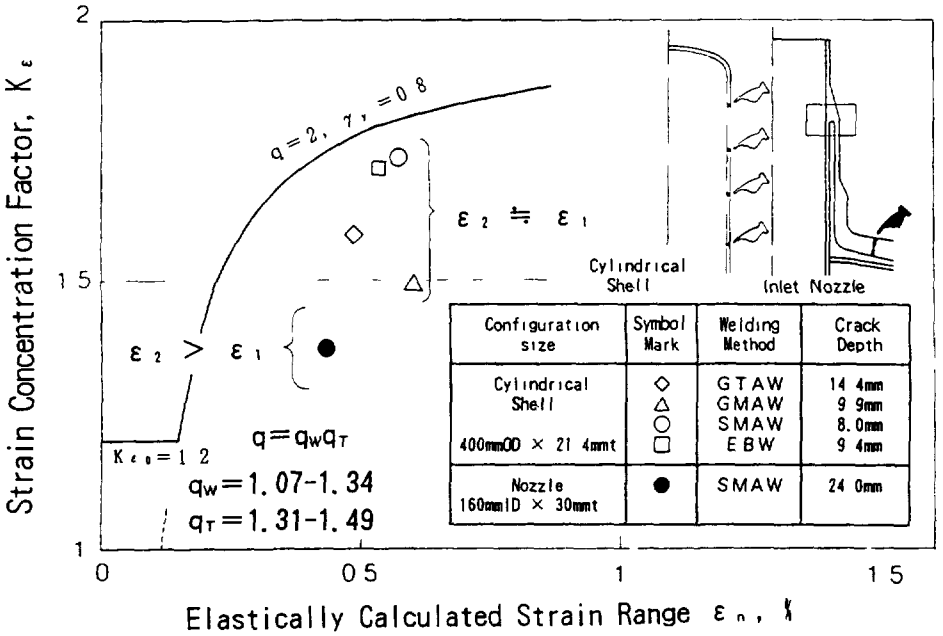

FIG 13 K_ε FACTOR OF CIRCUMFERENTIAL WELDED JOINT OF VESSEL TYPE STRUCTURE UNDER THERMAAL LOADING

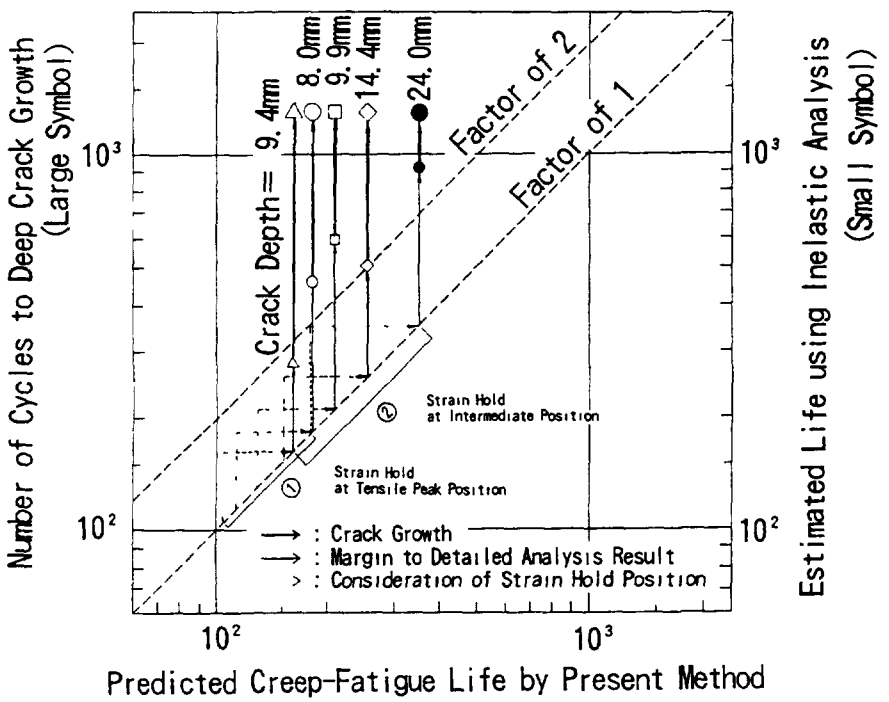

FIG.14 COMPARISON OF ESTIMATED LIFE BY PRESENT METHOD WITH DETAILED INELASTIC ANALYSIS[8]

For creep-fatigue strength of the above structure, creep damage can be calculated using PNC creep-fatigue life evaluation procedure for weldment. Furthermore considering that strain hold position is not at tensile peak, because in this test both hot and cold transient were loaded, creep damage is estimated using PNC proposed method[8], in which the initial value of stress relaxation is determined in the condition of strain range of $\varepsilon_t/2$ instead of ε_t. If the condition of the crack initiation is defined as Df+Dc=D, crack initiation life can be evaluated as shown in FIG.14. In this figure small symbol marks are estimated lives using inelastic analysis[7], and large ones are tested number of cycles(1300). Crack growth starts after initiation life, and deep cracks are observed at 1300 cycles.

From thermal transient test results on a vessel type structure, it is clarified that PNC creep-fatigue life evaluation procedure for weldment gives good prediction for creep and fatigue damages in structures.

4. CONCLUSIVE REMARKS

The strain concentration factor K_ε in vessel type structures is investigated, and the q_W value is estimated using the strain concentration factor; β and its value of 1.4(which leads to q_W=2 under uni-axial loading).

(1) Under uniaxial mechanical loading, q_W=2 is recommended for the transverse type, and for the longitudinal one the q_W value is nearly equal to 1 and the $K_{\varepsilon 0}$ value(=1.2) is dominant.
(2) Under thermal loading, q_W=1.5 for both of the longitudinal and the circumferential welded joints are recommended.
(3) PNC creep-fatigue life evaluation procedure is applied to weldment. The strain range ε_t is estimated from the K_ε factor, and fatigue damage can be estimated by the ε_t value. Creep damage can be evaluated using the damage diagram determined from the ε_t value. The diagram is given analytically using mechanical properties of base metal; the cyclic stress-strain curve, the creep strain-time relation and the creep rupture curve.

REFERENCES

[1] N.Kasahara, et al., "Advanced creep-fatigue evaluation rule for fast breeder reactor components: generalization of elastic follow-up model," Nuclear Engineering & Design, Vol.155(1995)499-518

[2] N.Kasahara, et al., "Application of elastic follow-up model to evaluate cyclic thermal transient strength of welded vessels," ASME PVP-313-2(1995)481-486

[3] T.Asayama, et al., "Creep-fatigue evaluation of SUS304 welded joint," Proc. SMiRT-11, Vol.E(1991)E06/5

[4] M.Tanigawa, et al., "Fatigue damage evaluation of welded joints under thermal stresses at elevated temperatures," Proc. SMiRT-10, Vol.E(1989)191-196

[5] Y.Wada, et al., "Study on mechanical behavior of weldments of Type 304 ss under creep-fatigue loading," ASME PVP-313-2(1995)487-492

[6] F.Ueno, et al., "A study on creep damage parameters in creep cavity growth dominant region under creep-fatigue loading," Proc. SMiRT-12, Vol.L(1993)L05/4

[7] N.Tanaka, et al., "Creep-fatigue failure test and analysis of a vessel type structure subjected to cyclic thermal transients," Nuclear Engineering & Design, Vol.140(1993)349-372

[8] T.Nagata, et al., "Advancement in elevated temperature structural design code for FBR," Proc. Post Conf. Seminar of 10th SMiRT, Construction Code & Engineering Mechanics(1989)1-35,paper NO.2A

HIGH TEMPERATURE FATIGUE OF AUSTENITIC STAINLESS STEEL WELDS AND WELDMENTS

K BHANU SANKARA RAO, M VALSAN,
V S SRINIVASAN, S L MANNAN
Indira Gandhi Centre for Atomic Research,
Kalpakkam, India

Abstract

A comparative evaluation of LCF lives and cyclic stress response of type 304 SS base metal, 308 SS weld metal and 304/308 SS weld joints, prepared by manual metal arc welding process, has been carried out at 823 and 923 K Further, a comparative evaluation of LCF behaviour of 316L(N) SS base metal, 316 SS weld metal and 316L(N)/316 weld joint has also been conducted at 773 and 873 K A detailed examination of the microstructural changes and crack initiation and propagation behaviour has been studied with a view to understanding the features which influence the cyclic stress response and fatigue lives of base metal, weld metal and composite specimens In particular, the role of delta ferrite on the LCF life has been examined The LCF resistance of 304 SS and its welds were in the order, 304 SS base metal > 308 SS weld metal > 304/308 weld joint, whereas the LCF resistance of 316 SS weld metal was found to be better than that of 316L(N) base metal 316L(N)/316 weld joints displayed the least fatigue resistance Detailed investigations have also been performed for assessing the importance of weld discontinuities such as porosity and slag inclusions, on strain controlled LCF behaviour of 308 SS welds Porosity on the specimen surface has been found to be particularly harmful and caused a life reduction by a factor of seven relative to sound weld metal Defect combination of porosity and slag inclusions was found to be more deleterious than the case when either the slag inclusions or porosity was present alone The higher volume fraction of δ-ferrite in weld metal was found to be harmful for fatigue life Creep-fatigue interaction behaviour of 304 SS base metal, 308 SS weld metal has also been evaluated at 923 K

1 INTRODUCTION

In the design of welded components for nuclear applications under low cycle fatigue (LCF) conditions, failure is prevented through the use of safety factors on stresses and strains, and by requiring the welds to be located in the regions of relatively low stresses The complexity of welds and the costs of fabricating and testing fairly large specimens in order to assess the geometric effects have resulted in the lack of sufficient data and understanding of the all-weld metal and weldment (base+all-weld+heat affected zone (HAZ)) behaviour of various joint designs In the absence of definitive data, *ASME Boiler and Pressure Vessel Code Case N-47* [1] imposed a limit on the design strains in weld regions to one half of the values permitted in the base material The deformation restriction arises from the general knowledge that the weld-deposited austenitic SS is often less ductile than the parent material The design rules are based on wrought material data, and they do not directly account for the property variations between the wrought materials and welds Therefore the characterization and better understanding of the LCF behaviour of all-weld and composite specimens would be required before variations in properties between the weld and the base material can be treated explicitly and quantitatively

A significant problem in the production of fully austenitic steel welds is their tendency to hot cracking and microfissuring To minimize this tendency, the compositions of welding materials are generally modified to produce small amounts of δ-ferrite (usually less than 10%) in the as welded structure However, when these materials are exposed to elevated temperatures (773-1173 K) for extended periods of time, the ferrite can transform to a hard brittle phase known as the σ-phase This transformation has been shown to lead to low ductility creep ruptures when sufficiently high stresses are applied at elevated temperatures However, the transformation behaviour of the δ-ferrite and its effects on LCF behaviour of SS welds and weldments has not been examined in detail Furthermore, the welding process produces local microstructural changes, local residual stresses well beyond the component design stress and frequently introduces weld discontinuities (slag and/or porosity) There has been no adequate information on the effects of weld discontinuities on the LCF behaviour of austenitic stainless steels

TABLE I CHEMICAL COMPOSITION OF BASE AND WELD MATERIALS (Wt%)

Alloy	C	Mn	Ni	Cr	Mo	N	S	P
316LN Base	0 021	1 75	12 0	17 0	2 4	0 078	0 002	0 023
316 SS Weld	0 060	1 42	11 9	18 8	2 0	-	0 01	0 009
304 SS Base	0 042	1 65	9 9	18 2	-	-	0 003	0 024
308 SS Weld	0 028	1 4	9 2	20 1	-	-	0 004	0 050

This paper deals with (i) a comparative evaluation of LCF lives and cyclic stress-strain properties of type 304 SS base metal, 308 SS weld metal and 304-308 SS weldments **and** 316LN base metal, 316 weld metal and 316LN/316 weld joint, prepared by the shielded metal arc welding process, (ii) the influence of weld discontinuities on LCF behaviour of 308 SS weld metal and (iii) creep-fatigue interaction behaviour of 308 SS weld metal

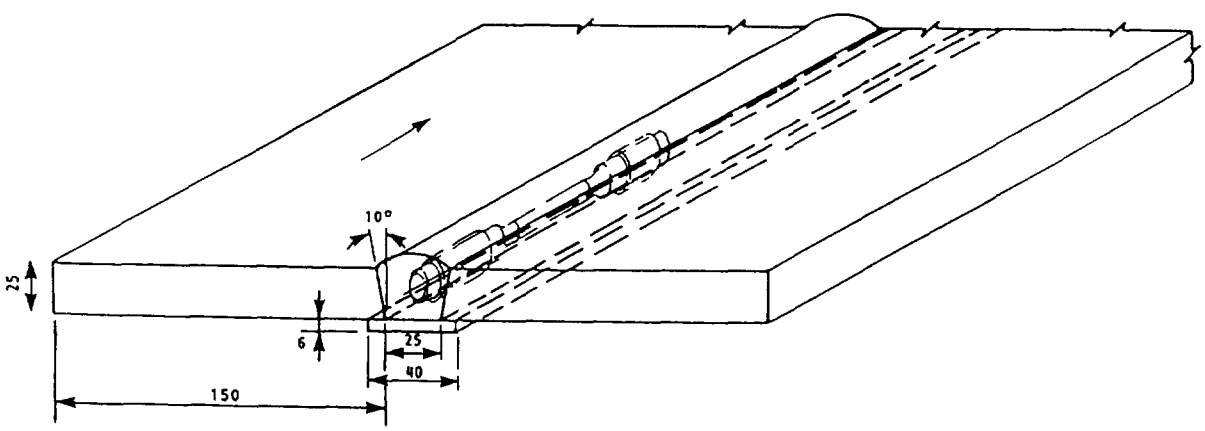

(a)

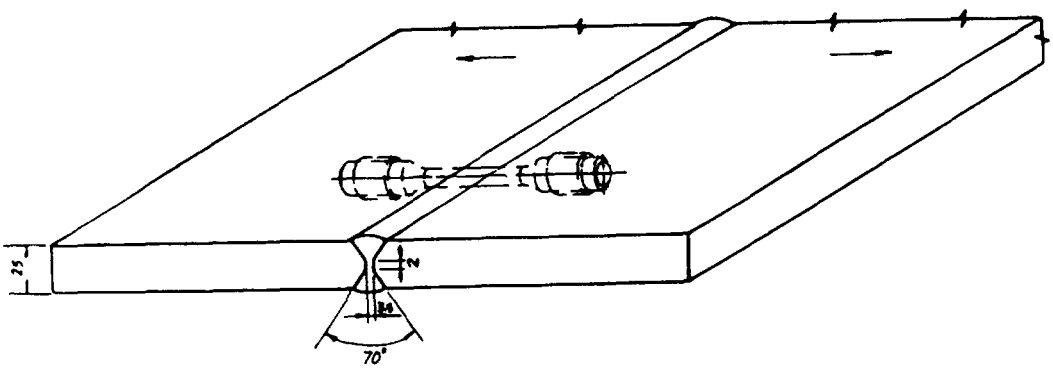

(b)

FIG 1 (a) Orientation of all-weld specimens in the single-V stainless steel weld joints and (b) Orientation of all-weld specimens a double-V joint The arrow indicates the base plate rolling direction (All dimensions are in mm)

2 EXPERIMENTAL DETAILS

Chemical composition of various materials used in this study (in Wt %) is given in Table I Manual metal arc welding process was employed for preparing the weld pads All-weld specimens were taken from the weld pads prepared with a 20° included angle V-groove joint geometry with a 25 mm root gap and a backing strip (Fig 1a) Typically, filling of this joint required 25 weld passes Weldment specimens were machined from the weld pads fabricated with a double-V configuration with an included angle of 70° and a root of 2 mm and a root gap of 3 15 mm (Fig 1b) The parameters used in welding process were documented in detail elsewhere [2-5] Subsequent to testing, the weld pads were examined non-destructively by X-radiography to ensure their soundness, followed by δ-ferrite measurement using a commercial Magne Gauge In order to study the effect of weld discontinuities on LCF properties, porosity and slag inclusions were deliberately introduced into the weld metal by grossly exaggerating the condition normally causing such flaws Cylindrical ridge LCF specimens (base, all-weld and weld joint) of 25 mm gauge length and 10 mm diameter were machined from essentially the central sections of sound weld pads as in the layout in Fig 1 Some of the LCF samples were fabricated by incorporating the porosity and slag inclusions into the gauge length of the specimens Fully reversed total axial strain controlled LCF tests were conducted in air on base, weld metal and weld joint specimens using a servo-hydraulic machine equipped with a radiant heating facility

3. RESULTS AND DISCUSSION

3.1. Strain controlled LCF behaviour of type 304 stainless steel base material, type 308 stainless steel weld metal and 304-308 stainless steel weldments

The average intercept grain size of the 304 SS base material was 75 μm and the microstructure was free from inclusions and undissolved carbides The microstructures of the as- deposited weld metal, made up of successively overlaid weld beads, were typical of type 308 SS weld metal and were composed of long columnar grains and δ-ferrite Typical morphologies of δ-ferrite seen in the multipass welds of a single-V joint are depicted in Fig 2 Figure 2a describes the skeletal morphology observed in the top pass whereas Fig 2b characterizes the lacy δ-ferrite seen in a few passes just below the top pass The vermicular morphology shown

TABLE II SUMMARY OF THE CONSTANTS IN THE STRAIN-LIFE RELATIONSHIPS

Temperature (K)	Material Condition	σ'_f	b	ε'_f	c
823	base	1550	-0 207	0 12	-0 502
823	all weld	1612	-0 158	0 34	-0 643
823	weldment	899	-0 146	0 4	-0 681
923	base	2812	-0 368	0 19	-0 56
923	all weld	1731	-0 284	0 23	-0 579
923	weldment	1110	-0 169	0 27	-0 642

in Fig 2c represents the actual δ-ferrite structure of the gauge portions of LCF specimens The ferrite content varied with its morphology, *i e* position in the weld The average δ-ferrite contents (average of 50 readings) of the single-V weld in skeletal, lacy and vermicular morphology regions has been estimated as 12 FN, 11 5 FN and 9 0 FN respectively It can be seen that the δ-ferrite dendrites in lacy and vermicular morphology regions contained finely distributed $M_{23}C_6$ Figure 3 shows the representative microstructure in the gauge portion of LCF specimens made out of double-V joint weldments The coarse grained region adjoining the weld metal depicts the HAZ, and its width is about approximately 1000 microns in size The average δ-ferrite content of the weld metal in the composite LCF specimens was 9 0 FN

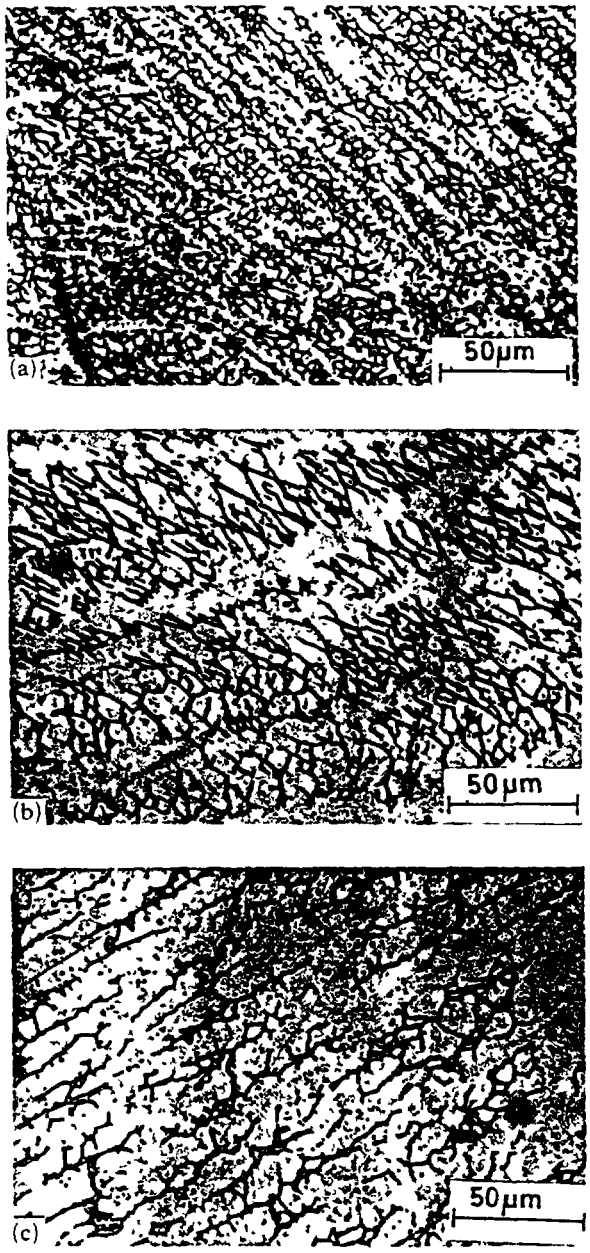

FIG 2 Morphology of δ-ferrite in different regions of a single-V 308 SS weld, (a) skeletal morphology in the top pass, (b) lacy morphology in the regions below the top pass, (c) vermicular morphology in the central regions (represents the microstructure in gauge portions of all-weld LCF specimens)

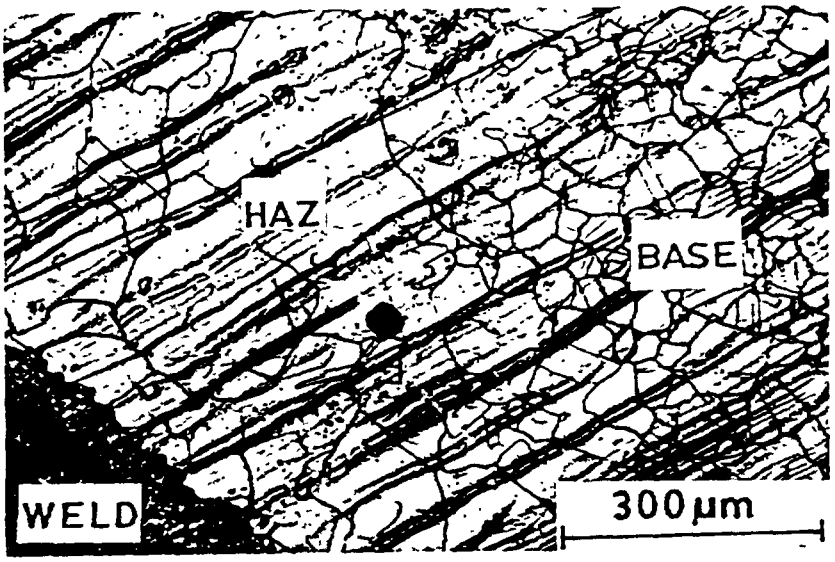

FIG. 3. Microstructure of the 304/308 SS weldment showing the all-weld. HAZ and base metal regions.

Figures 4 and 5 show the fatigue life results as double logarithmic plots of $\Delta\epsilon_t/2$ Vs $2N_f$ (number of reversals to failure) and $\Delta\epsilon_p/2$ Vs $2N_f$ at 823 and 923 K respectively The fatigue lives of the base, all-weld and weldment specimens at both the temperatures have been found to follow the strain-life relationships given by

$$\Delta\epsilon_t/2 = \Delta\epsilon_e/2 + \Delta\epsilon_p/2 = \sigma'_f/E\,(2N_f)^b + \epsilon'_f\,(2N_f)^c$$

where, σ'_f is the fatigue strength coefficient, b the fatigue strength exponent, ϵ'_f the fatigue ductility coefficient, c the fatigue ductility exponent and E the elastic modulus. The values of constants and the coefficients for the above equation as established by least squares analysis are summarized in Table II for the temperatures and material conditions investigated. In general, base metal displayed the highest endurance while weldments exhibited the least in terms of total and plastic strain amplitudes at both 823 and 923 K. All-weld samples had an intermediate fatigue life. The poor strain controlled fatigue resistance of weldments was not surprising considering the presence of coarse grains in the HAZ (Fig. 3) which could act as a metallurgical notch. At 823 K, in the base material and weldments, crack initiation occurred in persistent slip bands, which signifies the occurrence of planar slip. Since the grain size governs the slip length, a coarse grain size can be expected to develop larger slip steps at the surface, which would render the formation of intrusions and extrusions easier. Intrusions act as notches from which cracks originate. Therefore it is reasonable to assume that the coarse grain size in HAZ might have shortened the crack initiation stage. Furthermore, in alloys deforming by planar slip, an improved crack propagation resistance has been noticed with decreasing grain size and has been ascribed to the fact that the grain boundaries serve as the natural barriers to transgranular crack propagation, causing the crack front to be held back and necessitating a crack reinitiation event to occur in each new grain. At 823 K in the weldments, cracks propagated transgranularly in the HAZ containing a coarse grain size and therefore it can be argued that the crack propagation resistance in weldments is also reduced.

All-weld metal showed an inferior fatigue resistance compared with base metal at both 823 and 923 K. The reduction in fatigue life of all-weld material compared with base material is generally attributable to the reduced tensile ductility of weld material.Vermicular δ-ferrite present in the all-weld and weldment specimens transformed to carbides and σ-phase. Transformation of δ-ferrite was more rapid in weldment than in all-weld material at 923 K at all strain amplitudes. The proportion of δ-ferrite transformed increased with increasing temperature and number of cycles to failure in both weld and composite specimens (Fig. 6). The σ phase was believed to cause embrittlement locally and lead to the formation of microcracks at the austenite-σ interfaces

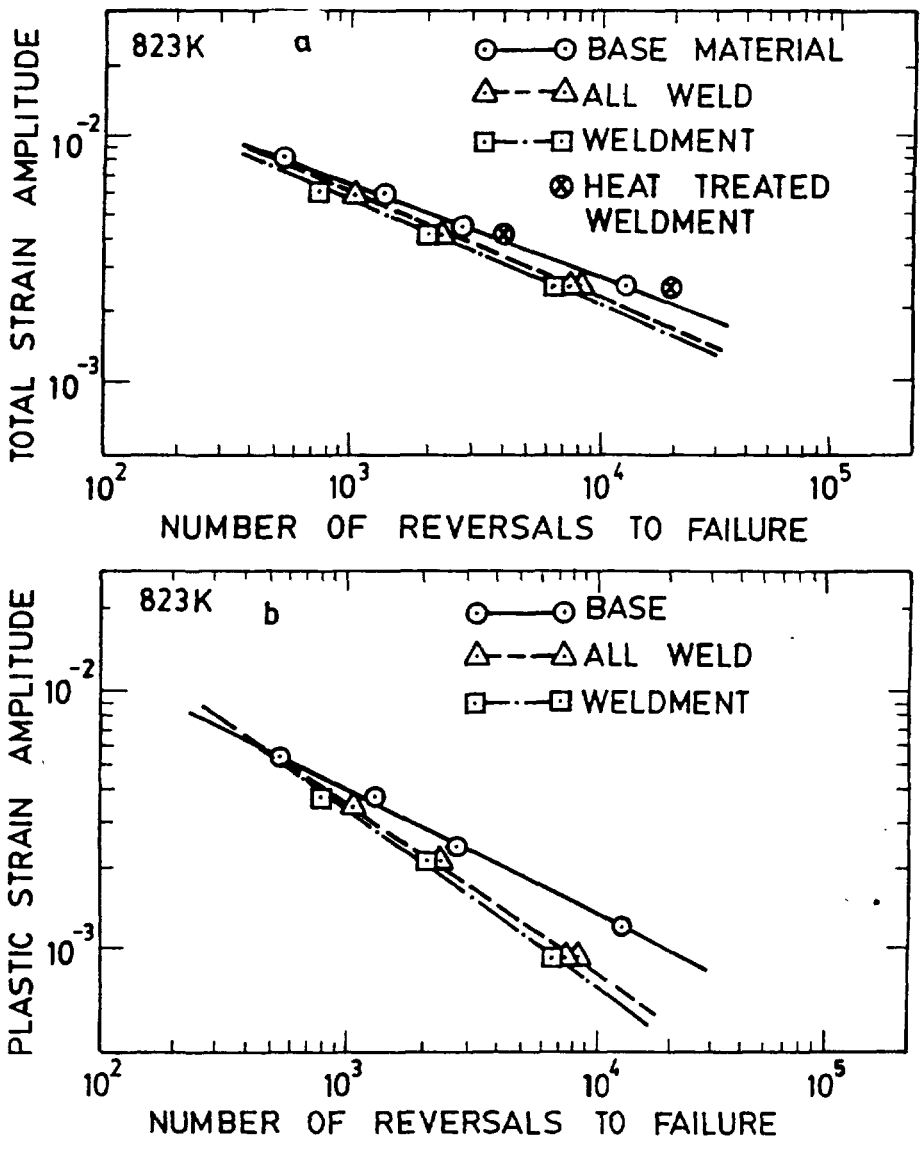

FIG. 4. Strain-life plots for 304 SS base, 308 SS all-weld and 304/308 SS weldment specimens at 823 K.

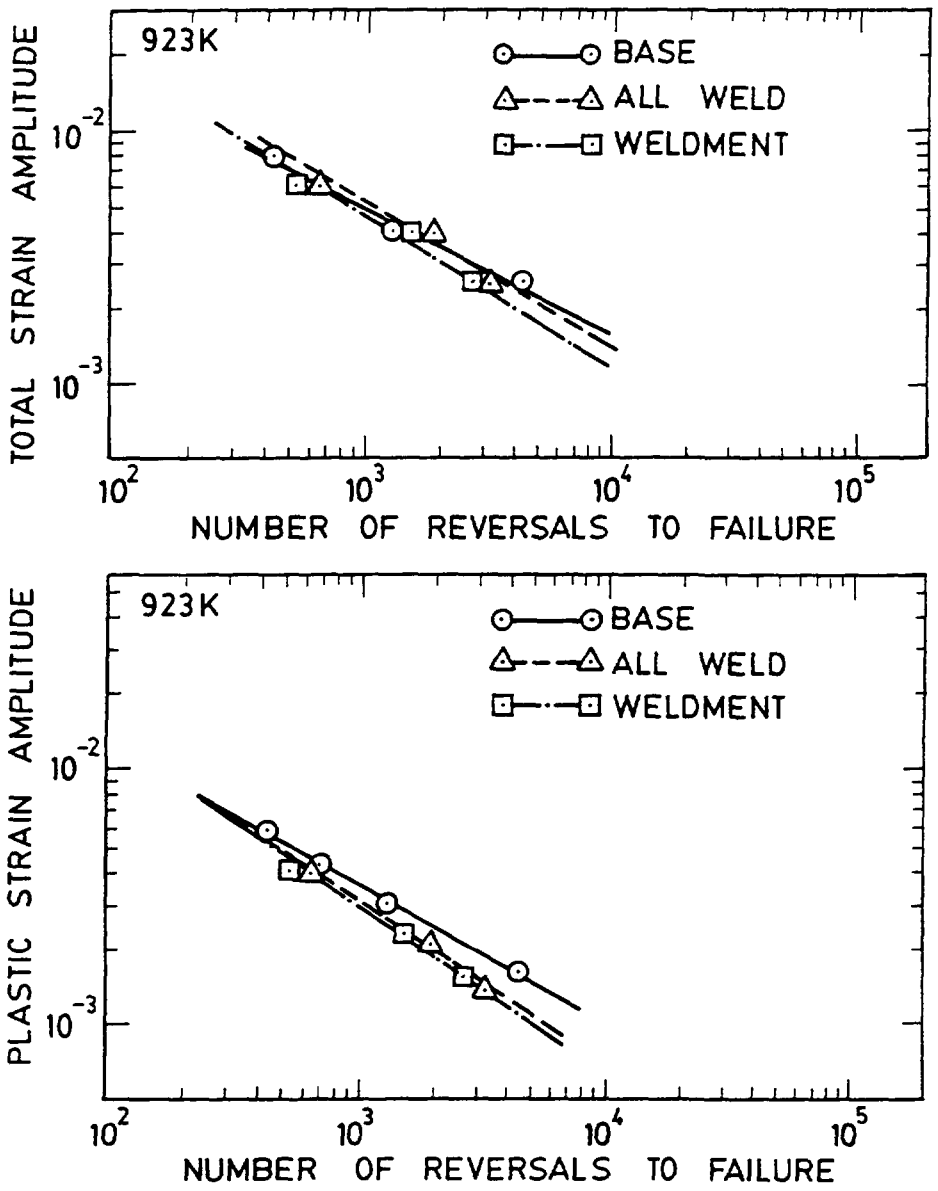

FIG. 5. Strain-life plots for 304 SS base, 308 SS all-weld and 304/308 SS weldment specimens at 923 K

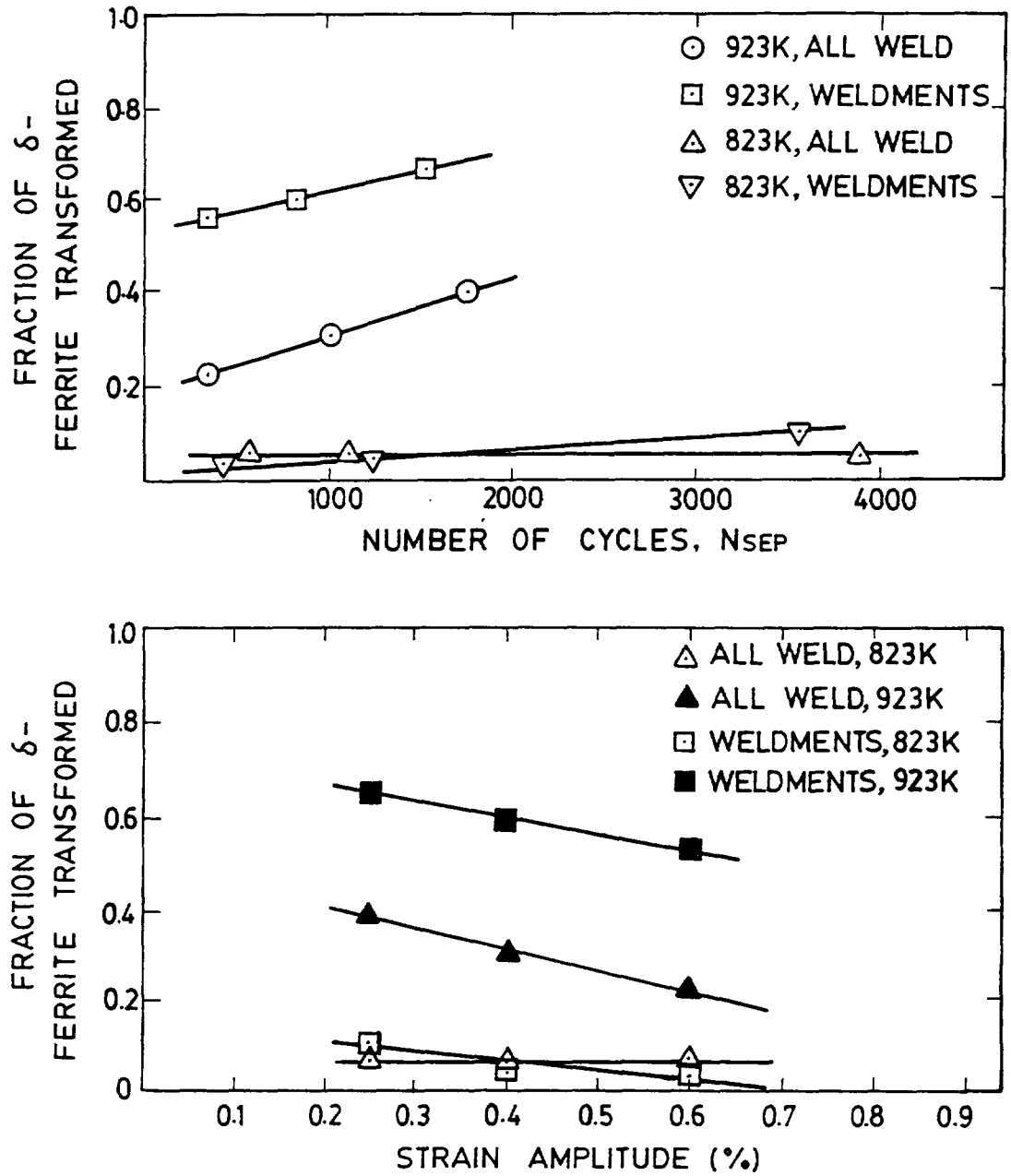

FIG. 6. Influence of testing variables on the fraction of δ-ferrite transformed during fatigue deformation.

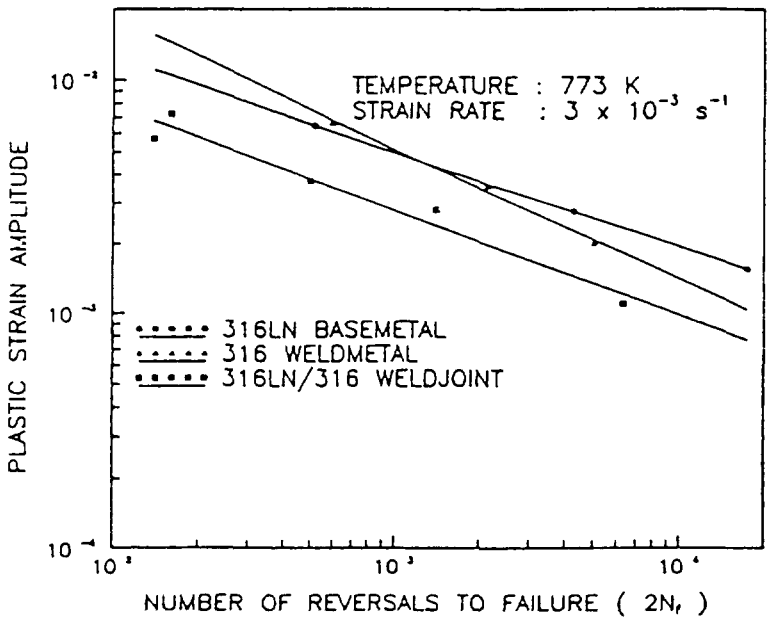

FIG. 7. Comparison of the fatigue lives of 316LN base metal, 316SS weld metal and 316LN/316 weld joint at 773 K.

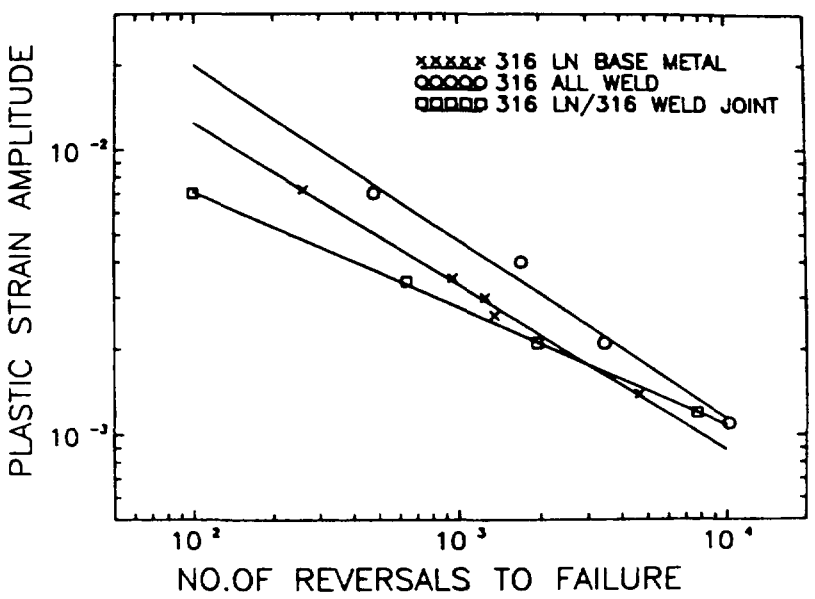

FIG. 8. Comparison of the fatigue lives of 316LN base metal, 316SS weld metal and 316LN/316 weld joint at 873 K.

leading to larger reduction in fatigue lives observed in the all-weld and weldment specimens at 923 K(particularly at low strain amplitudes) Joining of these microcracks with the main crack shortens the crack propagation stage and hence leads to an overall reduction in fatigue life Heat treating (at 1173 K for 3 h) the weldment prior to LCF testing improved the fatigue resistance significantly (Fig 4) This results from the relaxation of residual stresses and the beneficial changes that occur in the microstructure of the weld and HAZs

3.2. A comparative evaluation of low cycle fatigue behaviour of type 316LN base metal, 316 weld metal and 316LN/316 weld joint

A comparison of the LCF lives of 316LN base metal, 316SS weld metal and 316LN/316 weld joint specimens at 773 and 873 K is shown in Figs 7 and 8 respectively At 773 K, the base metal showed the highest fatigue resistance at most of the strain amplitudes, and the weld joint exhibited the least fatigue resistance at all strain amplitudes However, at 873 K, weld metal displayed an enhanced fatigue strength compared with the base metal Transmission electron microscopy of AISI 316 weld metal has been carried out on untested and on the samples tested at strain amplitudes of ±0 25 to ±1 0 % at 873 K Untested samples revealed very high dislocation density and extensive precipitation of carbides In the untested samples, dislocation structure was composed of mainly tangles distributed in the austenite matrix Delta ferrite also contained dislocations, though the density was much lower compared with the corresponding untested austenite matrix Occasionally, as welded matrix was found to be highly twinned with the twin bands extending upto δ-ferrite boundaries Carbides were noticed in the δ-ferrite/austenite boundaries, in the austenite matrix, and also in the twin bands After LCF testing, the dislocation density was seen to be much lower at regions away from the δ-ferrite/austenite boundary compared with the untested samples Furthermore, the δ-ferrite was completely free of dislocations, and the $M_{23}C_6$ carbides have coarsened considerably

The LCF life is generally governed by the tensile ductility of the material Therefore, one will expect lower fatigue life for 316SS weld metal (a cast structure), which is less ductile than 316LN base metal Contrary to this, weld metal showed a better fatigue life than the base metal at 873 K (Fig 8) This has occurred as a result of the crack propagation differences between the base and weld metals The fine duplex austenite-ferrite microstructure in the weld metal, with its many transformed phase boundaries, offered a greater resistance to the extension of fatigue cracks by causing deflection of the crack path than does the coarser structure of the base metal Furthermore, the increased resistance to crack propagation could also be attributed to the presence of heavily dislocated interphase boundaries between the austenite and delta phase A tangled dislocation structure near the phase boundary coupled with the brittle transformed interface leads to cracking of latter, resulting in a deflection of the crack path Crack deflection leads to reduced stress intensity at the crack tip and an associated reduction in crack propagation rate It must be pointed out that in 308 weld metal, microcracking of brittle sigma phase during fatigue testing at 923 K was found to decrease the fatigue life (section 3 1) The average δ-ferrite content reported in 308 weld metal was 9 FN in contrast to 4-5 FN found in 316 weld metal Enhanced interconnectivity among δ-ferrite colonies at higher δ-ferrite contents has led to linkup of microcracks, thus offsetting the advantages associated with crack deflection and crack branching

It has been found that a highly dislocated region near the γ-δ interface alone (without a brittle transformed region) was not sufficient to affect the crack path deflection This was evident in tests conducted at 773 K At 773 K, fatigue resistance of weld metal was lower at all strain amplitudes compared with the base metal (Fig 7) This is associated with the reduced degree of transformation of δ-ferrite to the brittle sigma phase and carbides at 773 K and the associated decrease in the degree of crack path deflection

The fatigue life of the weld joint was significantly lower than that of the weld metal and the base metal at both the temperatures investigated This decrease in life corresponded to a transition in crack initiation mode from purely transgranular in base and weld metals to an intergranular one in the HAZ of weld joint This intergranular crack initiation resulted as a consequence of the impingement of planar slip bands on the grain boundaries Movement of dislocations in planar slip bands led to the formation of dislocation pile-ups at the intersection of grain boundary and slip bands The stress concentration arising out of such pileups has been suggested to cause intergranular cracking more easily in coarse grained stainless steel Surface intergranular cracking shortens the crack initiation phase in weld joints and reduces the overall fatigue life

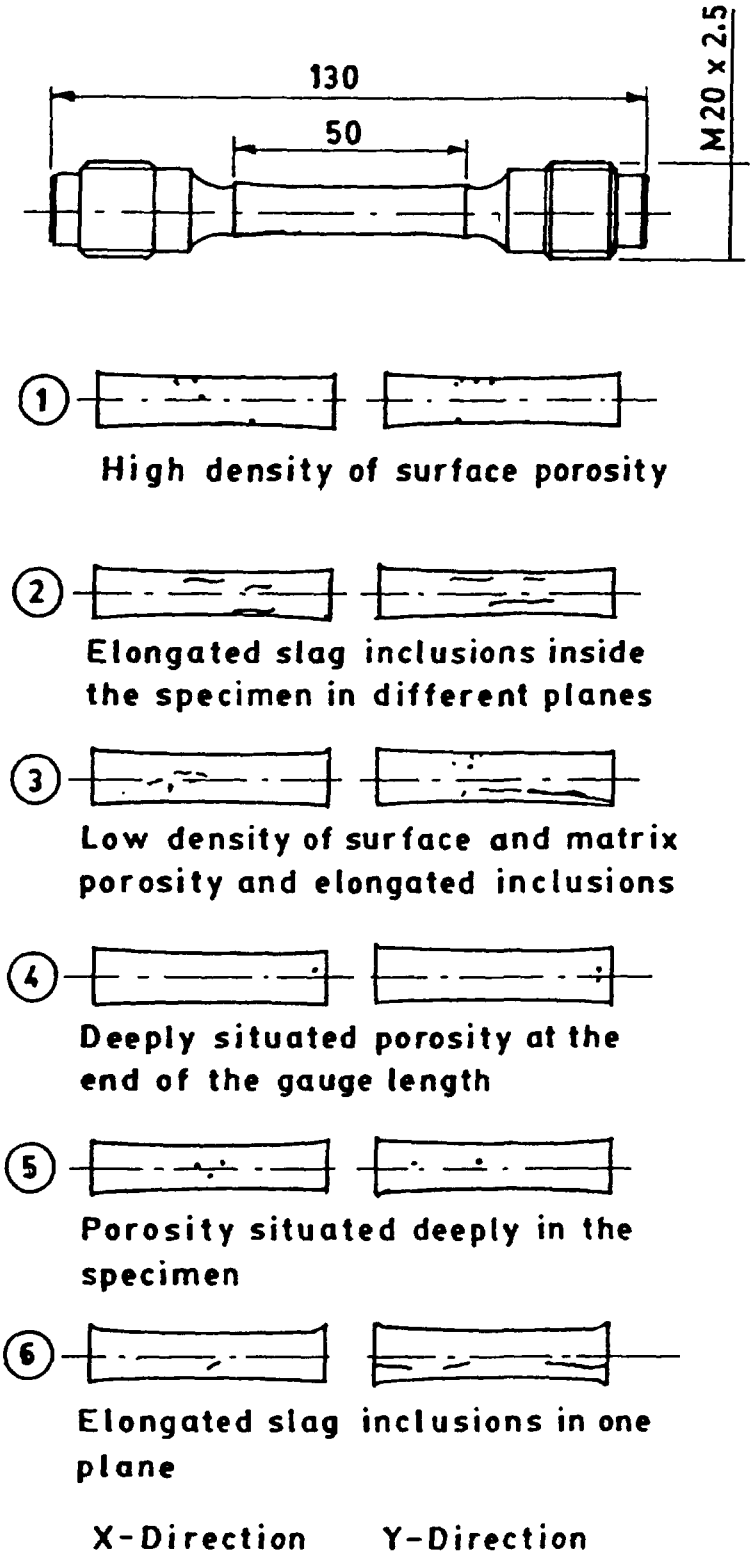

FIG. 9. Description and location of defects in LCF specimens of 308 SS weld metal

3.3. Influence of weld discontinuities on strain controlled fatigue behaviour of 308 stainless steel weld metal

The microstructure of as-deposited 308 SS sound weld metal was composed of long columnar grains and δ-ferrite (9 0 FN) distributed in the austenite matrix The orientation of the weld discontinuities with respect the loading axis and their location in the gauge length portion of six defective all-weld samples used in this investigation are described in Fig 9 The porosity in the weld metal was found in samples S1 and S3 in surface and near surface regions while the porosity in samples S4 and S5 was located in the interior regions Pores in S4 were situated at one end of the gauge length Samples S2, S3 and S6 contained slag inclusions and their orientation remained parallel to the LCF loading direction

Porosity is generally considered to result from the evolution of gases such as H_2, N_2 or O_2 from the weld metal The gas evolution takes place as a result of the decrease in solubility with decreasing temperature as the liquid metal solidifies or due to abrupt changes in solubility of gases during the liquid-solid reaction The use of damp electrodes for welding provides abundant supply of H_2 and O_2 leading to generation of pores The location of pores in different positions has been manipulated using the damp electrodes, only in those weld passes where the pores were desired

Defect-free welds exhibited continuous softening from the first cycle onwards to the onset of failure (Fig 10) Defective welds too exhibited cyclic softening and have generally supported smaller response stresses The cyclic response of defective welds was dependent on the type and location of defects The sample S1 containing surface porosity displayed much lower response stress than sample S6 having slag inclusions in a plane parallel to the loading direction The combination of porosity and slag inclusions in sample S3 was more effective in reducing the load bearing capacity of the specimen The discontinuities exerted their influence on cyclic stress response from the very first cycle onwards

TABLE III LOW CYCLE FATIGUE PROPERTIES OF BASE METAL, ALL WELD AND DEFECTIVE WELD METAL AT 823 K

Material condition	$\Delta\varepsilon_t/2$ (%)	$\Delta\varepsilon_t/2$ (%)	$(\Delta\sigma/2)_I$ (MPa)	$(\Delta\sigma/2)_{sat}$ (MPa)	N_I	N_f	N_{sep}
Base	0 25	0 13	140	208	4000	6211	6280
Base	0 4	0 16	159	271	725	1290	1475
Base	0 6	0 22	200	300	200	630	670
All weld	0 25	0 16	252	181	3000	3760	3900
all weld	0 4	0 2	278	220	900	1015	1120
all weld	0 6	0 24	288	245	375	528	560
Defective weld-S1	0 25	0 08	210	185	450	725	900
S2	0 25	0 09	220	166	2250	2552	2660
S3	0 25	0 08	223	172	800	935	1075
S4	0 25	0 09	226	178	3550	3700	3850
S5	0 25	0 08	233	175	1700	2050	2240
S6	0 25	0 08	239	175	3000	3385	3510

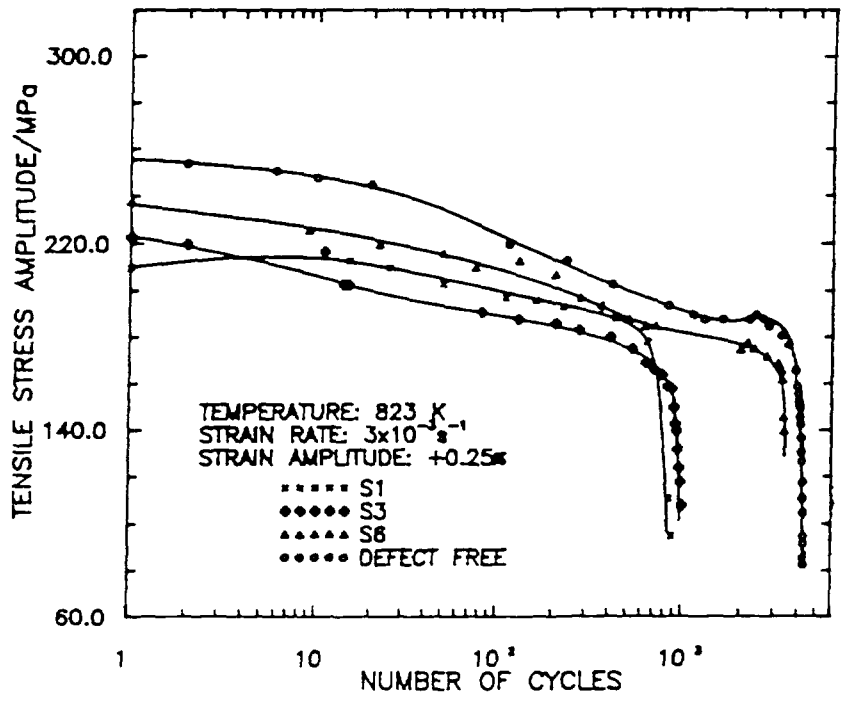

FIG. 10. Cyclic stress response in defect-free and defective 308 SS weld metal samples at 823 K. S1, S3 and S6 refer to the defective samples shown in Fig. 9.

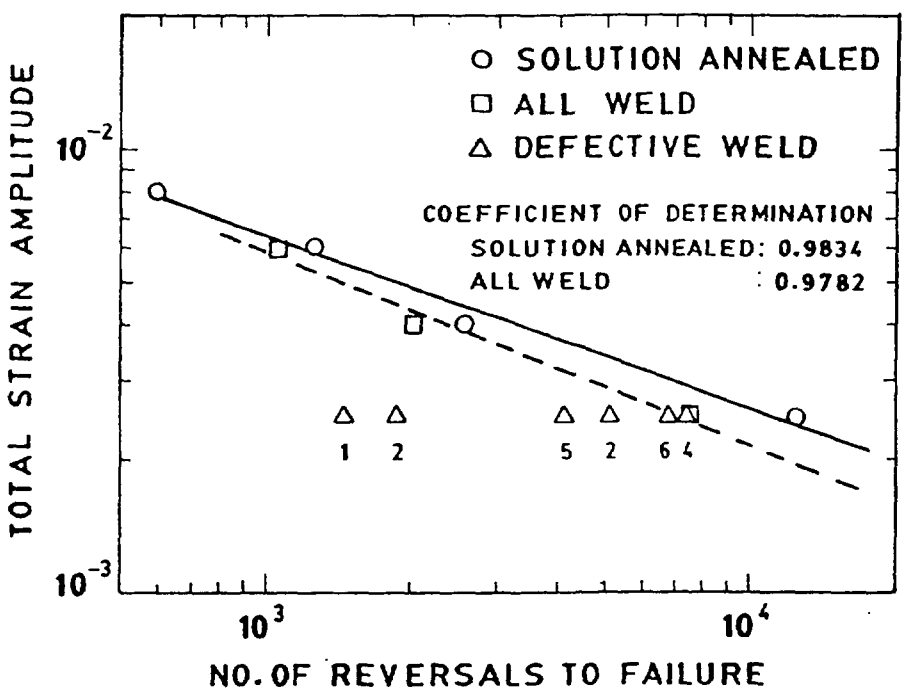

FIG. 11. Strain-life plots of 304 SS base and 308 SS sound weld and defective weld metal. Numbers at data points refer to the samples shown in Fig. 9.

The results of strain controlled fatigue tests on 304 SS base and 308 SS welds are given in Table III. Figure 11 shows the LCF life results as double logarithmic plots of total strain amplitude and number of reversals to failure. Fatigue resistance of defect free 308 SS weld metal was lower than 304 SS base material at low strain amplitudes. Discontinuities on and near the specimen surface (samples S1 and S3) have been found to reduce the LCF life drastically compared to the defects located in the interior regions of the samples (S4 and S6). Porosity on the specimen surface (S1) has been found to be particularly harmful and caused a reduction in life by a factor of seven relative to the sound weld metal. Defect combination of porosity and elongated inclusions (S3) was found to be more deleterious than the case when either the slag inclusions (S6) or porosity (S5) was present alone in the interior regions. Porosity at one end of the gauge length (S4) proved to be less harmful to LCF life of the weld metal. Crack initiation life was also found to be much smaller in the case of samples containing surface porosity, compared to sound weld metal. In this investigation the cycle number corresponding to the onset of rapid drop in tensile stress in cyclic stress response curves has been used as an estimate of the macrocrack initiation life (N_I). Shorter crack initiation and failure lives in defective welds were found to have correlation with the initiation of fatigue cracks at discontinuities. Although it has been generally accepted that inclusions are more deleterious to the performance of harder microstructures, the present investigation indicates that the relatively ductile stainless steel welds are also vulnerable to damaging effects exerted by inclusions in shortening the fatigue crack initiation and propagation phases.

3.4. Creep-Fatigue interaction behaviour of type 308 stainless steel weld metal and type 304 stainless steel base metal

The fatigue life results of the strain controlled LCF and creep-fatigue interaction (CFI) tests for 304 SS and 308 SS weld metal are shown in Table IV. Results clearly indicate a reduction in continuous cycling as well as CFI lives of 308 weld metal when compared with type 304 base metal under identical testing conditions. Hold-time effect on life was dependent not only on the material condition but also on the position of the hold in a cycle. Fatigue lives for 308 SS weld in the 1 min. hold-time tests were in the order : compression hold - continuous cycling-tension + compression hold - tension hold. Fatigue lives of 304 SS were in the order : continuous cycling - compression hold-tension+compression hold-tension hold. Significant reduction in the life of the weld metal was noted on increasing the duration of tension hold time to 10 min. However, the time to failure increased.

304 SS revealed a severe degradation in life with a tension hold compared with continuous cycling. The compression hold lowered life marginally while the hold in tension + compression exhibited life values in between the lives in tension only and compression only holds. It is of interest to examine the build up of mean stress in the course of fatigue deformation. The existence of appreciable mean stress is cited as the reason for the difference in fatigue life between tension and compression hold cycling. It was observed that the addition of either tension-only or compression-only holds led to no significant mean stresses in the hysteresis loops. The capacity of the material to develop mean stress depends on the ratio of inelastic to elastic strain in a cycle. If the inelastic strain is large relative to the elastic strain, as in the present experiments, the mean stress which can develop is very low, and consequently the influence of mean stresses on cyclic life under dwell conditions would be expected to be very small.

The damage behaviour during hold periods can be best described by characterizing the stress relaxation as a function of time elapsed in hold-time tests. The mid-life stress relaxation response curves for the different hold-time tests are shown in Figs. 12 and 13 respectively for 304 base and 308 SS welds. It can be seen that rapid relaxation to 60% of the maximum stress occurred in less than 5s. Further, the inelastic strain rate associated with relaxation strain decreased continuously with increasing fraction of hold time. Inelastic strain rates ($\varepsilon = (\sigma/E).\ 1/t$, where σ = stress at a given time t and E = the elastic modulus) found in the rapid relaxation period ($>10^{-4}\ s^{-1}$) correspond to those which are expected for precipitation-free matrix deformation, while those observed in the slow relaxation period ($<10^{-5} s^{-1}$) are typical of creep deformation. Inelastic strains accumulated in various hold-time tests are recorded in Table IV. The increase in inelastic strain occurring as a result of creep in a cycle under hold-time conditions would lead to a reduction in life.

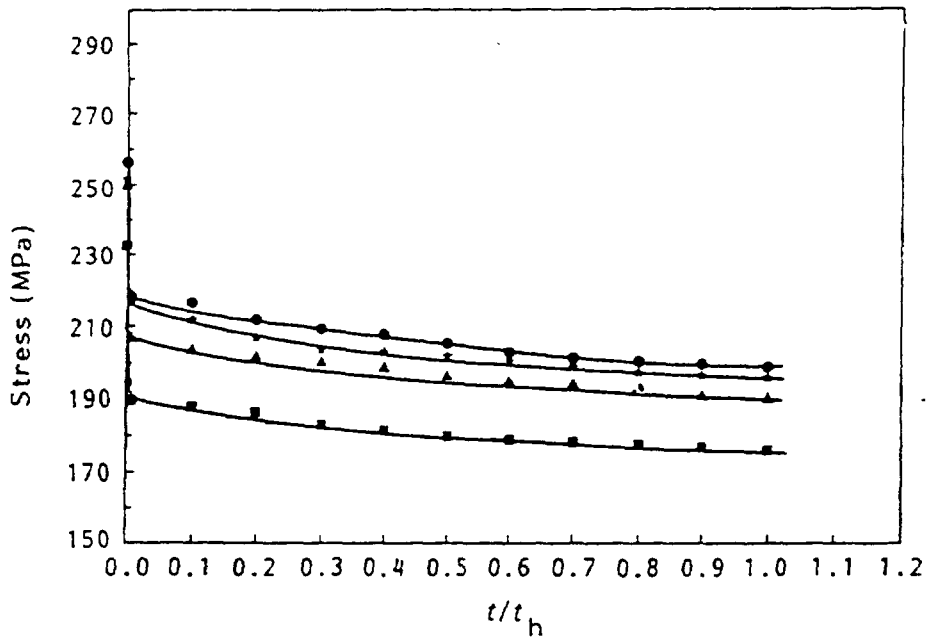

FIG. 12. Stress relaxation response for 304 SS base material at 923 K; ±0.5 %.

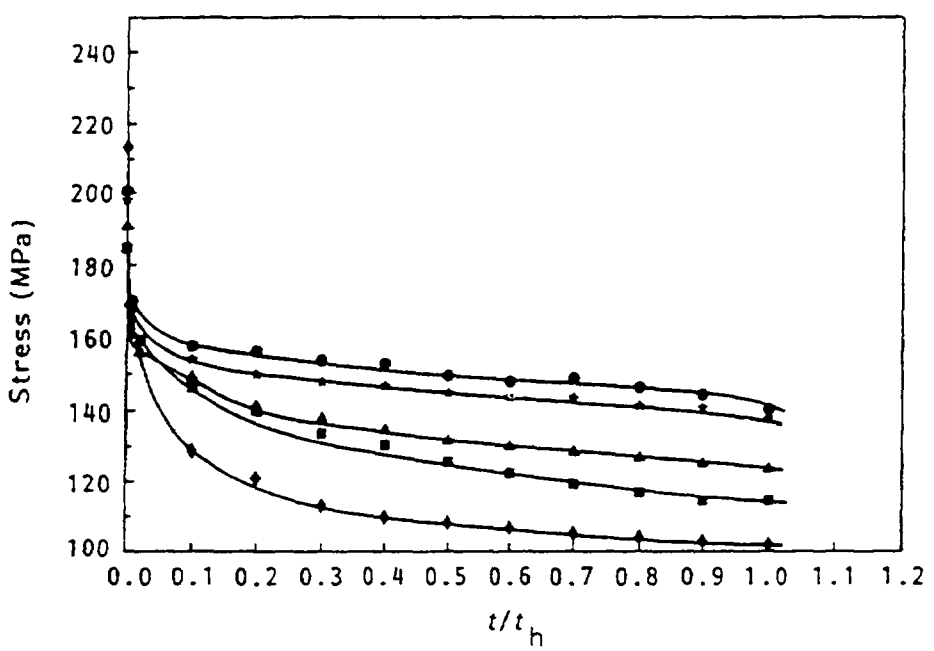

FIG. 13. Stress relaxation response for 308 SS all-weld material at 923 K; ±0.5 %.

TABLE IV LCF AND CREEP-FATIGUE INTERACTION PROPERTIES OF 304SS BASE AND 308 SS WELD MATERIAL

Material	Wave Shape[a]	Hold time (min)	Strain range (%)		Creep (%)	Stress amplitude (MPa)		N_{sep}	Duration of test (s)
			Total	Inelastic		First Cycle	Half life		
304 SS base	CC	0	1 0	0 73	0	127	266	900	6000
	TH	1	1 0	0 76	0 03	111	255	555	37000
	CH	1	1 0	0 75	0 02	123	250	880	58670
	TCH	1	1 0	0 84	0 11	131	242	695	46340
308 SS weld	CC	0	1 0	0 72	0	215	188	525	3500
	TH	1	1 0	0 73	0 01	217	188	385	25600
	CH	1	1 0	0 78	0 05	218	204	730	48670
	TCH	1	1 0	0 86	0 14	223	185	415	52570
	TH	10	1 0	0 83	0 11	245	210	160	97070

[a]CC- continuous cycling, TH-tension hold, CH-compression hold, TCH-tension plus compression hold

Fractographic investigations on 304 SS subjected to 1 min dwell periods have demonstrated that bulk creep damage effects are associated with tensile hold periods (Fig 14) whereas the fracture modes associated with compression holds and continuous cycling are very similar in nature, being dominated by ductile fatigue striations The larger reduction in life under tension holds occurred as a result of the introduction of grain boundary creep damage during low-strain-rate tensile deformation, which modified the failure process Premature failure and reduced fatigue life result primarily because the reduced crack length at failure is effectively shorter than that in the absence of creep cavitation Hales [6] proposed that a creep strain rate less than 10^{-4} s^{-1} and an accumulated relaxation strain of approximately 7% are necessary to accumulate grain boundary damage at second-phase particles As the process of initiation and early growth of internal grain boundary cavities which give rise to CFI failures require both shear and tensile stresses across a grain boundary, bulk damage is unlikely to occur during the period of compressive stresses Hence the larger life exhibited with compressive dwells could be attributed to the healing of effect of compressive creep In general, intergranular crack propagation occurs at a faster rate than transgranular cracking Therefore the fatigue lives of the specimens tested with tension hold times are shorter than those tested with symmetrical or compressive hold periods

308 SS weld generally showed a shorter life than 304 SS under identical loading conditions during CFI tests In weld metal, surface cracks initiated at austenite-ferrite boundaries (Fig 15) In this study, at 923 K, extensive transformation of ferrite to σ-phase occurred at γ-δ interfaces, providing a variety of interface boundaries to serve as fracture paths In fact, a larger number of microcracks were observed in the longitudinal sections of tension-hold specimens (Fig 16) owing to the cracking at the γ-σ interfaces Joining of these microcracks with the main crack probably shortens the crack propagation stage and hence leads to an overall reduction in life The compression hold exhibited longer life than the continuously cycled weld (Table IV) inspite of a larger amount of δ-ferrite transformation Weld specimens tested under compression hold did not reveal microcracking at γ-σ interfaces It can be inferred from these observations that the processes of initiation and early growth of γ-σ interface cracks require the normal tensile stresses across the interface Thus for cycles containing compression holds only, failure would be dominated by fatigue striation formation mechanisms

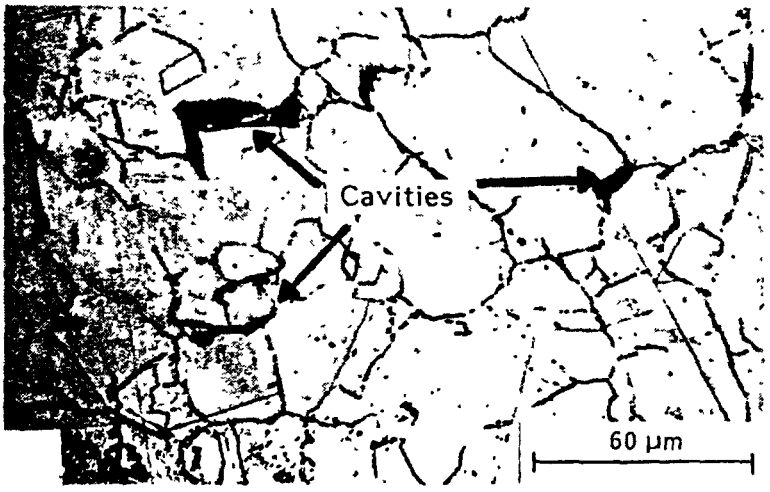

FIG 14 Bulk creep damage associated with 1 min. tensile hold period in 304 SS

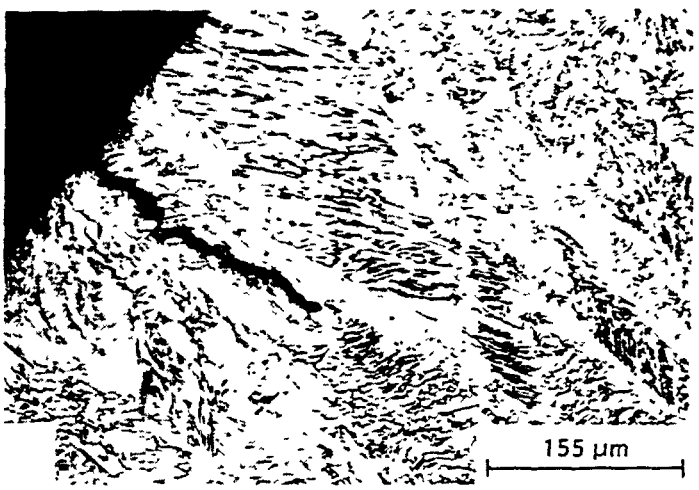

FIG 15 Crack initiation at austenite-ferrite interfaces in 308 SS weld metal under 1 min compression hold at 923 K

FIG. 16. (a) Microcracks at γ - transformed δ interfaces and (b) Microcrack growth and interlinkage (1 min. tension hold)

ACKNOWLEDGEMENTS

The authors wish to thank Dr.Placid Rodriguez, Director, IGCAR and Dr. Baldev Raj, Director, Metallurgy and Materials Group for their encouragement and many useful discussions. During the course of these investigations, cooperation rendered by Mrs. R. Sandhya is highly appreciated.

REFERENCES

[1] ASME Boiler and Pressure Vessel Code Case N-47, ASME, New York (1986).

[2] BHANU SANKARA RAO, K., et al., "Strain controlled LCF behaviour of type 304 stainless steel base material, type 308 stainless steel weld metal and 304-308 stainless steel weldments", Mater.Sci.Engng. **A130** (1990) 67-82.

[3] BHANU SANKARA RAO, K., et al., "Influence of weld discontinuities on strain controlled fatigue behaviour of 308 stainless steel weld metal", J.Engineering Materials and Technology **116** (1994) 193-199.

[4] BHANU SANKARA RAO, K., et al., "Creep-Fatigue interaction behaviour of type 308 stainless steel weld metal and type 304 stainless steel base metal", Intl.J.Fatigue **15** (1993) 221-229.

[5] VALSAN, M., et al., "A comparative evaluation of low cycle fatigue behaviour of type 316LN base metal, 316 weld metal and 316LN/316 weld joint", Metllurgical and Materials Transactions A **26A** (1995), 1207-1219.

[6] HALES, R., "A quantitative metallogarphic assessment of structural degradation of type 316 stainless steel during creep-fatigue", Fatigue Eng. Mater. Struct. **3** (1980) 339-356.

ASSESSMENT OF CREEP BEHAVIOUR OF AUSTENITIC STAINLESS STEEL WELDS

G. SASIKALA, M.D. MATHEW, K. BHANU SANKARA RAO,
S.L. MANNAN
Indira Gandhi Centre for Atomic Research,
Kalpakkam, Tamil Nadu, India

Abstract

The creep properties of a nitrogen alloyed type 316 L stainless steel (316LN SS) base metal and weld metal of nuclear grade were studied at 873 and 923 K in the range of applied stresses from 120 to 315 MPa The results were compared with those obtained on a nuclear grade type 316 SS Creep rupture lives of the weld metals were found to be lower than those of the respective base metals by a factor of 5 to 10 Both the base metal and the weld metal of 316LN SS exhibited better rupture lives compared to 316 SS base metal and weld metal respectively at identical test conditions At 923 K, the stress exponent for minimum creep rate was about 9 5 for both the base metals, whereas it was about 12 for the weld metals However, in the case of 316 SS, the weld metal exhibited higher creep rates compared to the base metal whereas for 316LN SS the creep rate of the weld metal was lower by a factor of 5 at high stress levels to 10 at lower stress levels, compared to that of its base metal Both the weld metals exhibited lower rupture elongation compared to that of the respective base metals at 873 and 923 K Comparison of rupture lives of the two steels with the ASME Code Case N-47 curves for the base and weld metals showed that in the case of 316 LN SS the specifications for maximum allowable stresses are over-conservative The creep rupture results are rationalised on the basis of evolving microstructure

1 INTRODUCTION

Type 316 austenitic stainless steel (SS) is being widely used as a major structural material for fast breeder reactor components in view of its good high temperature mechanical properties, compatibility with the liquid sodium coolant and adequate weldability However, in general, austenitic stainless steels have relatively poor resistance to intergranular stress corrosion cracking (IGSCC) in chloride and caustic environments In the marine environment, welded components of type 316 SS have been reported to fail by IGSCC in the heat affected zone (HAZ) due to the combined influence of sensitization and residual stresses A nitrogen alloyed low carbon (0 03 wt % max) version of this steel (316 LN SS) has been chosen for the high temperature structural components of the prototype fast breeder reactor being designed at Kalpakkam (For this steel nitrogen is specified as 0 08 wt % in order to compensate for the loss in solid solution strengthening due to reduced carbon content) Since very little information was available in the literature on the high temperature behaviour of 316 LN SS, design of the components operating in the creep range has until recently been based on ASME code case N-47 [1] with data available in the code on type 316 SS Differences in chemical composition, microstructure and its stability and thermomechanical history have been found to lead to wide variations in high temperature behaviour of austenitic stainless steels and their weld metals [2] The safety factors applied for designing for the allowable stresses in the welded components are supposed to take into account these differences In order to calculate the allowable stresses in the welded components, the design rules have been modified taking into account the weld metal creep rupture strength [3,4] Accordingly, the allowable stress in the weld is chosen as the lower value between (i) allowable stress intensity limit for the base metal which in turn is based on 67 percent of the stress to rupture, 80 percent of the stress to cause onset of tertiary and 100 percent of stress to cause 1 percent total strain and (ii) 0 8 σ_{min} *R where σ_{min} is the expected minimum stress to rupture for the base metal and R is the appropriate ratio of creep rupture strength of the weld metal to that of the base metal The allowable deformation in the weld is restricted to half the deformation permitted for the base metal since ductility of the weld metal at elevated temperatures is generally low The strength reduction factors proposed for 316 SS welds [4] were found to be adequate for a nuclear grade type 316 SS used for high temperature components in the fast breeder test reactor at Kalpakkam [5] However, applicability of these rules for designing 316 LN SS welds has not yet been examined A significant problem in the production of fully austenitic welds is their tendency to hot

cracking. In order to minimize hot cracking, the chemical composition of the welding consumable is adjusted to produce small amounts of δ–ferrite (usually, less than 10 %). However, the duplex microstructure consisting of austenite and ferrite phases is highly unstable at high temperatures and δ–ferrite can transform to brittle intermetallic phases such as σ. This transformation has been shown to lead to low ductility creep failures at elevated temperatures. It has been recognized that the creep properties of weld metals are significantly influenced by the kinetics of δ–ferrite transformation. Since the design of welded components of 316 LN SS operating in the creep range uses data on 316 SS weld metal, an attempt has been made in this investigation to obtain a comparative assessment of the creep behaviours of 316 SS and 316 LN SS and their welds.

2. EXPERIMENTAL

Constant-load creep rupture tests have been carried out on 316 SS base and all-weld specimens of 50 mm gage-length and 8 mm gage diameter while 316 LN base and weld specimens had 50 mm gage-length and 10 mm gage diameter. Creep tests were carried out at 873 and 923 K employing stress levels in the range 100 to 335 MPa. Temperature was controlled to within ±2 K along the gage length. All-weld specimens were taken from weld pads prepared by manual metal arc welding process, the details of which have been reported elsewhere [5]. The chemical compositions of the base and weld metals are given in Table 1. The base metals were tested in the solution treated condition and the weld metals in the as welded condition. The base metals had an equiaxed grain structure (Fig. 1(a)) with mean linear intercept grain size of 70 μm for 316 SS and 88 μm for 316 LN SS. The microstructure of both the weld metals consisted of δ-ferrite (~5 FN in 316 and ~7.5 FN in 316 LN, vermicular morphology) distributed uniformly in γ matrix (Fig. 1(b)).

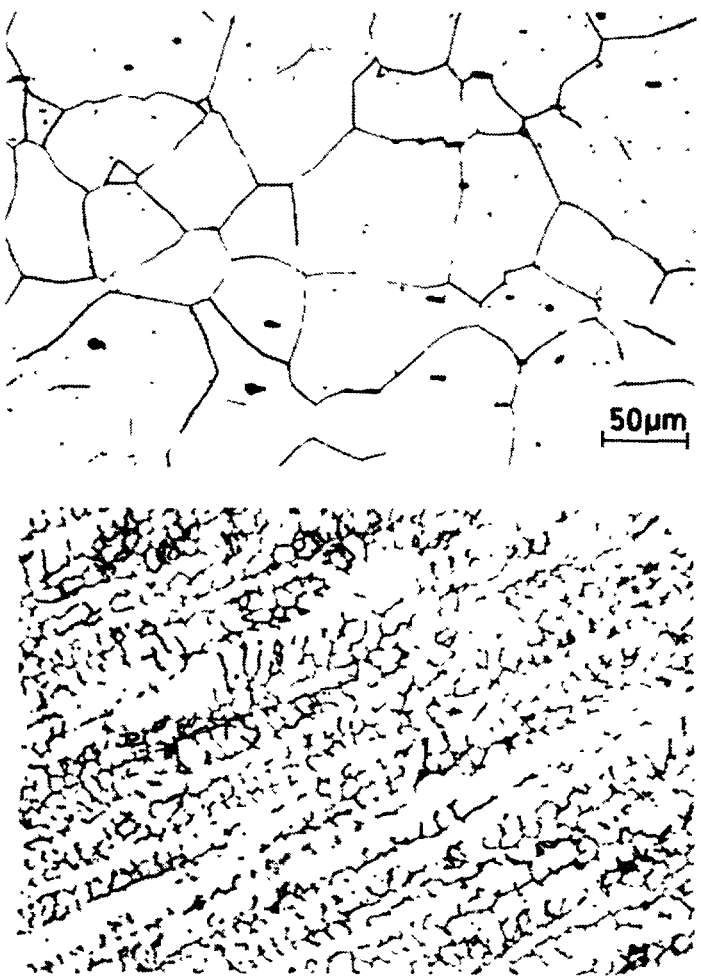

FIG.1. Typical microstructures before creep testing : (a) base metal (b) weld metal

TABLE I CHEMICAL COMPOSITIONS (IN WEIGHT%) OF THE BASE AND WELD METALS OF 316 SS AND 316 LN SS

Element	Base metal		Weld metal	
	316	316 LN	316	316 LN
C	0 048	0 023	0 060	0 052
Ni	12 48	12 21	11 9	11 5
Cr	16 10	17 12	18 8	18 6
Mo	2 11	2 31	2 06	2 20
Mn	1 73	1 65	1 42	1 74
Si	0 295	0 29	0 58	0 64
S	0 016	0 003	0 010	0 007
P	0 03	0 024	0 010	0 022
Cu	0 225	0 10	0 05	0 04
B	0 0005	0 0012	0 0005	0 0009
N	0 031	0 086	-	0 067

3 RESULTS AND DISCUSSION

3.1. Rupture life

The variation of rupture life with applied stress for both base and weld metals at 873 and 923 K are shown in Figs 2(a) and (b) respectively It may be noted that both the weld metals are weaker compared to the respective base metals 316 LN SS base metal exhibited the highest creep rupture strength and 316 SS weld metal the lowest It is interesting to note that 316 LN SS weld metal strength is comparable to that of 316 SS base metal The dashed lines in these figures represent the expected minimum stress to rupture specified by ASME Code Case N-47 for 316 SS base metal while the solid lines represent the values specified for 316 SS weld metal It may be noted that the rupture strength of even 316 SS weld metal (which is the weakest among the four materials examined here) is higher than the values specified by ASME code except at very high stresses corresponding to rupture lives smaller than 100 h Thus, for this material, the use of strength reduction factors employed in defining this curve beyond 100 h rupture life appers to be adequate However, it is clear from Figs 2(a) and 2(b) that the design of welded components of 316 LN SS in the creep regime using the data and strength reduction factors proposed for 316 SS weld metal could prove to be over-conservative Note that the rupture lives of 316 LN SS weld metal are higher by a factor of ~10 than that of 316 SS weld metal

3.2 Minimum Creep Rate

Variation of minimum creep rate ($\dot{\varepsilon}_s$) with applied stress (σ) at 923 K is given in Fig 3 A power law relationship between ε_s and σ is found to be obeyed for all the four material conditions, the stress exponent was ~ 9 5 for both the base metals and ~ 12 for the weld metals These values of stress exponent suggests that for all the material conditions, dislocation creep is the rate controlling mechanism Under the test conditions employed, creep rates for 316 SS base and weld metals are found to be similar The creep rates for 316 LN SS base metal are an order of magnitude lower compared to that for 316 SS base metal and are higher compared to 316 LN SS weld metal

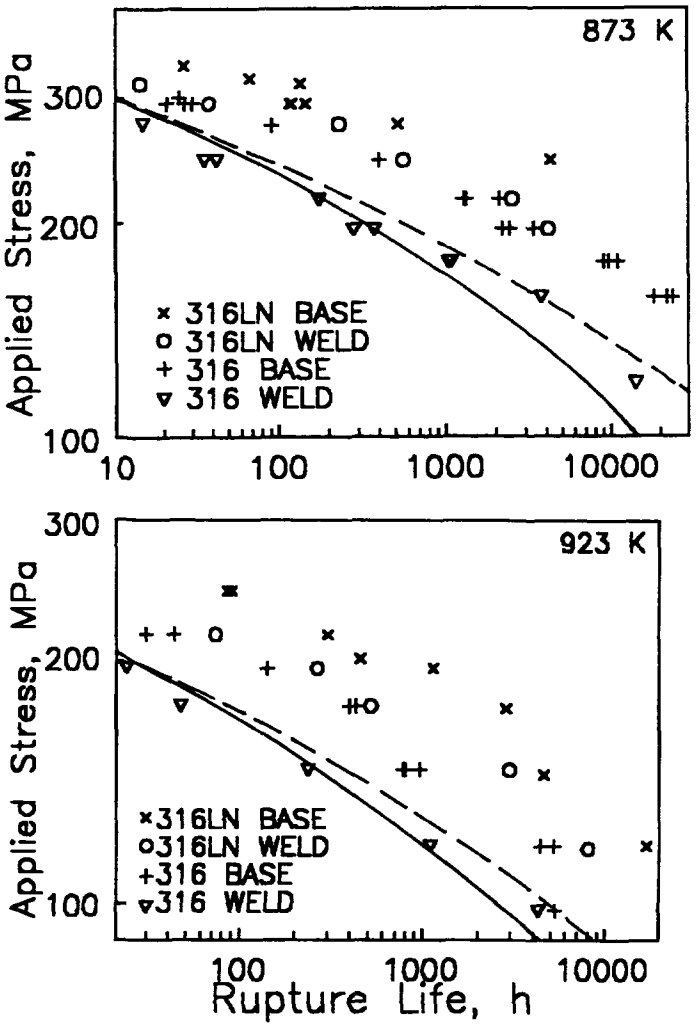

*FIG 2 Variation of rupture life with applied stress at (a) 873 K and (b) 923 K for base and weld metals of types 316 and 316LN SS The dashed lines represent the ASME curves for expected minimum stress to rupture (σ_{min}) for the base metal while the solid lines represent σ_{min} *R for the weld metal of 316 SS*

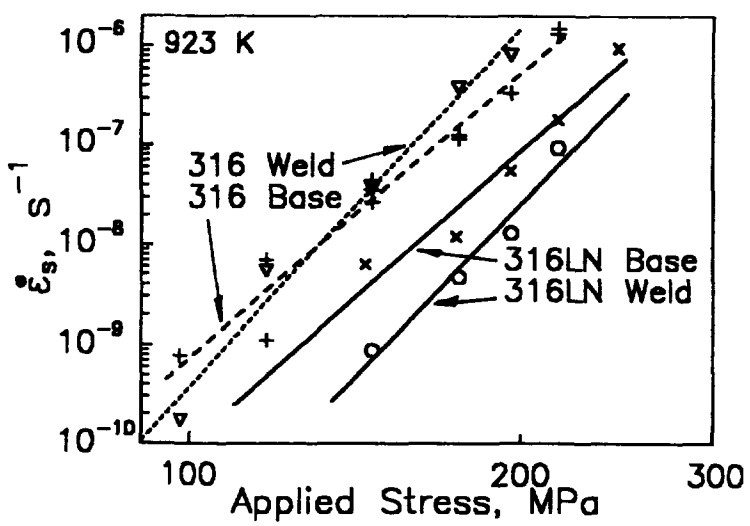

Fig 3.Variation of minimum creep rate with applied stress at 923 K for base and weld metals of types 316 and 316 LN SS

Factors controlling the creep deformation behaviour of type 316 SS have been widely studied [4,5,6-9]. Carbon is a good solid solution strengthener at lower temperatures and short durations. Longer exposures at higher temperatures lead to precipitation of carbides, initially on grain boundaries and subsequently on matrix dilocations [9,10]. While, fine carbides on grain boundaries reduce grain boundary sliding, the intragranular precipitation of carbides strengthen the matrix by retarding the glide and climb of dislocations [6]. Nitrogen is known to be a better solid solution strengthener compared to C [11,12] and has been suggested to .delay the onset of carbide precipitation and to retard the coarsening of carbides[13]. Thus the beneficial effects of cabide precipitation are retained to longer times in steels containing N. Precipitation of nitrides, however, have not been reported at the temperatures employed in this study when the N levels are less than 0.15 wt.%. It was shown that nitrogen rich clusters of Cr-N type form at very high temperatures during initial stages of ageing and subsequently develop into Cr_2N precipitates in 316 LN SS [14].

3.3. Rupture elongation

Variation of rupture elongation with applied stress for 316 SS and 316 LN SS is shown in Figs. 4 (a) and 4(b) respectively. It may be noted that in both the cases, weld metals exhibited very poor ductility compared to that of the respective base metals. A comparison of the elongation values for the two weld metals shows that 316 LN SS exhibits lesser elongation at rupture ompared to 316 SS weld metal; typically, at 120 MPa, the values are 20% for 316 SS weld metal and 3% for 316 LN SS weld metal. In the case of 316 SS, the difference in rupture elongation increased with decreasing stress levels, i.e., increasing rupture times, while in the case of 316 LN SS the difference was nearly the same at all stress levels. The weld metal of 316 SS showed complete transformation of δ-ferrite in about 1000 h. Extensive creep cavitation associated with coarse precipitates of σ - phase was observed (Fig. 5(a)). Growth and linkage of these cavities caused failures with low ductility. Similar type of fracture behaviour was displayed by 316 LN SS (Fig. 5(b)). However, the transformation was complete in less than 100 h. The longer rupture times of 316 LN SS weld samples compared to 316 SS weld samples at identical stress levels also led to coasening of σ - phase particles contributing to lowering of ductility.

In the as-welded state, both the weld metals contain δ-ferrite; ~5 FN in 316 and ~ 7.5 FN in 316 LN. The high temperature creep properties of δ-ferrite containing weld metals are generally controlled by the kinetics and the nature of the products of transformation of δ-ferrite. Influence of stress on the transformation of δ-ferrite in 316 SS weld metal was characterised extensively by following the transformation magnetically as well as metallographically in the stressed (gage section) and stress-free (shoulder) regions of the creep tested samples. Figures 6(a) and 6(b) show the optical micrographs of gage sections of type 316 SS weld metal crept at 923 K for different durations. Elevated temperature exposure for 1100 h has led to precipitation of $M_{23}C_6$ type carbides and intermetallic σ-phase. Prolonged exposure resulted in coarsening of σ-phase and partial dissolution of carbides, as seen in Fig. 6(b). These precipitates were observed both in gage section and shoulder regions. Figures 7(a) and 7(b) show the variation of % δ-ferrite transformed with rupture time as measured using Magne-gage on samples ruptured at various temperatures. Transformation occurred earlier and more extensively in the gage section as compared with the shoulder region. The percentage of δ-ferrite transformed increased with increasing temperature.

Figures 8(a) to (d) show the progressive changes in the microstructure of 316 LN weld metal undergoing creep at 923 K. It may be seen from this figure that during creep at 923 K, transformation of δ-ferrite takes place in the following sequence; (i) initially the δ-ferrite network breaks down forming carbides in about 50 h (Fig. 8(a)) (ii) continued exposure results in formation of an intermetallic phase σ (Fig. 8(b)) (iii) on further exposure the σ-phase particles coarsen to form large islands of σ-phase (Figs. 8(c) and (d)). The continuous decrease in ductility with decreasing stress (increasing duration of exposure) is found to have correlation with the formation and coarsening of σ-phase particles.

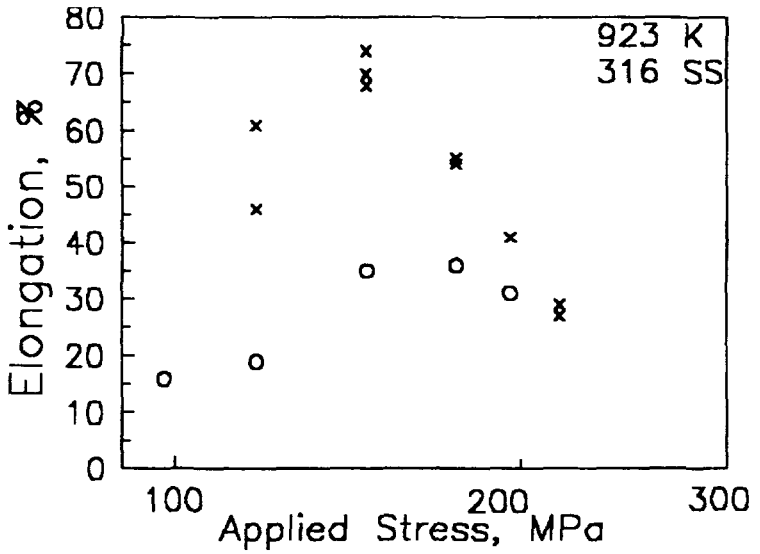

(a)

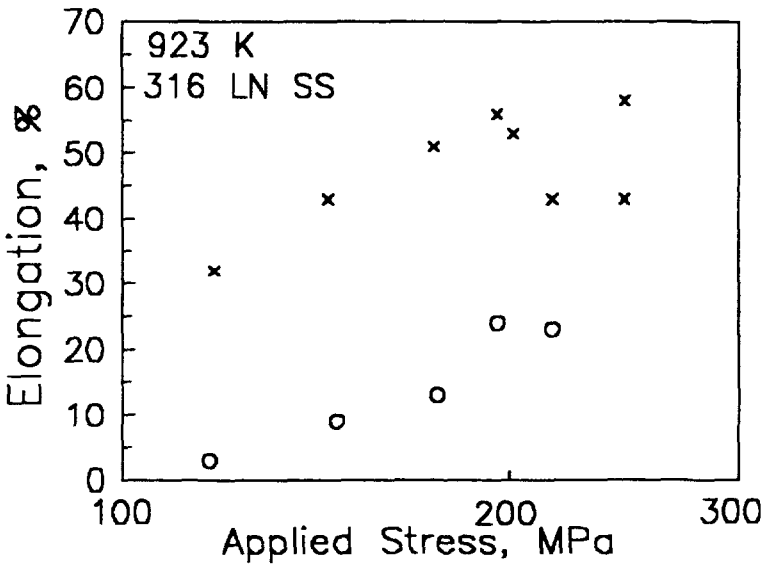

(b)

FIG 4 Comparison of the variation of rupture elongation with applied stress for the base (X) *and weld* (O) *metals of (a) 316 SS and (b) 316 LN SS*

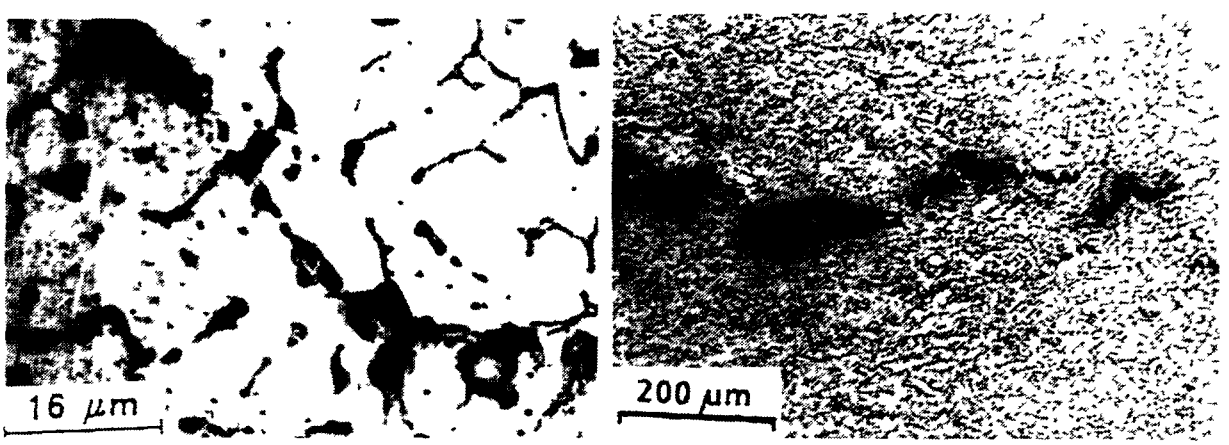

(a) (b)

FIG 5 Optical micrographs showing creep damage at 923 K in(a) 316 SS weld metal (b) 316LN SS

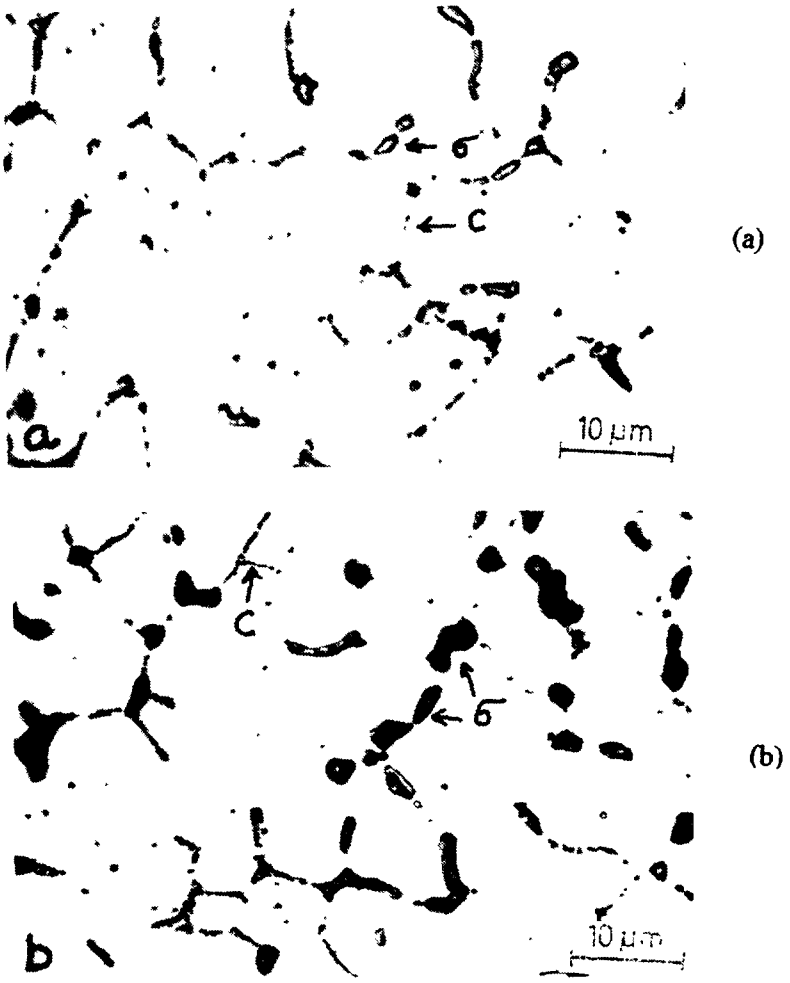

FIG. 6 Microstructure of type 316 SS weld metal creep tested at 923 K (a) 1100 h (b) 4300 h. Carbide and σ-phase shown by arrows

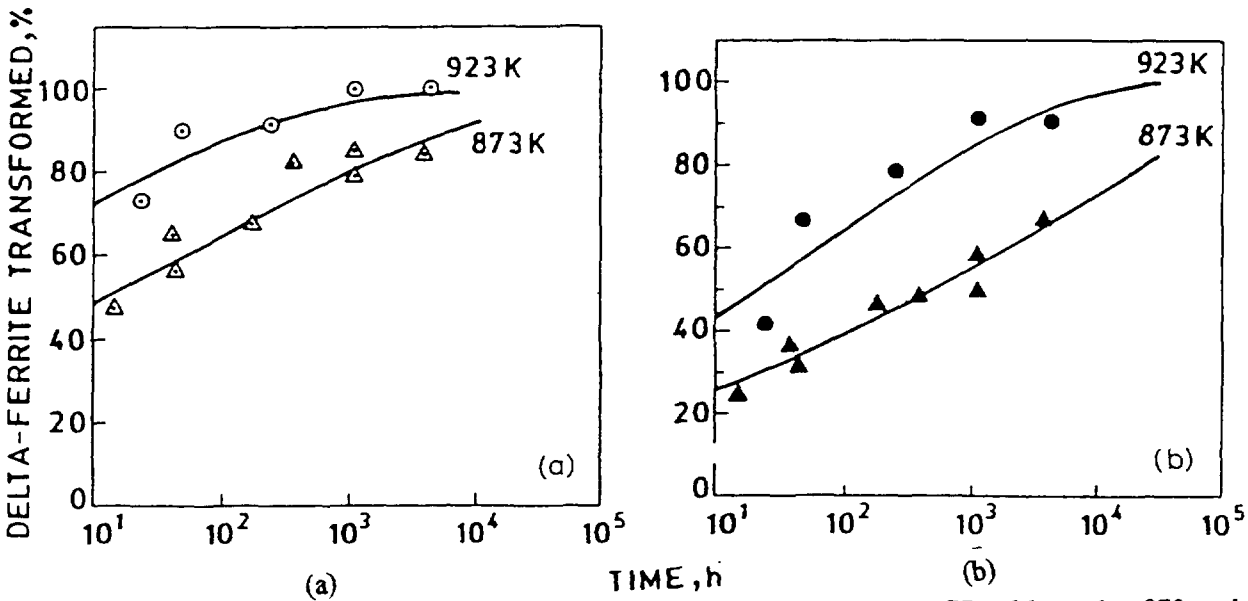

FIG. 7 Variation of percentage δ-ferrite transformed with creep time for 316 SS weld metal at 873 and 923 K. (a) gage section (b)shoulder region

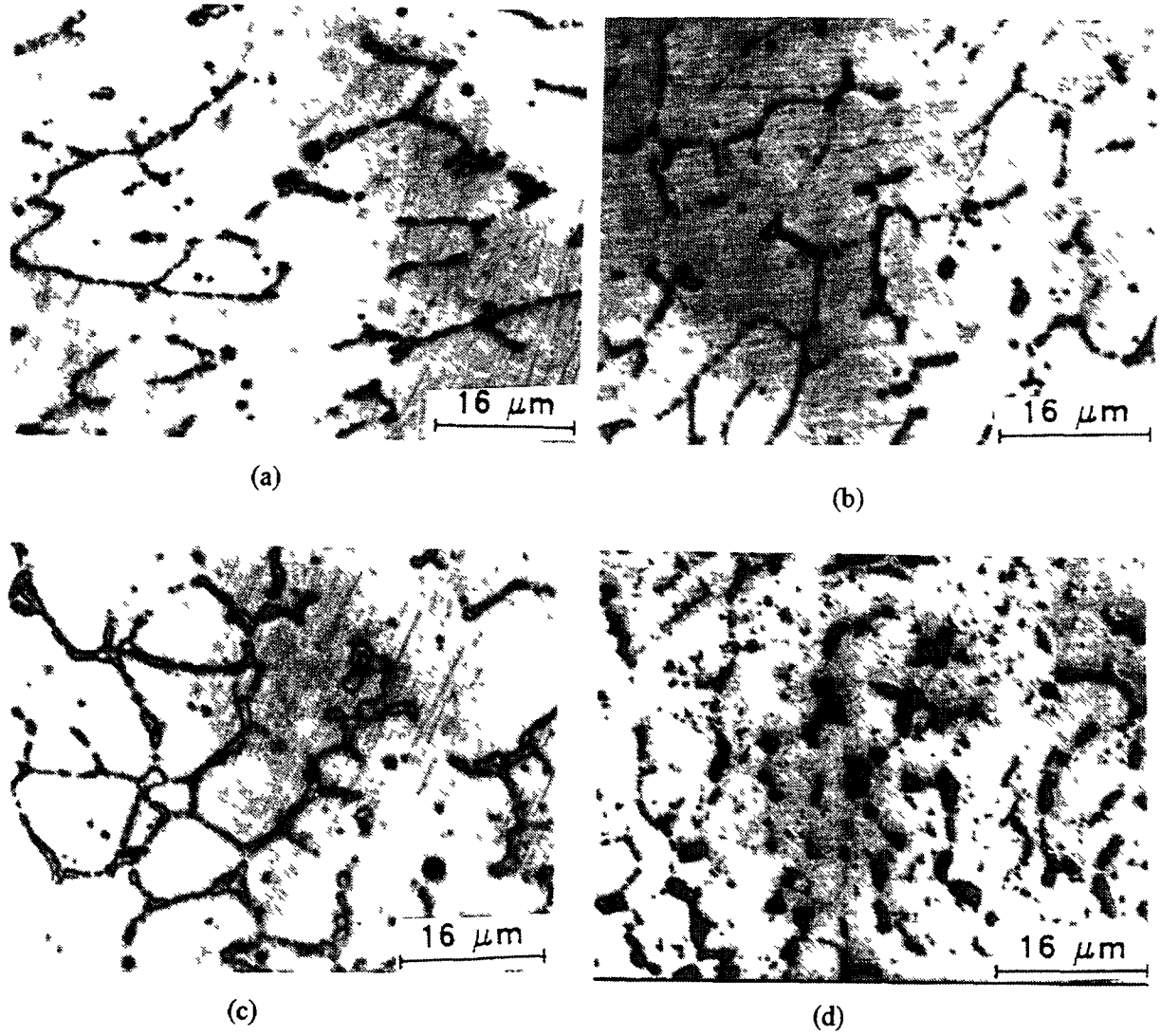

(a) (b)

(c) (d)

FIG 8 Microstructure of 316 LN SS weld metal after creep testing at 923 K for (a) 47 h (b)480 h (c)2300 h and (d) 5400 h

4 SUMMARY

1 Creep rupture properties of nuclear grade versions of type 316 SSand 316 LN SS and their weld metals were examined It was found that, the rupture lives of the weld metals were lower by a factor of 5 to 10 compared to the respective base metals

2 Both base metal and weld metal of 316 LN SS, exhibited better rupture lives compared to type 316 SS base metal and weld metal at identical stress levels

3 The minimum creep rates were lower for the 316 LN SS base and weld metals compared to that for 316 SS

4 The rupture elongations of 316 LN SS weld metal were lower compared to 316 SS weld metal

ACKNOWLEDGEMENTS

The authors wish to acknowledge Dr Placid Rodriguez, Director, IGCAR and Dr Baldev Raj, Director, Metallurgy and Materials Group, IGCAR, for many useful discussions and constant encouragement

REFERENCES

[1] ASME Boiler and Pressure Vessel Code, Code Case N-47, Amer Soc Mech Engrs , New York (1986)

[2] MARSHALL, P , Austenitic Stainless Steels Microstructure and Mechanical Properties. Elsevier Applied Science Publishers, London (1984)

[3] CORUM, J M , ASME J Pressure Vessel Technol **112** (1990) 333

[4] ASME Boiler and Pressure Vessel Code, Code Case N-47, Amer Soc Mech Engrs , New York (1992)

[5] MATHEW, M D ,et al , Trans ASME J Eng Mater Technol **115** (1993) 163

[6] MORRIS, D G HARRIES, D R , Met Sci **12** (1978) 525

[7] MATHEW, M D , et al , Nucl Technol **81** (1988) 114

[8] NAKAZAWA, T , et al , (Proc 6th Int Conf on Pressure Vessel Technology, Beijing, September 11-15,1988), (LIU CENGDIAN, NICHOLS, R.W , Eds), Pergamon Press (1988) 1041

[9] MORRIS, D G , Met Sci **12** (1978) 19

[10] WEISS, B , STICKLER, R., Metall Trans **3** (1972) 851

[11] MATSUO, T et al (Proc Int Conf on High Nitrogen Steels, Lille, May 18-20, 1988), (FOCT, J , HENDRY, A , Eds), Institute of Metals (1989) 213

[12] NAKAZAWA, T , et al , (Proc Int Conf on High Nitrogen Steels, Lille, May 18-20, 1988), (FOCT, J , HENDRY, A , Eds), Institute of Metals (1989) 218

[13] LAI, J K L , Mater Sci Eng **61** (1983) 101

[14] SUNDARARAMAN, D , et al , Metall Trans **27A** (1996) 1175

ASSESSMENT OF CREEP-FATIGUE DAMAGE USING THE UK STRAIN BASED PROCEDURE

S.K. BATE
AEA Technology plc,
Plant Support Services,
Risley, Warrington,Cheshire,
United Kingdom

Abstract

The UK strain based procedures have been developed for the evaluation of damage in structures, arising from fatigue cycles and creep processes. The fatigue damage is assessed on the basis of modelling crack growth from about one grain depth to an allowable limit which represents an engineering definition of crack formation. Creep damage is based up on the exhaustion of available ductility by creep strain accumulation. The procedures are applicable only when level A and B service conditions apply, as defined in RCC-MR or ASME Code Case N47. The procedures require the components of strain to be evaluated separately, thus they may be used with either full inelastic analysis or simplified methods. To support the development of the UK strain based creep-fatigue procedures an experimental program was undertaken by NNC to study creep-fatigue interaction of structures operating at high temperature. These tests, collectively known as the SALTBATH tests considered solid cylinder and tube-plate specimens, manufactured from Type 316 stainless steel. These specimens were subjected to thermal cycles between 250°C and 600°C. In all the cases the thermal cycle produces tensile residual stresses during dwells at 600°C. One of the tube-plate specimens was used as a benchmark for validating the strain based creep fatigue procedures and subsequently as part of a CEC co-operative study. This benchmark work is described in this paper. A thermal and inelastic stress analysis was carried out using the finite element code ABAQUS. The inelastic behaviour of the material was described using the ORNL constitutive equations. A creep fatigue assessment using the strain based procedures has been compared with an assessment using the RCC-MR inelastic rules. The analyses indicated that both the UK strain based procedures and the RCC-MR rules were conservative, but the conservatism was greater for the RCC-MR rules.

1. INTRODUCTION

To support the development of the UK strain based creep-fatigue procedures[1] an experimental program was undertaken by NNC to study creep-fatigue interaction of structures operating at high temperature. These tests, collectively known as the SALTBATH tests considered solid cylinder and tube-plate specimens, manufactured from Type 316 stainless steel. These specimens were subjected to thermal cycles between 250°C and 600°C. In all the cases the thermal cycle produce tensile residual stresses during dwells at 600°C.

One of the tube-plate specimens was used as a benchmark for validating the strain based creep fatigue procedures. The benchmark work is described in this paper. A thermal and inelastic stress analysis was carried out using the finite element code ABAQUS[2]. The inelastic behaviour of the material was described using the ORNL constitutive equations[3].

A creep fatigue assessment using the strain based procedures has been compared with an assessment using the RCC-MR elastic and inelastic rules.

This benchmark was subsequently used in a CEC co-operative exercise in the simulation of an experiment[4]. The predictions of inelastic calculations using various constitutive equations and non-linear finite element programs are compared. Some of these results were then used in a further CEC benchmark exercise on laws for damage assessment[5]. The predictions of the UK strain based method and RCC-MR are shown.

2. DESCRIPTION OF BENCHMARK

The specimen used for the benchmark was identified as a 'Type 2 Saltbath specimen' and is shown in Figure 1. The right-hand side (as shown in the figure), in particular the region around the 5mm radius, is intended to represent a typical geometrical feature of a tube-tubeplate junction. The left-hand side is a removable plug, allowing periodic inspection of the interior surface, and is not intended to be of structural significance.

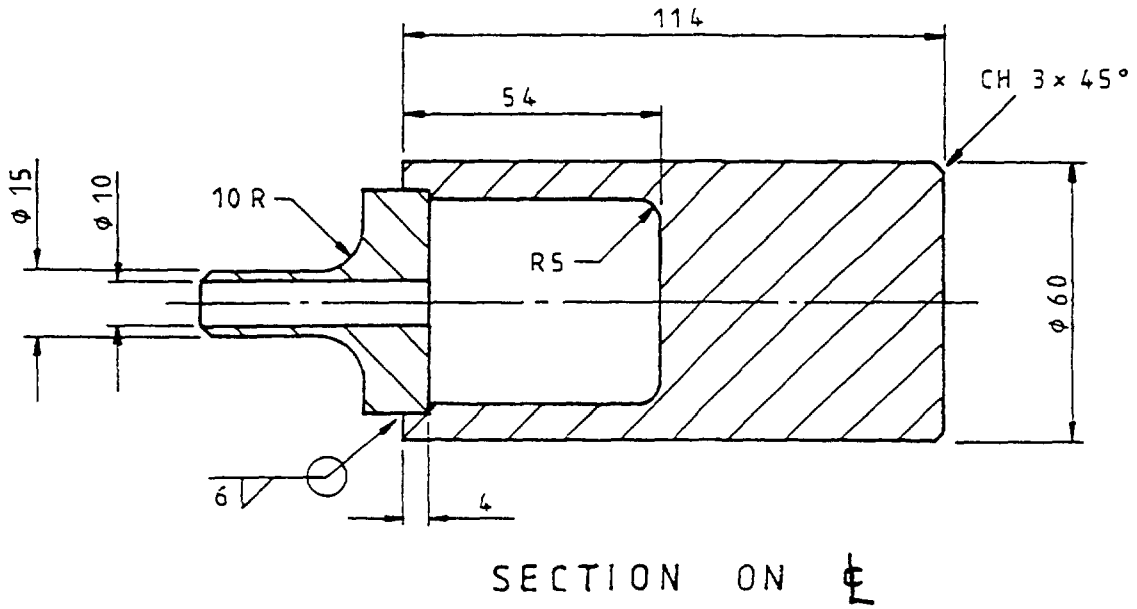

CYCLE DESCRIPTION

Step	Event
0	Initial condition - Uniform Temperature 600°C
1	Immerse in heat treatment salt at 250oC fro 30 seconds (step change in fluid temeprature). Heat transfer coefficient on external surfaces 3000 W/m2K. Internal surfaces adiabatic
2	Heat in air, fluid temperature 600oC. Heat transfer coefficient 80 W/m2K on external surfaces. Internal surfaces adiabatic
3	Hold at uniform temperature of 600oC for 15 hours
4	As step 1

Note

The design of this testpiece is such that discontinuity stresses at each end of the chamber have decayed to low levels at the mid length of the chamber

FIG. 1. Geometry of Tube-Plate Test Piece (Type 2) [7]

For the benchmark problem, the applied thermal cycle was a thermal downshock from 600°C to 250°C for 30 seconds, followed by heating at 600°C for one hour to attain a uniform temperature before a hold time of fifteen hours at 600°C. The thermal shocks were applied by immersing the specimens in heat treatment salt and then slowly re-heating in air to attain a uniform temperature at the dwell period.

3. FINITE ELEMENT ANALYSES

The specimen has been modelled using eight noded axisymmetric elements with symmetry conditions applied, see Figure 2. The finite element program ABAQUS was used for the analyses. The desired mesh refinement was obtained after making several elastic analyses and validating the results with those obtained in a previous analysis[6].

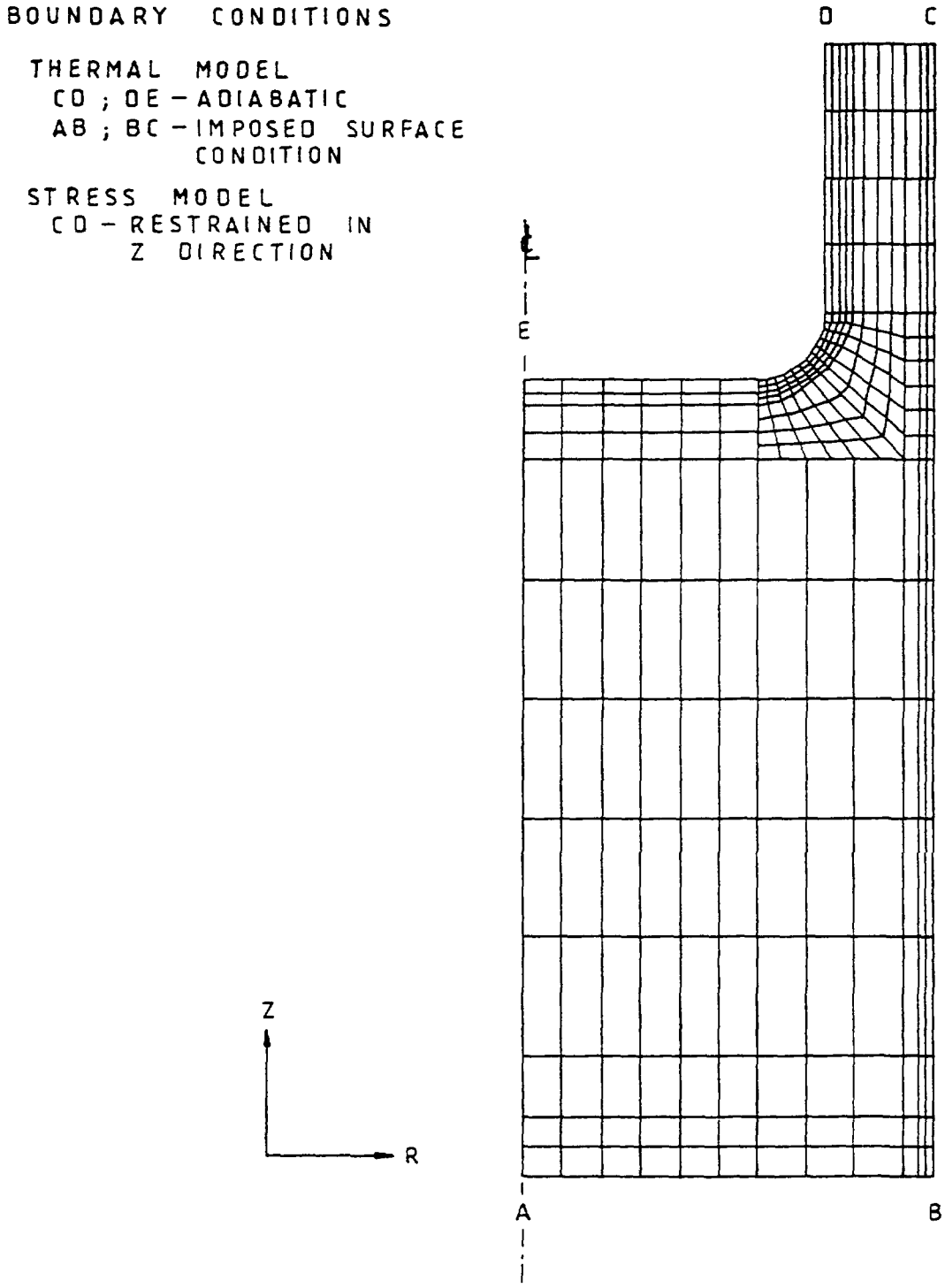

FIG.2. Finite Element Model and Boundary Conditions Applied

The finite element analysis consisted of :

(a) A thermal analysis (using ABAQUS DCAX8 elements): For the thermal cycle described previously a thermal analysis was completed and the results written to file to be used for the subsequent stress analyses.

(b) Inelastic Stress Analyses (using ABAQUS CAX8R reduced integration elements): Two cases were considered to examine the sensitivity of the ORNL constitutive equations with different plasticity parameters. Note, the parameters normally recommended for use with the ORNL constitutive equations are based upon 10th cycle data.

CASE 1 - This was based upon the 100th cycle curve[7]. An elastic-plastic slope was drawn based upon the slope of the curve and the yield stress was derived from the intersection of the elastic plastic slope with the elastic slope. The plastic slope required in ABAQUS was derived from these values.

The analysis used the alpha reset option and all the parameters were temperature independent. The initial and cyclic properties were assumed identical.

CASE 2 - This was also based upon the 100th cycle curve but an elastic-plastic slope based on the 10th cycle curve was used. The yield stress was derived by the intersection of the elastic and elastic plastic slope. The same conditions as case 1 were then assumed.

4. RESULTS OF THE ANALYSES

The rapid thermal loading of the outside surface can be seen in Figure 3. This leads to yielding of the whole area of this surface within a second of the downshock. There is also a small amount of yielding at the fillet. The faster cooling of the tube relative to the plate section leads to bending at the fillet section, see Figure 4.

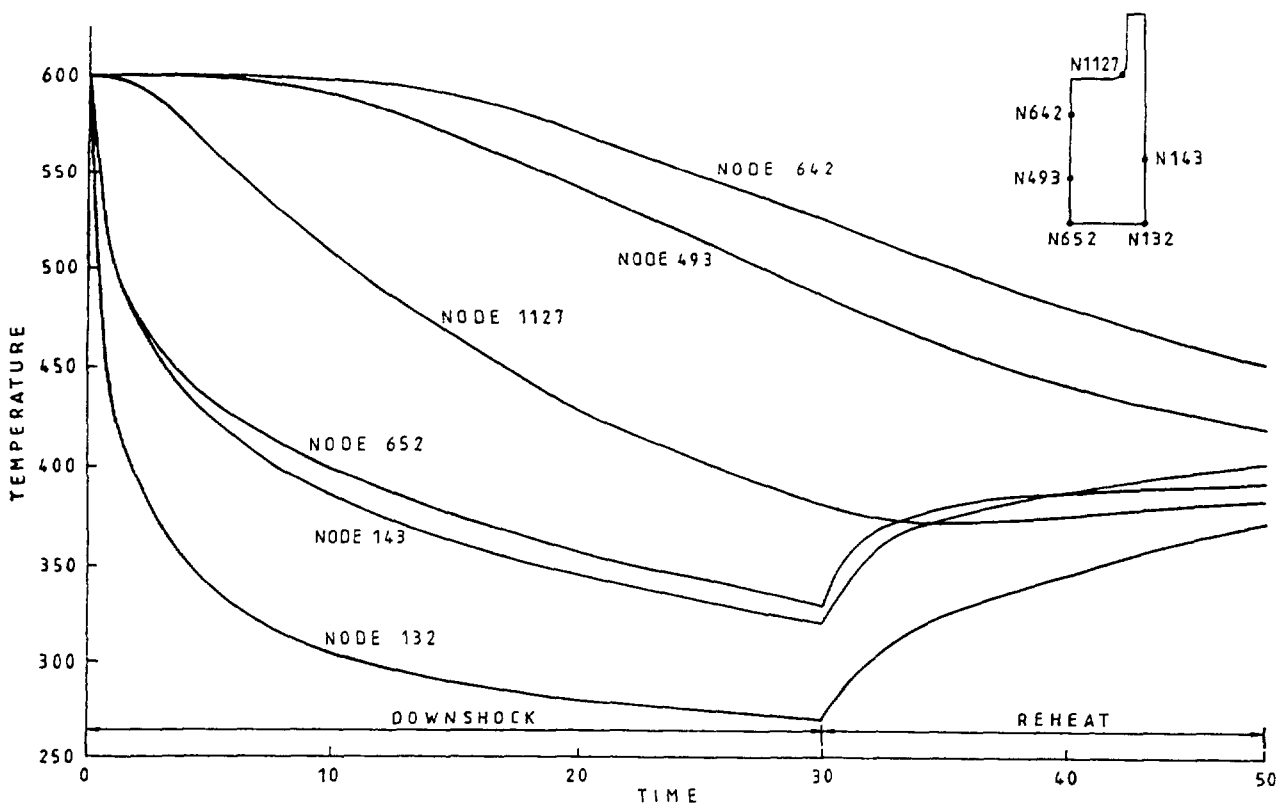

FIG. 3. Plot of Temperature against Time

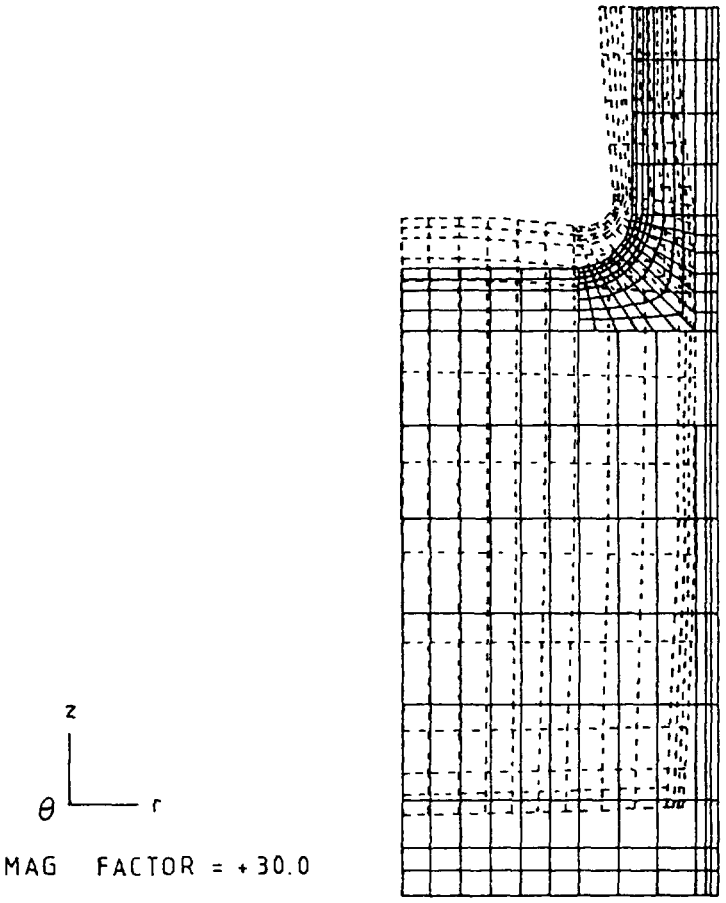

FIG. 4. Displacement Plot

Figure 5 shows the results obtained after five stress/strain cycles have been applied for CASE 2. The principal stress histories at the peak stress position are shown for the two cases in Figures 6 and 7. Figure 8 shows a hysteresis plot of the equivalent (Mises) stress and strain.

The results indicate that in the first second of the transient significant 'skin' stresses occur in the specimen. Shortly after this time, the plastic strain at the fillet accumulates as the secondary stresses start to dominate. This effect can be seen in the principal stress histories at the fillet. These figures show that the principal stress tangential to the fillet dominates throughout the cycle except at unloading. Both CASES indicate that through-wall yielding occurs at the fillet and all the outside surface. They show a peak stress at the fillet 15 seconds into the transient. The magnitude and distribution of inelastic strain within the specimen is dependent on the material parameters used in the ORNL constitutive equations.

The results of this analysis were compared in a CEC benchmark exercise between six participants, each using different combinations of constitutive equations and non-linear finite element programs. These combinations are shown in Table I with the predictions of strain range at a point where it is maximised.

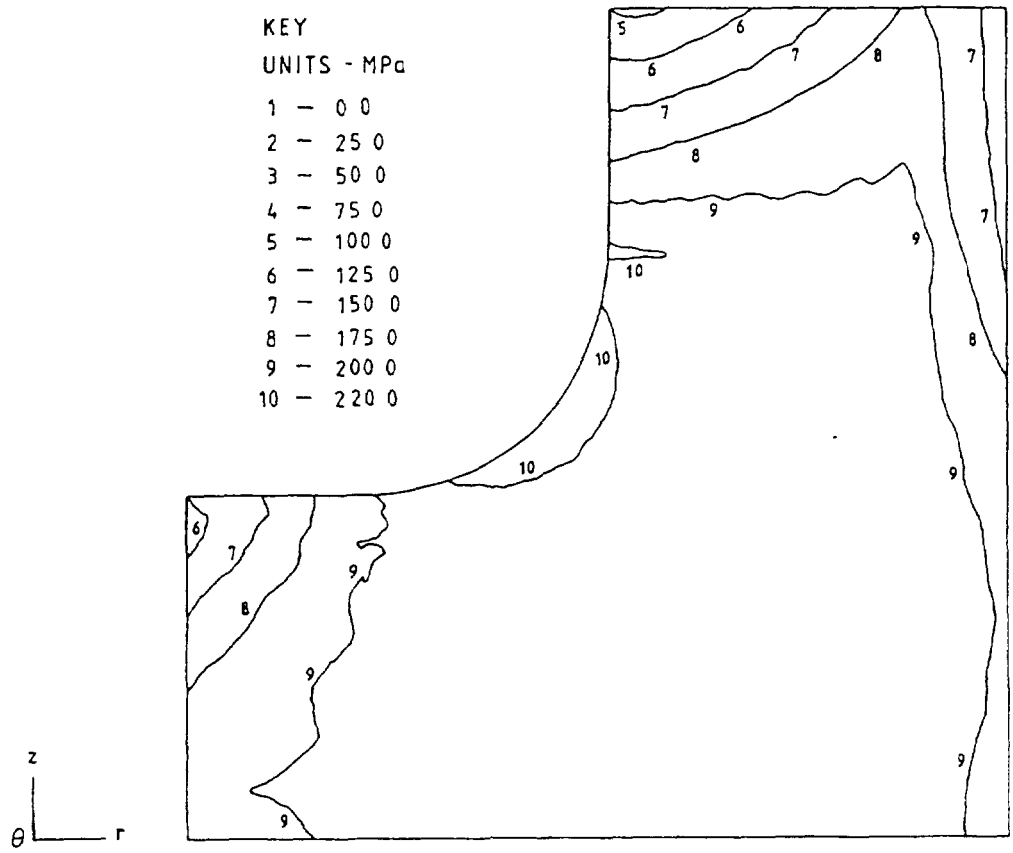

FIG 5a Von Mises Stress Distribution / Peak Stress at Fillet During Sixth Operational Cycle, CASE 2

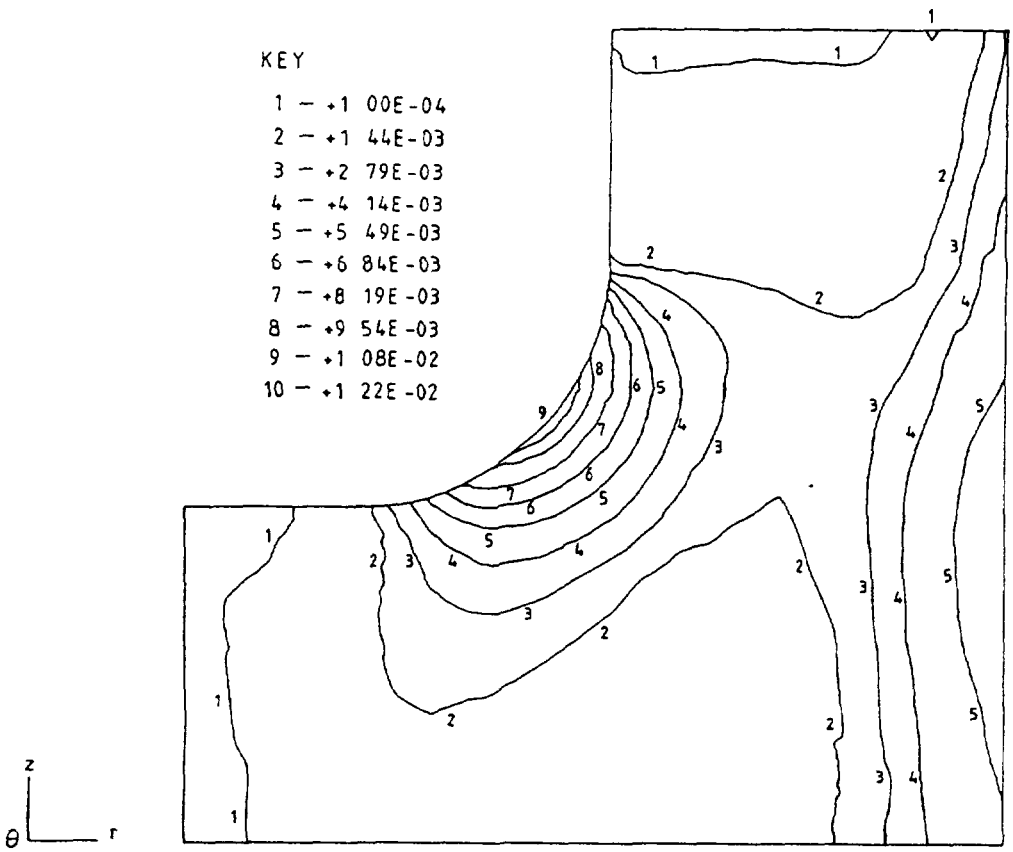

FIG 5b Plastic Strain Magnitude / Peak at Fillet During Sixth Operational Cycle, CASE 2

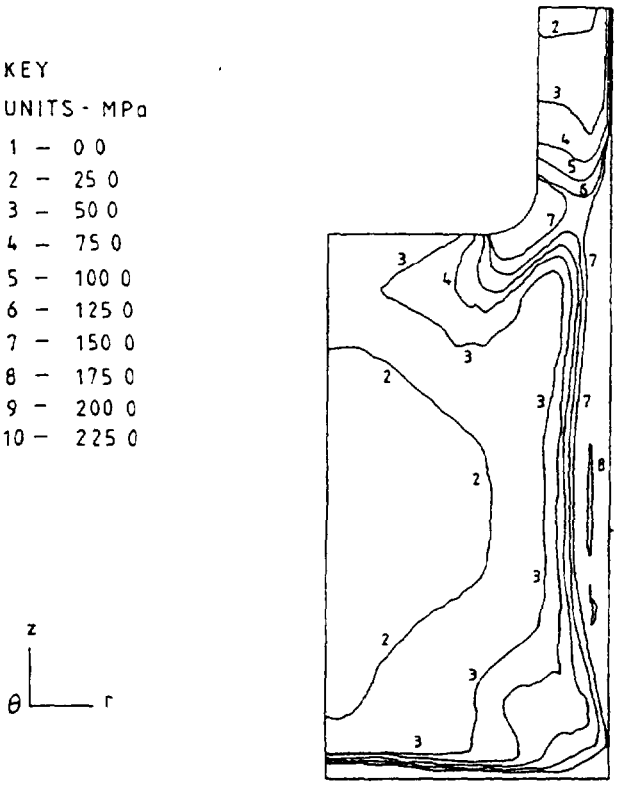

FIG. 5c. Von Mises Stress Distribution / At End of Reheat During Sixth Operational Cycle, CASE 2

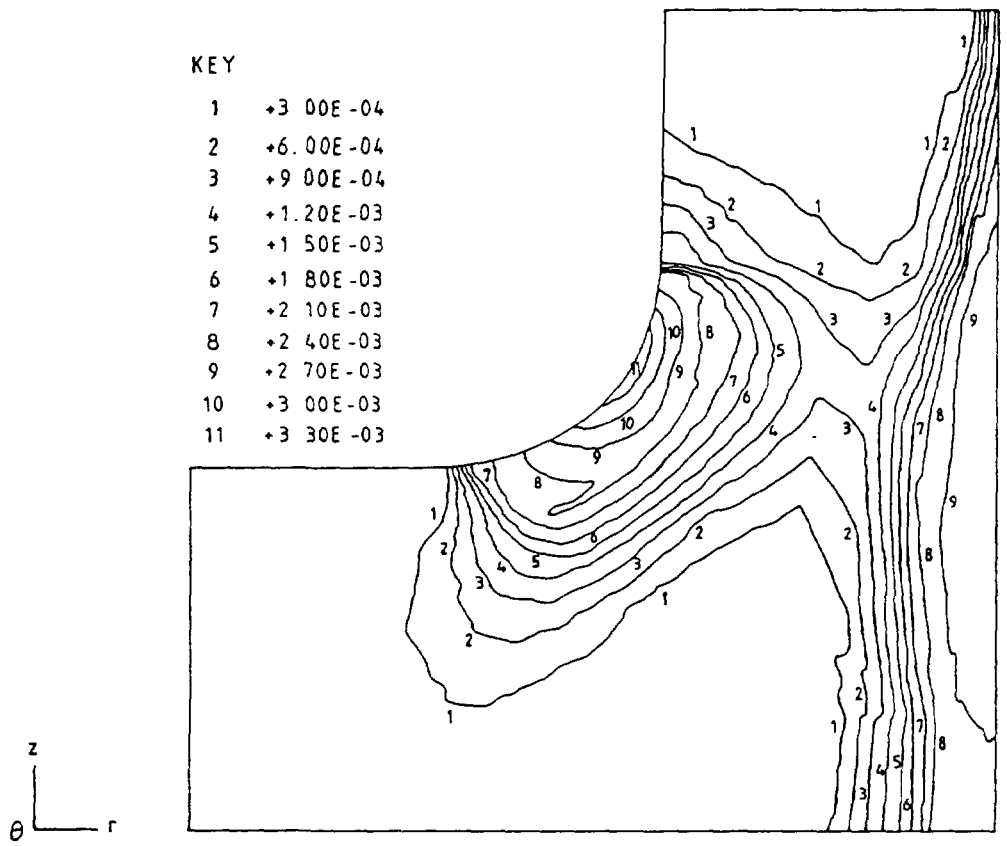

FIG. 5d. Creep Strain Magnitude After Five Cycles (Total Hold Time = 75 hours), CASE 2

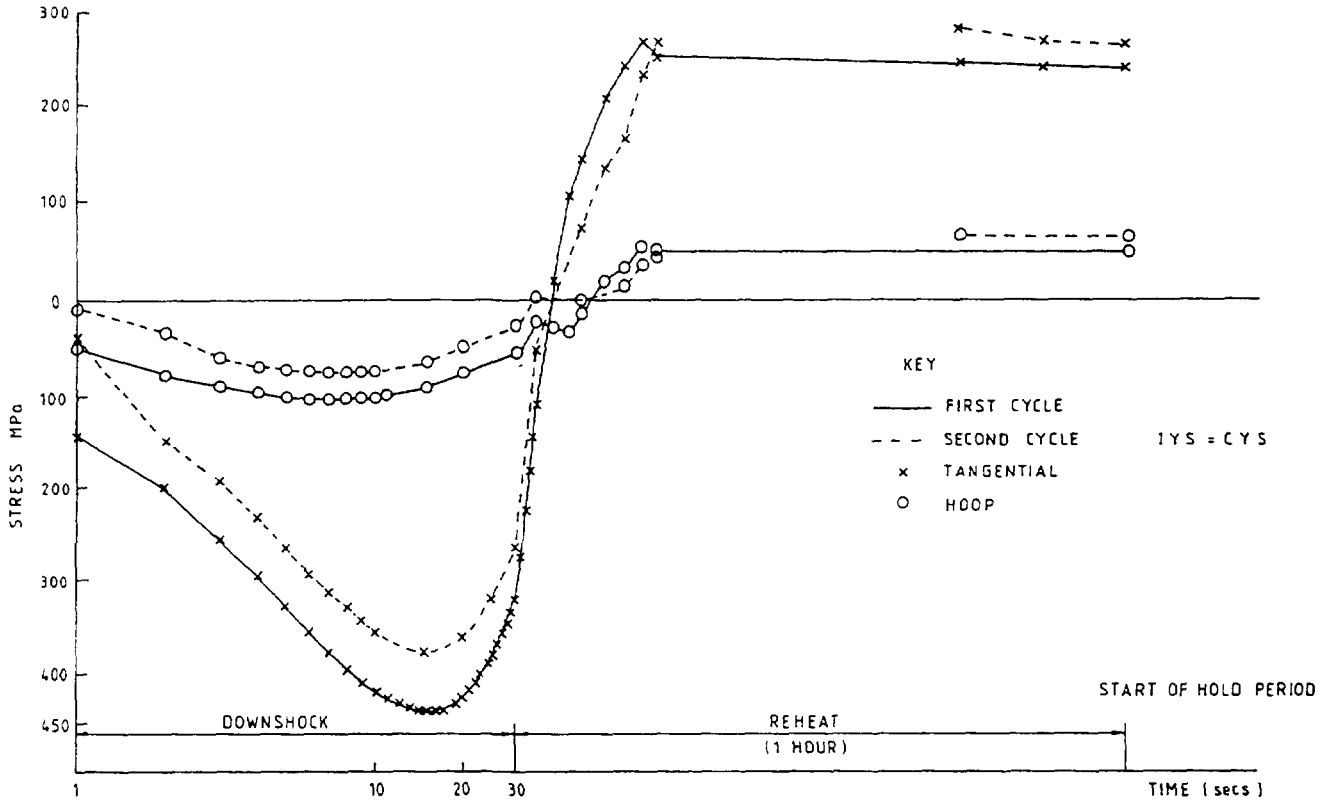

FIG. 6. Principal Stress History Over Downshock and Reheat (Using Hundreth Cycle Data Hundreth Cycle Plastic Slope)

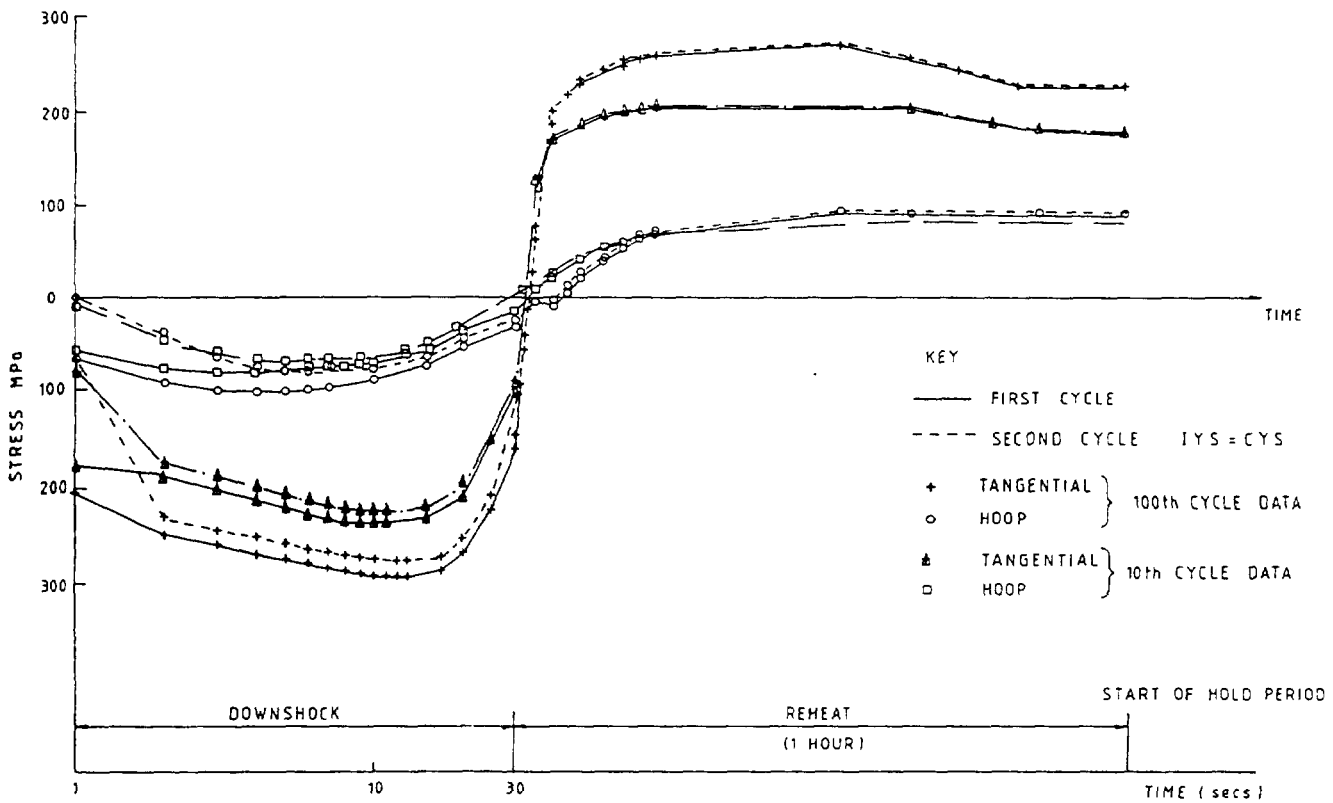

FIG 7 Principal Stress History Over Downshock and Reheat (Using Hundreth Cycle Data Tenth Cycle Plastic Slope)

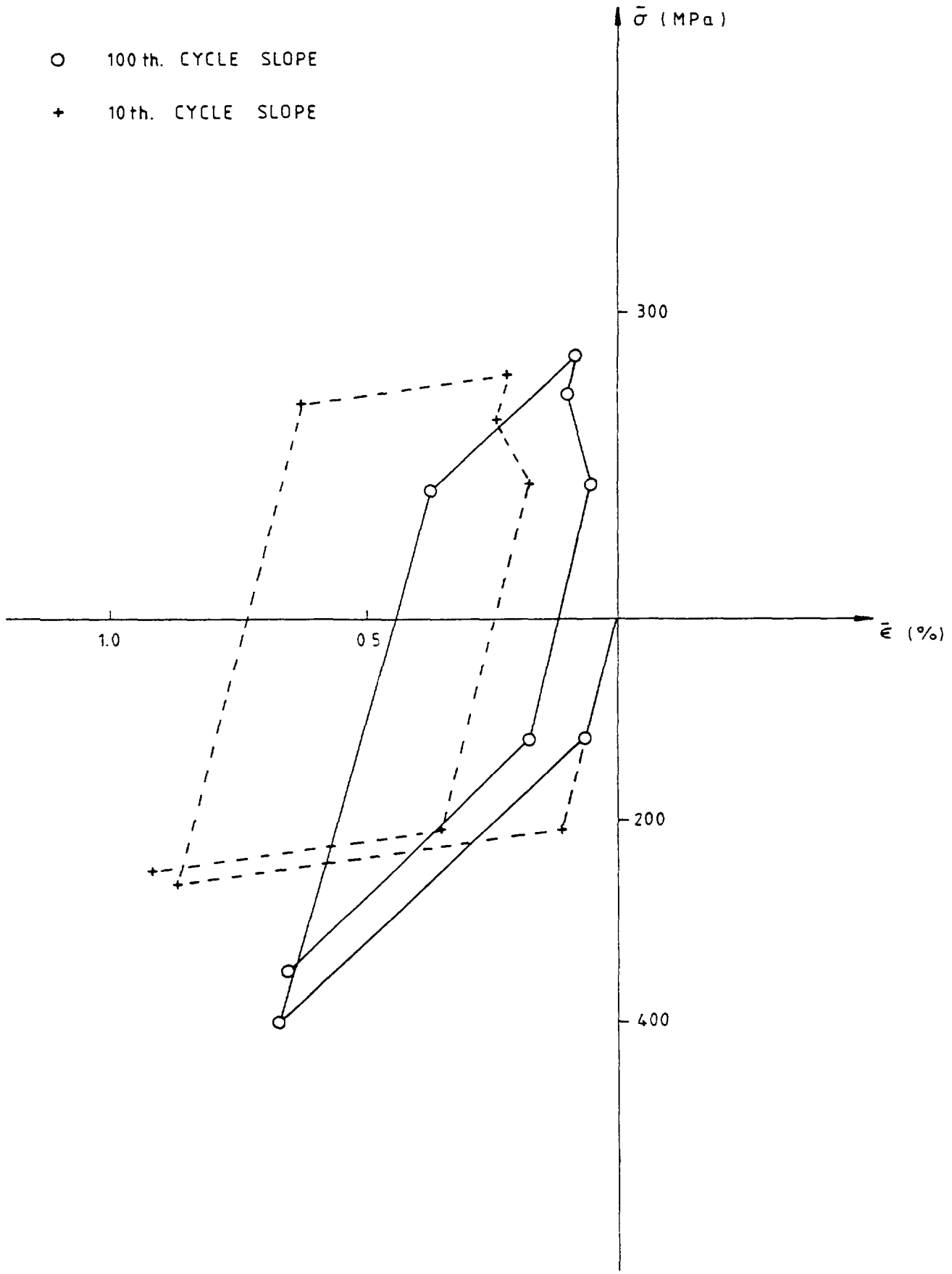

FIG. 8. Stress-Strain Hysteresis Loop (Using Hundreth Cycle Curve)

TABLE I STRAIN RANGES IN % AT MAXIMUM POINT [4]

FE CODE	MATERIAL MODEL		CYCLE					
			1	2	3	4	5	6
ABAQUS	ORNL	CASE 1	0 612				0 6014	
		CASE 2	0 748				0 7157	
ABAQUS	Fast Reactor State Variable		0 724	0 623	0 607	0 599	0 594	0 590
ANSYS	Bilinear Kinematic		0 63	0 63	0 63	0 63	0 63	
ABAQUS	Interatom		0 943	0 963	0 916	0 918	0 922	
SYSTUS	Chaboche		0 87	0 79	0 87	0 74	0 72	0 78
INCA	Chaboche		0 688	0 649	0 627			

Four solutions agreed fairly closely with a steady state maximum strain range of about 0 6% Two further solutions had values of about 0 72% and one solution 0 9% Examination of the results suggested that the reason for the differences lay in the basic test data used to form material parameters

Further comparison was made of the equivalent stress at four positions of the stress strain cycle maxima during the downshock and reheat, and values at the start and end of the hold period These results are shown in Table II

TABLE II VON MISES EQUIVALENT STRESSES (MPa) MAXIMA DURING DOWNSHOCK AND REHEAT, VALUES AT START AND END OF HOLD PERIOD [4]

FE CODE	MATERIAL MODEL	STAGE	CYCLE			
			1	3	5/6	12
ABAQUS	ORNL CASE 2	Downshock			250	
		Reheat			240	
		Start of Hold			197 3	
		End of Hold			160 6	
ABAQUS	Fast Reactor State Variable		178 2	234 8	250 1	263 7
			220 1	220 0	221 4	223 8
			220 1	220 0	221 4	223 8
			130 3	148 6	159 9	172 3
ANSYS	Bilinear Kinematic		314 0	331 0	346 0	
			137 0	123 0	108 0	
			84 9	72 8	61 1	
			76 9	65 4	54 4	
ABAQUS	Interatom		166 4	178 6	176 6	
			161 0	181 7	193 3	
			148 0	170 3	184 3	
			138 2	160 2	174 0	
SYSTUS	Chaboche				207 6	
					210 2	
					-	
					113 6	
INCA	Chaboche		195 3	244 1		
			180 1	239 1		
			-	-		
			132 3	177 8		

The results in Table II show, apart from the analysis using the bilinear kinematic model, a spread of up to 25% over all the stages. The most important aspect concerns the hold period when most of the time dependent (creep) damage is to be expected. The exact damage comparison would be dependent upon the specific damage rule used. This is related to in the next section where damage laws are compared.

Similar differences are also evident for the amount of relaxation. It is thought likely that the substantial differences are due to discrepancies in the underlying material data related to the creep tests.

5. CREEP FATIGUE DAMAGE ASSESSMENT

Using the UK strain based rules and RCC-MR[8] creep-fatigue rules an estimate of the design life has been based upon the results obtained after five cycles had been applied. Due to the effects of stress relaxation and creep a stable cycle had not been obtainable but the difference between each stress strain cycle was not causing a considerable difference in the life predicted by each cycle.

The estimates of design life are shown in Table III.

TABLE III. COMPARISON OF DESIGN LIFE PREDICTIONS

CASE	UK Strain Based Method				RCC-MR			
	Strain Range (%)	Fatigue Damage /Cycle	Creep Damage /Cycle	Allowable Design Cycles	Strain Range (%)	Fatigue Damage /Cycle	Creep Damage /Cycle	Allowable Design Cycles
1	0.7189	0.00128	0.00814	78	0.6014	0.0027	0.1098	9
2	0.8347	0.00214	0.00573	46	0.7157	0.004	0.0451	18

Notes: 1. UK procedures use Rankine strain range to evaluate fatigue damage

2. RCC-MR procedures use Von Mises strain to evaluate fatigue damage.

For CASE 1, a prediction of 78 cycles was obtained using the UK procedure whereas CASE 2 predicted a life of 46 cycles. This difference is due to the strain range (hence fatigue damage) predicted by each case. The difference in the amount of creep damage has no effect in the UK method but RCC-MR predicts a reduction in life due to the increased creep damage.

Further comparison can be drawn from the CEC benchmark exercise[5] where results from several of the inelastic analyses completed in Section 4 were used to evaluate creep fatigue damage using the UK strain based method and the RCC-MR rules. The predicted design life is shown in Table IV.

No cracks had been observed in the experimental specimens after 280 cycles. The results therefore indicate that both procedures, with the exception of the Chaboche and UK strain based method, provide a conservative estimate of the design life, with the UK strain based method providing a less conservative estimate.

The results show that the predicted failure can differ greatly depending on the constitutive model used. The main difference in this case being caused by the predicted stresses and strains during the steady state (creep) period. The creep damage assessment which is based on the viscoplastic strain for the strain based method was generally less severe than the stress based method of RCC-MR. The creep

TABLE IV. PREDICTED DESIGN LIFE USING VARIOUS CONSTITUTIVE MODELS [5]

Constitutive Model	Damage Assessment Model					
	UK Strain Based Method			RCC-MR		
	Cycles to Failure	Fatigue Damage per Cycle	Creep Damage per Cycle	Cycles to Failure	Fatigue Damage per Cycle	Creep Damage per Cycle
Interatom	177	5.65×10^{-3}	1.20×10^{-4}	48	1.24×10^{-2}	3.59×10^{-3}
Chaboche (SYSTUS)	473	2.11×10^{-3}	1.59×10^{-5}	71	6.25×10^{-3}	3.33×10^{-3}
ORNL CASE 2	46	2.15×10^{-3}	5.73×10^{-3}	18	4.13×10^{-3}	4.51×10^{-2}

damage per cycle was found to be negligible with the unified constitutive models (Interatom and Chaboche model. On the contrary, the non-unified ORNL model, the strain was non negligible and hence creep damage was more significant.

The other significant comparison came from the predicted mechanism governing damage. For the strain based damage law, the unified constitutive models predicted pure fatigue cracks, whereas the ORNL model predicted creep fatigue interaction.

Using the RCC-MR damage law, creep fatigue cracks were predicted in all three cases, with, however dominating creep damage for the ORNL model and dominating fatigue damage for the Interatom model. Unfortunately none of the specimens have been tested until crack initiation and these differences can not be checked.

6. CONCLUDING REMARKS

The conclusions of this analysis are reflected by the CEC benchmark studies and therefore it is worthy that some of the conclusions from these studies are reiterated here.

Constitutive Equations:

The simple kinematic model of plasticity, though agreeing with several other models with respect to strain range, gave very discrepant results for stresses at extreme stages of the cycle, including the hold period, and also in the distributions of stresses at different stages. This is considered to arise principally from an inappropriate relation between mean stress and stain in cycling. The model is therefore **not** recommended for other severe thermally loaded problems involving creep.

In view of the differences arising from use of different material data the value of comparison is reduced. Clearly a consistent base of raw data should be obtained for refitting of all constitutive equations intended for future use and development.

Damage Models:

Both the strain based and RCC-MR models appear to be conservative.

A characteristic feature is that the unified constitutive models predict a pure fatigue failure mechanism whilst the non-unified ORNL model predicted a creep-fatigue mechanism. The differences in the predicted stresses and strains during creep meant that the unified models generally predicted lower creep damage than the non-unified models.

REFERENCES

[1] PICKER, C., "UK Development of a Strain-Based Creep Fatigue Assessment Procedure for the Evaluation of Creep and Fatigue Damage in Fast Reactor Design", IAEA Technical Committee Meeting on Creep Fatigue Damage Rules to be Used in Fast Reactor Design, Manchester (1996)

[2] HIBBIT, D et al., ABAQUS Version 4.7

[3] CORUM, J.M., "Interim Guidelines for Detailed Inelastic Analysis of High Temperature Reactor System Components", ORNL-5014.

[4] WHITE, P.S., "A Co-operative Benchmark Exercise in the Simulation of an Experiment - Inelastic Analysis of Type 2 SaltBath Specimens", CEC Contract Number RA1.0161.UK.

[5] CABRILLAT, M.T., "Benchmark on Laws for Damage Assessment", CEC Contract Number RA1.CT91.0195

[6] BESTWICK, R.D.W., HUGHES, P.M., "Development of a Tube-Tubeplate Testpiece for use in the Saltbath Creep-Fatigue Test Programme", UK Fast Reactor Document

[7] BESTWICK, R.D.W., BUCKTHORPE, D.E., "Data for use in Assessments of Saltbath Creep Fatigue Tests", UK Fast Reactor Document

[8] RCC-MR Addendum No. 1 - November 1987

PREDICTION OF RATCHETING BEHAVIOUR OF 304 SS CYLINDRICAL SHELL USING THE CHABOCHE MODEL

HYEONG-YEON LEE, JONG BUM KIM,
JAE-HAN LEE, BONG YOO
Liquid Metal Reactor Development Team,
Korea Atomic Energy Research Institute,
Taejon, Republic of Korea

Abstract

Ratcheting, that is, a progressive cyclic inelastic deformation can occur in a component subjected to thermal secondary stress, mechanical stress or both in the presence of a primary stress. The circumferential plastic strain may be accumulated with the increase of the number of cycles when a cylinder is subjected to a temperature front moving cyclically in the axial direction. This phenomenon of liquid surface induced thermal ratcheting is important in the design of liquid metal reactor. The ratcheting behavior of a thin-walled 304 stainless steel cylinder under axially moving temperature distribution was analyzed using the constitutive theory of Chaboche. The constitutive model was implemented as a user subroutine of ABAQUS and it was verified through the comparison with the exact solutions for the uniaxial cyclic loading and test results available in the literature for the cylinder. In addition, ratcheting in pressurized push-pull pipes under loading conditions of ± 1% axial strain with steady hoop stress was analyzed with Chaboche model. It is shown that the elastic-plastic analysis using Chaboche model can evaluate properly the progressive strain accumulation under secondary cyclic loads.

1. INTRODUCTION

The operating condition of LMR(Liquid metal reactor) is generally characterized as high temperature of 500 ~ 550°C and low pressure of 1 ~ 10 bar. The temperature difference between inlet and outlet of reactor vessel is about 150°C , which is far higher than that of 30°C for light water reactor. Therefore, high level of alternating secondary stresses will act in LMR components.

In the design of high temperature structures which are subjected to severe thermal transients of liquid sodium, the progressive accumulation of deformation by thermal ratcheting should be prevented because excessive deformation may cause unacceptable radial deformation. The ratcheting in hollow cylinders subjected to an axial movement of a longitudinal temperature distribution is well known as a representative case. This type of ratcheting behavior under thermal stress alone is very important in the design of LMR components because the primary stress in those high temperature structure components is low. Among several types of ratcheting, the Bree type ratcheting has been mainly noticed, in which the ratchet strain occurs in combination of steady primary stress and cyclic secondary stress. This ratcheting behavior has been considered in the design codes such as ASME Code Case N-47[1], RCC-MR[2] and Japanese code[3,4].

In the present study, Chaboche model has been used to represent the material behavior of cyclic plasticity and implemented as ABAQUS user subroutine UMAT. An elastic-plastic analysis with Chaboche constitutive model has been performed for a simple structure of cylindrical shell. The analysis results show that thermal stresses are induced by axially moving temperature from 550°C to 350°C along the length of the shell and the plastic ratchet deformation increases cycle by cycle in the same pattern with the same amount of residual deformation. The validity of user subroutine UMAT has been verified with the exact solutions for uniaxial loading cases.

In the mean time, the integrity of pressurized vessels and large piping runs is of particular concern, especially when they are subjected to high strain, low cycle fatigue conditions in case of seismic excitations. Stresses due to both pressure and seismic loads are classified within the code as

primary stresses[1]. Experimental evidence, however, shows that the failure mode of pipework subjected to reversed dynamic loads is by ratcheting and fatigue[5]. It could therefore be argued that seismically induced stresses should be treated as secondary rather than primary. In the present study, strain-controlled cyclic analysis with push-pull conditions of ±1% axial strain for the cylinder has also been performed and the ratchet behavior has been evaluated.

2. THEORETICAL BACKGROUND

The constitutive modeling of cyclic plasticity has made considerable progress during the last two decades. One of the unsolved difficulties concerns the problem of ratcheting. The description of ratcheting in terms of constitutive equations is mainly related to kinematic hardening which corresponds to a translation of elastic domain of equipotential surface in stress space during viscoplastic flow. The development of an efficient constitutive model and analysis program for the prediction of ratcheting generally requires a lot of time and endeavor.

The viscoplastic constitutive theory proposed by Chaboche assumes a yield condition and the assumed normality of the infinitesimal strain rate to the yield surface defines the structure of the flow rule. The model considered is of the overstress type with hardening as well as recovery terms in the evolutionary equations of the internal variables. Based on the general viscoplastic relations, Chaboche model can be described as follows[6-8]. Under the assumptions of small strain and small rotations,

the total strain rate($\dot{\varepsilon}$) is the sum of the elastic($\dot{\varepsilon}^e$), inelastic ($\dot{\varepsilon}^p$) and thermal strain rates($\dot{\varepsilon}^{th}$).

$$\dot{\varepsilon}_{ij} = \dot{\varepsilon}^e_{ij} + \dot{\varepsilon}^p_{ij} + \dot{\varepsilon}^{th}_{ij} \tag{1}$$

The elastic strain rate and the stress rate are related by Hooke' s law,

$$\dot{\sigma}_{ij} = E_{ijkl}\,\dot{\varepsilon}^e_{kl} + T\frac{\partial E_{ijkl}}{\partial T}\,\dot{\varepsilon}^e_{kl} \tag{2}$$

The thermal strain rate is expressed as

$$\dot{\varepsilon}^{th}_{ij} = \gamma \dot{T} \delta_{ij} \tag{3}$$

where γ is temperature dependent material parameter.

The inelastic strain rate is governed by a flow law,

$$\dot{\varepsilon}^p_{ij} = f(J_2(\Sigma_{kl}), \kappa, T)\Sigma'_{ij}\,, \tag{4}$$

where

$\Sigma_{ij} = \sigma_{ij} - \alpha_{ij}$ is the difference between the applied stress σ and the back stress α,

and $\Sigma'_{ij} = \sigma_{ij} - \alpha'_{ij}$,

$$f = \frac{3}{2}\frac{p}{J_2(\Sigma_{ij})}\,, \tag{5}$$

$$p = \frac{J_2(\Sigma_{ij}) - \kappa - k}{K}^{n} \tag{6}$$

A prime mark on second order tensor is used to indicate the deviatoric part. The model can be described by kinematic equations for the internal state variables α'_{ij},

$$\alpha'_{ij} = h(\sigma'_{kl}, \alpha'_{kl}, \kappa, \varepsilon_{kl}, p, T)\varepsilon^{p\prime}_{ij} - r(\sigma'_{kl}, \alpha'_{kl}, \kappa, \varepsilon_{kl}, p, T)\,\alpha'_{ij} \tag{7}$$

$$h = \frac{2}{3}C,$$

$$r = \gamma\, p$$

and a set of arbitrary number of isotropic hardening variables κ

$$\kappa = \Gamma(p,T)\,p + \Theta(p,T)\,T \tag{8}$$

The nonlinear functions f, h, r, Γ, and Θ depend on κ and temperature, T, and possibly additional external variables on the invariants of σ' and α',

$$J_2(\sigma') = \frac{1}{2}\sigma' : \sigma', \tag{9a}$$

$$J_2(\alpha') = \frac{1}{2}\alpha' : \alpha', \tag{9b}$$

$$J_2(\Sigma_{ij}) = \frac{1}{2}\Sigma_{ij}\Sigma_{ij} \tag{9c}$$

and an accumulated variable η, which may be chosen according to either strain-hardening,

$$\eta = \int (d\varepsilon'^{p} : d\varepsilon'^{p}) \tag{10}$$

or work hardening,

$$\eta = \int \sigma' : d\varepsilon'^{p} \tag{11}$$

The model under consideration uses only one drag stress.

$$\Gamma = b(Q - \kappa). \tag{12}$$

where K, n, C, γ, b, Q, and κ are material parameters dependent on temperature. The above formulation on viscoplastic constitutive equation can be applied for the analysis of cyclic plasticity, thermal ratcheting with or without creep effect and creep-fatigue.

3. ANALYSIS OF THERMAL RATCHETING

3.1. Loading condition

In order to simulate LMR operating condition, the test by Tanaka et al[9,10] was performed with a test cylinder moving up into Ar gas and down into the sodium pool of 350°C in the axial direction. The ratchet behavior under the test condition was simulated in the present analysis. The cylinder shown in Fig.1 has an initial temperature of 550°C. At t = 0, the bottom for the cylinder reaches the sodium pool of 350°C and the cylinder submerges continuously into the pool with the

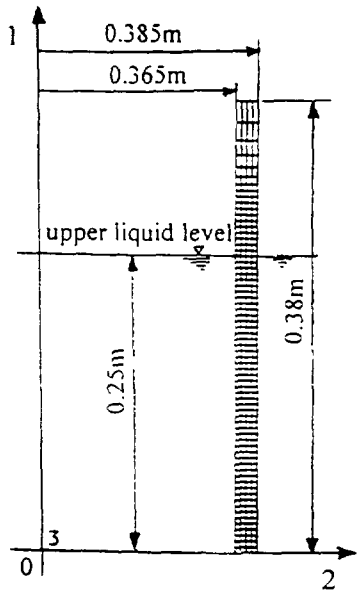

FIG. 1. Finite element model

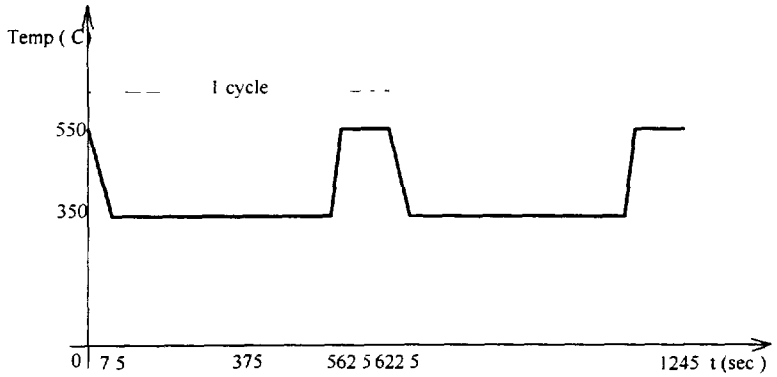

FIG. 2. Variation of bulk temperature with time

dipping speed of 0.04 m/min. As soon as the cylinder reaches the depth of 0.25 m, it is lifted with the rate of 0.08 m/min. After the whole cylinder is lifted into the Ar gas atmosphere, it is heated at 550°C during 1 minute intensively by electric heater in order to reach the target temperature. It is assumed that heat transfer during the heating period is dominated by convection. This type of heating and cooling cycles are repeated 10 times and the ratcheting deformation was computed. The bulk temperature near the cylinder varies from 350°C to 550°C as shown in Fig. 2. It should be noted that heat transfer coefficients for the elements below the height of 0.25m will vary continuously with time as the cylinder submerges into sodium pool, is lifted into Ar gas atmosphere and fully withdrawn into heating environments.

3.2. FE modeling

The analysis model of Fig.1 is 1/10 scale of the reference LMR design and the dimensions are shown in the figure. The model consists of axisymmetric 8-node isoparametric 272 elements with totally 961 nodes. The element types for thermal and stress analyses are DCAX8R and CAX8R of ABAQUS code. The surface of cylinder will be in contact with sodium repeatedly below the height of 0.25 m. It is assumed that creep effect is negligible with short duration of thermal loading, and inelastic deformation will be caused by the plastic properties of the material. The material properties used in the analysis are listed in Table 1. The dependence of material properties upon temperature over the range of 350~550°C was neglected, and the constant values were used in the analysis.

3.3. Thermal stress analysis

Since the bulk temperature varies continuously with time during the thermal cycles, the variations of bulk temperature and heat transfer coefficients should be considered in thermal analysis. The lower parts of the cylinder below the height of 0.25m will be subjected to severe cyclic thermal loading. In this analysis, the variations of the bulk temperature and heat transfer coefficients with time were considered.

3.4. Verification of user subroutine UMAT

Based on the previous theoretical background, Chaboche constitutive model has been implemented in ABAQUS user subroutine, UMAT so that general high temperature analysis may be

TABLE 1. MATERIAL PROPERTIES OF 304 STAINLESS STEEL

Parameter	Value
thermal conductivity	21 W/m°C
specific heat	500 Wsec/kg°C
density	7.9 kg/m^3
Young`s modulus	163.3 GPa
Poisson ratio (ν)	0.34
thermal expansion coeff.	$17.9x10^{-6}$ 1/°C

possible. Since equations (2), (6), (7) and (8) reduce to the first order differential equations with initial conditions, exact solutions can be obtained with Runge-Kutta method in uniaxial loading problems. In the present study, uniaxial hardening analysis and uniaxial cyclic hardening analysis were performed to verify UMAT. The analysis results by FEM agree well with those of Runge-Kutta solutions as shown in Fig. 3 for uniaxial hardening case and in Fig. 4 for uniaxial cyclic hardening case.

4. ANALYSIS OF RATCHETING IN PRESSURIZED PIPING

The plastic deformation of thin-walled cylinder has been analyzed for strain controlled push-pull loading conditions of ±1% axial strain at a rate of 0.1 %/min. Thin-walled push-pull cylinder with a nominal gage length 0f 0.04m, an outer diameter of 0.022m and bore of 0.02m has been additionally loaded by internal pressure applied hydraulically so that it allows the cyclic loading to be combined with static tensile hoop stress of 1/2 of the uniaxial yield stress. The finite element model of this problem will be very similar to the previous model of Fig.1 and the same element types for thermal and stress analysis with the previous model were used.

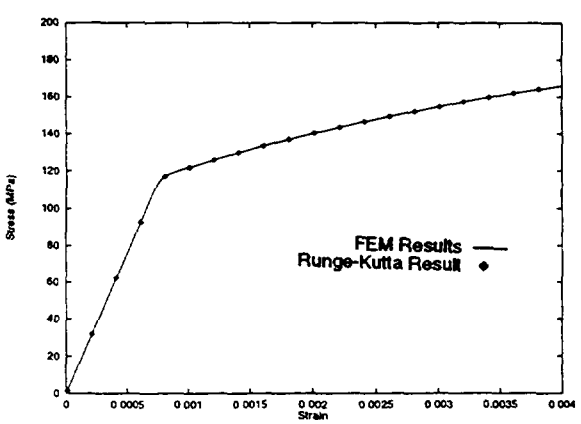

FIG. 3. Comparison of results by FEM and Runge-Kutta solutions for uniaxial hardening case.

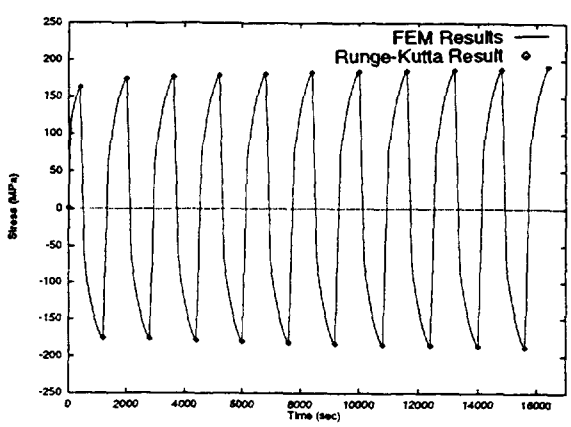

FIG. 4. Comparison of results by FEM and Runge-Kutta solutions for uniaxial cyclic hardening case.

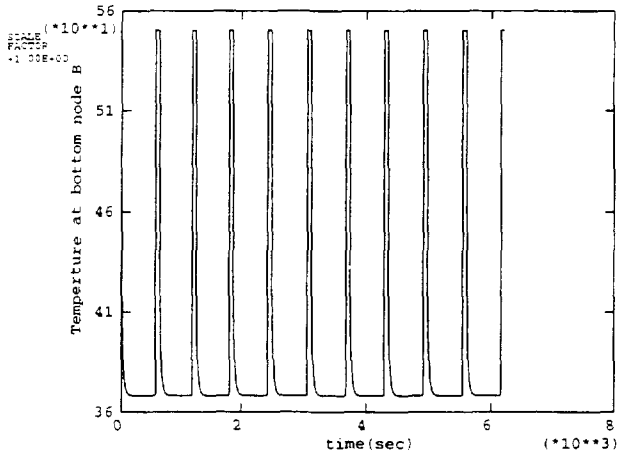

FIG. 5. Temperature history at bottom of the cylinder

5. RESULTS AND DISCUSSIONS

5.1. Thermal ratcheting

5.1.1 Temperature distribution

Fig. 5 shows the temperature history at the bottom of the cylinder during ten cycles of cooling and heating. As shown in the figure, the bottom experiences the cyclic thermal loading over the range of 368.2°C ~ 550°C. Heat transfer of the upper shell part in contact with Ar gas atmosphere is dominated by conduction and of lower part in sodium atmosphere is dominated by convection so that the axially moving temperature distribution between top(550°C) and bottom(368.2°C) induces thermal ratcheting. The steep temperature gradient occurs near the contact zone of sodium and Ar gas.

5.1.2. Thermal ratchet behavior

Fig. 6a which shows the deformed shape of the cylinder magnified 80 times after first cooling into the sodium pool, that is, at t=375 sec, represents the circumferential contraction in the lower part of the cylinder.

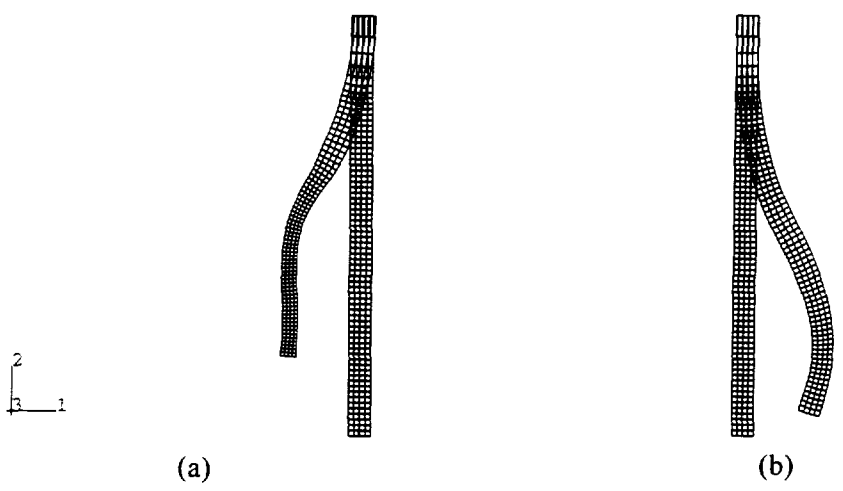

FIG. 6.. Deformed profile (a) after first cooling , (b) after 10 cycles

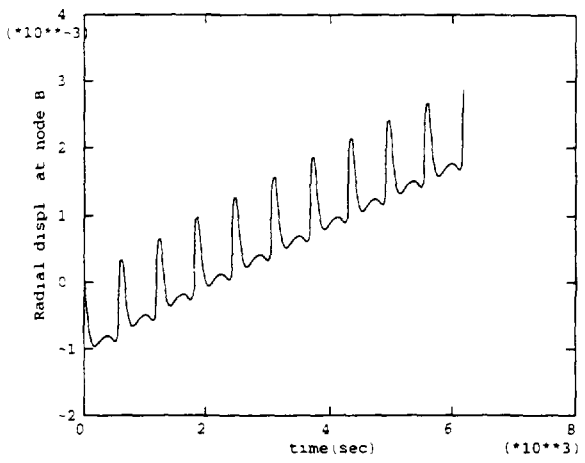

FIG. 7 History of radial displacement

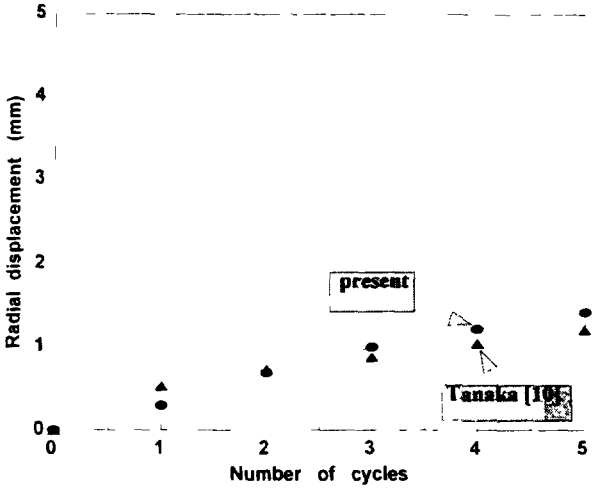

FIG. 8. Comparison of the results by test and FEM

The maximum radial contraction was computed as 0.86 mm in the outer surface, lower part of the cylinder. In the meantime, the deformed profile after 10 cycles of heating and cooling at t = 6225 sec as shown in Fig. 6b shows radial expansion due to heating in Ar gas atmosphere. It can be seen that the heating after complete withdrawal from the sodium pool for 1 minute at 550°C overcomes the cooling in the sodium pool, which leads to the progressive accumulation of the residual deformation. That is, the cylinder contracts when it submerges and expands when it is lifted completely and exposed high temperature environments. The history of radial displacement at the bottom of the cylinder versus time is shown in Fig. 7. As shown in the figure, the radial displacement of the cylinder no longer contracts below zero after the third cycle even though it is submerged into the pool. It is shown that the radial displacement due to thermal load can lead to an excessive deformation.

The present results by FE analysis were compared with those of the test[10] as shown in Fig.8. The difference of radial expansion after ten cycles is rather small producing 0.8 mm when the test result shows expansion of 2.2 mm. It can be shown that the present FE analysis can evaluate properly the thermal ratchet behavior of 304 SS cylinder.

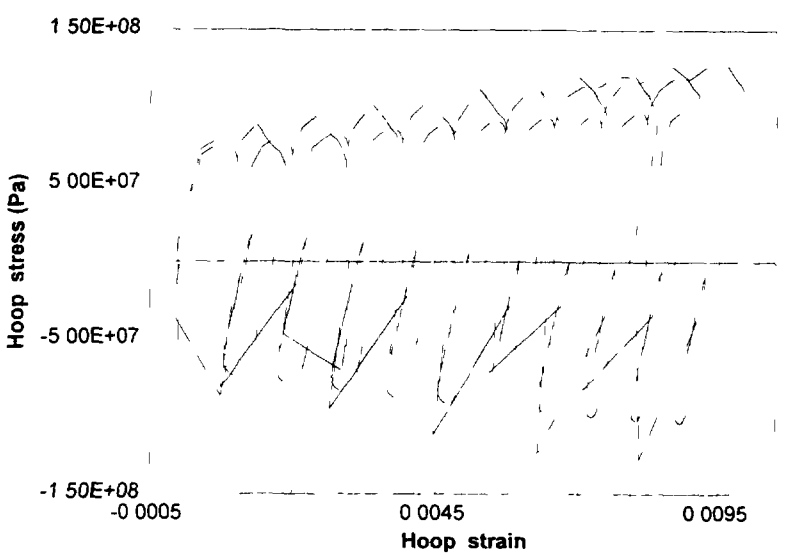

FIG. 9. Hoop stress-strain hysteresis curve

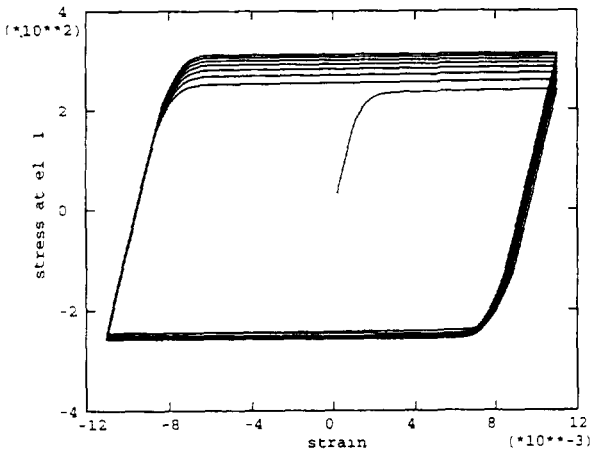

FIG. 10. Hoop stress-strain hysteresis curve of pressurized pipe.

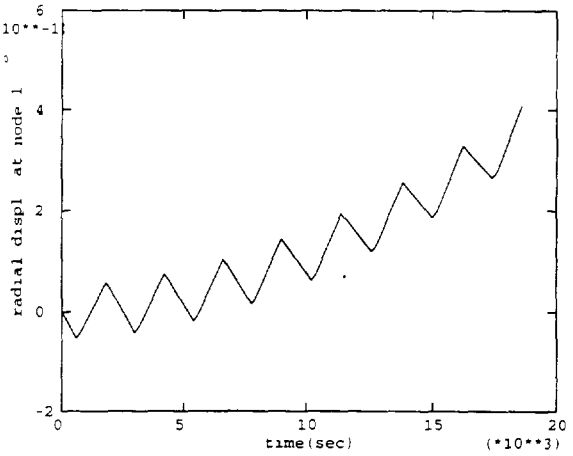

FIG. 11. History of radial displacement of pressurized pipe.

It should be noted that the stress-strain hysteresis loop develops progressive propagation to the right direction rather than hardens to a stable hysteresis loop as shown in Fig. 9. Since the loop is for an axisymmetric structure, the propagation aspects shows a rather complex one. The analysis results clearly show that ratchet deformation is one of the dominant factors for structural integrity for this type component.

5.2. Ratcheting in pressurized pipe

Fig. 10 shows the hoop stress-strain hysteresis loop of the pressurized pipe. The material hardens to a stable hysteresis loop. Fig. 11 shows the history of progressive accumulation of radial displacement. It can be shown that externally appied cyclic strain can induce progressive inelastic deformation for the pipe runs.

6. CONCLUSIONS

Thermal ratchet behavior of 304SS cylinder caused by axial moving temperature distribution and racheting in a pressurized pipe have been evaluated using elastic-plastic analysis with Chaboche constitutive model. The constitutive model was implemented in ABAQUS user subroutine UMAT and the validity of the implementation was verified through the comparison of results by analysis and test. The analysis results of thermal ratcheting showed that residual thermal deformation was continuously accumulated cycle by cycle due to the axially moving temperature distribution. The allowable ratchet deformation during its service life should be carefully limited in the design because the progressive deformation caused by secondary cyclic load may result in functional failure. A further study on creep and relaxation effect in the constitutive model and implementation to accommodate efficient creep ratcheting analysis is necessary.

REFERENCES

[1] ASME Boiler and Pressure Vessel Code (1992 edition) Code Case N-47-29.
[2] RCC-MR Code, Section I, Subsection RB-3000, AFCEN (1985).
[3] IIDA,K., et.al., "Simplified analysis and design for elevated temperature components of Monju", Nucl.Engrg.& Des., **98** (1987) 305-317.
[4] OZAKI, H et al., "Evaluation of inelastic strain in elevated temperature components," ASME PVP. **262** (1993) 19-25.

[5] CHARLES,I.D., et al., "Racheting in pressurized piping," SMIRT-12, L08/2 (1993) 197-202.
[6] CHABOCHE, J-L., "Viscoplastic constitutive equations for the description of cyclic and creep deformation : Part I, Equations, development and analytical procedures" , J.Eng. Mat'l and Tech. (1976) 96 pp.
[7] CHABOCHE, J-L.,"Cyclic viscoplastic constitutive equations, Part I : A Thermodynamically consistent formulations," J. Appl. Mech., **60** (1993) 813 pp.
[8] LEMAITRE, J and CHABOCHE, J-L., Mechanics of solid materials, Cambridge university press (1990) .
[9] OHSIMA, I., TANAKA, N., et al., "Structural Integrity of DFBR internal structure under severe thermal loading (2) : Thermal ratchet deformation" , ASME PVP. **163** (1989) 47-55.
[10] TANANKA, N., et al., "Simulation of Thermal Ratcheting of 304 SS Cylindrical Shell" , SMIRT **11**, L04/4 (1991) 97- 101.

FRENCH RECENT DEVELOPMENTS IN SUPPORT TO RULES FOR CREEP AND CREEP-FATIGUE ANALYSES

F. TOUBOUL, D. MOULIN
CEA DRN/DMT/SEMT,
CEN Saclay, France

Abstract

RCC-MR proposes Design rules for creep and creep-fatigue damage evaluation in zones with no geometrical discontinuities. Rules have been developed, based on the σ_d concept, in order to consider zones with geometrical discontinuities. Rules for Weld are proposed in the paragraph relative to *shell design rules* and reduction coefficient due to material properties are given in Appendix A9. For fatigue analysis, last version of RCC-MR (1993) has proposed a reduction factor on fatigue curves (Jf value), derived from preliminary tests performed within European program. Studies have been carried out in order to have a better understanding of the phenomena involved in these fatigue reduction factors.

Tests have been performed on large plates, with varying applied displacements, weld geometry, plate thickness, weld direction,...

It appears that material effect is not the only purpose to be considered but that it is necessary to think about the geometrical effect, linked to the welded zone dimensions, and the elastic follow-up effect between the two materials: base metal and weld metal. As a first approach, simplified calculations have been achieved with precise material characterization. Roche's method and Zarka method's give conservative result in comparison to tests results.

1. INTRODUCTION

RCC-MR [1] proposes Design rules for creep and creep-fatigue damage evaluation in zones with no geometrical discontinuities. Rules have been developed, based on the σ_d concept, in order to consider zones with geometrical discontinuities.

Rules for Weld are proposed in the paragraph relative to *shell design rules* and reduction coefficient due to material properties are given in Appendix A9. For fatigue analysis, last version of RCC-MR (1993) has proposed a reduction factor on fatigue curves (Jf value), derived from preliminary tests performed within European program. Studies have been carried out both experimental and analytical, in order to have a better understanding of the phenomena involved in these fatigue life reduction factors.

2. TESTS PRESENTATION

Tests have been performed in AEA/Risley on butt welded large plates in 316L (N), with varying applied displacements ($\Delta\varepsilon$: 0.3 à 1%), weld geometry (simple V or double V), plate thickness (10 mm, 25 mm), and weld direction (longitudinal or transverse). Test temperature is 550°C.

AEA has carried out a first tests campaign of 17 tests[1] :

- 9 tests on 10 mm thick plates:
  5 fatigue tests
  3 creep-fatigue tests, with 1 hour hold period
  1 creep-fatigue tests, with 5 hours hold period
- 8 tests on 25 mm thick plates:
  4 fatigue tests
  4 creep-fatigue tests, with 1 hour hold period

An additional testing matrix has been defined with CEA, in order to be performed by AEA ("SOUFFLE program). The weld considered in this second campaign are non dressed one:

- 4 tests on 10 mm thick plates:
  2 fatigue tests
  2 creep-fatigue tests, with 1 hour hold period
- 6 tests on 25 mm thick plates:
  2 fatigue tests
  3 creep-fatigue tests, with 1 hour hold period
  (including one test with capacitance strain gauges)
  1 creep-fatigue tests, with 5 hour hold period

The experimental device imposes a cyclic displacement (Δd) in circular bending. $\Delta \varepsilon$ is derived from Δd measurements. $\Delta d / \Delta \varepsilon$ has been adjusted on plates without welds, at 20°C.

The number of cycles to rupture (plate separation into 2 parts) is given as a result of the tests, as well as the cyclic variation of the applied load.

SOUFFLE program fatigue tests results are given in the following table:

Plate		Weld		strain	Rupture	
(mm)	Orientation	Type		(%)	N (cycles)	Location
590x125x10	*Transverse*	Single Vee	MMA + TIG	0.983	1295	Weld toe
590x125x10	*Transverse*	Single Vee	MMA + TIG	0.6	3932	Weld toe
1600x220x25	*Transverse*	Double Vee	MMA	0.3	114670	
1600x220x25	*Longitudinal*	Double Vee	MMA	0.6	8480	P&W

A accompanying characterization program has been performed in CEA in order to evaluate the cyclic and fatigue behaviour of the base metal and MMA weld metal. It has been found that MMA metal shows a very slight cyclic hardening. As a consequence the over-matching between weld and base metal on the first cycle becomes an under-matching after some cycling, especially for high strain levels. Fatigue tests have shown that fatigue life is very similar between 316L(N) steel and MMA steel.

3. TESTS INTERPRETATION

RCC-MR *RB3361* provide rules for weld, based on a fatigue strength reduction factor **f** and a coefficient of weld fatigue characteristics J_f.

[1] Work performed within the framework of the EFR programm.

f depends on the type of welding joint and the examination performed. It is a multiplying factor of the elastic strain range, that is used for the calculation of the elasto-plastic strain range enhancement (Neuber's rule).

$$\Delta\sigma \Rightarrow \mathbf{f} \times \Delta\sigma$$

f is set to 1 for butt welding, fully examined.

Computed elasto-plastic strain range is entered on fatigue curves. When the weld material fatigue behaviour is unknown, the base material can be used and the strain range is divided by $\mathbf{J_f}$ before entering the curves.

Last version of RCC-MR (1993) has proposed a reduction factor on fatigue curves:

$\mathbf{J_f} = 1.25$ for 316L(N) steel

Considering the fact that, in the *SOUFFLE* program, the experimentally determined weld metal fatigue curve is similar to the base metal one, $\mathbf{J_f}$ should be taken as 1 in our case. On the other end, butt welding are considered, with full radiographic examination, leading to a **f** value of 1.

Nevertheless, tests have shown fatigue life reduction and a so-called $(J_f)_{exp}$ factor can be determined by:

$$(J_f)_{exp} = \frac{\Delta\varepsilon(N_r)}{\Delta\varepsilon_{ap}}$$

where $\Delta\varepsilon_{ap}$ is the applied strain range, and $\Delta\varepsilon(N_r)$ is the strain range corresponding to the experimental number of cycle to rupture N_r and is derived from a base metal fatigue curve.

It is to be noted that the experimental value $(J_f)_{exp}$ is comparable to the $\mathbf{J_f}$ codified one, in term of application purpose, but does not represent the same phenomena.

In order to interpret the *SOUFFLE* tests, we have considered the "best-fit" fatigue curve from which the codified curve (RCC-MR A3.1S) has been deduced by using the 2 and 20 reduction coefficients.

$$J_f = \frac{\Delta\varepsilon_{A3.1S}(N_r)}{\Delta\varepsilon}$$

Experimental results are given in the following table:

Plate (mm)	Orientation	Weld Type		strain (%)	J_f
590x125x10	*Transverse*	Single Vee	MMA + TIG	0.983	1.14
590x125x10	*Transverse*	Single Vee	MMA + TIG	0.6	1.34
1600x220x25	*Transverse*	Double Vee	MMA	0.3	1.39
1600x220x25	*Longitudinal*	Double Vee	MMA	0.6	1.10

Mean value obtained for $\mathbf{J_f}$ on these tests is very close to the RCC-MR codified one (1.24). But this value cannot be attributed to a weld metal fatigue curve effect.

Moreover, the value varies much from one test to another. As a matter of fact, longitudinal weld endurance is much larger than the transverse weld one. But it is also to be noticed that there is a non negligible influence of the strain amplitude as the $(J_f)_{exp}$ factors decreases for high strain ranges. We can so assume that the experimental $(J_f)_{exp}$ factor should not be linked to a reduction in endurance (reduction in the abscissa of the fatigue curve) but represent a strain enhancement (co-ordinate of the fatigue curve). This enhancement can be connected to the elastic follow-up effect that exist between the two different materials. Strain cyclically accumulates in the weaker part of the structure.

From the experimental SOUFFLE program, we can so conclude that:

- For MMA weld metal, the coefficient of weld fatigue characteristic should be taken as 1.
- Even for butt welding, there is a strain concentration due to elastic follow-up effect between the two materials of dissimilar characteristics.

In order to verify the latest assumption, we have carried out simplified elasto-plastic calculations that allow to estimate strain enhancement in the weld. As there is a cyclic under-matching of the weld metal in comparison to the base metal, strain effectively accumulates in the weld zone.

4. LOCAL STRAIN EVALUATION

Elasto-plastic simulations have been achieved with precise material characterization: the cyclic behaviour has been introduced by the consideration of the cyclic curve for the material. As well, more simplified calculations have been performed, based on elastic computations and analytical corrections, and allowing for parametric studies. Two procedure have been studied:

- Roche's method
- Zarka's method

Application has been made on the following case:

- fatigue test
- 25 mm thick plate
- dressed
- transverse: simple V
  TIG root MMA cap

4.1 Simplified methods presentation

4.1.1 Roche's method [2]

R. Roche has proposed to determine the elasto-plastic strain range using the results of an elastic computation and the determination of an elastic follow-up factor. The amount of elastic follow-up depends on the variation of loading and/or mechanical (or geometrical) properties within the structure. Heterogeneity of mechanical properties in the plate, due to the presence of the weld, imposes the accumulation of strains in the weld.

The method proposes to take into account the effect of plasticity on the imposed strain variation distribution. As shown on the figure below, an attempt is made to determine the co-ordinates of point 3 (inelastic solution) when the results of the elastic calculation (point 0) are known, regardless of geometry, loading and material.

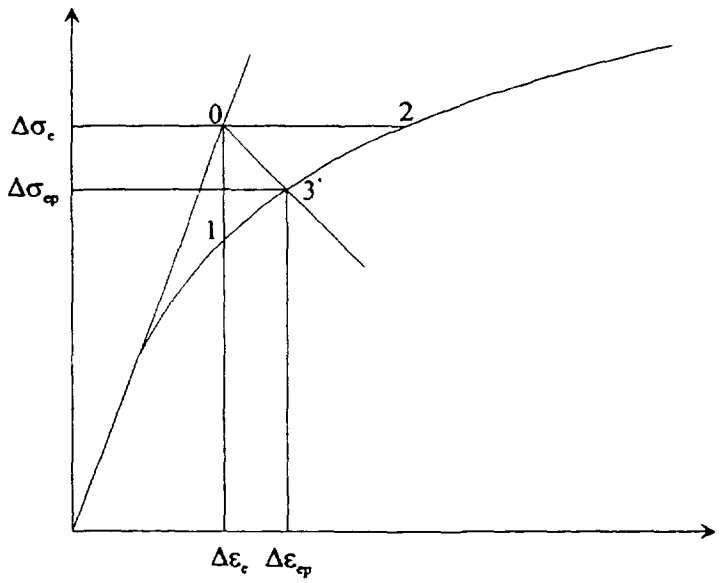

To solve the problem, the author uses the Kachanov approximation. Plastic strain does not alter the spatial stress distribution. If, at one point in a structure, the elastic stress is $\Delta\sigma_e$ the elastoplastic stress is $\Delta\sigma_{ep} = \Phi\Delta\sigma_e$, where Φ is a function independent of the point in question. The stresses remain proportional, regardless of the plastic strain. The cyclical behaviour of the material is represented by a Ramberg-Osgood's law :

$$\Delta\varepsilon_{ep} = \frac{\Delta\sigma_{ep}}{E} + \left(\frac{\Delta\sigma_{ep}}{K}\right)^n$$

with n = 1/m

With Kachanov's approximation, the elastoplastic strain variation is expressed as follows:

$$\Delta\varepsilon_{ep} = \Phi\frac{\Delta\sigma_e}{E} + \Phi^n\left(\frac{\Delta\sigma_e}{K}\right)^n$$

It can be demonstrated with the principle of complementary works that Φ is the solution of the equation :

$$(\Phi - 1)\,T + \Phi^n = 0 \qquad \text{where} \qquad T = \frac{\int \Delta\sigma_e{}^2 dV}{\int \frac{\Delta\sigma_e{}^2}{t} dV}$$

$$\text{and} \qquad t = \frac{\Delta\varepsilon_e}{\Delta\varepsilon_p}$$

where $\overline{\Delta\varepsilon_p}$ is the plastic strain variation corresponding to $\overline{\Delta\sigma_e}$ obtained from the cyclic consolidation curve.

Some modifications of the procedure are necessary in the case of the welded plates because the structure is composed of two different materials, so that the parameters n and K are not the same in the two cases. In opposition to $\Delta\varepsilon_e$, $\Delta\varepsilon_p$ is not calculated independently of K and n. The t factor has to be calculated separately in the weld and in the base metal; then, t will not be continuous at the limit between the two materials. To calculate the factor T on the total structure, the equation $(\Phi - 1).T + \Phi^n = 0$ is solved separately on the two materials and the elastoplastic strain is deduced.

4.1.2 Zarka's method [3]

Zarka's method allows to determine the total strain range by performing two elastic computations, considering a bilinear modelisation of the cyclic curve. The second computation, for an homogenous material, can consider one or two fictitious areas, with or without iterations (GATT modification). The two zones method with iterations has been shown to be the more conservative, without being two expansive, and has been applied in the present case.

The calculation with Zarka's method follows the recommendations of annexe A10, RCC-MR, which requires some hypotheses :

- The model of mathematical behaviour is based on the Von Mises's plasticity criterion, a plastic flow law and a kinematic strain hardening law of bilinear type.
  The plasticity criterion is $f(S-\alpha) \le {\sigma_0}^2$ where σ_0 is the elastic limit.
  $S = \sigma - \frac{1}{3}\mathrm{tr}(\sigma)$ is the deviator of the total stress σ, $\mathrm{tr}(\sigma)$ is the trace of stress tensor.
  α is the intern strain hardening parameter of the material : $\alpha = C\varepsilon_p$
  C is a strain hardening operator : $C = \frac{2}{3}hI$
  h is the strain hardening modulus of the material and I the identity matrix.

- The characteristics of the material required for the application of this model are :
  - The cyclic curves, modified by dividing the co-ordinates by 2 ($\Delta\sigma/2$, $\Delta\varepsilon/2$), so that they are comparable with monotone curves. In the following, these curves will be called reduced cyclic curves. This curve is bilinearized in order to applied the method. A maximum strain is postulated in order to calculate the tangent modulus.
  - The Young's modulus as a function of the temperature.

The method is based on the introduction of modified parameters. The total stress $\sigma = \sigma^{el} + \rho$ is composed of the elastic stress and the residual stress. In term of deviator, we have $S = S^{el} + \text{dev}\,\rho$. The modified parameter $\hat{\alpha}$ is introduced in order to suppress the inelastic stresses in the plasticity criterion : $\hat{\alpha} = \alpha - \text{dev}(\rho)$

The criterion is then : $f(S^{el} + \text{dev}(\rho) - \alpha) \leq {\sigma_0}^2$ or $f(S^{el} - \hat{\alpha}) \leq {\sigma_0}^2$

The calculation is carried on in the modified parameters space and the local solution is built.

4.2 Results of the simplified methods

Results of the application of the simplified methods are given in the following table:

		Δε maximum	*Δε far from the weld zone*
ROCHE'S METHOD	middle size weld	1.648	0.674
	maximum size weld	1.611	0.675
	middle size weld, $\Delta\varepsilon T_{max}$= 1%	0.829	0.620
ZARKA'S METHOD	maximum size weld, $\Delta\varepsilon T_{max}$= 1%	0.847	0.620
	middle size weld, $\Delta\varepsilon T_{max}$ = 0.8%	0.770	0.613
	middle size weld, $\Delta\varepsilon T_{max}$ = 2%	0.968	0.646
	middle size weld, $\Delta\varepsilon T_{max}$ = 8%	1.273	0.694

Strain enhancement between the welded zone and the rest of the plate varies from 1.2 to 2.5. It depends on the method used, on the weld dimension and, for ZARKA's method, on the postulated maximum strain.

Comparison between the simplified methods and the elasto plastic calculation is made on the following table:

		Δε maximum	*Δε point A4*
ROCHE'S METHOD	middle size weld	1.648	0.674
ZARKA'S METHOD	middle size weld, $\Delta\varepsilon T_{max}$= 1%	0.829	0.620
Elasto-plastic calculation	middle size weld	1.35	0.63

The experimental strain enhancement is close to 1.2. All the numerical methods give conservative results, Roche's method is closer to the elasto-plastic simulation.

The elasto-plastic calculation is simplified as it has been considered only the stabilized behaviour of the material. A full cyclic elasto-plastic simulation should have given results closer to the experimental ones. In particular, it seems necessary to simulate the fact that the dissimilarity between the two materials varies with the number of applied cycles.

4. CONCLUSION

Reduced fatigue life of welded structure is not related to a lower fatigue endurance of weld metal but to a strain enhancement in cyclic plasticity due to dissimilar materials. This elasto-plastic follow-up effect can be easily represented by simplified methods, used as post-processors to elastic calculations. These methods (Roche's method, Zarka's method) allow for parametric study on weld metal or weld geometry and give satisfactory results.

More precise analyses are now being performs in order to understand the redistribution of strain, and especially the evolution of strain localization with varied applied number of cycles.

Parameter analyses are also necessary in order to codified the approach in different situations and to limit the applicability of each coefficient.

REFERENCES

[1] RCC-MR, Design and Construction rules for mechanical components of FBR nuclear islands, edited by AFCEN, may 1993.

[2] R.L. ROCHE, Analyse à la fatigue : détermination de la variation réelle de déformation à partir d'un calcul élastique, Note CEA N.2523, avril 1987.

[3] J. ZARKA, A new approach in inelastic analysis of structures, Martinis Nijhoff Publishers, 1990.

CREEP-FATIGUE ASSESSMENT OF A THERMINA TEST SPECIMEN USING THE R5 PROCEDURE

P. BOOTH*, S.K. BATE**, P.J. BUDDEN*

*Nuclear Electric plc,
Barnwood, Gloucester

**AEA Technology,
Risley, Warrington, Cheshire

United Kingdom

Abstract

A creep-fatigue life assessment of an axisymmetric 316 stainless steel test specimen under constant mechanical and cyclic thermal shock loading using the R5 Procedure is described in this paper. This test was carried out at CEA, France, and formed part of the 'Thermina' series. Stress analysis has been carried out using both full inelastic finite element analysis and also the simplified shakedown methods, based on elastic calculation, within R5. The estimates of strain range and the stress at the start of the creep dwell have then been used with R5 to estimate creep and fatigue damage per cycle and hence to make predictions of component life. The predicted lives are compared with the lives observed in the tests. The simplified R5 estimate of life, based on development of a crack of depth 200 microns, is 260 cycles using best-estimate material properties. Experimentally, cracks of depth at least 150 microns were observed in between 526 and 650 cycles, for two similar tests. The simplified R5 route therefore leads to an estimate of life which is conservative but not unduly so on this component. Detailed cyclic inelastic analysis using the ORNL constitutive model and the ABAQUS finite element code to estimate the strain range and dwell stress led to a best estimate of 618 cycles to crack initiation using R5.

1. INTRODUCTION

The design and assessment of power plant components operating at high temperature requires validated methods for estimating component life under conditions of creep and fatigue. The interaction of these two mechanisms needs to be taken into account. R5 [1] is a comprehensive set of procedures developed within the UK for the assessment of the high temperature response of structures. In particular, methods are given in R5, based on simplified shakedown and reference stress techniques, for calculating life. For an initially defect-free component, failure may be defined following Volume 3 of R5 as initiation of a crack of specified depth under creep fatigue loading. Other volumes of R5 consider propagation of defects. This paper presents validation of the R5 Volume 3 initiation procedure on an austenitic steel test specimen subjected to a severe thermal shock loading. The magnitude of the loading is strictly outside the creep-modified shakedown limits of R5, which formally permit up to 20% of any structural section to cyclically yield. As such, it is considered to represent a critical test of the R5 procedure.

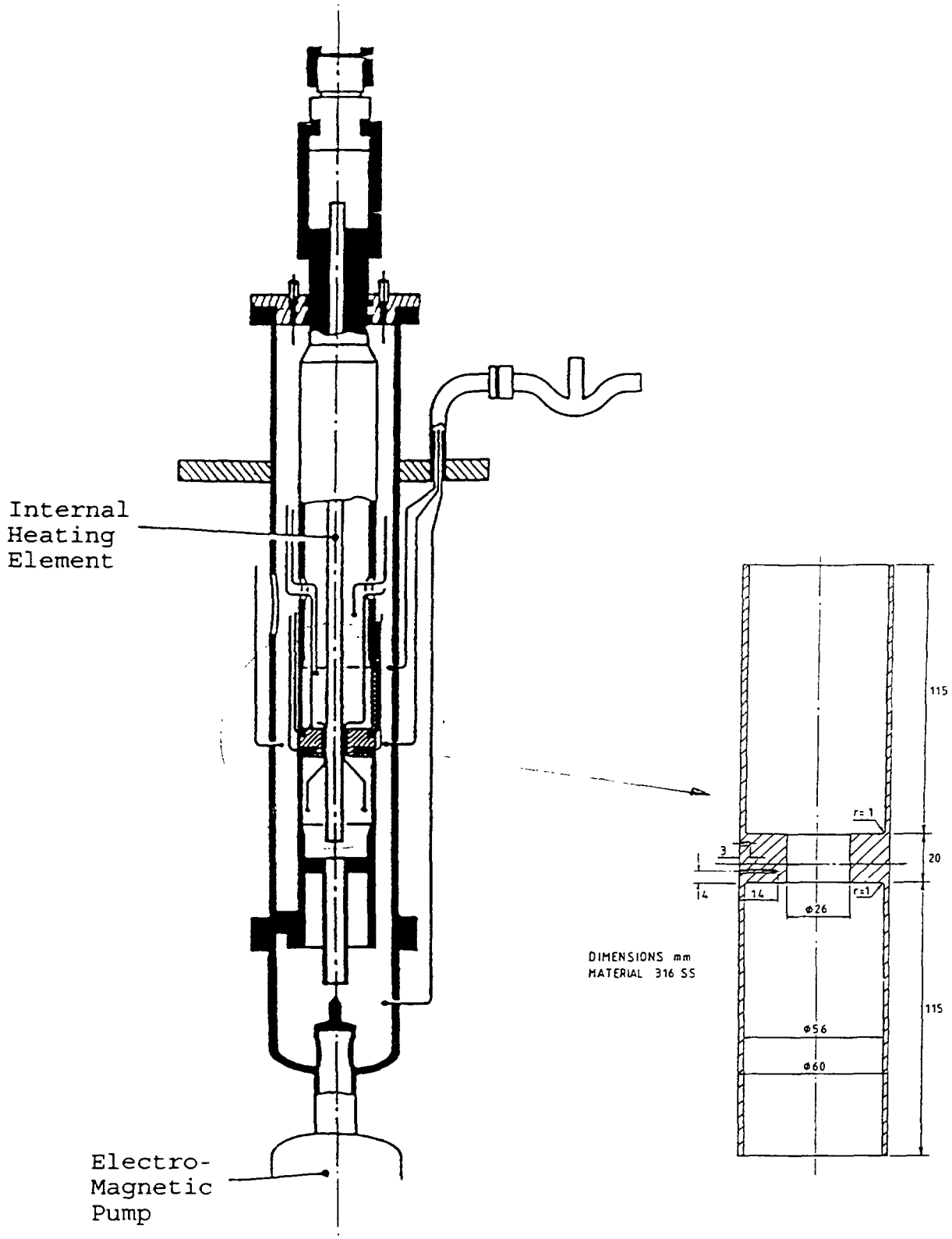

FIG.1. Drawing of THERMINA test rig showing details of test specimen

The Thermina test specimen is described in Section 2. Following a brief description of the R5 method in Section 3, a shakedown calculation to derive estimates of the strain range and stress at the start of the creep dwell is then described in Section 4. Detailed cyclic inelastic finite element calculations using both ORNL and Fast Reactor State Variable (FRSV) constitutive models are outlined in Section 5. The results of both the elastic and inelastic analyses are used to estimate the number of cycles to initiate a crack of depth 200 microns using Volume 3 of R5. The results are compared with other predictions and with the experimental observations.

2. THE THERMINA TEST

The Thermina series of tests have been carried out at CEA Cadarache, France [2,3]. The design of the experimental test rig is shown in Figure 1 together with the main features of the specimen chosen for analysis. Thermina samples are filled with sodium and maintained at 600°C by means of an internal electric element. Thermal shock is induced by forcing cooler liquid sodium onto the outside surface of the specimen for 20 seconds by means of a submerged electromagnetic pump. Subsequently the internal heater causes the temperature to return to 600°C where it is maintained for a hold period before being subjected to repeated shocks.

The specimen analysed consists of an internal flange within a thin walled cylinder subjected to periodic cooling by liquid sodium at a temperature of 400°C alternating with hold periods of 6 hours at 600°C during which creep can take place. Because the flange responds more slowly than the cylinder wall to the thermal shock, high thermal stresses are generated in the transition region between the flange and the cylinder wall.

The results published for two specimens subjected to this loading during the Thermina test programme indicated crack development of at least 150μm after 526 and 650 cycles respectively.

3. THE R5 PROCEDURE FOR CREEP-FATIGUE CRACK INITIATION

Endurance under creep-fatigue loading is estimated in Volume 3 of R5 [1] by calculating fatigue damage and creep damage and equating the sum of the two to unity at crack initiation:

$$D \equiv D_f + D_c = 1$$

Comparisons between the R5 approach and alternative design code approaches to crack initiation, such as in ASME N-47 [4] and RCC-MR [5], are discussed in [6].

Endurance is defined in Volume 3 as the number of cycles to initiate a crack of specified depth a_0, defined by the user. This corresponds to microscopic initiation (a crack of depth 20 microns) and propagation to depth a_0. For thick-section components, a_0 is generally taken as the diameter, a_f say, of conventional uniaxial endurance specimens used to derive the baseline endurance data. For thin-section components, however, a_0 may be a small fraction of the cross section, say 10%, and less than a_f. A size correction is applied by R5 to the baseline endurance data in this latter case. The fatigue damage per cycle, d_f, is the reciprocal of this modified endurance. Total fatigue damage, D_f, then follows by summation over the cycle history.

Creep damage per cycle, d_c, is defined by the ductility exhaustion integral over the dwell period t_h:

$$d_c = \int_0^{t_h} \frac{\dot{\epsilon}_c}{\epsilon_f(\dot{\epsilon}_c)} dt$$

where the creep ductility, ϵ_f, is a function of creep strain rate, $\dot{\epsilon}_c$, in general. For a stress drop, $\Delta\sigma'$, in the dwell with elastic follow-up factor Z, this equation may be conservatively simplified to

$$d_c = \frac{Z\Delta\sigma'}{E'\epsilon_L}$$

where ϵ_L is a lower bound creep ductility which is assumed to be independent of strain rate and $E'=3E/2(1+\nu)$ is Young's Modulus modified for the difference in Poisson's ratios between elastic and inelastic response. The total creep damage, D_c, is then simply the sum of d_c over the various cycles.

Estimates of cyclic strain range, stress drop and elastic follow-up factor are required to calculate damage factors and hence endurance using the R5 procedure. These quantities can be calculated using simplified shakedown and reference stress methods as described in Volume 2 of R5, or they may be determined using detailed inelastic methods. Life estimates for the Thermina specimen are given in Sections 4 and 5 which follow, for simplified and full inelastic routes, respectively.

4. ELASTIC FINITE ELEMENT ANALYSIS

4.1. Material Properties

Both 0.2% yield stresses and cyclic stress strain data were obtained from RCC-MR [5] using the correct steel grade in the unaged condition to provide best estimate data.

The Norton creep law chosen for the monotonic creep calculation to estimate elastic follow up described in Section 4.4 was chosen following the advice in Goodman [7] such that $\epsilon_c = 10^{-17}\ \sigma^5\ t$ for stress σ in MPa and time t in hours.

A creep ductility of 56% was chosen for this analysis based on creep characterisation tests carried out on samples of representative material [8] and also on tests from Thermina samples [2].

The values of the general properties used in the elastic finite element analysis are given in Table 1 and were chosen for consistency to be the same as those used in the non-linear analysis described in Section 5. They agree closely with values quoted in RCC-MR [5].

TABLE 1. MATERIAL PROPERTIES USED IN ELASTIC FINITE ELEMENT ANALYSIS

Property	Temperature		
	400°C	500°C	600°C
Thermal Conductivity (Steel)	19.39W/m/°C	20.82W/m/°C	22.25W/m/°C
Thermal Conductivity (Sodium)	71.00W/m/°C	66.50W/m/°C	62.00W/m/°C
Coefficient of Expansion (Steel)	17.1×10^{-6}/°C	17.56×10^{-6}/°C	18.01×10^{-6}/°C
Young's Modulus (Steel)	169700MPa	162200MPa	154700MPa
Poisson's Ratio	0.29	0.29	0.29
Density (Steel)	7717kg/m^3	7717kg/m^3	7717kg/m^3
Density (Sodium)	808kg/m^3	808kg/m^3	808kg/m^3
Specific Heat (Steel)	549.8J/kg/°C	570.9J/kg/°C	592.1J/kg/°C
Specific Heat (Sodium)	1278J/kg/°C	1262J/kg/°C	1255J/kg/°C

4.2. Finite Element Mesh

It was shown in both the inelastic analysis described in Section 5 and in [9] that the stagnant sodium pool needed to be modelled to obtain correct thermal response. The mesh used in the analysis (Fig.2) therefore consists of a total of 1008 8-node quadrilateral isoparametric elements, 283 in the specimen and 725 in the pool.

4.3. Thermal Analysis

This was carried out using the FLHE [10] finite element thermal analysis program. The internal heater was represented by a forced convection heat transfer coefficient of 400W/m^2°C. The thermal downshock was modelled by the use of a forced convection heat transfer coefficient of 20kW/m^2°C together with a temperature drop from 600°C to 400°C in 0.25 seconds. The results of this analysis are shown in Figure 3a and 3b compared with results from the analysis described in Section 5 and [9].

4.4. Elastic Analyses

The linear elastic stress analysis was carried out using the BERSAFE [11] finite element stress analysis program. The analysis included a primary mechanical load of 50MPa together with the secondary thermal loading described in Section 4.3 and was performed at several different times during the thermal cycle to determine both the position of maximum stress in the specimen and the time in the cycle when the stresses were at their maximum values. The results are shown in Figure 4 compared with the results of the analysis described in Section 5. Two specific cases identifying the extremes of the loading cycle were chosen for use in the shakedown analysis and are detailed in the following sub-sections.

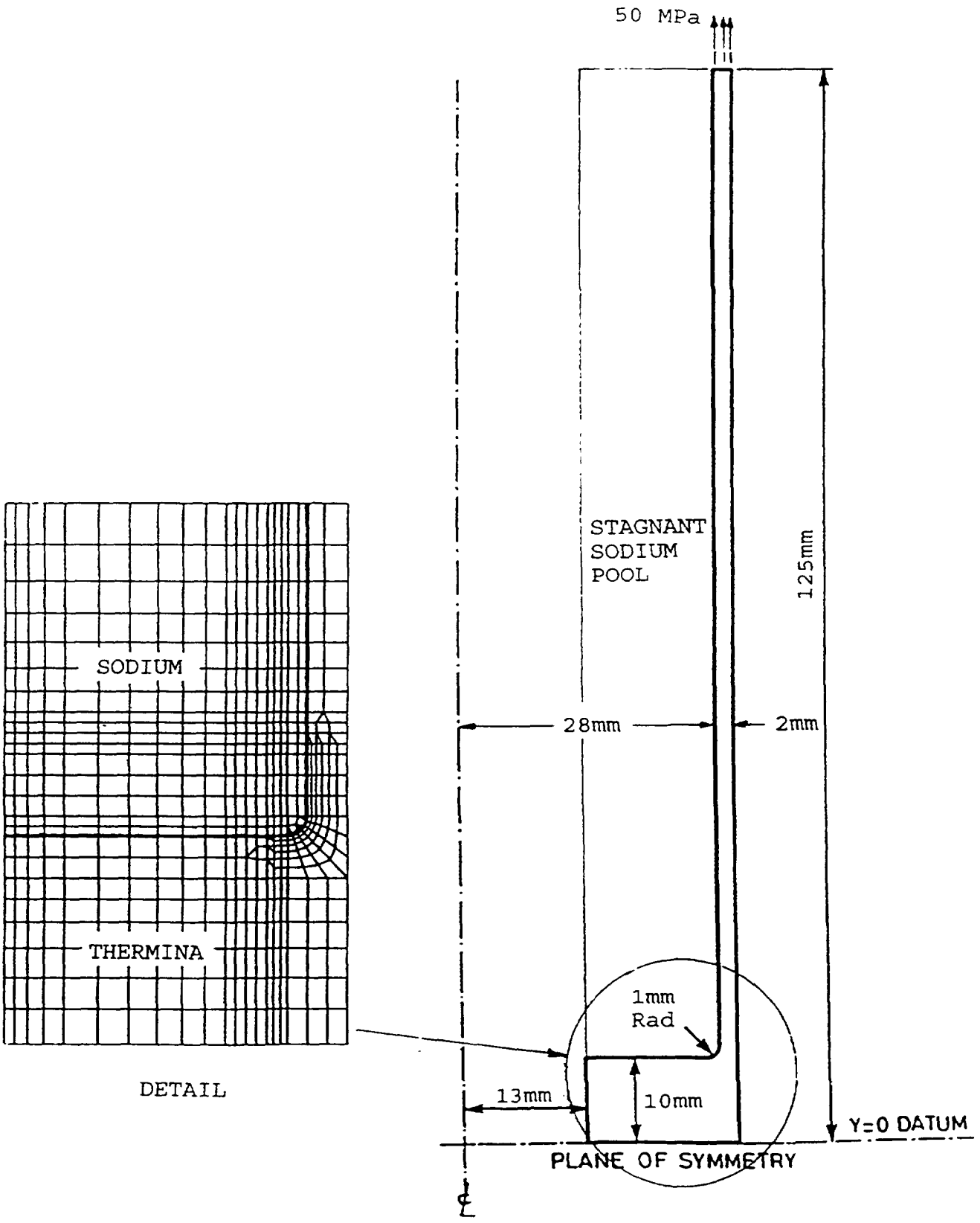

FIG. 2. The finite element mesh showing details of the modelling of the sodium pool.

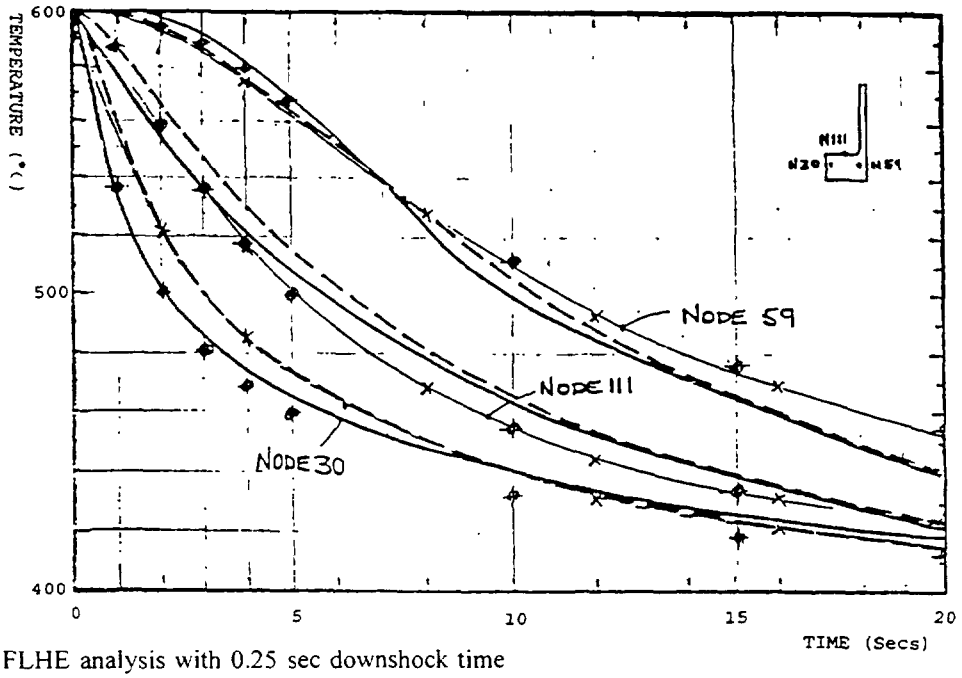

FLHE analysis with 0.25 sec downshock time
Calculated values [9]
Experimental Values [9]
ABAQUS Calculations [13]

FIG. 3a. Temperature response of the flange

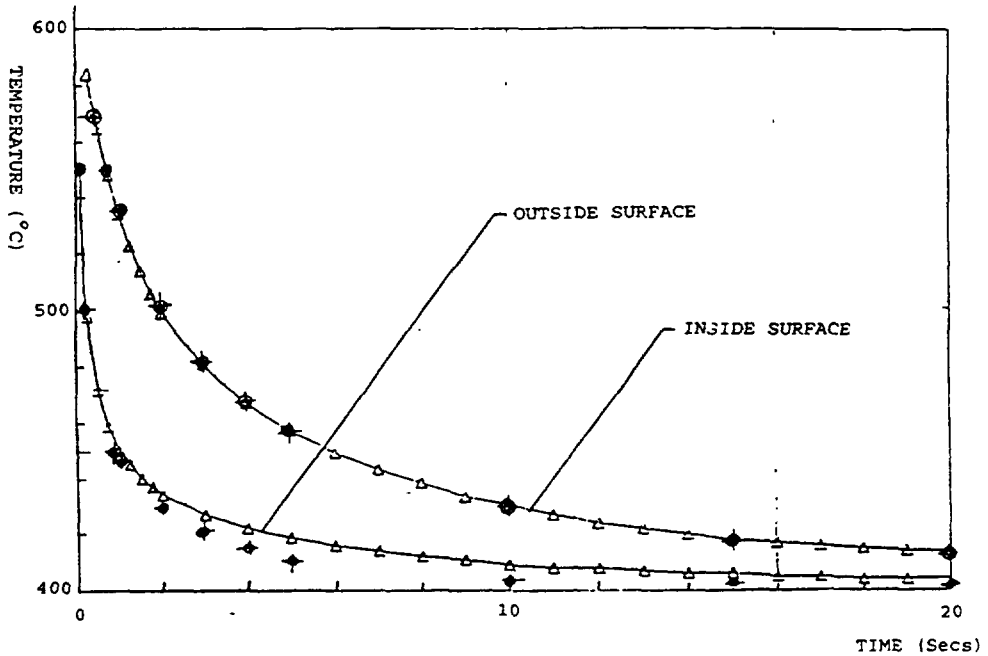

FLHE analysis with 0.25 sec downshock time
ABAQUS Calculations [13]

FIG. 3b. Temperature response of the cylinder

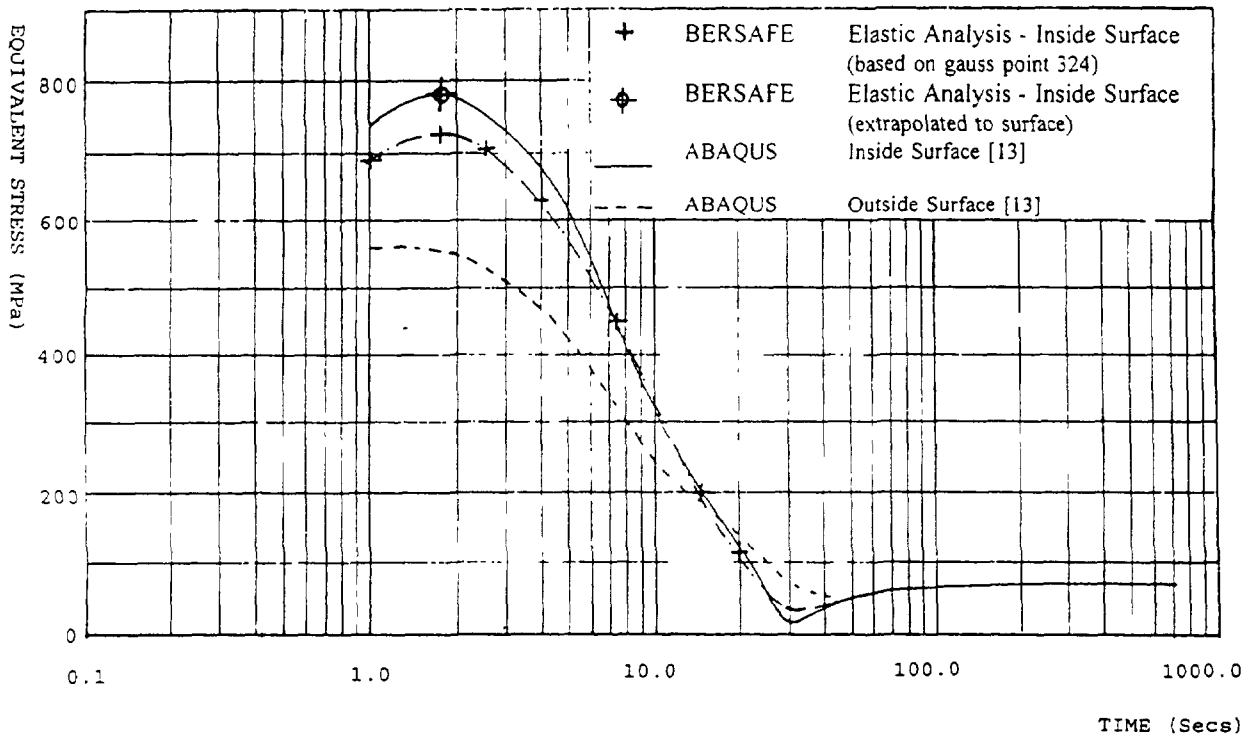

FIG 4 Variation of maximum stress during the thermal loading history

4.4.1 Peak Combined Loading

This is the time in the thermal cycle when the elastic stresses are at their maximum values. It occurs at 1.75 seconds after the commencement of the thermal downshock and the distribution of component stresses is shown in Figure 5. These are plotted on Section AA which is shown inset. The maximum axial stress occurs on the inside surface and has a magnitude of -655.2MPa, the equivalent stress at this point being 710MPa.

4.4.2 Steady State Loading

This is the loading during the steady state dwell period when the specimen temperature is uniform at 600°C and occurs at the start of the thermal cycle. Figure 6 shows the through thickness component stress distribution on Section AA (shown inset on Figure 5) and has a peak axial value of 58MPa at the inner surface.

4.5 Elastic Follow-up

Elastic follow-up in the dwell was estimated using a monotonic creep calculation starting from the elastic stress distribution calculated in Section 4.4.1 and continuing until the peak stresses had relaxed to below 100MPa. From this an elastic follow-up factor Z=3.57 was calculated.

4.6 Shakedown Analysis

The R5 procedure [1] requires a shakedown analysis to be performed. This is the superposition of a self-equilibrating residual stress field, constant at all times in the cycle, onto

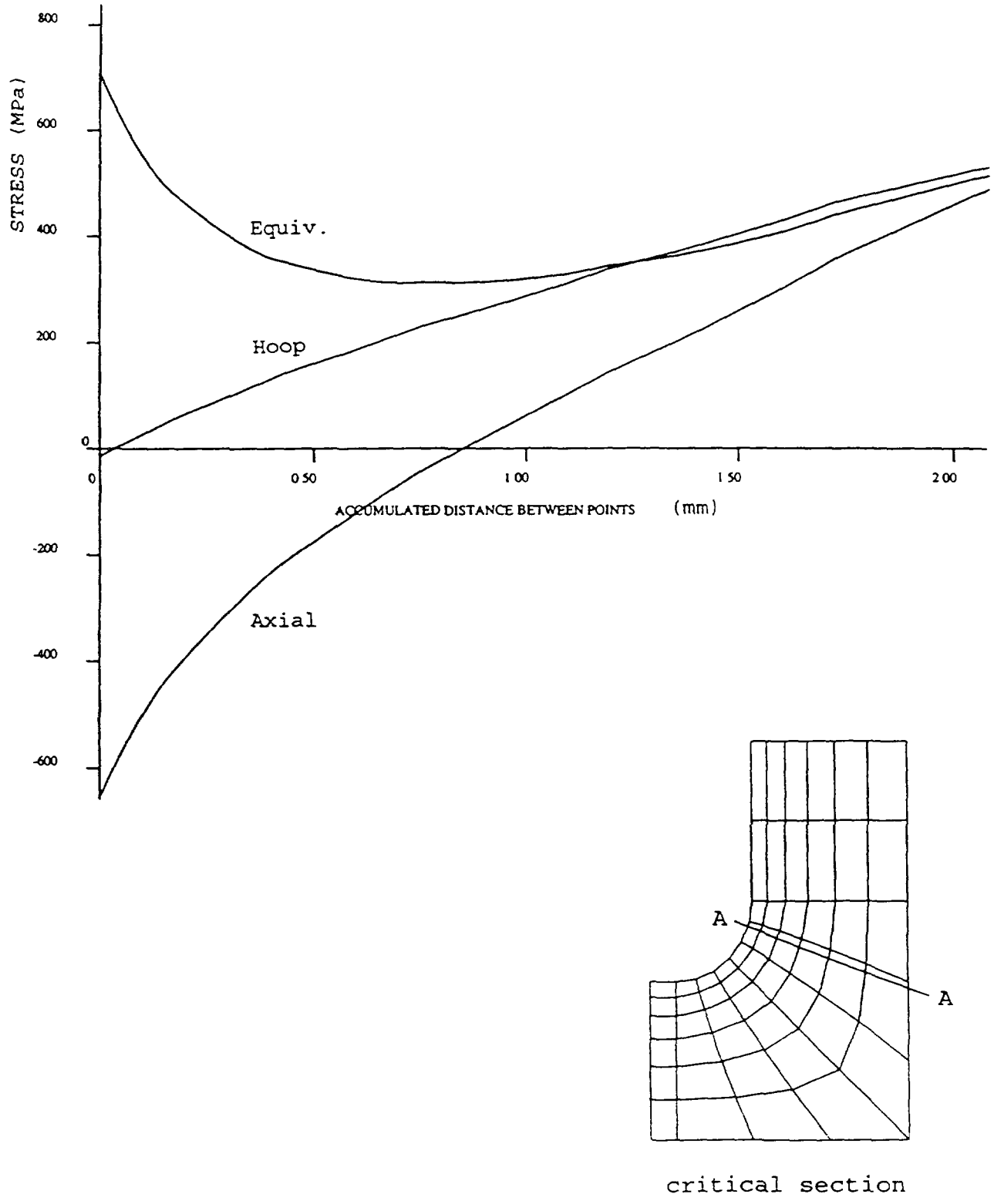

FIG 5 Through thickness component stress distributions for the peak combined loading case

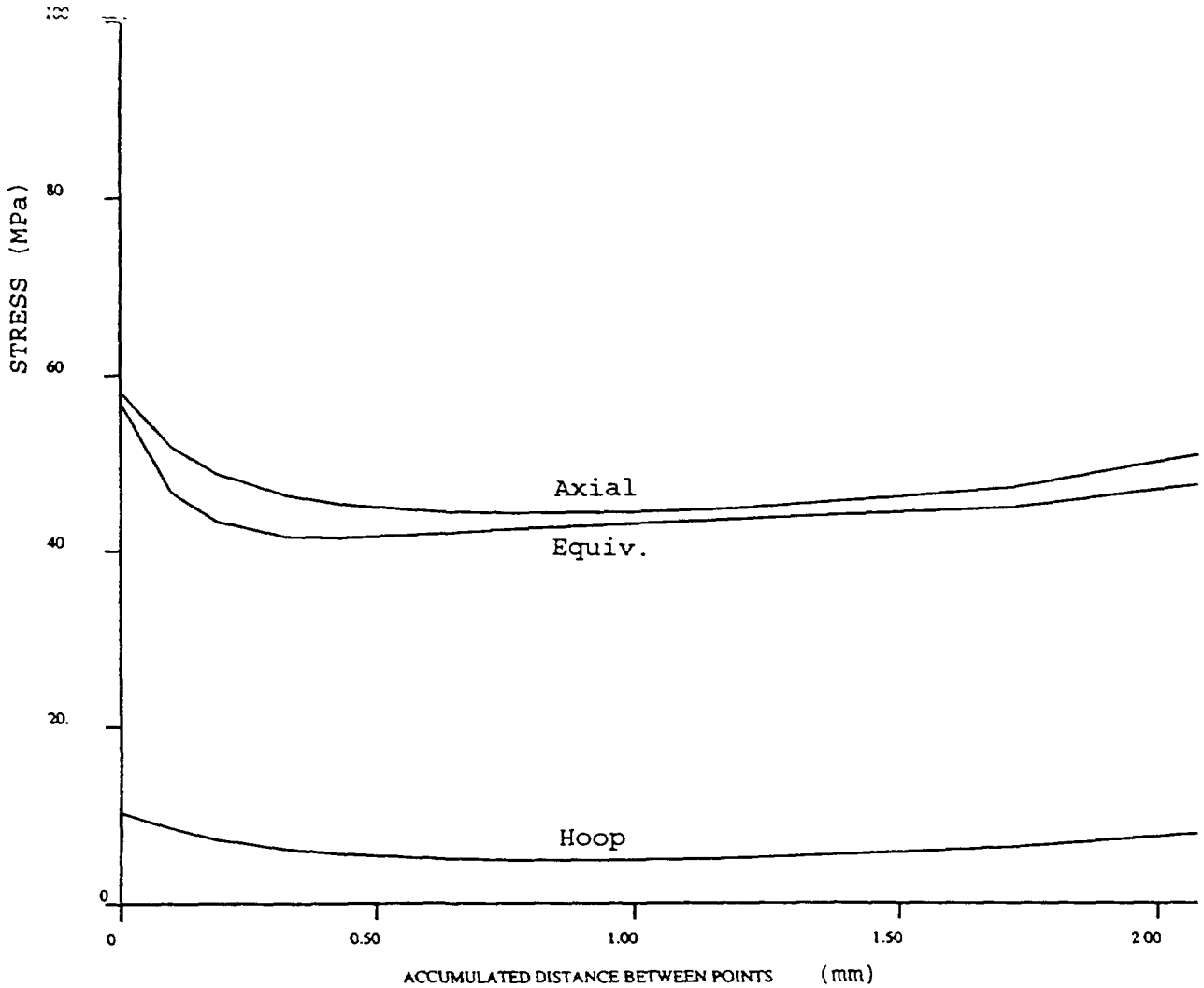

FIG 6 Through thickness component stress distributions for the steady state case

the extremes of the loading cycles described in Section 4.4.1 and 4.4.2. If the resultant shakedown stress distributions are below yield at all positions in the structure, then strict shakedown has been achieved. However, a less rigorous condition known as global shakedown is acceptable if no more than 20% of any cross section is outside yield.

Due to the requirement for being self-equilibrating, candidate residual stress fields may be successfully generated from thermal loadings. The field chosen for this analysis was the combination of factored thermal stresses generated as in Section 4.4.1 in the absence of primary loading, and a stress field caused by a localised region of high temperature on the outer surface of the specimen opposite to the transition region between flange and cylinder.

The resultant shakedown stress distributions are shown in Figure 7 for the peak combined loading case and Figure 8 for the steady state case. The residual stress field was adjusted so that the peak excursions above yield were equal for both cases and the proportions of the cross section outside yield were approximately the same. For this geometry under these loading conditions it was not possible to demonstrate global shakedown.

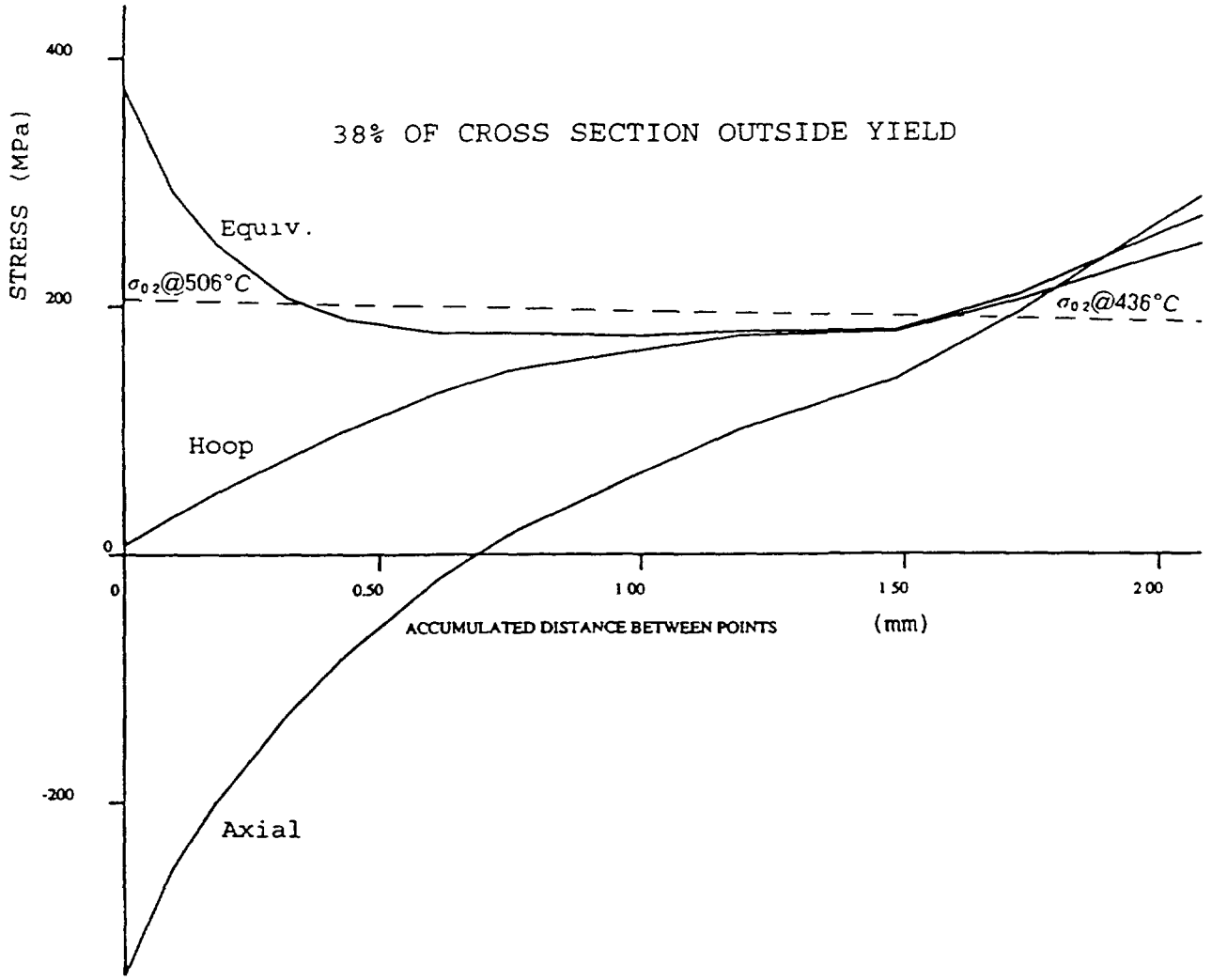

FIG 7 Through thickness component stress distributions for the shakedown solution, peak loading case

4.7 R5 Volume 3 assessment

A life assessment is made by combining fatigue and creep damage as outlined in Section 3. The strain range for the fatigue damage is calculated using the approximation methods of R5 Volume 2 as outlined below using the stress difference between the peak and steady state dwell loads.

4.7.1 Fatigue damage

The fatigue strain range is calculated from the equivalent elastic stress range $\Delta\bar{\sigma}_{el}$ together with an allowance for enhancement of the strain range due to plasticity and creep. $\Delta\bar{\sigma}_{el}$ is calculated using the differences in component stresses between the peak combined loading case and the steady state case. The effect of creep on the fatigue strain range is allowed for by adding $2(1+\nu)\Delta\sigma_{rD}/3E$ to the elastic strain range, where $\Delta\sigma_{rD}=\sigma_0 B''\ln(bt+1)$ is the stress relaxation stress drop, σ_0 is the creep reference stress, i.e. the maximum stress in the steady

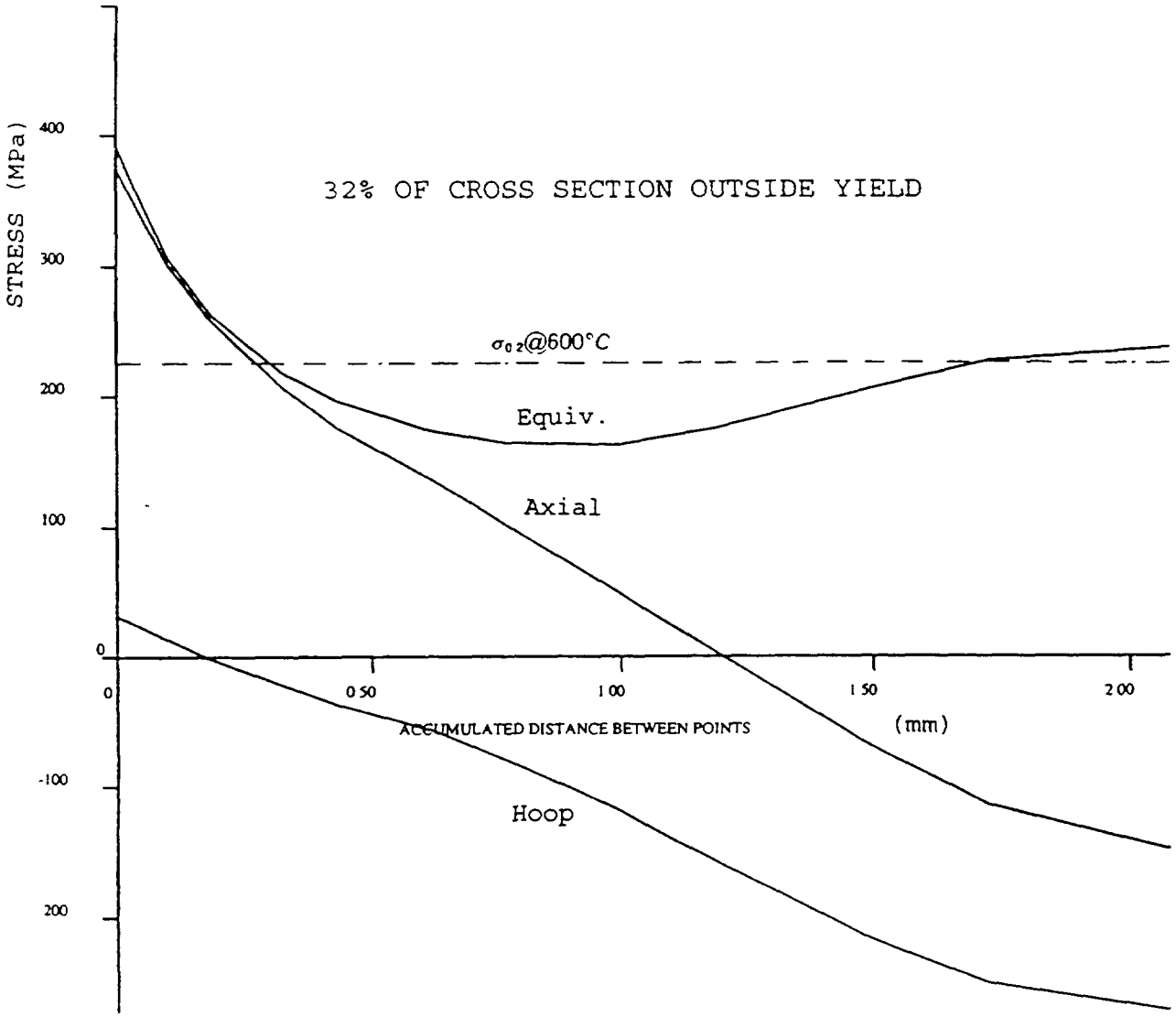

FIG 8 Through thickness component stress distributions for the shakedown solution, steady state case

state case, and $B^{//}$ and b are constants [1]. The enhancement of the fatigue strain range due to plasticity is calculated by the use of the Neuber procedure as shown in Figure 9. A further correction factor $\Delta\bar{\varepsilon}_{vol}$ [1] is made to allow for the fact that elastic straining takes places with ν=0.29, whereas for inelastic straining ν=0.5.

Using the procedure described above a total fatigue strain range of 0.893% per cycle was calculated which when applied to the appropriate fatigue data supplied in R66 [12] indicated failure after N_L=1766 cycles, where N_L refers to the failure of a test specimen typically 8mm in diameter. As the critical cross section is only 2mm thick, the procedure of R5 [1] Volume 3 was used to estimate crack initiation after 637 cycles and that cracks of 200μm (the failure criterion) would occur after N_o=1197 cycles.

4.7.2 Creep damage

The creep damage per cycle d_c was estimated following the R5 [1] procedure such that $d_c=Z\Delta\sigma'/E'\varepsilon_L$ where $\Delta\sigma'=\sigma_0 B^{//}\ln(bt/Z+1)$, $E'=3E/2(1+\nu)$ is the multi-axial elastic modulus and ε_L is the creep ductility. Using the values of material properties from Section 4.1 the creep damage was calculated as d_c=0.003.

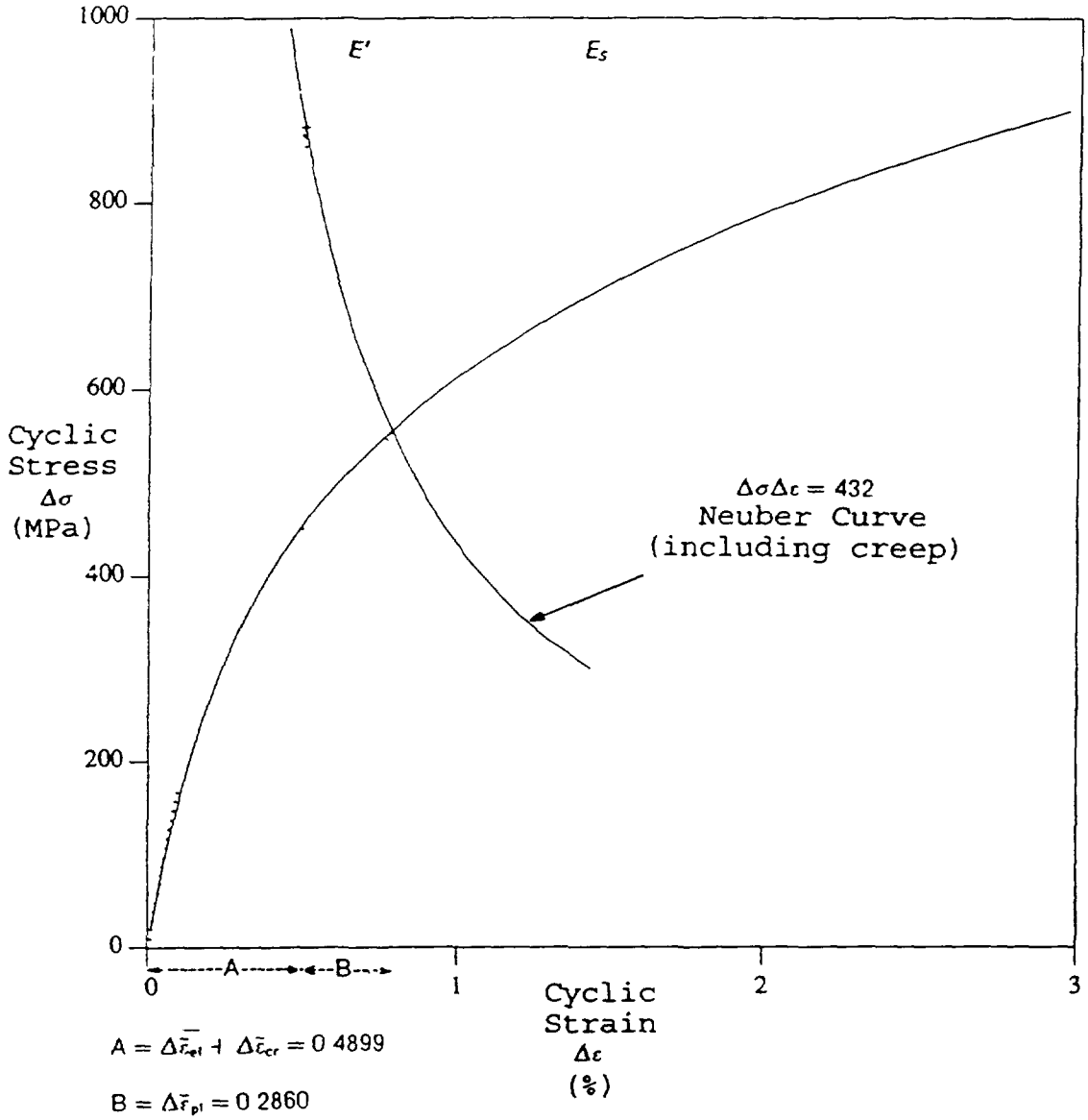

FIG 9 Derivation of fatigue strain range components using the Neuber construction

4 7 3 Total damage

The total damage per cycle is $d_t=1/N_0+d_c$ and the creep-fatigue endurance then $N_0^*=1/d_t$. Using $N_0=1197$ and $d_c=0\ 003$ gives $N_0^*=260$ cycles.

5. INELASTIC FINITE ELEMENT ANALYSIS

Detailed inelastic finite element analysis was used to define the strain range, elastic follow-up factor and creep stress drop for use in the R5 initiation assessment as described in Section 3 The analyses were performed using the ORNL constitutive model within a user-defined (UMAT) subroutine written for ABAQUS version 5.2. Some additional analysis was however also carried out using the Fast Reactor State Variable (FRSV) constitutive model for comparison.

5.1. Material properties

In general, except for non-linear data, the material properties chosen for this analysis were the same as those chosen for the elastic analysis described in Section 4 so that meaningful comparisons could be made.

For the ORNL model, zoning of plasticity parameters was used based on the assessed strain ranges and the values used in the analysis are shown in Tables 2a to 2c and in Fig. 9.

TABLE 2a. 0.2% SEMI-STRAIN RANGE PLASTICITY PARAMETERS

Cycle Number	Plastic Strain	Stress (MPa)			
	(absolute)	300°C	450°C	550°C	625°C
1	0.0	128	115	110	108
	0.01	341	328	323	321
10	0.0	164	130	133	133
	0.01	377	324	346	346

TABLE 2b. 0.3% SEMI-STRAIN RANGE PLASTICITY PARAMETERS

Cycle Number	Plastic Strain	Stress (MPa)			
	(absolute)	300°C	450°C	550°C	625°C
1	0.0	140	126	120	118
	0.01	245	231	225	223
10	0.0	198	151	156	155
	0.01	303	256	261	260

TABLE 2c. 0.5% SEMI-STRAIN RANGE PLASTICITY PARAMETERS

Cycle Number	Plastic Strain	Stress (MPa)			
	(absolute)	300°C	450°C	550°C	625°C
1	0.0	152	136	130	128
	0.01	205.2	189.2	183.2	181.2
10	0.0	242	180	185	180
	0.01	295.2	233.2	238.2	233.2

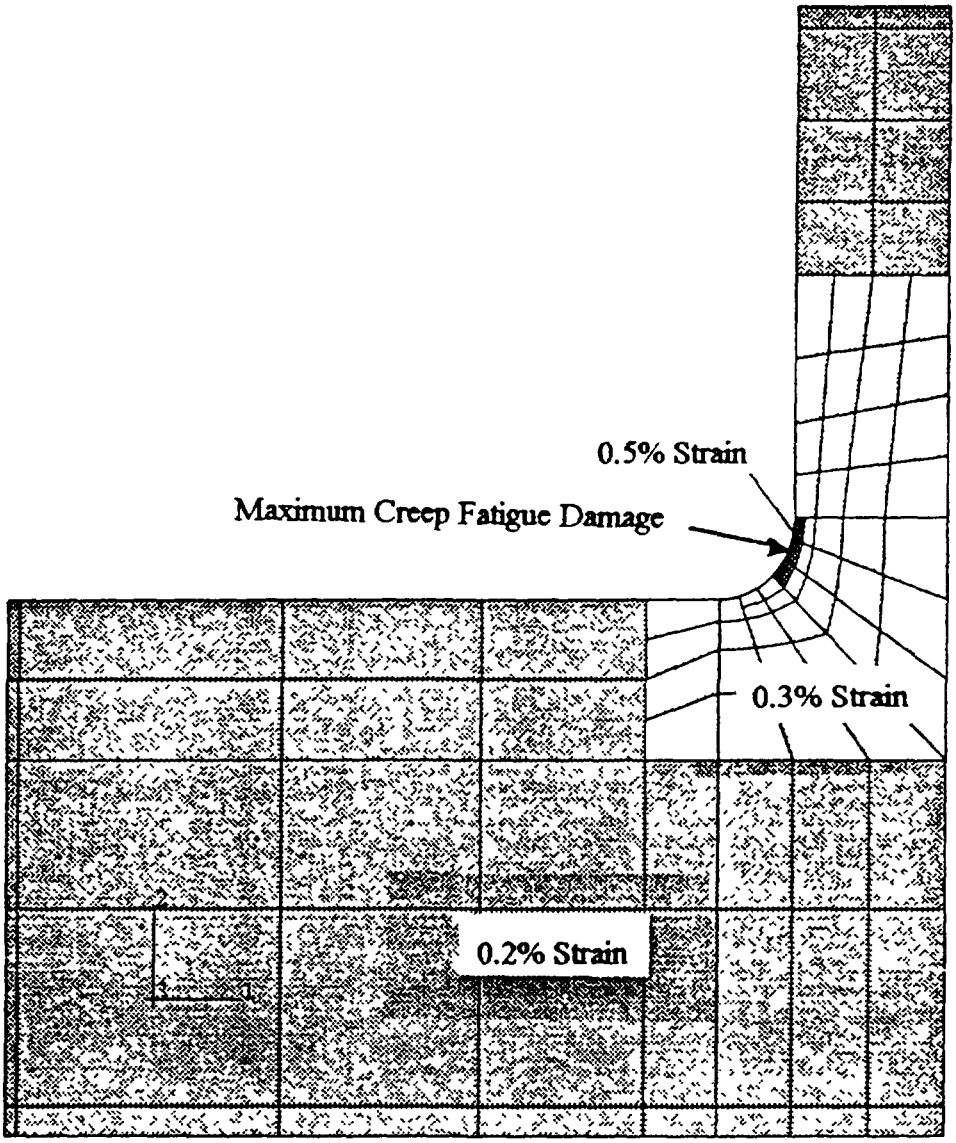

FIG 10 Detail of the finite element mesh used in the inelastic analysis showing the zoning of material properties and position of maximum creep damage

Tenth cycle data were used in the inelastic analysis described in Section 5 3 after the application of the first complete cycle.

The creep behaviour was described by the currently recommended properties [13] using a creep subroutine developed for use with the finite element program used

5.2. Finite element mesh

Details of the finite element mesh used in the analysis are shown in Figure 10, which also indicates the zoning of material properties and the region of maximum damage. The model is made up axisymmetric eight noded elements and consists of 120 elements and 461 nodes.

5.3. Inelastic Analysis

The thermal analysis and an initial elastic analysis are described in [14]. The inelastic analysis was performed using the ABAQUS [15] finite element stress analysis program. This was

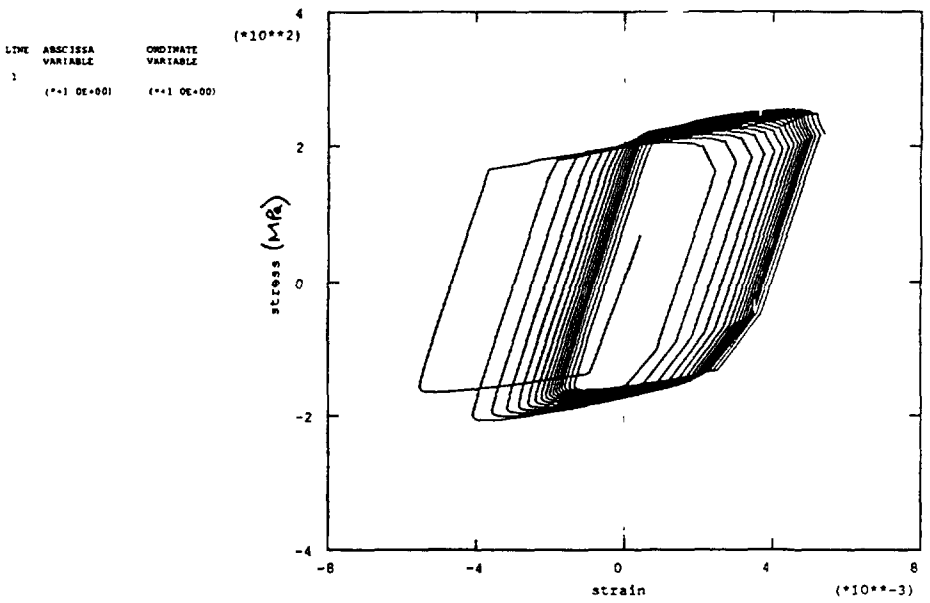

FIG 11a The axial stress-strain hysteresisloops for the ORNL constitutive model

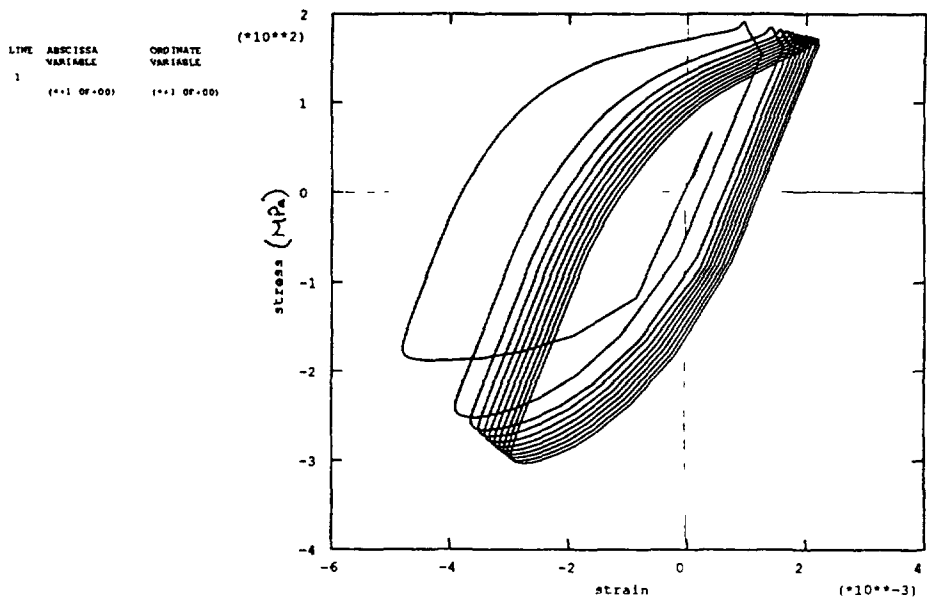

FIG 11b The axial stress-strain hysteresis loops for the FRSV constitutive model

carried out, firstly, using the ORNL constitutive model within ABAQUS, initially subjecting the model to 10 complete thermal cycles of loading. After inspection of the results, this was followed by a further 7 cycles until stable hysteresis loops had been achieved. An error was however found to exist with the ORNL model used which consequently failed to provide the specified creep-fatigue interaction. To correct this problem, an ABAQUS user subroutine (UMAT) was provided by HKS, the authors of ABAQUS. The results using the UMAT are given in Section 5.4 below.

The second inelastic analysis was carried out over 10 complete cycles using the Fast Reactor State Variable (FRSV) constitutive model [13]. This model has been developed in order to give improvements over the ORNL model. For this case, the creep-plasticity description has been encoded as a UMAT subroutine for the ABAQUS program, treating creep with the same strain hardening formulation as in the ORNL model.

5.4. Results

Neither the ORNL nor the FRSV constitutive models reached full stabilisation, the ORNL model predicting a positive increasing mean stress and the FRSV model a negative decreasing mean stress as shown in the axial stress-strain hysteresis loops of Figure 11a and 11b. Comparisons have been made with a French inelastic analysis by Cabrillat and Carbonnier [16] for two constitutive models. The first is a linear kinematic model based on the reduced cyclic curve at 600°C. The second is a nonlinear kinematic hardening Chaboche model, this latter model being the only one which apparently symmetrises. Table 3 gives a comparison of the predicted starting stress for creep and fatigue strain range.

TABLE 3. COMPARISON OF PREDICTED STRAIN RANGE AND STRESS

Constitutive Model	Stress at beginning of hold time (MPa)	Strain Range (%)
ORNL	237.4	0.790
FRSV	172.8	0.564
Linear Kinematic	164.7	0.700
Chaboche	245.0	0.563

In general, there is reasonable agreement over the predicted strain ranges, the major difference between the models being the stress at the commencement of the hold period, and hence the amount of predicted creep damage.

5.5. R5 Volume 3 assessment

Table 4 above summarises the life predictions and corresponding damage fractions at initiation as obtained from various analyses, including the elastic analysis described in Section 4 and an elastic analysis [3] based on the methods of RCC-MR [5].

TABLE 4. COMPARISON OF LIFE PREDICTIONS

Assessment Method	Strain Range (%)	Fatigue-Creep Life (cycles)	Fatigue Damage Fraction D_f	Creep Damage Fraction D_c
RCC-MR Elastic	0.666	13	0	1
Linear Kinematic	0.700	1080	0.15	0.65
Chaboche	0.563	100	0.01	~1
R5 Elastic (Section 4)	0.893	260	0.22	0.78
R5 Inelastic ORNL	0.790	618	0.38	0.62

6. DISCUSSION

The Thermina tests lead to a severe creep-fatigue load history on the specimen, with up to 40% of the critical cross-section outside yield at shakedown. It therefore provides a demanding test of the R5 methodology.

The shakedown route of R5 Volume 2 based on elastic analysis and reference stress techniques gave a best-estimate of 260 cycles to initiate a crack of 0.2mm. The detailed inelastic methods led to an estimate of 618 cycles using the ORNL model. These compare with the experimental observation of between 526 and 650 cycles as measured on two specimens.

In addition to the results given above, Cabrillat and Martin [3] derived life estimates using RCC-MR [5]. Using the 1985 version gave 14 cycles whereas using the first addendum (1987) which takes account of secondary stress relaxation gave 212 cycles.

7. CONCLUDING REMARKS

The R5 procedure has been applied to estimate the endurance of a test specimen subjected to controlled mechanical and cyclic thermal loading. The simplified route based on shakedown analysis and using best estimate materials data resulted in an estimated endurance of about half the observed endurance. The result is closer than existing design codes and retains a degree of conservatism.

Detailed inelastic finite element analysis resulted in a life estimate in good agreement with experiment.

REFERENCES

[1] AINSWORTH R. A. (Editor), R5: Assessment procedure for the high temperature response of structures, Issue 2, Nuclear Electric, 1995.

[2] CABRILLAT M. T., MARTIN Ph., Creep-fatigue interaction on Thermina samples experimental and numerical results, SMIRT 10. August 1989, Session L.

[3] CABRILLAT M. T., MARTIN Ph., Assessment of the creep-fatigue damage by the elastic route of the RCC-MR. Some lessons drawn from in sodium test. SMIRT 10. Div.E, August 1989.

[4] Cases of ASME boiler and pressure vessel code, case N-47-29, American Society of Mechanical Engineers, 1990.

[5] RCC-MR, Design and construction rules for mechanical components of FBR nuclear islands, ACFEN, 1985.

[6] AINSWORTH R.A., BUDDEN P.J., Design and assessment of components subjected to creep, J Strain Analysis, 29, 201-208, 1994.

[7] GOODMAN A.M., BOOTH P., Approximate methods for estimating elastic follow-up in creeping structures, Nuclear Electric Report TD/SE/REP/0002, November 1992.

[8] CABRILLAT M.T.,Thermina: material characterisation tests, STRA/LDCS/SDCS/86.125np, June 1986.

[9] CABRILLAT M.T., Thermina - Calculs thermiques, STRA/LDCS/85.070, March 1985.

[10] KEAVEY M.A., A user's guide to FLHE, CEGB, July 1987.

[11] HELLEN T.K., A user's guide to BERSAFE, CEGB, February 1988.

[12] R66, AGR materials data handbook, Issue 2, Nuclear Electric, July 1992.

[13] WHITE P.S, SIWG recommendation on constitutive equations for Type 316 (LN) steel - revised version, FRDCC/SIWG/P(88) 608 Rev 1.

[14] BATE S.K., Inelastic finite element analysis of a Thermina test specimen interim report, AEA Report AEA-RS-1303, March 1993.

[15] HIBBITT, KARLSSON, SORENSON, ABAQUS/STANDARD user's guide version 5.2.

[16] CABRILLAT M.T., CARBONNIER J.L., Creep-fatigue interaction in small mock-ups subjected to thermal shocks and primary stresses, Res Mechanica 27 (1989) p323-333

LIST OF PARTICIPANTS

Bate, S.K.	Structural Assessments Department, AEA Technology, Building RD3/Room 103, Risley, Warrington, Cheshire WA3 6AT, United Kingdom
Booth, P.	Nuclear Electric Ltd, Barnett Way, Barnwood, Gloucester, GL4 3RS, United Kingdom
Buckthorpe, D.	NNC Ltd, Booths Hall, Chelford Road, Knutsford, Cheshire WA16 8QZ, United Kingdom
Hales, R.	Nuclear Electric Ltd, Barnett Way, Barnwood, Gloucester, GL4 3RS, United Kingdom
Lee, H.-Y.	Korea Atomic Energy Research Institute, Mechanical Structure Design Development, P.O.Box 105, Yusung Post Office, Taejon, Republic of Korea 305-600
Michel, B.	CEA, DER/SERA/LDCS, Bat. 204, CEA de Cadarache, F-13108 St. Paul-lez-Durance Cedex, France
Picker, C. *(Chairman)*	AEA Technology, Risley, Warrington, Cheshire WA3 6AT, United Kingdom
Poette, C.	Structural Integrity Laboratory, CEA/CEN Cadarache, Bat. 204, F-13108 St. Paul-lez-Durance Cedex, France
Ramesh, R.	Nuclear Systems Division, Indira Gandhi Center for Atomic Research, Kalpakkam - 603 102, Tamil Nadu, India
Rao B. Sankara, K.	Indira Gandhi Center for Atomic Research, Kalpakkam - 603 102, Tamil Nadu, India
Rinejski, A. *(Scientific Secretary)*	Division of Nuclear Power and the Fuel Cycle, Internationa Atomic Energy Agency, Wagramerstrasse 5, P.O. Box 100, A-1400 Vienna, Austria

Riou, B.	Framatome, 10 rue Juliette Récamier, F-69456 Lyon Cedex 06, France
Spindler, W.	Nuclear Electric Ltd, Barnett Way, Barnwood, Gloucester, GL4 3RS, United Kingdom
Touboul, F.	CEA/CEN Saclay, F-91191 Gif-sur-Yvette Cedex, France
Townley, C.	Rodborough House, Butterrow West, Stroud, Gloucestershire, GL5 3TZ, United Kingdom
Wada, Y.	Structure and Material Research Section, Oarai Engineering Center, Power Reactor & Nuclear Fuel Development Corporation, 4002 Narita, Oarai-machi, Higashi-ibaraki-gun, Ibaraki-ken, 311-13 Japan
Zhukov, V.	Structural Analysis Department, OKBM, 603 603 Nizhny Novgorod -74, Burnakovsky proezd 15, Russian Federation